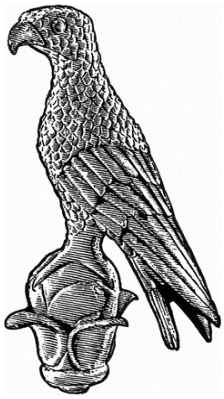

ΠΑΝΕΠΙΣΤΗΜΙΟ ΙΩΑΝΝΙΝΩΝ
ΣΧΟΛΗ ΘΕΤΙΚΩΝ ΕΠΙΣΤΗΜΩΝ
ΤΜΗΜΑ ΦΥΣΙΚΗΣ

Φαινομενολογία και Κοσμολογία Επεκτάσεων του Καθιερωμένου Προτύπου με Κλασική Συμμετρία Κλίμακας

Αλέξανδρος Καράμ

Διδακτορική διατριβή

ΙΩΑΝΝΙΝΑ 2018

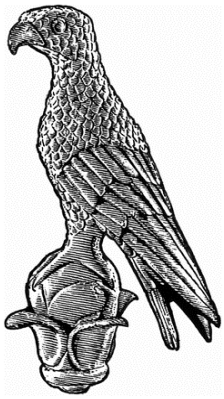

UNIVERSITY OF IOANNINA
DEPARTMENT OF PHYSICS

Phenomenological and Cosmological Implications of Classically Scale-Invariant Standard Model Extensions

Alexandros Karam

PhD thesis

IOANNINA 2018

Three-member advisory committee:

1. Kyriakos Tamvakis (Supervisor) – Professor, Physics Department, University of Ioannina
2. Athanasios Dedes – Professor, Physics Department, University of Ioannina
3. Ioannis Rizos – Professor, Physics Department, University of Ioannina

Seven-member PhD thesis examination committee:

1. Kyriakos Tamvakis (Supervisor) – Professor, Physics Department, University of Ioannina
2. Athanasios Dedes – Professor, Physics Department, University of Ioannina
3. Ioannis Rizos – Professor, Physics Department, University of Ioannina
4. Panagiota Kanti – Professor, Physics Department, University of Ioannina
5. Georgios Leontaris – Professor, Physics Department, University of Ioannina
6. Alex Kahagias – Professor, Physics Department, National Technical University of Athens
7. Vassilis Spanos – Associate Professor, Department of Physics, University of Athens

"Theoretical physics research is like music. It can be beautiful but also chaotic. It takes (a lot of) time to master the theoretical background and creativity to construct something new and original. The end result can be a matter of taste, but if the foundations are sound (pun intended) it will likely reach the eyes/ears of a large audience and make an impact on society."

Abstract

In this thesis, we investigate the phenomenology and cosmological consequences of classically scale-invariant Standard Model extensions. We explore how models with classical scale invariance, where all mass scales are dynamically generated, can address various contemporary high-energy physics problems without destabilizing the Higgs mass. The vacuum stability, dark matter and neutrino mass problems are simultaneously addressed in an $SU(2)_X$ extension. We also explore an $SU(3)_X$ extension due to its rich phenomenology regarding dark matter. Finally, we address the dynamical generation of the Planck scale in conjunction with the theory of cosmic inflation and study various aspects pertaining to the inflationary observables.

ΠΕΡΙΛΗΨΗ

Μια συναρπαστική εποχή βρίσκεται σε εξέλιξη για τη Φυσική Υψηλών Ενεργειών και την Κοσμολογία. Η πρόσφατη ανακάλυψη του μποζονίου Higgs από τον επιταχυντή LHC στο CERN και η παρατήρηση βαρυτικών κυμάτων που προήλθαν από συγχωνευόμενες μελανές οπές από τον ανιχνευτή LIGO, έχουν επιβεβαιώσει ξανά τους μακρόχρονους ακρογωνιαίους λίθους της κατανόησής μας για τη Φυσική του Σύμπαντος, ήτοι, το Καθιερωμένο Πρότυπο (SM) των στοιχειωδών σωματιδίων και τη Γενική Θεωρία της Σχετικότητας (GR) του Einstein. Αμφότερες θεωρίες έχουν αντέξει στο πέρασμα του χρόνου και έχουν επιβεβαιωθεί πειραματικά σε πολυάριθμες περιπτώσεις από την απαρχή τους κι έπειτα. Παρά την επιτυχία τους όμως, το SM και η GR αποτυγχάνουν να εξηγήσουν κάποια φαινόμενα ενώ περιέχουν και μερικά έμφυτα προβλήματα.

Πρόσφατες παρατηρήσεις της κοσμικής ακτινοβολίας υποβάθρου (CMB) έχουν καθορίσει πως το Σύμπαν είναι επίπεδο και ομοιογενές σε μεγάλες κλίμακες. Επεκτείνοντας την GR με ένα βαθμωτό πεδίο μπορούμε να οδηγηθούμε σε μια πληθωριστική εποχή στα πρώιμα στάδια του Σύμπαντος, η οποία μπορεί να εξηγήσει την επιπεδότητα και ομοιογένειά του. Εξετάζοντας τον *πληθωρισμό* με κβαντομηχανικό τρόπο, η θεωρία μπορεί να μας παράσχει τους σπόρους για την μετέπειτα δημιουργία δομής που παρατηρούμε (άστρα, γαλαξίες, κ.τ.λ.). Τα πρόσφατα αποτελέσματα της αποστολής Planck έχουν περιορίσει τον παραμετρικό χώρο των πληθωριστικών παρατηρούμενων ποσοτήτων και έχουν ουσιαστικά αποκλείσει πολλά από τα προταθέντα θεωρητικά μοντέλα, συμπεριλαμβανομένων των απλούστερων όπου ένα βαθμωτό πεδίο έχει ελάχιστη σύζευξη με τη βαρύτητα. Από την άλλη, ελαφρώς πιο περίπλοκα μοντέλα όπως το Starobinsky και τα μη-ελάχιστα μοντέλα, δείχνουν να κείνται μέσα στο επιτρεπόμενο εύρος. Αυτά τα μοντέλα ανήκουν στην οικογένεια των θεωριών *βαθμωτής-τανυστικής* (ST) βαρύτητας. Στα ST μοντέλα, ένα (ή περισσότερα) βαθμωτό πεδίο έχει εν γένει μη-ελάχιστη σύζευξη με τη βαρύτητα και μπορεί να οδηγήσει σε πληθωρισμό. Μια τέτοια μη-ελάχιστη σύζευξη είναι ενδιαφέρουσα κι υπό άλλη έννοια: εάν το βαθμωτό πεδίο αναπτύξει αναμενόμενη τιμή κενού (VEV), τότε η κλίμακα Planck μπορεί να γεννηθεί με δυναμικό τρόπο. Η κλίμακα Planck (περί τα 10^{19} GeV) είναι μία εκ των δύο γνωστών κλιμάκων μάζας στη Φυσική. Η άλλη είναι η ηλεκτρασθενής (EW) κλίμακα (περί τα 250 GeV), σχετιζόμενη με τη VEV του πεδίου Higgs. Δε γνωρίζουμε ακόμα γιατί αυτές οι δύο κλίμακες απέχουν τόσο πολύ.

Το CMB υποδεικνύει επίσης πως γύρω στο 85% της μάζας που περιέχεται στο Σύμπαν είναι σε μορή η οποία δεν ακτινοβολεί. Η *σκοτεινή ύλη* πιστεύεται ότι είναι σωματιδιακής φύσης, με την οικογένεια των *ασθενώς αλληλεπιδρώντων έμμαζων σωματιδίων* (WIMPs) να είναι η πιο επιτυχής στην περιγραφή της. Τα WIMPs συνήθως εδρεύουν σε σκοτεινούς τομείς οι οποίοι επικοινωνούν με το SM μέσω αλληλεπιδράσεων πύλης (portal interactions). Πολυάριθμα πειράματα βρίσκονται σε

λειτουργία ή αναμένεται σύντομα να λειτουργήσουν, με στόχο την εξεύρεση της σκοτεινής ύλης, είτε άμεσα είτε έμμεσα.

Με την ανακάλυψη του μποζονίου Higgs, έχουμε πλέον προσδιορίσει όλες τις παραμέτρους του SM. Παρολαυτά, το SM δεν μπορεί να εξηγήσει τη φύση της σκοτεινής ύλης, πώς τα νετρίνα αποκτούν μάζα, την προέλευση της ασυμμετρίας ύλης-αντιύλης ή γιατί η QCD φαίνεται να μην παραβιάζει την CP συμμετρία (strong CP problem). Επιπλέον, η μετρούμενη τιμή για τη μάζα του Higgs υποδηλώνει ότι το κενό μας βρίσκεται σε μια μετασταθή (metastable) κατάσταση από την οποία μπορεί ενδεχομένως να υποστεί αυθόρμητη μετάπτωση, με καταστροφικά αποτελέσματα για το Σύμπαν μας. Αυτό οφείλεται στο γεγονός ότι η σταθερά αυτο-σύζευξης του Higgs μεταβάλλεται με την ενέργεια και αποκτά αρνητικό πρόσημο σε ενέργειες πάνω από περίπου 10^{10} GeV. Το πρόβλημα της ευστάθειας του κενού μπορεί να εξαλειφθεί εάν εισάγουμε ένα ή περισσότερα βαθμωτά πεδία τα οποία συζεύγνυνται με το Higgs. Νέα πεδία, φερμιονικά ή μποζονικά, μπορούν επίσης να παράσχουν λύσεις για τα υπόλοιπα προβλήματα του SM. Παρολαυτά, εξαιτίας κβαντικών φαινομένων, η μάζα του Higgs παρουσιάζει μια τετραγωνική ευαισθησία στις κλίμακες μάζας που εισάγουμε μαζί με τα νέα πεδία. Χρειαζόμαστε λοιπόν ένα τεράστιο ποσό μικρο-ρύθμισης (fine-tuning) για να εξαλείψουμε τις τετραγωνικές αποκλίσεις και να ανακτήσουμε την παρατηρούμενη μάζα του Higgs. Αυτό το πρόβλημα της *φυσικότητας* της μάζας του Higgs μετριάζεται σε υπερσυμμετρικές επεκτάσεις του SM, εφόσον η υπερσυμμετρία σπάει ήπια σχετικά κοντά στην ηλεκτρασθενή κλίμακα. Δυστυχώς, κανένα υπερσυμμετρικό σωματίδιο δεν έχει παρατηρηθεί από τον LHC ή άλλους επιταχυντές μέχρι τώρα, κάτι το οποίο έχει παρακινήσει την εξερεύνηση εναλλακτικών ιδεών.

Μια ιδέα η οποία έχει λάβει αρκετή προσοχή τα τελευταία χρόνια είναι αυτή της *κλασικής συμμετρίας κλίμακας*. Η κλασική συμμετρία κλίμακας αξιώνει πως η Lagrangian του κλασικού επιπέδου μιας θεωρίας δε θα πρέπει να περιέχει οποιαδήποτε ad hoc παράμετρο με διαστάσεις μάζας. Η μόνη τέτοια παράμετρος στο SM είναι η παράμετρος μάζας του Higgs η οποία οδηγεί στο σπάσιμο την ηλεκτρασθενή συμμετρία. Θέτοντας αυτήν την παράμετρο ίση με το μηδέν ενισχύουμε τη συμμετρία του SM. Πηγαίνοντας στο κβαντικό επίπεδο, η μεταβολή των συζεύξεων της θεωρίας με την ενέργεια επιφέρει σπάσιμο της συμμετρίας, αλλά αυτό δεν επανεισάγει τις τετραγωνικές αποκλίσεις. Συνεπώς, η θεωρία είναι από τεχνικής άποψης φυσική. Ο μηχανισμός που ευθύνεται για το σπάσιμο της συμμετρίας αναπτύχθηκε από τους S. Coleman και E. Weinberg. Αν εφαρμόσουμε, όμως, αυτόν το μηχανισμό στο SM με κλασική συμμετρία κλίμακας (CSI) βρίσκουμε ταχυονική μάζα για το Higgs εξαιτίας της μεγάλης μάζας του top κουάρκ. Αυτό σημαίνει πως για να δουλέψει ο μηχανισμός Coleman-Weinberg χρειάζεται να προσθέσουμε νέα (μποζονικά) πεδία στο SM. Εάν αυτά είναι βαθμωτά πεδία τότε η σύζευξή τους με το Higgs μπορεί να συνεισφέρει θετικά στη μεταβολή της αυτο-σύζευξης του Higgs και να βοηθήσει στη σταθεροποίηση του δυναμικού.

Νέα πεδία μπορούν επίσης να αποτελέσουν υποψήφιους για σκοτεινή ύλη. Αυτοί οι υποψήφιοι μπορούν να είναι βαθμωτά, φερμιόνια, διανυσματικά μποζόνια ή να έχουν μεγαλύτερα σπιν. Σε κάθε περίπτωση, θα πρέπει να υπάρχει μια συμμετρία η οποία θα καθιστά τους υποψήφιους αυτούς ευσταθείς σε κοσμολογική κλίμακα, καθότι σε άλλη περίπτωση θα είχαν διασπαστεί κατά την εξέλιξη του Σύμπαντος και δε θα υπήρχαν σήμερα. Τέτοιες σταθεροποιητικές συμμετρίες συνήθως επιβάλλονται στις θεωρίες, μπορούν όμως και να προκύψουν αυθόρμητα σαν εσωτερικά χαρακτηριστικά νέων συμμετριών βαθμίδας.

Στο επόμενο κεφάλαιο, ξεκινάμε κάνοντας μια σύντομη ανασκόπηση του ευρέως αποδεκτού μοντέλου ΛCDM, γνωστό επίσης σαν το Καθιερωμένο Πρότυπο της Κοσμολογίας. Αφότου σκιαγραφήσουμε τα βασικά του χαρακτηριστικά, συζητούμε τα προβλήματα του ορίζοντα και της επιπεδότητας τα οποία έχουν κοινή λύση εφόσον το Σύμπαν υπέστη μια πληθωριστική εποχή στα πρώιμα στάδιά του.

Στο κεφάλαιο 3, εξερευνούμε το πρότυπο του κοσμολογικού πληθωρισμού. Αρχικά κάνουμε ανασκόπηση της απλούστερης περίπτωσης ενός βαθμωτού πεδίου ελάχιστα συζευγμένου με τη βαρύτητα το οποία, με τη βοήθεια ενός κατάλληλου δυναμικού, δύναται να οδηγήσει τον πληθωρισμό. Έπειτα, χειριζόμαστε τον πληθωρισμό με κβαντομηχανικό τρόπο και εξετάζουμε τη φυσική πίσω από τις κοσμολογικές διαταραχές οι οποίες πιστεύεται ότι ήταν οι σπόροι για τη δημιουργία της δομής που παρατηρούμε σήμερα στο Σύμπαν. Για να κάνουμε σύνδεση με το πείραμα, υπολογίζουμε τους φασματικούς δείκτες καθώς και τον τανυστικό-προς-βαθμωτό λόγο και τους εκφράζουμε συναρτήσει των slow-roll παραμέτρων. Κατόπιν, γενικεύουμε στην περίπτωση των ST θεωριών οι οποίες περιέχουν μη-ελάχιστη σύζευξη μεταξύ του βαθμωτού πεδίου και του βαθμωτού Ricci. Μια τέτοια μη-ελάχιστη σύζευξη μας ενδιαφέρει υπό την έννοια ότι στα πλαίσια της κλασικής συμμετρίας κλίμακας η VEV του πεδίου δύναται να γεννήσει δυναμικά την κλίμακα Planck.

Στο κεφάλαιο 4, κάνουμε μια σύντομη ανασκόπηση των βασικών συστατικών του Καθιερωμένου Προτύπου των Στοιχειωδών Σωματιδίων το οποίο έχει αντέξει στο πέρασμα του χρόνου για πάνω από τέσσερις δεκαετίες. Έπειτα, σκιαγραφούμε τα προβλήματα και τις ελλείψεις του μοντέλου πριν επικεντρωθούμε σε αυτά που μας ενδιαφέρουν περισσότερο στην παρούσα διατριβή.

Στο κεφάλαιο 5, εμβαθύνουμε στο πρόβλημα της σκοτεινής ύλης. Ξεκινάμε σκιαγραφώντας τα κύρια αποδεικτικά στοιχεία που υποστηρίζουν την ύπαρξη της σκοτεινής ύλης. Έπειτα, κάνουμε μια σύντομη ανασκόπηση των ιδιοτήτων μερικών από τους πιο διάσημους υποψήφιους για σκοτεινή ύλη πριν επικεντρωθούμε στο πρότυπο WIMP και τα διάφορα χαρακτηριστικά του. Τέλος, παρουσιάζουμε την κατάσταση των ερευνών που αφορούν τη σκοτεινή ύλη.

Στο κεφάλαιο 6, ξεκινάμε αξιώνοντας πως η διάσταση του χωρόχρονου είναι ο λόγος πίσω από την εμφάνιση μόνο (υπερ-)επανακανονικοποιήσιμων τελεστών στη Lagrangian του SM. Έπειτα, ισχυριζόμαστε πως η κλασική συμμετρία κλίμακας

ευθύνεται για το γεγονός αυτό και συζητούμε εν συντομία τα κύρια χαρακτηριστικά της συμμετρίας πριν εξετάσουμε το πως μια κλίμακα μπορεί να γεννηθεί μέσω κβαντικών διορθώσεων χάρη στη μεταβολή των σταθερών σύζευξης στα πλαίσια του μηχανισμού Coleman-Weinberg. Κατόπιν, γενικεύουμε τον μηχανισμό Coleman-Weinberg στην περίπτωση πολλαπλών βαθμωτών πεδίων και συζητάμε τα κύρια χαρακτηριστικά διαφόρων CSI μοντέλων που έχουν προταθεί στη βιβλιογραφία. Τέλος, εξερευνούμε το πώς η κλίμακα Planck μπορεί να γεννηθεί δυναμικά σε CSI τρόπο από τη VEV ενός βαθμωτού πεδίου το οποίο μπορεί επίσης να οδηγήσει τον πληθωρισμό.

Στο κεφάλαιο 7, θεωρούμε το CSI SM επεκταμένο με μια σκοτεινή $SU(2)_X$ συμμετρία βαθμίδας. Αυτή η νέα συμμετρία βαθμίδας σπάει τελείως από τη VEV ενός βαθμωτού πεδίου στη θεμελιώδη αναπαράσταση μέσω του μηχανισμού Coleman-Weinberg. Μέσω μιας αλληλεπίδρασης πύλης με το πεδίο Higgs, το σπάσιμο της συμμετρίας μεταδίδεται στον ηλεκτρασθενή τομέα. Τα τρία σκοτεινά διανυσματικά μποζόνια αποκτούν ίσες μάζες, είναι ευσταθή χάρη σε μια εσωτερική $Z_2 \times Z_2'$ διάκριτη συμμετρία και μπορούν επομένως να αποτελέσουν υποψήφιους για σκοτεινή ύλη. Προσθέτοντας μια πραγματική βαθμωτή ισομονάδα η οποία συζεύγνυται με τα υπόλοιπα βαθμωτά και τρία δεξιόστροφα νετρίνα, τα νετρίνα του SM μπορούν να αποκτήσουν μάζα μέσω ενός seesaw μηχανισμού τύπου-I. Αυτό σημαίνει πως η ηλεκτρασθενής κλίμακα μάζας καθώς και οι κλίμακες μάζας της σκοτεινής ύλης και των νετρίνων ενδέχεται να έχουν μια κοινή, δυναμική προέλευση. Εξατάζοντας την εξέλιξη της ομάδας επανακανονικοποίησης των συζεύξεων του μοντέλου βρίσκουμε ότι το βαθμωτό δυναμικό μπορεί εύκολα να σταθεροποιηθεί. Τα βαθμωτά μπορούν να προσφέρουν στοιχεία της ύπαρξής τους μέσω της μίξης με το Higgs εάν μια καθολική απόκλιση από τις προβλεπόμενες τιμές για τις συζεύξεις του SM Higgs βρεθεί στον LHC. Επιπροσθέτως, τα σκοτεινά διανυσματικά μποζόνια αποτελούν ενδιαφέροντες υποψήφιους για σκοτεινή ύλη καθότι, πέραν των διδακασιών εξαΰλωσης, η αριθμητική τους πυκνότητα μπορεί να μεταβληθεί και μέσω ημι-εξαϋλώσεων. Μπορούν να αναπαράγουν τη μετρούμενη αφθονία σκοτεινής ύλης, να αποφύγουν τα ισχύοντα όρια άμεσης ανίχνευσης αλλά παρολαυτά να είναι ανιχνεύσιμα από μελοντικά πειράματα.

Στο κεφάλαιο 8, εξετάζουμε το CSI SM επεκταμένο με μια σκοτεινή $SU(3)_X$ συμμετρία βαθμίδας. Ο νέος τομέας αποτελείται από οκτώ σκοτεινά διανυσματικά μποζόνια και δύο μιγαδικές βαθμωτές τριπλέτες. Κάτω από ήπιες υποθέσεις για τις παραμέτρους του βαθμωτού δυναμικού του μοντέλου, οι βαθμωτές τριπλέτες μπορούν να αποκτήσουν μη-μηδενικές VEVs και να σπάσουν την $SU(3)_X$ τελείως μέσω του μηχανισμού Coleman-Weinberg. Οκτώ από τους δώδεκα βαθμωτούς βαθμούς ελευθερίας απορροφώνται από τα σκοτεινά διανυσματικά μποζόνια, τα οποία καθίστανται όλα έμμαζα. Επικεντρωνόμαστε και αναλύουμε την απλούστερη περίπτωση στην οποία το πρότυπο τους σπασίματος συμμετρίας περιέχει δύο VEVs. Σαν αποτέλεσμα της σύζευξης του Higgs με τα σκοτεινά βαθμωτά, το σπάσιμο της σκοτεινής συμμετρίας πυροδοτεί το σπάσιμο της ηλεκτρασθενούς συμμετρίας και το κενό σταθεροποιείται. Από τα οκτώ έμμαζα σκοτεινά διανυσματικά μποζόνια, τα τρία

ελαφρύτερα είναι σχεδόν εκφυλισμένα στη μάζα και επίσης ευσταθή χάρη σε μια εσωτερική $Z_2 \times Z_2'$ διάκριτη συμμετρία της $SU(3)_X$. Αυτά τα τρία διανυσματικά μποζόνια είναι βιώσιμοι υποψήφιοι για σκοτεινή ύλη. Αφότου αναγνωρίσουμε τις σχετικές διεργασίες σκοτεινής ύλης (εξαϋλώσεις, ημι-εξαϋλώσεις, συν-εξαϋλώσεις και μετατροπές σκοτεινής ύλης), κατασκευάζουμε το σετ των πεπλεγμένων εξισώσεων Boltzmann, οι οποίες περιγράφουν την εξέλιξη της αριθμητικής πυκνότητας των υποψηφίων σκοτεινής ύλης ούτως ώστε να πάρουμε την ολική αφθονία και να τη συγκρίνουμε με τη μετρούμενη τιμή. Οι εξισώσεις Boltzmann λύνονται αριθμητικά για δύο περιπτώσεις οι οποίες καθορίζονται από τις VEVs των βαθμωτών πεδίων της $SU(3)_X$. Στη μία περίπτωση, πιθανές επιδράσεις συν-εξαϋλώσεων πρέπει να ληφθούν υπόψη. Παρολαυτά, προκύπτει πως και στις δύο περιπτώσεις η κυρίαρχη επίδραση είναι η μετατροπή σκοτεινής ύλης μεταξύ των τριών υποψηφίων και πως ο ελαφρύτερος από αυτούς είναι η κυρίαρχη συνιστώσα της σκοτεινής ύλης. Τέλος, δείχνουμε ότι οι υποψήφιοι για σκοτεινή ύλη έχουν βιώσιμες προοπτικές για να ανιχνευτούν άμεσα από υπόγεια μελλοντικά πειράματα.

Στο κεφάλαιο 9, στο πλαίσιο των ST θεωριών βαρύτητας υπολογίζουμε τους φασματικούς δείκτες με διορθώσεις τρίτης τάξης στην προσέγγιση slow-roll. Ο υπολογισμός πραγματοποιείται εφαρμόζοντας τη μέθοδο της συνάρτησης Green για βαθμωτές και τανυστικές διαταραχές στα Einstein και Jordan συστήματα αναφοράς. Έπειτα, χρησιμοποιώντας τις σχέσεις μεταξύ των Hubble παραμέτρων slow-roll στα δύο συστήματα αναφοράς βρίσκουμε ότι αυτά είναι ισοδύναμα ως την τρίτη τάξη. Καθόσον οι Hubble παράμετροι slow-roll σχετίζονται με τις παραμέτρους slow-roll του δυναμικού, εκφράζουμε τις παρατηρούμενες ποσότητες συναρτήσει των τελευταίων οι οποίες είναι αναλλοίωτες κάτω από σύμμορφους μετασχηματισμούς της μετρικής και επαναπαραμετροποιήσεις του βαθμωτού πεδίου. Παρολαυτά, η ίδια μεταβολή του inflaton μπορεί να οδηγήσει σε διαφορετικές προβλέψεις στα δύο συστήματα αναφοράς καθότι ο ορισμός του αριθμού των e-folds διαφέρει. Για να διευκρινίσουμε το ζήτημα, θεωρούμε ένα μη-ελάχιστο πληθωριστικό μοντέλο όπου η κλίμακα Planck γεννιέται δυναμικά και βρίσκουμε ότι η διαφορά στις προβλέψεις μεγαλώνει όσο μεγαλώνει η μη-ελάχιστη σύζευξη και μπορεί πράγματι να είναι μεγαλύτερη από τη διαφορά μεταξύ των αποτελεσμάτων πρώτης και τρίτης τάξης για τις παρατηρούμενες ποσότητες. Τέλος, επιδεικνύουμε τα αποτελέσματα διαφόρων συνθηκών για το τέλος του πληθωρισμού στις παρατηρούμενες ποσότητες. Αυτές οι διαφορές θα σημαντικές για τις αναλύσεις πληθωριστικών μοντέλων ενόψει της βελτιωμένης ευαισθησίας των μελλοντικών πειραμάτων.

Τέλος, στο κεφάλαιο 10 παραθέτουμε τα συμπεράσματά μας και συζητάμε πιθανές μελλοντικές κατευθύνσεις. Χρήσιμοι τύποι δίνονται στα παραρτήματα.

Acknowledgements

I thank my supervisor Professor Kyriakos Tamvakis and all those who stood by my side these last few years. Part of the research presented in this thesis has been cofinanced by the European Union (European Social Fund - ESF) and Greek national funds through the Operational Program Education and Lifelong Learning of the National Strategic Reference Framework (NSRF) - Research Funding Program: *ARISTEIA - Investing in the society of knowledge through the European Social Fund.*

Contents

Dedicated to my family and friends

Chapter 1

Introduction and Summary

An exciting era is underway for high-energy Physics and Cosmology. The recent discovery of the Higgs boson at the LHC in CERN and the observation of gravitational waves originating from merging black holes at LIGO have reaffirmed the long-standing pillars of our understanding of the physics of the Universe, namely, the Standard Model (SM) of Particle Physics and Einstein's theory of General Relativity (GR). Both theories have stood the test of time and have been validated in numerous occasions since their inception. Despite their successes though, the SM and GR fail to explain some phenomena and also contain a few innate problems of their own.

Recent observations of the cosmic microwave background (CMB) have determined the Universe to be almost flat and homogeneous at large scales. Supplementing GR with a scalar field can lead to an inflating era in the early moments of the Universe, which can explain its flatness and homogeneity. When treated quantum-mechanically, the theory of *inflation* can also provide the seeds for the large-scale structure we observe (galaxy clusters and filaments). The recent results from the Planck mission [1] have constrained the parameter space of the inflationary observables and essentially ruled out many of the proposed models, including the simplest ones where a scalar field is minimally coupled to gravity. On the other hand, slightly more involved models such as the Starobinsky and non-minimal models, seem to lie within the allowed range. These models belong to the class of *scalar-tensor* (ST) theories [2]. In ST models, one (or more) scalar field is generally non-minimally coupled to gravity and can drive inflation. Such a non-minimal coupling is also interesting from another point of view: if the scalar field develops a vacuum expectation value (VEV), then the Planck scale can be generated in a dynamical way. The Planck scale (around 10^{19} GeV) is one of the two known mass scales in physics. The other one is the electroweak (EW) scale (around 250 GeV), related to the VEV of the Higgs field. We still do not know why these two scales are so vastly separated.

The CMB also indicates that around 85% of the mass content of the Universe is in a form which does not radiate. *Dark matter* (DM) is believed to be of particulate nature, with the class of *weakly interacting massive particles* (WIMPs) being the most successful in describing it. WIMPs usually reside in *dark sectors* which communicate with the SM through portal interactions. Numerous experiments are currently operating or are expected to become operational in the next few years, with the aim of detecting DM, either directly or indirectly.

With the discovery of the Higgs boson, we have now determined all the parameters of the SM. Nevertheless, the SM still cannot explain the nature of DM, how neutrinos obtain their mass, the origin of the matter-antimatter asymmetry or why QCD does not violate the CP symmetry (strong CP problem). Furthermore, the measured value of the Higgs mass suggests that our vacuum is in a metastable state and could potentially decay [3, 4] with catastrophic results. This is due to the fact that the Higgs self-coupling evolves with energy and the measured values of the Higgs and top quark masses suggest that it becomes negative at energies above circa 10^{10} GeV. The vacuum stability problem can be remedied if we introduce one or more scalar fields that couple to the Higgs.

New fields, fermionic or bosonic, can also provide solutions for the rest of the problems of the SM. However, due to quantum effects, the Higgs mass displays a quadratic sensitivity to the mass scales we introduce along with the new fields. We then need an enormous amount of fine-tuning in order to cancel the quadratic divergences and retrieve the observed Higgs mass. This problem of the *naturalness* of the Higgs mass is mitigated in supersymmetric extensions of the SM, as long as supersymmetry is softly broken not too far away from the EW scale. Unfortunately, no supersymmetric particles have been observed by the LHC or other colliders so far, which has prompted the exploration of alternative ideas.

An idea that has received a lot of attention in recent years is that of *classical scale invariance*. Classical scale invariance posits that the tree-level Lagrangian of a theory should not contain any ad hoc mass parameters. The only mass parameter in the SM is the Higgs mass parameter which drives EW symmetry breaking. Setting this parameter to zero enhances the symmetry of the SM [5]. Going to the quantum level, the running of the couplings of the theory with energy induces symmetry breaking, but this does not reintroduce the quadratic divergences [6]. Thus, the theory is technically natural. The mechanism responsible for breaking the symmetry was developed by S. Coleman and E. Weinberg [7]. If we apply, however, this mechanism to the classically scale-invariant (CSI) SM we find a tachyonic mass for the Higgs due to the large mass of the top quark. This means that for the Coleman-Weinberg mechanism to work we need to add new (bosonic) fields to the SM. If these are scalar fields then their couplings to the Higgs field can contribute positively to the running of the Higgs self-coupling and also help stabilise the potential.

New fields can also provide candidates for DM. These candidates can be scalars, fermions, vector bosons or have higher spins. In any case, there should be a symmetry that renders the DM candidates stable, since otherwise they would have decayed during the evolution of the Universe and would not be present today. Such a stabilizing symmetry is usually “put by hand", but it can also arise naturally as an intrinsic feature of new gauge symmetries.

In the next chapter, we begin by briefly reviewing the widely accepted ΛCDM model, also known as the Standard Model of Cosmology. After outlining its basic ingredients, we discuss the problems of horizon and flatness which can be simultaneously solved if the Universe underwent an inflationary era in its early stages.

In Chapter 3, we explore the paradigm of cosmic inflation. First, we review the simplest case of a real scalar field minimally coupled to gravity which, with a suitable potential, can drive inflation. Then, we treat inflation in a quantum-mechanical way and we examine the physics behind cosmological perturbations which are believed to have been the seeds of all structure we observe today in the Universe. To make a connection with experiment, we compute the spectral indices and tensor-to-scalar ratio and express them in terms of the so-called slow-roll parameters. After that, we generalize to the case of ST theories which contain a non-minimal coupling between the scalar field and the Ricci scalar. We are interested in such a non-minimal coupling since, in the context of classical scale invariance, the VEV of the field is able to dynamically generate the Planck scale.

In Chapter 4, we briefly review the basic ingredients that comprise the Standard Model of Particle Physics which has stood the test of time for over four decades. Then, we outline its problems and shortcomings before focusing on the ones that are of interest to us in this thesis.

In Chapter 5, we delve into the problem of dark matter. We begin by outlining the main evidence supporting the existence of DM. Then, we briefly review the properties of some of the most popular DM candidates before focusing on the WIMP paradigm and its various aspects. Finally, we present the status of the ongoing DM searches.

In Chapter 6, we begin by conjecturing that the dimensionality of spacetime is the reason behind the appearance of only (super-)renormalizable operators in the Lagrangian of the Standard Model.

Then, we argue that classical scale invariance is responsible for this fact and briefly discuss the main features of the symmetry before examining how a scale can be radiatively generated due to the running of the coupling constants in the context of the Coleman-Weinberg mechanism. After that, we generalize the Coleman-Weinberg mechanism to the case of multiple scalar fields and discuss the main features of the various CSI models found in the literature. Finally, we explore how the Planck scale can be dynamically generated in a CSI manner by the VEV of a scalar field that can also drive inflation.

In Chapter 7, we consider the CSI SM extended by a dark $SU(2)$ gauge symmetry. This new gauge symmetry gets completely broken by a scalar field in the fundamental representation via the Coleman-Weinberg mechanism. Through a portal interaction with the Higgs field, symmetry breaking is then communicated to the electroweak sector. The three dark gauge bosons obtain equal masses, are stable due to an intrinsic $Z_2 \times Z_2'$ discrete symmetry and can therefore constitute DM candidates. By adding a real scalar singlet which couples to the other scalar fields and three right-handed sterile neutrinos, the SM neutrinos can obtain their mass through a type-I seesaw mechanism. This means that the electroweak, the DM, and the neutrino mass scales may have a common, dynamical origin. By examining the renormalization group evolution of the couplings of the model we find that the scalar potential can be easily stabilized. The scalars may offer hints of their existence via their mixing with the Higgs if a universal deviation of the predicted SM Higgs couplings is found at the LHC. Furthermore, the dark gauge bosons are interesting DM candidates since, apart from annihilation processes, their number density can change through semi-annihilations as well. They can reproduce the measured DM relic density, evade the current direct detection limits but nevertheless be detectable by ongoing and future experiments.

In Chapter 8, we examine a CSI extension of the SM, enlarged by a weakly-coupled dark $SU(3)_X$ gauge group. The new sector consists of eight dark gauge bosons and two complex scalar triplets. Under mild assumptions on the parameters of the scalar potential of the model, the scalar triplets can develop non-vanishing VEVs and break the extra $SU(3)_X$ completely via the Coleman-Weinberg mechanism. Eight of the twelve scalar degrees of freedom are absorbed by the dark gauge bosons, rendering them all massive. We focus on and analyze the case in which the symmetry breaking pattern involves two VEVs. As a result of the portal couplings of the dark scalars to the Higgs field, the dark gauge symmetry breakdown triggers electroweak symmetry breaking and the vacuum can be stabilised. Out of the eight massive dark gauge bosons, the lightest three of them are almost degenerate in mass and also stable due to an intrinsic $Z_2 \times Z_2'$ discrete symmetry of $SU(3)_X$. These are viable DM candidates. After identifying the relevant DM processes (annihilations, semi-annihilations, co-annihilations, and DM conversions), the set of coupled Boltzmann equations is constructed, describing the number density evolution of the DM candidates in order to obtain their total relic density and compare it to the measured value. The Boltzmann equations are solved numerically in two cases defined by the VEVs of the $SU(3)_X$ scalar fields. In one of these cases, possible co-annihilation effects have to be taken into account. However, it turns out that in both cases the dominant effect is DM conversion between the DM species and that the lightest candidate is the predominant DM component. Finally, we determine that the DM candidates have viable prospects of being directly detected by future underground experiments.

In Chapter 9, in the context of scalar-tensor theories of gravity we compute the third-order corrected spectral indices in the slow-roll approximation. The calculation is carried out by employing the Green's function method for scalar and tensor perturbations in both the Einstein and Jordan frames. Then, using the interrelations between the Hubble slow-roll parameters in the two frames we find that the frames are equivalent up to third order. Since the Hubble slow-roll parameters are related to the potential slow-roll parameters, we express the observables in terms of the latter which are manifestly invariant under a conformal transformation of the metric and a reparametrization of the scalar field. Nevertheless, the same inflaton excursion leads to different predictions in the two

frames since the definition of the number of e-folds differs. To illustrate this effect we consider a non-minimal inflationary model where the Planck scale can be dynamically generated and find that the difference in the predictions grows with the non-minimal coupling and it can actually be larger than the difference between the first and third order results for the observables. Finally, we demonstrate the effect of various end-of-inflation conditions on the observables. These effects will become important for the analyses of inflationary models in view of the improved sensitivity of future experiments.

Finally, in Chapter 10, we present our conclusions and discuss possible future directions. Useful formulae are presented in the appendices.

Notation

Throughout this thesis we will use the natural units

$$c = k_B = \hbar = 1\,.$$

We will also use the reduced Planck mass

$$M_{\rm Pl} = (8\pi G)^{-1/2}\,,$$

and often set it equal to one. We will also adopt the Einstein summation convention where repeated indices are summed over. Greek indices will take the values $\mu, \nu = 0, 1, 2, 3$ and Latin letters are used as spatial indices $i, j = 1, 2, 3$. For conformal time we use the letter τ. The letter η is used for the second slow-roll parameter. Derivatives with respect to cosmic time are indicated by overdots, while derivatives with respect to conformal time are denoted by primes.

Chapter 2

The Standard Model of Cosmology

Ever since we evolved into humans, we would look at the stars and start imagining how our Cosmos came to be. In this way, the first myths and religions were created and everything we could not understand was attributed to unknown forces. Later on, as our civilization also evolved and science progressed, the first scientists began getting a clearer picture of the history of our Universe and what it entails. Most of the progress has occurred during the last hundred years.

In the early 20th century, Albert Einstein unified space and time in his theory of General Relativity (GR) [8] and showed, through his elegant field equations, how matter and energy curve spacetime. He found that the solutions to these equations could describe a Universe which is either expanding or contracting. Since this came into conflict with his philosophy of a static Universe, he introduced a constant to negate the effects of any possible expansion or contraction, which later became known as the *cosmological constant*. As Edwin Hubble observed, though, most of the galaxies are hurdling away from the Milky Way, which means the Universe is actually expanding. Another surprising twist took place in the 1990s when astronomers found that the Universe is not only expanding, but it does so at an accelerating rate.

Such a behaviour can be encoded in the aforementioned cosmological constant, which is believed to be a constant energy density that fills space in a homogeneous way and has been dubbed *dark energy*. Recent observations from the Planck mission [1] suggest that dark energy accounts for around 69% of the energy budget of the Universe. *Ordinary matter* – described by the *Standard Model of Particle Physics* (to be discussed in detail in Chap. 4) – takes up around 5% of the energy budget. The rest 26% is in a form that gravitates but does not emit electromagnetic radiation and has thus been called *dark matter* (to be discussed in detail in Chap. 5).

As you can see, we still attribute phenomena we do not understand to unknown forces, but we believe these to be of physical origin. Let us now imagine that the Universe is one majestic film nearly 14 billion years long and start rewinding it. As we go back in time we would see the galaxies coming together and spacetime shrinking until density and temperature reached immeasurable values, leading to the singularity known as the *Big Bang*. In 1965, the afterglow of the Big Bang was discovered in the famous Cosmic Microwave Background radiation (CMB) [9]. The CMB contains a lot of information which we have been decoding since its discovery. Fast forward to today and we have constructed the *Standard Model of Cosmology*, also known as the *ΛCDM model* [10–12].

This chapter is organized as follows: In the next section we present a short history of the main events of the Universe as inferred by various observations and theoretical considerations. Then, in Section 2.2, we outline the basic ingredients of the ΛCDM model which is based on the theory of General Relativity and the cosmological principle. Finally, in Section 2.3, we discuss two of the problems of the standard Big Bang Cosmology, namely the horizon and flatness problems, and then entertain their possible inflationary solutions.

2.1 A Short History of the Universe

Before we delve into the specifics of the ΛCDM model, let us first present a qualitative summary of what we know and what we speculate about the evolution of the Universe between the Big Bang and today (see Fig.2.1).

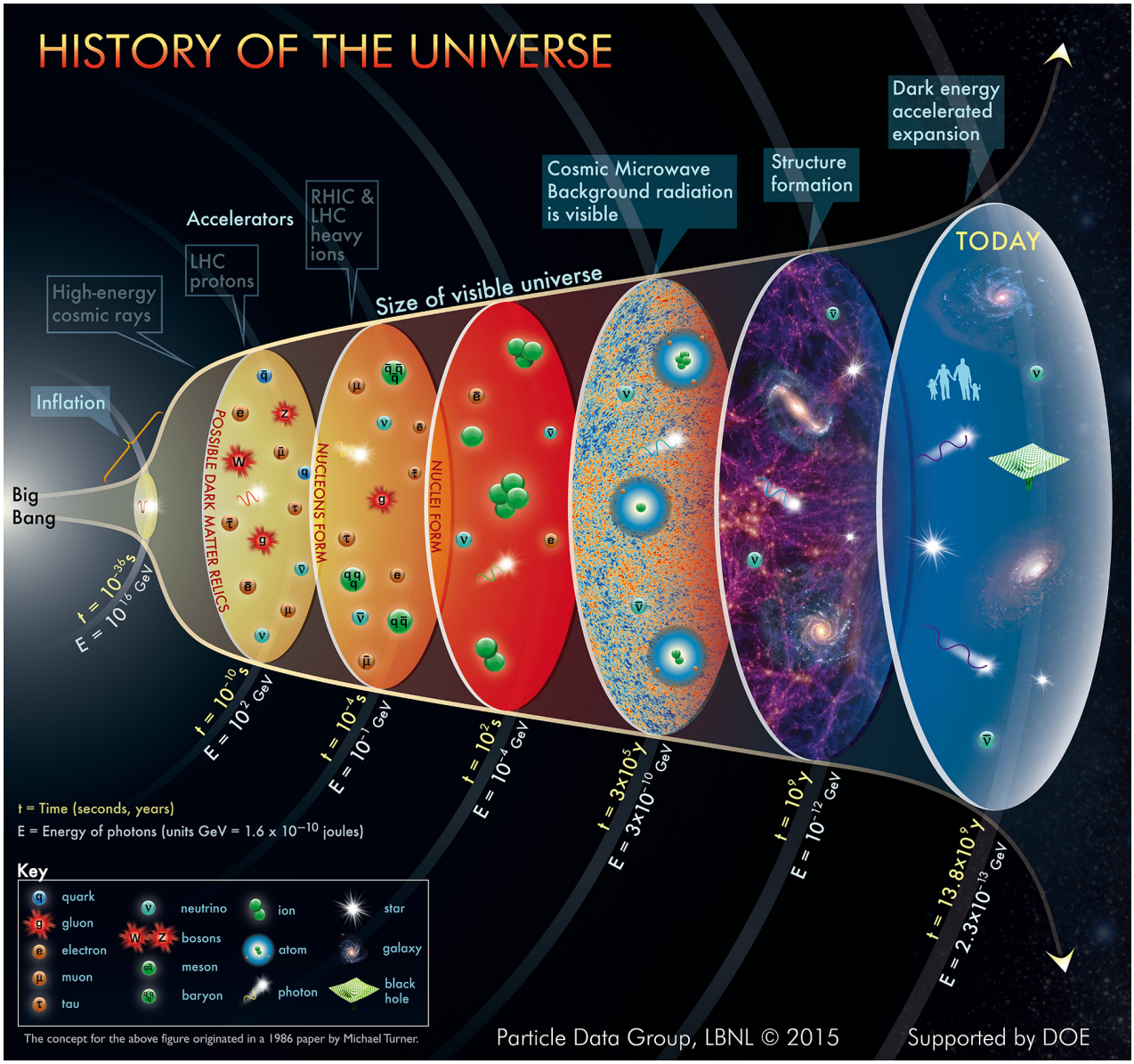

Figure 2.1: The history of the Universe. Credit: Particle Data Group at Lawrence Berkeley National Lab.

The Universe is assumed to have started as an extremely hot and dense plasma which eventually cooled down during the subsequent expansion. Its very early moments are unknown to us since they occurred at very high energies (above $\sim 10^{18}$ GeV) and we still have not settled on an acceptable theory for quantum gravity.

Inflation. Around 10^{-36} s after the Big Bang (or $\sim 10^{16}$ GeV) an inflationary epoch is thought to have occurred. During *inflation* (to be discussed in detail in Chap. 3), the Universe underwent an

Table 2.1: Major events in the thermal history of the Universe.

Event	Time t	Redshift z	Energy E
Planck Epoch?	$< 10^{-43}$ s	–	$> 10^{18}$ GeV
Inflation	10^{-34} s	–	10^{15} GeV
Baryogenesis	?	?	?
Dark Matter Freeze-Out	?	?	?
EW Phase Transition	20 ps	10^{15}	100 GeV
QCD Phase Transition	20 μs	10^{12}	150 MeV
Neutrino Decoupling	1 s	6×10^9	1 MeV
Electron-Positron Annihilation	6 s	2×10^9	500 keV
Big Bang Nucleosynthesis	3 min	4×10^8	100 keV
Matter-Radiation Equality	60 kyr	3400	0.75 eV
Recombination	$260 - 380$ kyr	$1100 - 1400$	$0.26 - 0.33$ eV
Photon Decoupling	380 kyr	$1000 - 1200$	$0.23 - 0.28$ eV
Reionization	$100 - 400$ Myr	$11 - 30$	$2.6 - 7.0$ meV
Dark Energy-Matter Equality	9 Gyr	0.4	0.33 meV
Today	13.8 Gyr	0	0.24 meV

exponential expansion during which the scale factor a grew as $a(t) = \exp(Ht)$, where t is the cosmic time and H the Hubble factor.

Inflation was originally proposed as a solution to the *horizon* and *flatness* problems. The horizon problem is related to the fact that measurements from the CMB indicate that the Universe has almost the same temperature in all directions in the sky. This means, however, that two distant patches cannot have been in causal contact in the past since they would not have enough time to have communicated if the standard evolution is assumed. If, however, a period of exponential expansion is assumed, as is the case in inflation, then the patches which were in causal contact before the end of inflation could have become stretched and widely separated after the end of inflation.

The flatness problem is related to the fact that the curvature of spacetime at large scales is estimated to be almost exactly zero [1], which means the matter and energy density of the Universe must have a critical value. Such a value seems to be extremely fined-tuned, since otherwise the Universe would be open or closed. Furthermore, because in a non flat Universe the curvature increases as we go back in time, the curvature energy density in the early universe must have had a density even closer to the critical density, deviating from it by at most one part in 10^{62}. Of course, we can

always invoke the anthropic principle in order to explain away this amount of fine-tuning. In a physical context, however, the exponential expansion during inflation dilutes the curvature and an initial value of zero can remain zero when inflation ends.

The horizon and flatness problems can simultaneously be solved if inflation lasted for at least 50 – 60 e-folds, a dimensionless number that measures the exponential change of the scale factor and is defined as

$$N := \ln\left(\frac{a_2}{a_1}\right) = \int_{t_1}^{t_2} H \mathrm{d}t. \tag{2.1}$$

In most models of inflation, a real scalar field ϕ, called the *inflaton*, behaves like a cosmological constant as it slowly rolls down its potential $V(\phi)$ and drives an inflationary epoch. When the inflaton reaches the minimum of the potential, inflation ends. Then, as the inflaton starts oscillating around the minimum it decays into other particles, in a process called *reheating*.

After reheating, the evolution of the Universe is characterized by two principles: *i)* particles freeze out as soon as their interaction rate Γ becomes smaller than the expansion rate H, and *ii)* symmetries in the fundamental laws of physics which are broken now may be restored at high energies.

Baryogenesis. One of the great puzzles of Particle Physics and Cosmology is the mechanism behind baryogenesis. Relativistic quantum field theory predicts the existence of anti-matter, giving rise to processes such as $e^- + e^+ \rightarrow \gamma + \gamma$. But since everything around us is made up only of matter, an asymmetry must have occurred during the early phases of the Universe which resulted in the observed baryon-to-photon ratio

$$\frac{n_b}{n_\gamma} \sim 10^9. \tag{2.2}$$

Dark matter freeze-out. As the Universe is expanding and cooling, the pair annihilations between dark matter particles become more rare and then eventually stop as their interaction rate becomes smaller than the expansion rate, $\Gamma \lesssim H$. After that point, which is called *dark matter freeze-out*, the dark matter particles fall out of equilibrium with the thermal bath and settle on their constant relic abundance which we detect today (see Chapter 5).

Electroweak phase transition. Around 100 GeV the Higgs mechanism occurs (see Chapter 4) and the electroweak symmetry $SU(2) \times U(1)$ breaks to the electromagnetic $U(1)$. In this way, the leptons, quarks and gauge bosons obtain the masses we observe at the experiments.

QCD phase transition. As the Universe further cools down below 150 MeV, the interactions between the quarks and gluons become important. After that, quarks and gluons are confined into *hadrons*. Three-quark states are called *baryons*, while quark-antiquark pairs are called *mesons*.

Neutrino decoupling. At around 1 MeV neutrinos decouple from the plasma since the interaction rate of scattering processes such as $e^- + e^+ \leftrightarrow \nu_e + \bar{\nu}_e$ becomes slower than the expansion rate of the Universe. At this point, the relic neutrinos give rise to the *Cosmic Neutrino Background* which is nevertheless very hard to directly detect since these neutrinos have extremely low energy.

Electron-positron annihilation. Shortly after neutrino decoupling, the energy densities of electrons and positrons get transferred to the photons (but not the neutrinos) through the annihilation process $e^- + e^+ \rightarrow \gamma + \gamma$. As a result, the photons are reheated, which is why the temperature of the photons today is higher than the neutrino temperature.

Big Bang nucleosynthesis. Around the famous 3 minute mark [13], the energy of the photons is not enough to break the nuclear binding energy and hadron scatterings can now produce the light nuclei, namely deuterium, helium, and lithium. Heavier elements form later inside stars and during violent events such as supernovae explosions.

Recombination. Below the temperature of 1 eV a matter-radiation equality is reached and then the matter energy density dominates the evolution of the Universe. Electrons and nuclei combine to form neutral atoms, mostly hydrogen through the reaction $e^- + p^+ \rightarrow H + \gamma$. At this point, the photons can no longer break the electron-nucleus binding energy and matter stops being ionized.

Photon decoupling. After recombination, at 380,000 years after the Big Bang, Thomson scattering ($e^- + \gamma \rightarrow e^- + \gamma$) becomes inefficient due to the sharp drop in the density of free electrons. As a result, the photons decouple and can now freely stream through the Universe. We observe them today as the CMB radiation.

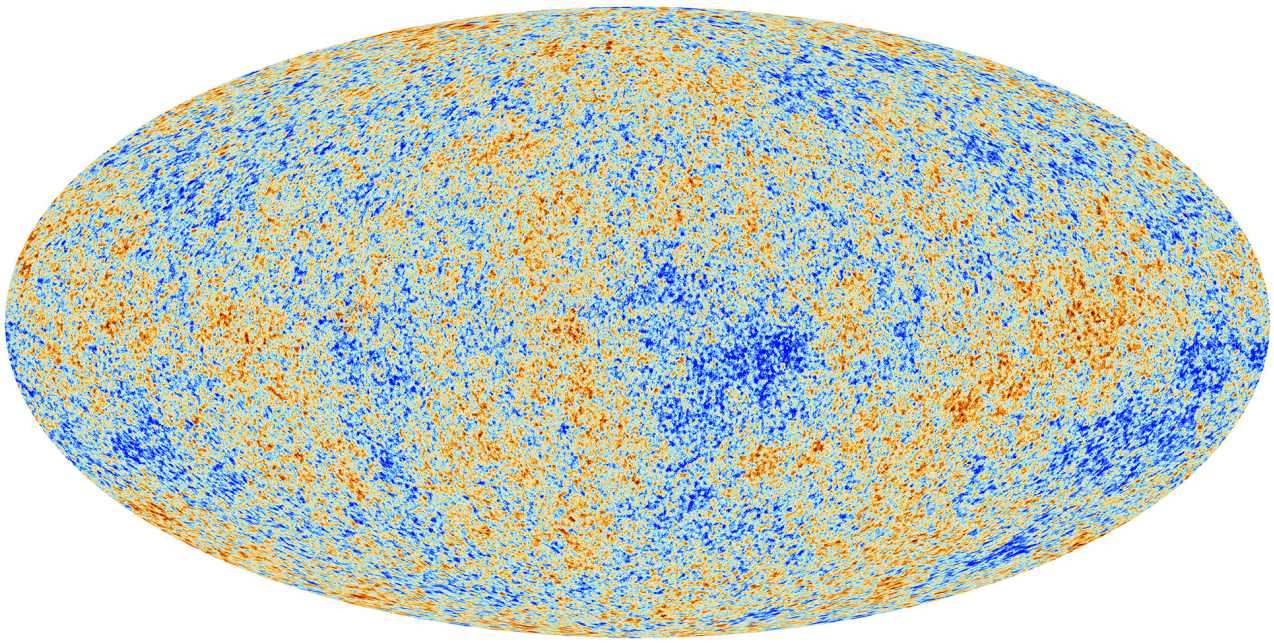

Figure 2.2: The anisotropies of the cosmic microwave background (CMB), as observed by the European Space Agency's Planck satellite. The CMB is a snapshot of the oldest light in our Universe, imprinted on the sky when the Universe was just 380000 years old. It shows tiny temperature fluctuations that correspond to regions of slightly different densities, representing the seeds of all future structure: the stars and galaxies of today. Credit: ESA and the Planck Collaboration

Reionization. At around 100 million years, gravity takes over and hydrogen atoms start coalescing. They radiate energy and the plasma becomes ionized once again. The matter perturbations generated during inflation evolve into stars, galaxies, and filaments.

Dark energy domination. Finally, around 9 billion years after the Big Bang, matter and radiation have diluted enough for the density of dark energy to start dominating. After this point, the Universe is expanding with an accelerating rate due to the effect of the cosmological constant.

After this qualitative summary of the main events in the history of the Universe, we will outline the basic ingredients of the ΛCDM model, where Λ refers to the cosmological constant and CDM stands for cold dark matter. After that, we will briefly discuss the flatness and horizon problems.

2.2 The ΛCDM Model

2.2.1 Cosmic Expansion

There is good evidence that we live in an expanding Universe [14, 15]. This means that at earlier times distant galaxies were closer to us than they are today. We can quantify the expanding behaviour of the Universe with the help of the scale factor $a = a(t)$, where today we have[1] $a_0 = a(t_0) = 1$ and $a(t < 0) < 1$. The scale factor can be used to define the so-called *comoving distance* L_{com}. Two points that are at rest in an expanding Universe have the same comoving distance throughout its evolution since the comoving distance does not change with time. The *physical distance* L_{phys}, on the other hand, is proportional to the scale factor which means it evolves with time. We have

$$L_{\text{phys}} = a(t) L_{\text{com}}. \tag{2.3}$$

By differentiating Eq. (2.3) with respect to cosmic time t, we obtain

$$v = \frac{\mathrm{d}L_{\text{phys}}}{\mathrm{d}t} = \frac{\dot{a}}{a} L_{\text{phys}} = H L_{\text{phys}}, \tag{2.4}$$

where

$$H := \frac{\dot{a}}{a} \tag{2.5}$$

is the *Hubble factor* or *Hubble parameter* which has the unit of inverse time and is positive for an expanding Universe (and negative for a contracting Universe).Equation 2.4 is also known as the *Hubble law*. The most recent measurements from the Planck mission [1] for the current value of H give

$$H_0 = 67.74 \pm 0.46 \text{km/s/Mpc} = 100\, h\, \text{km/s/Mpc}\ , \tag{2.6}$$

where h is the reduced Hubble parameter, which is also often used. From the Hubble parameter we can define the *Hubble time*, which is just its inverse

$$t_H := \frac{1}{H_0} = 4.55 \times 10^{17}\ s = 14.4 \text{ billion years}. \tag{2.7}$$

The Hubble time is different from the age of the Universe $t_0 \approx 13.8$ billion years, since the expansion has not been linear throughout its evolution. By multiplying the Hubble parameter with the speed of light c, we can also define the *Hubble length* $cH^{-1} = 14.4$ billion light years, which is interpreted as the distance between the Earth and the galaxies which are currently receding from us at the speed of light.

2.2.2 The Friedmann – Lemaître – Robertson – Walker Metric

In General Relativity, the geometrical properties of spacetime can be described with the help of the metric $g_{\mu\nu}$, which depends on the spacetime coordinates $x^\mu = (x^0, x^i)$, where $x^0 = t$ is the time-like component and x^i are the 3 spatial components. The distance between two points is given by the invariant square of an infinitesimal line element,

$$\mathrm{d}s^2 := g_{\mu\nu} \mathrm{d}x^\mu \mathrm{d}x^\nu\ . \tag{2.8}$$

[1] The subscript 0 will be used to denote the values of the related quantities today.

Since the metric $g_{\mu\nu}$ must be a symmetric 4×4 tensor, we are left with 10 independent coefficients. A Universe which is homogeneous and isotropic is described by the Friedmann - Lemaître - Robertson - Walker Metric (FLRW) metric [16–23]. Homogeneity suggests there are no privileged observers in the Universe, therefore $g_{\mu\nu}$ must not depend on the spatial coordinates. Furthermore, isotropy of the Universe suggests there is no preferred direction, which implies that the off-diagonal entries of $g_{\mu\nu}$ ($\mu \neq \nu$) must vanish. For a local observer in a flat Minkowski spacetime, we obtain the limit of special relativity with $\eta_{\mu\nu} = \mathrm{diag}(-1, +1, +1, +1)$, while the metric is approximated as

$$g_{\mu\nu} = \begin{pmatrix} -1 & 0 & 0 & 0 \\ 0 & a^2(t) & 0 & 0 \\ 0 & 0 & a^2(t) & 0 \\ 0 & 0 & 0 & a^2(t) \end{pmatrix} \tag{2.9}$$

and the line element becomes

$$\mathrm{d}s^2 = -\mathrm{d}t^2 + a^2(t)\delta_{ij}\mathrm{d}x^i\mathrm{d}x^j \,, \tag{2.10}$$

where $\delta_{ij} = \mathrm{diag}(+1, +1, +1)$ is the Kronecker delta in an Euclidean space.

In general, the Universe can be open, flat, or closed. We can encode the spatial curvature in a discrete parameter $\mathcal{K} = -1, 0, 1$. Then, using spherical coordinates, the line element (2.8) can be written as

$$\mathrm{d}s^2 = -\mathrm{d}t^2 + a^2(t)\left[\frac{\mathrm{d}r^2}{1-\mathcal{K}r^2} + r^2(\mathrm{d}\theta^2 + \sin^2\theta\mathrm{d}\phi^2)\right] \tag{2.11}$$

$$= -\mathrm{d}t^2 + a^2(t)\gamma_{ij}(x)\mathrm{d}x^i\mathrm{d}x^j \,, \tag{2.12}$$

where (r, θ, ϕ) are the standard spherical coordinates and

$$\gamma_{11} = \gamma_{rr} = \frac{1}{1-\mathcal{K}r^2} \,, \quad \gamma_{22} = \gamma_{\theta\theta} = r^2 \,, \quad \gamma_{33} = \gamma_{\phi\phi} = r^2\sin^2\theta \,. \tag{2.13}$$

It is often convenient to use, instead of t, the conformal time coordinate τ defined as

$$\mathrm{d}\tau := \frac{\mathrm{d}t}{a} \,. \tag{2.14}$$

Then the line element (2.12) can be rewritten as

$$\mathrm{d}s^2 = a^2(\tau)\left[-\mathrm{d}\tau^2 + \gamma_{ij}(x)\mathrm{d}x^i\mathrm{d}x^j\right] \,. \tag{2.15}$$

We can also define the conformal Hubble parameter

$$\mathcal{H}(\tau) := \frac{\mathrm{d}a/\mathrm{d}\tau}{a} = \frac{a'}{a} \,. \tag{2.16}$$

Then, the Hubble parameter in cosmic and conformal time are related to one another by

$$\mathcal{H} = aH \,. \tag{2.17}$$

In order to study the motion of a particle in a spacetime described by a metric $g_{\mu\nu}$, it proves useful to employ the *Christoffel symbols* $\Gamma^\rho_{\mu\nu}$, which are symmetric in the μ and ν indices:

$$\Gamma^\rho_{\mu\nu} := \frac{g^{\rho\tau}}{2}\left(\partial_\mu g_{\nu\tau} + \partial_\nu g_{\mu\tau} - \partial_\tau g_{\mu\nu}\right) \,, \tag{2.18}$$

where we also introduced the notation $\partial_\mu g_{\nu\tau} = \partial g_{\nu\tau}/\partial x^\mu$. The Christoffel symbols enter in the geodesic equation

$$\frac{\mathrm{d}^2 x^\mu}{\mathrm{d}\lambda^2} = -\Gamma^\mu_{\alpha\beta}\frac{\mathrm{d}x^\alpha}{\mathrm{d}\lambda}\frac{\mathrm{d}x^\beta}{\mathrm{d}\lambda}\,, \tag{2.19}$$

which describes the motion of particles in nontrivial coordinate systems and where λ is a scalar monotonic parameter that increases along the particle's path. In FLRW spacetime, the Christoffel symbols are calculated to be

$$\Gamma^0_{0\mu} = \Gamma^0_{\mu 0} = 0\,, \tag{2.20}$$

$$\Gamma^0_{ij} = \gamma_{ij}\,\dot{a}\,a\,, \tag{2.21}$$

$$\Gamma^i_{0j} = \Gamma^i_{j0} = \delta_{ij}\,\frac{\dot{a}}{a}\,, \tag{2.22}$$

$$\Gamma^i_{\alpha\beta} = 0 \quad \text{otherwise.} \tag{2.23}$$

With the help of the Christoffel symbols we can define the *Ricci tensor*, which has the following expression:

$$R_{\mu\nu} := \partial_\alpha\Gamma^\alpha_{\mu\nu} - \partial_\nu\Gamma^\alpha_{\mu\alpha} + \Gamma^\alpha_{\beta\alpha}\Gamma^\beta_{\mu\nu} - \Gamma^\alpha_{\beta\nu}\Gamma^\beta_{\mu\alpha}\,. \tag{2.24}$$

Taking the trace of the Ricci tensor, we obtain the *Ricci scalar*:

$$R := R^\mu{}_\mu = g^{\mu\nu}R_{\mu\nu}, \tag{2.25}$$

where $g^{\mu\nu}$ is the inverse of $g_{\mu\nu}$. The Ricci tensor is diagonal and its components are found to be

$$R_{00} = -3\frac{\ddot{a}}{a}\,, \tag{2.26}$$

$$R_{ij} = \gamma_{ij}\left(2\dot{a}^2 + a\ddot{a} + 2\mathcal{K}\right)\,, \tag{2.27}$$

while the Ricci scalar is:

$$R = 6\left(\frac{\ddot{a}}{a} + \frac{\dot{a}^2}{a^2} + \frac{\mathcal{K}}{a^2}\right). \tag{2.28}$$

2.2.3 Einstein Field Equations

In order to obtain the Einstein field equations we start from the Einstein-Hilbert action, which reads

$$S_{\mathrm{EH}} = \frac{1}{2}M_{\mathrm{Pl}}^2\int \mathrm{d}^4x\sqrt{-g}\,(R - 2\Lambda)\,, \tag{2.29}$$

where $g = \det(g_{\mu\nu})$ is the determinant of the metric tensor matrix. To this action we should add a part describing matter, namely

$$S_{\mathrm{m}} = \int \mathrm{d}^4x\sqrt{-g}\mathcal{L}_{\mathrm{m}}\,, \tag{2.30}$$

where $\mathcal{L}_{\mathrm{m}}$ is the matter Lagrangian density. By varying these two action terms with respect to the metric $g_{\mu\nu}$, we obtain the *Einstein tensor* $G_{\mu\nu}$ which measures the "spacetime curvature" of the Universe, given by

$$G_{\mu\nu} + \Lambda g_{\mu\nu} := \frac{2}{M_{\mathrm{Pl}}^2\sqrt{-g}}\frac{\partial S_{\mathrm{EH}}}{\partial g_{\mu\nu}} = R_{\mu\nu} - \frac{1}{2}Rg_{\mu\nu} + \Lambda g_{\mu\nu} \tag{2.31}$$

for the gravity part, and the *energy-momentum tensor* which measures the matter content of the Universe, given by

$$T_{\mu\nu} =: -\frac{2}{\sqrt{-g}}\frac{\partial S_{\rm m}}{\partial g_{\mu\nu}} = g_{\mu\nu}\mathcal{L}_{\rm m} - 2\frac{\delta \mathcal{L}_{\rm m}}{\delta g_{\mu\nu}} \tag{2.32}$$

for the matter part. Then, using the action principle we obtain the *Einstein equations*

$$G_{\mu\nu} + \Lambda g_{\mu\nu} = M_{\rm Pl}^{-2} T_{\mu\nu}\,. \tag{2.33}$$

Let us now deconstruct the two tensors $G_{\mu\nu}$ and $T_{\mu\nu}$. In a FLRW spacetime described by the metric (2.12), we obtain

$$G_{00} = 3\left(H^2 + \frac{\mathcal{K}}{a^2}\right), \qquad G_{ij} = -g_{ij}\left(H^2 + 2\frac{\ddot{a}}{a} + \frac{\mathcal{K}}{a^2}\right). \tag{2.34}$$

In order to define the energy-momentum tensor of the Universe, we first consider the case of a general imperfect fluid. Denoting with $u^\mu := \frac{{\rm d}x^\mu}{{\rm d}\tau}$ the 4-velocity (of the fluid relative to the observer), $\rho = T_{\mu\nu}u^\mu u^\nu$ the matter energy density, $P = \frac{1}{3}T_{\mu\nu}t^{\mu\nu}$ the isotropic pressure, $q_\mu = -t_\mu^{\ \alpha}T_{\alpha\beta}u^\beta$ the energy-flux vector, and $\Sigma_{\mu\nu} = t_{\langle\mu}^{\ \ \alpha}\gamma_{\nu\rangle}^{\ \ \beta}T_{\alpha\beta}$ the symmetric and trace-free anisotropic stress tensor, the energy-momentum tensor can be written in the form

$$T_{\mu\nu} = \rho u_\mu u_\nu + P t_{\mu\nu} + 2q_{(\mu}u_{\nu)} + \Sigma_{\mu\nu}\,, \tag{2.35}$$

where we also defined the tensor $t_{\mu\nu} := g_{\mu\nu} + u_\mu u_\nu$ and used the notation $t_{\langle\mu\nu\rangle} = \gamma_{(\mu}^{\ \ \alpha}\gamma_{\nu)}^{\ \ \beta}t_{\alpha\beta} - \frac{1}{3}\gamma^{\alpha\beta}t_{\alpha\beta}\gamma_{\mu\nu}$ and $t_{(\mu\nu)} = \frac{1}{2}(t_{\mu\nu} + t_{\nu\mu})$. Now, for a perfect fluid that satisfies the requirements of isotropy and homogeneity there exists a unique 4-velocity such that $q_\mu = \Sigma_{\mu\nu} = 0$, and the energy-momentum tensor simplifies to

$$T^\mu_{\ \nu} = g^{\mu\alpha}T_{\alpha\nu} = (\rho + P)\,u^\mu u_\nu - P\,\delta^\mu_\nu\,, \tag{2.36}$$

For an observer comoving with the fluid we may choose $u^\mu = (1,0,0,0)$ and the energy-momentum tensor becomes

$$T^\mu_{\ \nu} = \begin{pmatrix} \rho & 0 & 0 & 0 \\ 0 & -P & 0 & 0 \\ 0 & 0 & -P & 0 \\ 0 & 0 & 0 & -P \end{pmatrix}. \tag{2.37}$$

Next, combining Eq. (2.34) with (2.37) we obtain the following two coupled, non-linear ordinary differential equations:

$$\boxed{H^2 = \left(\frac{\dot{a}}{a}\right)^2 = \frac{1}{3}\rho - \frac{\mathcal{K}}{a^2} + \frac{\Lambda}{3}}, \tag{2.38}$$

and

$$\boxed{\dot{H} + H^2 = \frac{\ddot{a}}{a} = -\frac{1}{6}(\rho + 3P) + \frac{\Lambda}{3}}. \tag{2.39}$$

The first equation is called the *Friedmann equation* [16], while the second one takes its name after *Raychaudhuri* [24]. Combining Eqs. (2.38) and (2.39) yields the "continuity equation"

$$\boxed{\dot{\rho} + 3H(\rho + P) = 0}. \tag{2.40}$$

The above equation can also be derived by the covariant conservation of the energy-momentum tensor,

$$D_\mu T^\mu_{\ \nu} := \partial_\mu T^\mu_{\ \nu} + \Gamma^\mu_{\alpha\mu}T^\alpha_{\ \nu} - \Gamma^\alpha_{\mu\nu}T^\mu_{\ \alpha} = 0\,. \tag{2.41}$$

In order to solve Eq. (2.40), it proves useful to define the equation of state parameter

$$w := \frac{P}{\rho} \,. \tag{2.42}$$

Then, Eq. (2.40) takes on the form

$$\frac{d\ln\rho}{d\ln a} = -3(1+w)\,, \tag{2.43}$$

which may be integrated to give

$$\rho \propto a^{-3(1+w)} \,. \tag{2.44}$$

Now, neglecting the curvature and cosmological constant terms, the Friedmann equation (2.38) can be integrated to give the time evolution of the scale factor

$$a(t) \propto \begin{cases} t^{\frac{2}{3(1+w)}} & w \neq -1\,, \\ e^{Ht} & w = -1\,. \end{cases} \tag{2.45}$$

For a flat ($\mathcal{K} = 0$) Universe dominated by non-relativistic or cold matter ($w = 0$) we have $a(t) \propto t^{2/3}$, for a Universe dominated by radiation or relativistic matter ($w = \frac{1}{3}$) we have $a(t) \propto t^{1/2}$ and for a Universe where the cosmological constant dominates ($w = -1$) we have $a(t) \propto \exp(Ht)$. Furthermore, in a Universe where the spatial curvature dominates ($w = -\frac{1}{3}$) we find $a(t) \propto t$, while for a Universe dominated by a scalar field (as is the case during inflation) the equation of state parameter becomes[2] $w = -1 + 2\epsilon_H/3$ and the scale factor evolves as $a(t) \propto t^{1/\epsilon_H}$.

Table 2.2: FLRW solutions for a flat universe dominated by radiation, matter or a cosmological constant.

fluid	equation of state parameter w	$\rho(a)$	$a(t)$	$a(\tau)$
cold matter	0	a^{-3}	$t^{2/3}$	τ^2
radiation	$\frac{1}{3}$	a^{-4}	$t^{1/2}$	τ
spatial curvature	$-\frac{1}{3}$	a^{-2}	t	e^{τ}
cosmol. constant	-1	a^{0}	e^{Ht}	$-\tau^{-1}$
scalar field	$-1+2\frac{\epsilon_H}{3}$	$a^{-2\epsilon_H}$	t^{1/ϵ_H}	$(-\tau/\epsilon_H)^{-\epsilon_H}$

In our Universe, the total energy density ρ and pressure P receive contributions from various matter and energy species (dark energy, baryons, dark matter, photons, neutrinos, etc.),

$$\rho := \sum_i \rho_i \,, \qquad P := \sum_i P_i \,. \tag{2.46}$$

For each different species 'i' we may define the present ratio of the energy density with respect to the *critical energy density*

$$\rho_{\rm crit} := 3H_0^2 \tag{2.47}$$

[2]The parameter ϵ_H will be discussed in full detail in Chapter 3.

as

$$\Omega_i := \frac{\rho_0^i}{\rho_{\text{crit}}}. \tag{2.48}$$

The corresponding equation of state parameter becomes

$$w_i := \frac{P_i}{\rho_i}. \tag{2.49}$$

Then, the Friedmann equation yields

$$H^2 = H_0^2 \left(\Omega_\Lambda^0 + \Omega_\mathcal{K}^0 a^{-2} + \Omega_m^0 a^{-3} + \Omega_r^0 a^{-4} \right), \tag{2.50}$$

with $\Omega_\text{K}^0 := -\mathcal{K}/a_0^2 H_0^2$. Today, the scalar factor is normalized to be $a_0 = a(t_0) := 1$ and we obtain the consistency relation

$$\Omega_\Lambda^0 + \Omega_\mathcal{K}^0 + \Omega_m^0 + \Omega_r^0 = 1\,. \tag{2.51}$$

Observations of the CMB from the Planck mission [1] constrain the above ratios to be $\Omega_\Lambda^0 \simeq 0.69$ for the cosmological constant, $\Omega_\text{CDM}^0 \simeq 0.26$ for cold dark matter, $\Omega_b^0 \simeq 0.05$ for baryons ($\Omega_m^0 \simeq \Omega_\text{CDM}^0 + \Omega_b^0$), and $\Omega_r^0 \simeq 10^{-5}$ for the relativistic components. Finally, the Universe appears to be flat, with $\Omega_\mathcal{K}^0 = 0.000 \pm 0.005$ (see also Fig. 2.3).

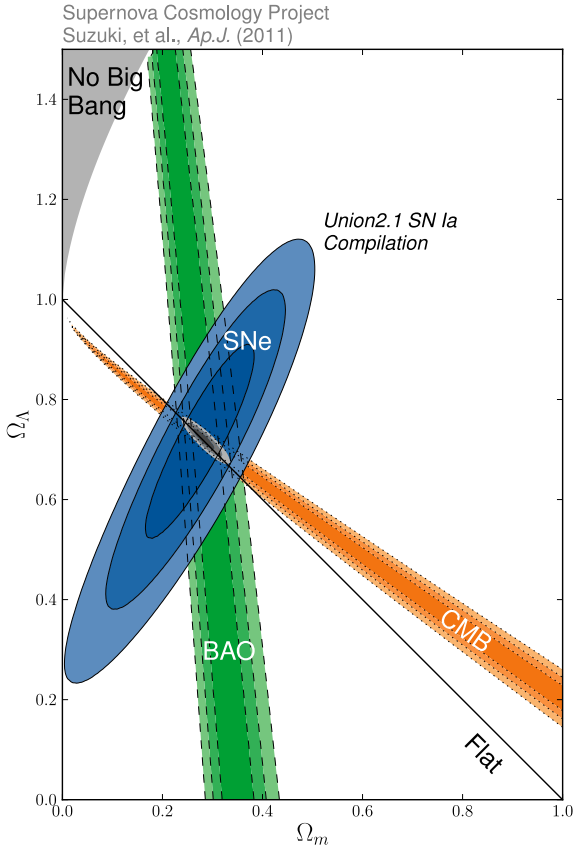

Figure 2.3: 68.3%, 95.4%, and 99.7% confidence regions of the $(\Omega_m, \Omega_\Lambda)$ plane in the ΛCDM model from type Ia supernovae combined with the constraints from BAO and CMB. Credit: Ref. [25]

2.2.4 Particles in Equilibrium

The CMB suggests that the early Universe was in local thermal equilibrium. As we outlined in Section 2.1, the expansion of the Universe resulted in non-equilibrium dynamics which allowed massive particles to acquire their cosmological abundances. A species i achieves thermal equilibrium when it is both in kinetic and chemical equilibrium. *Kinetic equilibrium* occurs when the particles of the species exchange energy and momentum in an efficient way. This results in a state of maximum entropy. Thus, in phase space, the distribution functions of the species obey the *Fermi-Dirac* (FD) and *Bose-Einstein* (BE) statistics

$$f(|\mathbf{p}|) = \frac{1}{e^{(E(|\mathbf{p}|)-\mu)/T} \pm 1} \tag{2.52}$$

where $+$ is for fermions and $-$ for bosons. The chemical potential μ is defined as the derivative of the entropy S with respect to the number of particles N, at fixed volume V and energy U,

$$\mu = -T \left(\frac{\partial S}{\partial N} \right)_{U,V} , \tag{2.53}$$

and it can be used to indicate which way a reaction proceeds. *Chemical equilibrium* is achieved when the sum of the chemical potentials of the reacting particles is equal to the sum of the chemical potentials of the produced particles. For processes of the form $1 + 2 \leftrightarrow 3 + 4$ this translates to

$$\mu_1 + \mu_2 = \mu_3 + \mu_4 \, . \tag{2.54}$$

Now, because of homogeneity, the distribution function is independent of the position $\mathbf{x}$ and due to isotropy it depends only on the magnitude of the momentum $|\mathbf{p}|$. Leaving the time dependence implicit, the number density n_i and the energy density ρ_i for a species i with g_i internal degrees of freedom are given by

$$n_i = g_i \int \frac{\mathrm{d}^3 p}{(2\pi)^3} f_i(|\mathbf{p}|) \, , \qquad \rho_i = g_i \int \frac{\mathrm{d}^3 p}{(2\pi)^3} f_i(|\mathbf{p}|) E_i(|\mathbf{p}|) \, , \tag{2.55}$$

where

$$E_i(|\mathbf{p}|) = \sqrt{|\mathbf{p}|^2 + m_i^2} \, . \tag{2.56}$$

At early times, the chemical potentials of all particles were small enough to be neglected. We may consider two limits. In the relativistic limit ($T_i \gg m_i$), we have

$$n_i = g_i \begin{cases} \frac{\zeta(3)}{\pi^2} T_i^3 & \text{(BE)} \\ \frac{3}{4} \frac{\zeta(3)}{\pi^2} T_i^3 & \text{(FD)} \end{cases} , \qquad \rho_i = g_i \begin{cases} \frac{\pi^2}{30} T_i^4 & \text{(BE)} \\ \frac{7}{8} \frac{\pi^2}{30} T_i^4 & \text{(FD)} \end{cases} , \tag{2.57}$$

where $\zeta(3) \simeq 1.20206$. In the non-relativistic limit ($T_i \ll m_i$) bosons and fermions are indistinguishable and can be described by the Maxwell-Boltzmann distribution

$$n_i = g_i \left(\frac{m_i T_i}{2\pi} \right)^{3/2} e^{-m_i/T_i} , \qquad \rho_i = n_i m_i \, . \tag{2.58}$$

Notice that as the temperature falls below the mass of the particle, the number density and energy density of the species drop exponentially. This is interpreted as annihilations of particles and antiparticles. At higher energies these annihilations are balanced by the production of particle-antiparticle pairs but as temperature drops the available energy of the thermal bath is inadequate for pair production.

Let us now consider the Universe during radiation domination. The total radiation energy density is

$$\rho_{\rm rad} = g_* \frac{\pi^2}{30} T^4 , \qquad g_* = \sum_{i=\text{bosons}} g_i \left(\frac{T_i}{T}\right)^4 + \frac{7}{8} \sum_{i=\text{fermions}} g_i \left(\frac{T_i}{T}\right)^4 , \tag{2.59}$$

where T is the photon (CMB) temperature. For high temperature ($T \geq 300\,\text{GeV}$) we can include all the SM degrees of freedom and we get $g_* = 106.75$. In a radiation dominated Universe the Friedmann equation has the form

$$H^2 = g_* \frac{\pi^2}{90} T^4 . \tag{2.60}$$

We can scale out the effect of the expansion by introducing the number density in a comoving volume. We take as comoving volume the entropy density $\mathbf{s}$, defined as

$$\mathbf{s} = \frac{2\pi^2}{45} g_{*s} T^3 , \qquad g_{*s} = \sum_{i=\text{bosons}} g_i \left(\frac{T_i}{T}\right)^3 + \frac{7}{8} \sum_{i=\text{fermions}} g_i \left(\frac{T_i}{T}\right)^3 . \tag{2.61}$$

For very high temperature all the relativistic species are in thermal equilibrium and therefore $g_{*\mathbf{s}} = g_*$. We are able to use the total entropy to define the comoving volume since it is conserved during the expansion, $\mathbf{s} \propto a^{-3}$. Thus, the comoving number density or *yield* is defined as

$$Y := \frac{n}{\mathbf{s}} . \tag{2.62}$$

The yield is a useful quantity since it scales out the expansion of the Universe. It is also a dimensionless variable and can therefore be used to numerically solve the Boltzmann equation (see Chapter 5).

2.3 Problems of the Big Bang Theory and their Inflationary Solutions

Despite its successes, the Big Bang Theory model is endowed with some problems which are mostly connected to the initial conditions of the Universe. In this Section, we will focus on the horizon and flatness problems and we will see how these problems are naturally solved if one assumes that the Universe underwent a period of inflationary expansion in its early stages.

2.3.1 The Horizon Problem

The Universe has existed for a finite amount of time, which means that photons have travelled a finite distance during this time. The propagation of light in an expanding Universe is best studied using conformal time, also called the *comoving particle horizon*,

$$\Delta\tau = \int_{t_i}^{t} \frac{\mathrm{d}t}{a} = \int_{a_i}^{a} \frac{\mathrm{d}a}{a\dot{a}} = \int_{\ln a_i}^{\ln a} \mathrm{d}\ln a \, (aH)^{-1} , \tag{2.63}$$

where $a_i := 0$ corresponds to the Big Bang singularity. Furthermore, the quantity $(aH)^{-1}$ is called the *comoving Hubble radius* and plays a crucial role in inflation. In an isotropic spacetime, we can define the coordinate system so that photons are travelling towards us ($\mathrm{d}\theta = \mathrm{d}\phi = 0$). Then, the line element becomes

$$\mathrm{d}s^2 = a^2(\tau) \left[-\mathrm{d}\tau^2 + \mathrm{d}r^2\right] , \tag{2.64}$$

and since light travels along null geodesics, $ds^2 = 0$, its path is determined by

$$\Delta r(\tau) = \pm \Delta\tau \,, \tag{2.65}$$

where the plus (minus) sign corresponds to outgoing (incoming) photons.

For a Universe dominated by a fluid with a constant equation of state parameter w, we obtain

$$(aH)^{-1} = H_0^{-1} a^{\frac{1}{2}(1+3w)} \,. \tag{2.66}$$

Matter and radiation satisfy the strong energy condition, $(1+3w) > 0$, so it used to be assumed that the comoving Hubble radius grows monotonically as the Universe expands. Using (2.66) in (2.63), we obtain

$$\tau - \tau_i = \frac{2H_0^{-1}}{(1+3w)} \left[a^{\frac{1}{2}(1+3w)} - a_i^{\frac{1}{2}(1+3w)} \right] . \tag{2.67}$$

We see that the integral in (2.63) is dominated by the upper limit, while early times give vanishing contributions

$$\tau_i = \frac{2H_0^{-1}}{(1+3w)} a_i^{\frac{1}{2}(1+3w)} \xrightarrow[w>-1/3]{a_i \to 0} 0 \,. \tag{2.68}$$

Measurements from the CMB suggest that the Hubble radius was roughly 100 Mpc at that time, which corresponds to around 1° in the sky. This implies that spots in the CMB separated by more than 1° cannot have been in causal contact since they have non-overlapping past light cones. Nevertheless, the CMB radiation is extremely homogeneous and isotropic, up to tiny fluctuations of the order of $\delta T/T \simeq 10^{-5}$, and consists of at least 10^4 disconnected patches of space which apparently did not have enough time to communicate. This is the *horizon problem*.

A simple solution to the horizon problem presents itself if we postulate a phase of decreasing Hubble radius in the early Universe,

$$\frac{\mathrm{d}}{\mathrm{d}t} (aH)^{-1} < 0 \,. \tag{2.69}$$

This means we need a fluid which violates the strong energy condition, that is, $1+3w < 0$. Now, the integral in (2.63) is dominated by the lower limit,

$$\tau_i = \frac{2H_0^{-1}}{(1+3w)} a_i^{\frac{1}{2}(1+3w)} \xrightarrow[w<-1/3]{a_i \to 0} -\infty \,, \tag{2.70}$$

and the Big Bang singularity is pushed to negative conformal time (see Fig. 2.4). The time $\tau = 0$ now becomes a transition point between the inflationary era and the standard Big Bang evolution. This transition point is now replaced by the period of reheating. All points in the CMB are now causally connected since they have overlapping past light cones.

2.3.2 The Flatness Problem

Let us now see how inflation also solves the flatness problem.

The Friedmann equation (with zero cosmological constant),

$$H^2 = \frac{1}{3}\rho - \frac{\mathcal{K}}{a^2} \,, \tag{2.71}$$

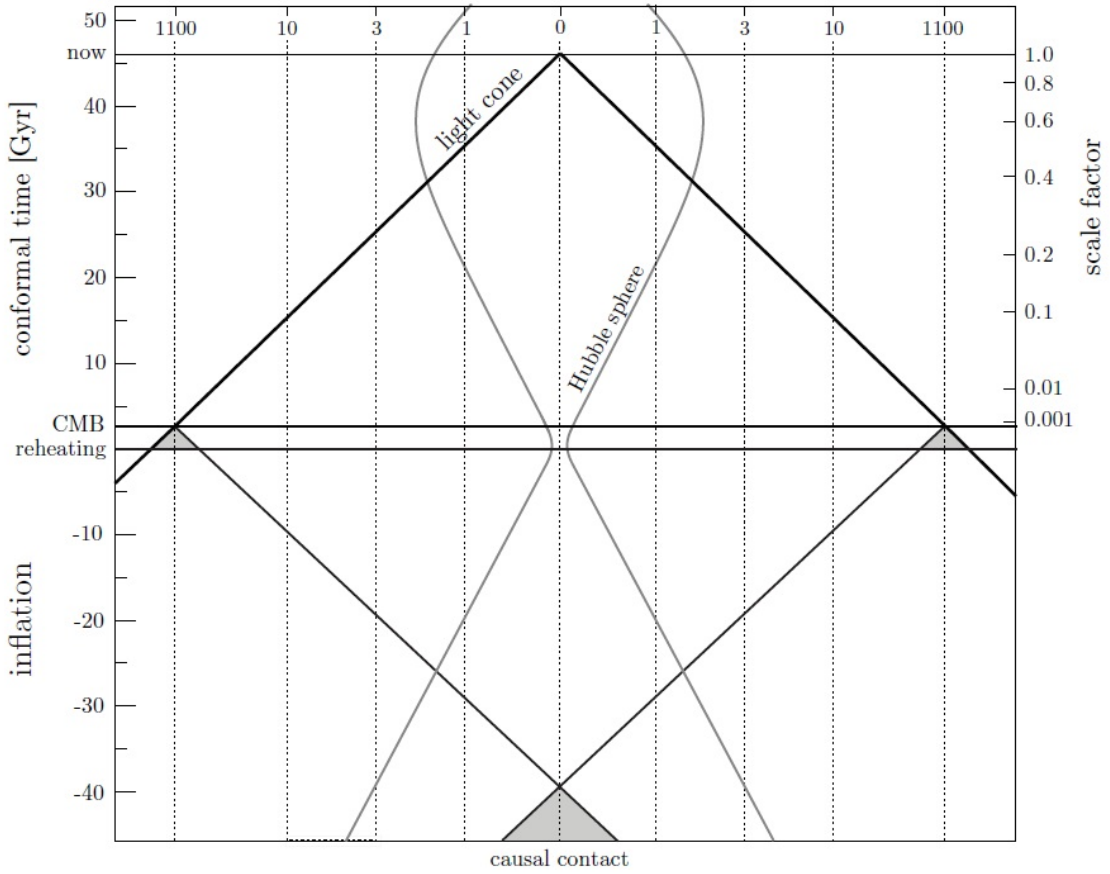

Figure 2.4: The horizon problem can be solved if we assume an inflationary period before $\tau = 0$ where the Hubble sphere is shrinking instead of expanding (as is the case in the standard Big Bang evolution until dark energy takes over at $a \sim 0.5$). All points in the CMB are now causally connected since they have overlapping past light cones. Credit: Cosmology lectures by Daniel Baumann

can be written as

$$1 - \Omega(t) = \frac{-\mathcal{K}}{(aH)^2} \,. \tag{2.72}$$

Notice that $\Omega(t)$ now depends on time. For some earlier time t_i we can write

$$\begin{aligned} 1 - \Omega(t_i) &= [1 - \Omega(t_0)] \, \frac{H^2(t_0) a^2(t_0)}{H^2(t_i) a^2(t_i)} \\ &= [1 - \Omega(t_0)] \left(\frac{\dot{a}(t_0)}{\dot{a}(t_i)} \right)^2 . \end{aligned} \tag{2.73}$$

In a Universe dominated by matter, the scale factor grows as $a \propto t^{2/3}$. Given the current age of the Universe $t_0 \simeq 4.3 \times 10^{17}$s, at the time of radiation-matter equality, $a \propto t^{1/2}$, we obtain

$$1 - \Omega(t_{\rm rec}) = [1 - \Omega(t_0)] \left(\frac{t_0}{t_{\rm rec}} \right)^{-2/3} < 10^{-4} \,, \tag{2.74}$$

where $t_{\rm rec} \simeq 2.0 \times 10^{12}$s. This implies that at recombination the Universe was very close to being flat. Now, during radiation domination the scale factor grows as $a \propto t^{1/2}$. Going back to the time of

Big Bang Nucleosynthesis, $t_{\rm BBN} \sim 10^2$s, we obtain

$$1 - \Omega(t_{\rm BBN}) = [1 - \Omega(t_0)] \left(\frac{t_0}{t_{\rm BBN}}\right)^{-1} < 10^{-17} \,. \tag{2.75}$$

If we go even further back to the Planck time, $t_{\rm P} \sim 5 \times 10^{-44}$s, we find

$$1 - \Omega(t_{\rm P}) < 10^{-64} \,. \tag{2.76}$$

All of this discussion shows that the density parameter must have been extremely close to "unity" in the early Universe despite the fact that the critical value $\Omega = 1$ is an unstable fixed point. This is the so-called *flatness problem*. During inflation, we will see that the Hubble parameter H_I is almost constant, which means the scale factor grows as

$$a(t) \simeq a_{\rm end} \exp\left[H_I \left(t - t_{\rm end}\right)\right] = \exp\left[-N(t)\right] \,, \tag{2.77}$$

where $t_{\rm end}$ is the time when inflation ends. If inflation lasted around $N(t) \simeq 60$, then the exponentially decreasing value of Ω is driven towards unity and will remain close to it even after inflation ends

$$1 - \Omega \propto e^{-2N} \to 0 \,. \tag{2.78}$$

The above discussion clearly demonstrates why inflation is generally considered as the natural solution to the horizon and flatness problems.

Chapter 3

Inflation

The theory of cosmic inflation was originally advocated as a solution to the flatness and horizon problems [26, 27] of the Big-Bang cosmology. When treated quantum-mechanically, inflation can also provide a mechanism for the generation of the perturbations that have resulted in the anisotropies observed in the CMB [28–31]. It is usually formulated in terms of a single scalar field, minimally coupled to gravity, whose potential energy dominates over its kinetic energy for a short period of time and drives the accelerated expansion of the universe. This phase can be most easily achieved if the scalar potential $V(\phi)$ has a relatively flat plateau and the scalar field can slowly roll down until it reaches the minimum of the potential.

This chapter is organized as follows: In the next section, we present the simplest scenario that can realize inflation: one real scalar field minimally coupled to gravity. Then, in Section 3.2, we study the scalar and tensor perturbations in the minimal case and derive the corresponding power spectra and spectral indices in terms of slow-roll parameters. In Section 3.2.5, we present an example of chaotic inflation from a polynomial potential which shows that minimally coupled models are in tension with observations. We are thus led to explore non-minimally coupled models. These can be studied in the general context of scalar-tensor theories of gravity, which we review in Section 3.3.

3.1 Minimal Inflation

3.1.1 Scalar Field Dynamics

Let us consider a real scalar field, hereby called the *inflaton*, which is governed by the Lagrangian

$$\mathcal{L} = \frac{1}{2} g^{\mu\nu} \partial_\mu \phi \partial_\nu \phi - V(\phi)\,, \tag{3.1}$$

where $V(\phi)$ is the inflaton potential, which we leave unspecified for the moment. By minimally coupling the inflaton to gravity, we obtain the following action[1]

$$S = \int \mathrm{d}^4x \sqrt{-g} \left[\frac{R}{2} - \frac{1}{2} g^{\mu\nu} \partial_\mu \phi \partial_\nu \phi - V(\phi) \right] = S_{\mathrm{EH}} + S_\phi\,. \tag{3.2}$$

By varying S_ϕ with respect to the metric, we obtain the energy-momentum tensor

$$T^{(\phi)}_{\mu\nu} = -\frac{2}{\sqrt{-g}} \frac{\delta S_\phi}{\delta g_{\mu\nu}} = \partial_\mu \phi \partial_\nu \phi - g_{\mu\nu} \left(\frac{1}{2} \partial^\sigma \phi \partial_\sigma \phi + V(\phi) \right)\,. \tag{3.3}$$

[1] Henceforth, we use units where $M_{\mathrm{Pl}} = 1$.

Next, by varying S_ϕ with respect to the scalar field we obtain the inflaton equation of motion

$$\frac{\delta S_\phi}{\delta \phi} = \frac{1}{\sqrt{-g}}\partial_\mu\left(\sqrt{-g}\,\partial^\mu\phi\right) + \frac{\mathrm{d}V(\phi)}{\mathrm{d}\phi} = 0\,. \tag{3.4}$$

In a FLRW Universe described by the metric (2.12) and assuming a homogeneous field $\phi(t,\mathbf{x}) =: \phi(t)$, the scalar energy-momentum tensor describes a perfect fluid with

$$T^0_{\ 0} = \rho_\phi \Rightarrow \quad \rho_\phi = \frac{1}{2}\dot{\phi}^2 + V(\phi)\,, \tag{3.5}$$

$$T^i_{\ j} = -P_\phi \delta^i_{\ j} \Rightarrow P_\phi = \frac{1}{2}\dot{\phi}^2 - V(\phi)\,. \tag{3.6}$$

The equation of state parameter for the inflaton has the form

$$w_\phi = \frac{P_\phi}{\rho_\phi} = \frac{\frac{1}{2}\dot{\phi}^2 - V(\phi)}{\frac{1}{2}\dot{\phi}^2 + V(\phi)}\,. \tag{3.7}$$

As one can see, a scalar field can produce negative pressure ($w_\phi < 0$) and lead to an accelerated expansion ($w_\phi < -1/3$) if its potential energy V dominates over its kinetic energy $\frac{1}{2}\dot{\phi}^2$. The Friedmann equation (2.38) now reads (assuming a flat Universe and zero cosmological constant)

$$\boxed{H^2 = \frac{1}{3}\left[\frac{\dot{\phi}^2}{2} + V\right]}\,. \tag{3.8}$$

Taking the time derivative of (3.8), $2H\dot{H} = \frac{1}{3}\left[\dot{\phi}\ddot{\phi} + V'\dot{\phi}\right]$, and using $\dot{H} = -\left(\rho_\phi + P_\phi\right)/2$, we obtain

$$\boxed{\dot{H} = -\frac{1}{2}\dot{\phi}^2}\,. \tag{3.9}$$

Finally, Eq. (3.4) gives the Klein-Gordon equation

$$\boxed{\ddot{\phi} + 3H\dot{\phi} + V' = 0}\,. \tag{3.10}$$

3.1.2 Slow-roll Approximation

Let us rewrite the Raychaudhuri equation (2.39) as

$$\frac{\ddot{a}}{a} = H^2(1 - \epsilon_H)\,, \tag{3.11}$$

where

$$\boxed{\epsilon_H := -\frac{\dot{H}}{H^2} = 2\left(\frac{H'(\phi)}{H(\phi)}\right)^2 = \frac{3\dot{\phi}^2}{\dot{\phi}^2 + 2V}} \tag{3.12}$$

is the first *Hubble slow-roll parameter* (HSRP) [32]. Equation (3.11) shows that accelerated expansion can occur if $\epsilon_H < 1$, while inflation ends *exactly* when $\epsilon_H = 1$. Furthermore, the limit $\epsilon_H \to 0$ corresponds to de Sitter space and occurs when the potential energy of the inflaton dominates over its kinetic energy,

$$V(\phi) \gg \dot{\phi}^2\,. \tag{3.13}$$

For inflation to last sufficiently long enough in order to solve the problems of the Big Bang theory described in Sec. 2.3, we must also impose that the second time derivative of ϕ be small, that is,

$$|\ddot{\phi}| \ll |3H\dot{\phi}|, \, |V'| \, . \tag{3.14}$$

This behaviour can be encoded in the second HSRP,

$$\boxed{\eta_H = -\frac{\ddot{\phi}}{H\dot{\phi}} = -\frac{1}{2}\frac{\ddot{H}}{\dot{H}H} = 2\frac{H''(\phi)}{H(\phi)}} \, . \tag{3.15}$$

In general, one can define a hierarchy of HSPRs [32]

$${}^{n}\beta_H = 2\left(\frac{(H')^{n-1}\, H^{(n+1)}}{H^n}\right)^{\frac{1}{n}} \, . \tag{3.16}$$

Within the slow-roll approximation, the Friedmann (3.8) and Klein-Gordon (3.10) equations become

$$H^2 \approx \frac{1}{3}V(\phi) \tag{3.17}$$

$$\dot{\phi} \approx -\frac{V'}{3H} \, . \tag{3.18}$$

In order to realize the slow-roll conditions (3.13) and (3.14), one usually considers an inflaton potential with a relatively flat part where the scalar field can slowly roll down towards the minimum and give rise to the quasi-exponential growth of the scale factor (see Fig. 3.1) (see [33–36] for reviews on inflation). After inflation ends, the scalar field rapidly oscillates around the minimum of the potential and eventually decays to other particles (including the Standard Model ones), in a process dubbed *reheating* (see [37–39] for reviews on reheating).

The shape of the potential can be encoded in the *potential slow-roll parameters* (PSRPs). The first two are defined as

$$\boxed{\epsilon_V := \frac{1}{2}\left(\frac{V'}{V}\right)^2} \, , \tag{3.19}$$

$$\boxed{\eta_V := \frac{V''}{V}} \, , \tag{3.20}$$

while higher-order PSRPs are given by the hierarchy [32]

$${}^{n}\beta_V = \left(\frac{(V')^{n-1}\, V^{(n+1)}}{V^n}\right)^{\frac{1}{n}} \, . \tag{3.21}$$

The HSPRs can be related to the PSRPs through the equations (3.8)–(3.10). One finds

$$\epsilon_V = \epsilon_H\left(\frac{3-\eta_H}{3-\epsilon_H}\right)^2 \, , \tag{3.22}$$

$$\eta_V = \sqrt{2\epsilon_H}\frac{\eta_H'}{3-\epsilon_H} + \left(\frac{3-\eta_H}{3-\epsilon_H}\right)(\epsilon_H + \eta_H) \tag{3.23}$$

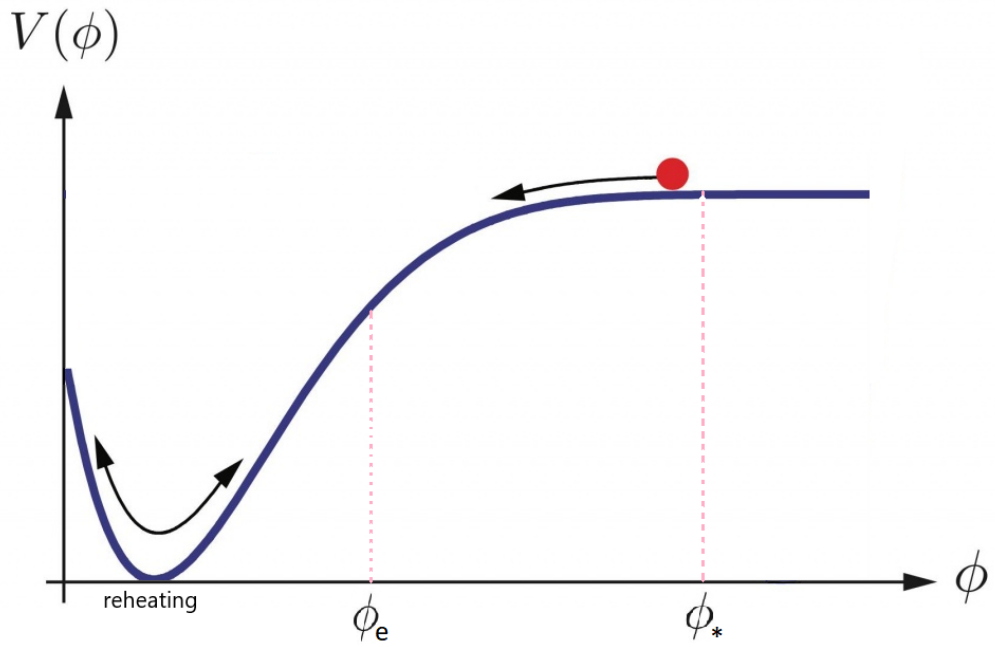

Figure 3.1: In the standard picture of inflation, the scalar field rolls down its potential, which generally needs to have a relatively flat plateau in order for the required $50-60$ e-folds to occur. Inflation ends when $\epsilon_H(\phi_e) = 1$. Then, the inflaton oscillates around the minimum of the potential and fuels the reheating era.

These equations are exact, but in the slow-roll regime we can approximate them using a Taylor expansion as [32]

$$\epsilon_H \approx \epsilon_V \tag{3.24}$$
$$\eta_H \approx \eta_V - \epsilon_V \,. \tag{3.25}$$

The above relations are usually assumed to be sufficient for the determination of the inflationary observables. However, as we will see in Chapter 9, the increasing sensitivity of the experiments forces us to be more careful in our considerations regarding what approximation to use. There, we will see that keeping higher-order terms in the Taylor expansion, or using other types of approximations altogether can lead to considerably different results.

Finally, in the slow-roll approximation the number of e-folds can be written as

$$N(\phi) = \int_t^{t_{\rm end}} H \mathrm{d}t = \int_\phi^{\phi_{\rm end}} \frac{H}{\dot\phi} \mathrm{d}\phi \approx \int_{\phi_{\rm end}}^{\phi} \left(\frac{V}{V'}\right) \mathrm{d}\phi \,, \tag{3.26}$$

or, using the slow-roll parameters, as

$$\boxed{N(\phi) = \int_{\phi_{\rm end}}^{\phi} \frac{\mathrm{d}\phi}{\sqrt{2\epsilon_H}} \approx \int_{\phi_{\rm end}}^{\phi} \frac{\mathrm{d}\phi}{\sqrt{2\epsilon_V}}} \,. \tag{3.27}$$

As we saw in Section 2.3, the flatness and horizon problems can be solved if we take the number of e-folds to be around $N \sim 60$ (see also [40, 41]), a number consistent also with the generation of the CMB anisotropies.

3.2 Cosmological Perturbations

Perhaps the most appealing feature of the theory of inflation is that, when treated quantum-mechanically, it can produce the small inhomogeneities of order 10^{-5} observed in the CMB. The generation of these inhomogeneities is best studied with the help of the cosmological perturbation theory. Thus far, we have only examined the classical FLRW evolution of the inflationary background. Going to the quantum theory, we will have to consider quantum fluctuations of the fields.

3.2.1 The Scalar-Vector-Tensor Decomposition

During inflation, perturbations around the homogeneous classical background solutions for the metric $\bar{g}_{\mu\nu}(t)$ and the inflaton $\bar{\phi}(t)$ are defined as

$$\delta g_{\mu\nu} := g_{\mu\nu}(\tau, \mathbf{x}) - \bar{g}_{\mu\nu}(\tau)\,, \quad \delta\phi := \phi(\tau, \mathbf{x}) - \bar{\phi}(\tau)\,. \tag{3.28}$$

Due to the underlying symmetries of the spatially flat, homogeneous and isotropic background space-time, general metric and energy-tensor perturbations can be decomposed into independent scalar (S), vector (V), and tensor (T) components. The *SVT decomposition theorem* then states that these perturbations will evolve independently (at linear level).

For the perturbed metric we have

$$\delta g_{\mu\nu} := \delta_S g_{\mu\nu} + \delta_V g_{\mu\nu} + \delta_T g_{\mu\nu}\,. \tag{3.29}$$

Now, even though we have split our fields into background and perturbed quantities and are in a position to study the three types of perturbations individually, we have not yet considered how a change of coordinates or the *gauge choice* affects the perturbations. For example, an infinitesimal coordinate transformation

$$x^\mu \to \tilde{x}^\mu = x^\mu + \xi^\mu \tag{3.30}$$

leads to a change in the perturbations. To demonstrate this fact, let us consider an unperturbed homogeneous FLRW Universe with energy density $\rho = \rho(\tau)$ and perform a coordinate transformation of the conformal time $\tau \to \tilde{\tau} = \tau + \xi^0(\tau, \mathbf{x})$. Then, the perturbed energy density will transform as [42]

$$\delta\rho \to \tilde{\delta\rho} = \delta\rho + \rho'\xi^0(\tau, \mathbf{x})\,. \tag{3.31}$$

Therefore, even though we started with $\delta\rho = 0$, by transforming to a new coordinate system we ended up with perturbations in the energy density, $\tilde{\delta\rho} = \rho'\xi^0(\tau, \mathbf{x}) \neq 0$, which are not physical. In order to avoid such ambiguities and get rid of fictitious extra modes, one can either fix a specific gauge or more ideally work with gauge-invariant combinations of perturbations.

Using the SVT decomposition, it can be shown that the perturbed line element takes the form [43, 44]

$$\mathrm{d}s^2 = a^2(\tau)\left\{-(1+2A)\,\mathrm{d}\tau^2 - 2\,(\partial_i B)\,\mathrm{d}x^i\mathrm{d}\tau + \left[(1+2\psi)\,\delta_{ij} + 2\partial_i\partial_j E + h_{ij}\right]\mathrm{d}x^i\mathrm{d}x^j\right\}. \tag{3.32}$$

Notice that we have not included vector perturbations since they are not produced during scalar field inflation and in any case decay fast during the evolution of the Universe. For the scalar and tensor perturbations, which correspond to density fluctuations and gravitational waves in the late Universe, we have a total number of ten degrees of freedom. Four of these can be eliminated through a coordinate transformation and we end up with six physical degrees of freedom. Tensor perturbations are gauge invariant by construction, but scalar perturbations behave non-trivially

under a change of coordinates. In the following we will focus only on scalar perturbations since the results for the tensor perturbations can be obtained in a similar manner.

There are two scalar gauge transformations

$$\tau \to \tilde{\tau} = \tau + \xi^0 \quad \text{and} \quad x^i \to \tilde{x}^i = x^i + \delta^{ij}\partial_j \xi \,. \tag{3.33}$$

Under these, the scalar degrees of freedom A, B, ψ and E transform as

$$\begin{aligned} A &\to \tilde{A} = A + \mathcal{H}\xi^0 + \left(\xi^0\right)' \,, \quad \psi \to \tilde{\psi} = \psi + \mathcal{H}\xi^0 \,, \\ B &\to \tilde{B} = B + \xi^0 - \xi' \,, \qquad\quad E \to \tilde{E} = E + \xi \,. \end{aligned} \tag{3.34}$$

where a prime now denotes differentiation with respect to the conformal time τ and $\mathcal{H} := a'/a = aH$. By taking linear combinations of the scalar degrees of freedom we can construct the gauge-invariant Bardeen potentials [45]

$$\Phi_B := A - \frac{1}{a}\left[a\left(B - E'\right)\right]' \quad \text{and} \quad \Psi_B := \psi - \mathcal{H}\left(B + E'\right) \,. \tag{3.35}$$

At this point, it is useful to also introduce the Mukhanov-Sasaki variable [46, 47]

$$v := a\left(\delta\phi_{gi} + \frac{\bar{\phi}'}{\mathcal{H}}\Phi_B\right) \,, \tag{3.36}$$

where $\delta\phi_{gi}$ is the gauge-invariant scalar field perturbation constructed with the help of (3.34)

$$\delta\phi_{gi} := \delta\phi - \bar{\phi}'\left(B + E'\right) \,. \tag{3.37}$$

Under (3.33), $\delta\phi_{gi}$ transforms as

$$\delta\phi \to \tilde{\delta\phi} = \delta\phi + \xi^0\bar{\phi}' \,. \tag{3.38}$$

Next, we wish to derive an equation of motion for $v(\tau, \mathbf{x})$. By expanding the action (3.2) around a FLRW background up to second order in the perturbations, one finds [48]

$$\delta^2 S = \frac{1}{2}\int \mathrm{d}\tau \mathrm{d}^3x \left(v'^2 - \partial_i v \partial_j v \delta^{ij} + \frac{z''}{z}v^2\right) = \int \mathrm{d}\tau \mathrm{d}^3x \mathcal{L}_{\text{eff}} \,, \tag{3.39}$$

where

$$z := \frac{a}{\mathcal{H}}\bar{\phi}' = \frac{a}{H}\dot{\bar{\phi}} \,. \tag{3.40}$$

We can also rewrite the Mukhanov-Sasaki variable v as

$$v = z\mathcal{R} \,, \tag{3.41}$$

with

$$\mathcal{R} = \psi + \mathcal{H}\frac{\delta\phi}{\bar{\phi}'} = \psi + \frac{H}{\dot{\bar{\phi}}}\delta\phi \,. \tag{3.42}$$

$\mathcal{R}$ is called the *comoving curvature perturbation* and is an important quantity since for adiabatic perturbations[2] it is conserved on large scales. This means that the value of $\mathcal{R}$ computed at horizon crossing ($k = aH$) will not evolve on super-horizon scales ($k \ll aH$) and remain unaltered until later times. Geometrically, $\mathcal{R}$ measures the spatial curvature of comoving hypersurfaces (surfaces of constant ϕ). During slow-roll inflation and also on super-horizon scales, $\mathcal{R}$ in fact coincides with

[2] Adiabatic perturbations normally occur during single-field inflation, which is of interest to us in this thesis.

the *curvature perturbation on uniform-density hypersurfaces*

$$-\zeta := \psi + \frac{H}{\dot{\bar{\rho}}}\delta\rho \simeq \psi + \frac{H}{\dot{\bar{\phi}}}\delta\phi = \mathcal{R}\,. \tag{3.43}$$

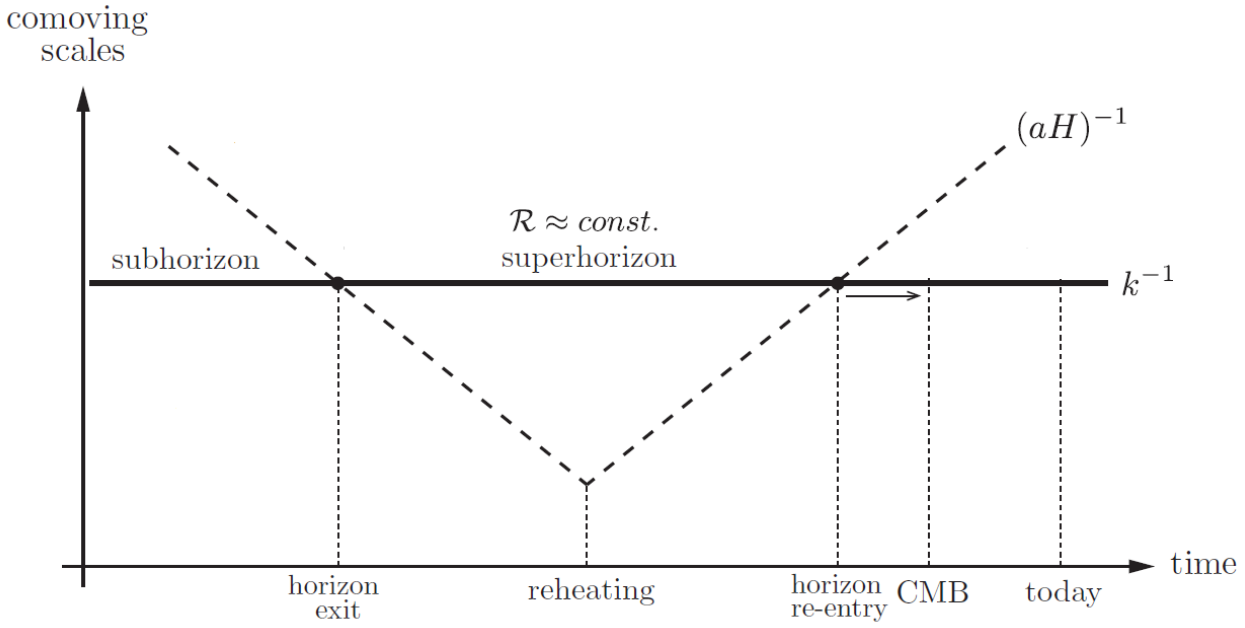

Figure 3.2: The evolution of curvature perturbations during and after inflation. The comoving horizon $(aH)^{-1}$ becomes smaller during inflation and then grows during the standard Big Bang evolution. This means that the comoving scales k^{-1} cross the horizon twice at different epochs in our observable universe. Since the curvature perturbations $\mathcal{R}$ are almost frozen during the superhorizon evolution, we can directly relate the predictions made at horizon exit (high energies) to the observables after horizon re-entry (low energies). Credit: Cosmology lectures by Daniel Baumann

3.2.2 Quantization of Fluctuations

We are now in a position to derive the primordial power spectrum of scalar perturbations. In order to do so, we promote the scalar field v into an operator and quantize it in a canonical way. The conjugate momentum is given by

$$\pi_v := \frac{\partial \mathcal{L}_{\rm eff}}{\partial v'} = v' \tag{3.44}$$

while the commutation relations read

$$\begin{aligned} \left[\hat{v}(\mathbf{x},\tau), \hat{v}(\mathbf{x}',\tau')\right]_{\tau=\tau'} &= \left[\hat{\pi}_v(\mathbf{x},\tau), \hat{\pi}_v(\mathbf{x}',\tau')\right]_{\tau=\tau'} = 0 \\ \left[\hat{v}(\mathbf{x},\tau), \hat{\pi}_v(\mathbf{x}',\tau')\right]_{\tau=\tau'} &= i\delta^{(3)}\left(\mathbf{x}-\mathbf{x}'\right)\,. \end{aligned} \tag{3.45}$$

The field operator $\hat{v}$ can be decomposed in Fourier space into creation and annihilation operators

$$\hat{v} = \frac{1}{2\,(2\pi)^{3/2}} \int \mathrm{d}^3k \left(\hat{a}_{\mathbf{k}} v_k^*(\tau) e^{i\mathbf{k}\cdot\mathbf{x}} + \hat{a}_{\mathbf{k}}^\dagger v_k(\tau) e^{-i\mathbf{k}\cdot\mathbf{x}}\right)\,. \tag{3.46}$$

Since v is a real field, we have $v_k = v^*_{-k}$. The creation and annihilation operators satisfy the commutation relations

$$\begin{aligned} [\hat{a}_k, \hat{a}_{k'}] &= \left[\hat{a}^\dagger_k, \hat{a}^\dagger_{k'}\right] = 0\,, \\ W\left[v_k, v^*_k\right] \times \left[\hat{a}_k, \hat{a}^\dagger_{k'}\right] &= \delta^{(3)}\left(\mathbf{k} - \mathbf{k}'\right)\,, \end{aligned} \tag{3.47}$$

where the Wronskian W is given by

$$W\left[v_k, v^*_k\right] := i\left(v^*_k v'_k - v_k (v^*_k)'\right) = 1 = \langle v|v\rangle\,. \tag{3.48}$$

Now, by varying the action (3.39) in Fourier space, we obtain what is known as the Mukhanov-Sasaki equation [46, 47]

$$\boxed{v''_k + \left(k^2 - \frac{z''}{z}\right) v_k = 0}\,, \tag{3.49}$$

with the mode- and time-dependent frequency

$$\omega_k(\tau) := k^2 - \frac{z''(\tau)}{z(\tau)}\,. \tag{3.50}$$

During slow-roll inflation, the HSPR parameter ϵ_H is assumed to be constant and the conformal time τ can be integrated to give

$$\tau = \int \frac{\mathrm{d}\tau}{a} = \int \frac{\mathrm{d}a}{a^2 H} = \frac{-1}{aH} + \int \frac{\epsilon_H}{a^2}\frac{\mathrm{d}a}{H}\,, \tag{3.51}$$

or, at leading order,

$$\boxed{\tau = -\frac{1}{aH}\frac{1}{1-\epsilon_H}} \simeq -\frac{1+\epsilon_H}{aH}\,. \tag{3.52}$$

The above result can be extended to any order by repeated integration [49][3]. For example, up to third order we have

$$\tau = -\frac{1}{aH}\left[1 + \epsilon_H + 3\epsilon_H^2 - 2\epsilon_H\eta_H + 15\epsilon_H^3 - 20\epsilon_H^2\eta_H + 4\epsilon_H\eta_H^2 + \epsilon_H\zeta_H^2\right]\,. \tag{3.53}$$

Now, in the de Sitter limit, $\epsilon_H \to 0$, the term z''/z in (3.49) simplifies to

$$\frac{z''}{z} = 2\,(aH)^2 = \frac{2}{\tau^2}\,. \tag{3.54}$$

Next, the vacuum state is defined as

$$\hat{a}_{\mathbf{k}}|0\rangle = 0\,, \tag{3.55}$$

for every mode $\mathbf{k}$, and is identified with the Minkowski vacuum of a comoving observer in the far past (i.e. when all comoving scales were well inside the Hubble horizon), $\tau \to -\infty$, or $|k\tau| \gg 1$ or $k \gg aH$. In this *sub-horizon limit*, the Mukhanov-Sasaki equation reduces to

$$v''_k + k^2 v_k = 0\,, \tag{3.56}$$

which is just the equation describing a simple harmonic oscillator, and has two independent solutions, namely $v_k \propto e^{\pm ik\tau}$. Positivity of the normalization condition $\langle v|v\rangle$ selects the minus sign,

[3] The slow-roll parameters we use here are related to those of Ref. [49] as $\epsilon_1 = \epsilon_H$, $\epsilon_2 = 2\epsilon_H - 2\eta_H$, $\epsilon_2\epsilon_3 = 4\epsilon_H^2 - 6\epsilon_H\eta_H + 2\zeta_H^2$.

while proper normalization ($\langle v|v\rangle = 1$) results in the asymptotic boundary condition

$$\lim_{\tau\to-\infty} v_k = \frac{e^{-ik\tau}}{\sqrt{2k}}\,, \tag{3.57}$$

also known as the Bunch-Davies boundary condition [50]. Now, again in the de Sitter limit, the Mukhanov-Sasaki has the form

$$v_k'' + \left(k^2 - \frac{2}{\tau^2}\right) v_k = 0\,, \tag{3.58}$$

which has an exact solution

$$v_k = \alpha\frac{e^{-ik\tau}}{\sqrt{2k}}\left(1 - \frac{i}{k\tau}\right) + \beta\frac{e^{ik\tau}}{\sqrt{2k}}\left(1 + \frac{i}{k\tau}\right)\,. \tag{3.59}$$

The boundary conditions (3.48) and (3.57) fix $\alpha = 1$, $\beta = 0$ and we end up with the unique Bunch-Davies mode functions

$$v_k = \frac{e^{-ik\tau}}{\sqrt{2k}}\left(1 - \frac{i}{k\tau}\right)\,. \tag{3.60}$$

Finally, in the *super-horizon limit* ($k \ll aH$ or $k|\tau| \to 0$) we find

$$\lim_{k|\tau|\to 0} v_k = -\frac{i}{\sqrt{2}k^{3/2}\tau}\,. \tag{3.61}$$

In this case, we can neglect the k^2 in (3.49) and the growing modes behave as

$$v_k \propto z \tag{3.62}$$

The above relation and Eq. (3.41) imply that the comoving curvature scalar remains constant during the super-horizon evolution

$$\mathcal{R} = \frac{v}{z} = \text{const.} \tag{3.63}$$

This feature is of great importance for the estimation of the power spectrum of the fluctuations. It means that once the modes cross the horizon they "freeze" and are unaffected by the details of the reheating phase. This fact allows us to connect the predictions made at horizon exit with the observable perturbations at horizon re-entry.

3.2.3 Power Spectra and Spectral Indices

The comoving curvature scalar has the Fourier transform

$$\hat{\mathcal{R}}\,(\tau, \mathbf{x}) = \frac{1}{(2\pi)^{3/2}}\int \mathrm{d}^3k\hat{\mathcal{R}}_{\mathbf{k}}(\tau)e^{i\mathbf{k}\cdot\mathbf{x}}\,, \tag{3.64}$$

with

$$\hat{\mathcal{R}}_{\mathbf{k}}(\tau) = \frac{v_k(\tau)}{z}\hat{a}_{\mathbf{k}} + \frac{v_k^*(\tau)}{z}\hat{a}^\dagger_{-\mathbf{k}}\,. \tag{3.65}$$

Then, the power spectrum of the comoving curvature perturbations $\mathcal{P}_\mathcal{R}$ is defined via the two-point correlation function in k-space

$$\langle 0|\hat{\mathcal{R}}_{\mathbf{k}}(\tau)\hat{\mathcal{R}}^\dagger_{\mathbf{k}'}|0\rangle =: \frac{2\pi^2}{k^3}\mathcal{P}_\mathcal{R}\delta^{(3)}\left(\mathbf{k} - \mathbf{k}'\right)\,, \tag{3.66}$$

and is related to v_k and z by

$$\mathcal{P}_{\mathcal{R}} = \frac{k^3}{2\pi^2}\frac{|v_k(\tau)|^2}{z^2}\,. \tag{3.67}$$

Let us now move away from pure de Sitter space and see what happens during the slow-roll regime $\epsilon_H \ll 1$. We begin by writing the z''/z term in (3.49) as

$$\frac{z''}{z} = 2a^2H^2\left(1+\epsilon_H-\frac{3}{2}\eta_H+\frac{1}{2}\eta_H^2-\frac{1}{2}\epsilon_H\eta_H+\frac{1}{2}\frac{1}{H}\dot{\epsilon}_H-\frac{1}{2}\frac{1}{H}\dot{\eta}_H\right)\,. \tag{3.68}$$

Using (3.52), we find during slow-roll

$$\frac{z''}{z} \simeq \frac{2+2\epsilon_H-3\eta_H}{\tau^2\left(1-\epsilon_H\right)^2} \simeq \frac{2+6\epsilon_H-3\eta_H}{\tau^2}\,, \tag{3.69}$$

which is of the form

$$\frac{z''}{z} = \frac{\nu_S^2-1/4}{\tau^2}\,, \tag{3.70}$$

with

$$\nu_S^2 = \frac{9}{4}+6\epsilon_H-3\eta_H \quad \Rightarrow \quad \nu_S = \frac{3}{2}+2\epsilon_H-\eta_H+\mathcal{O}(2)\,. \tag{3.71}$$

This means that the Mukhanov-Sasaki equation (3.49) has a general solution in terms of Hankel functions of the first and second kind $H_{\nu_S}^{(1,2)}\left(-k\tau\right)$ that reads

$$v_k(\tau) = \frac{\sqrt{\pi}}{2}\exp\left[i\left(\nu_S+\frac{1}{2}\right)\frac{\pi}{2}\right]\sqrt{-\tau}\,H_{\nu_S}^{(1)}\left(-k\tau\right)\,, \tag{3.72}$$

where $\left[H_{\nu_S}^{(1)}\left(-k\tau\right)\right]^* = H_{\nu_S}^{(2)}\left(-k\tau\right)$. The early time limit of the Hankel functions is

$$\lim_{\tau\to-\infty} H_{\nu_S}^{(1,2)}\left(-k\tau\right) = \sqrt{\frac{-2}{\pi k\tau}}\exp\left[\mp i\left(k\tau+\frac{\pi}{4}\left(2\nu_S+1\right)\right)\right]\,. \tag{3.73}$$

Having specified and normalized the mode functions in the infinite past, we now take the late time limit, $\tau\to 0$. Using

$$iH_{\nu_S}^{(1)}(z) \simeq \frac{\Gamma(\nu_S)}{\pi}\left(\frac{z}{2}\right)^{-\nu_S}\,, \qquad \text{as} \quad z\to 0\,, \tag{3.74}$$

the amplitude $|v_k(\tau)|$ in the super-horizon limit is given by

$$|v_k(\tau)| \simeq C(\nu_S)\frac{1}{\sqrt{2k}}\left(\frac{k}{aH}\right)^{-\nu_S+1/2}\,, \quad C(\nu_S) := 2^{\nu_S-3/2}\frac{\Gamma(\nu_S)}{\Gamma(3/2)}\left(1-\epsilon_H\right)^{\nu_S-1/2}\,. \tag{3.75}$$

During slow roll, we have $\nu_S \simeq 3/2$ and we can also approximate $C(\nu_S)\simeq 1$. Then, by substituting $z = a\dot{\phi}/H$, we finally obtain the scalar power spectrum

$$\mathcal{P}_{\mathcal{R}}(k) \simeq \left(\frac{H}{2\pi}\right)^2\left(\frac{H}{\dot{\phi}}\right)^2\left(\frac{k}{aH}\right)^{3-2\nu_S} \simeq \left(\frac{H}{2\pi}\right)^2\left(\frac{H}{\dot{\phi}}\right)^2\Bigg|_{k=aH}\,. \tag{3.76}$$

The above result is first order in the slow-roll approximation. It is measured to be $\mathcal{P}_{\mathcal{R}}(k_*)\simeq 2.14\times 10^{-9}$ [51], with $k_*/(a_*H_*) = 1$, and it is almost scale invariant. Deviation of the scalar power spectrum from scale invariance is measured by the scalar spectral index (also known as primordial

tilt) n_S, defined as

$$\boxed{n_S := 1 + \frac{\mathrm{d}\ln\mathcal{P}_\mathcal{R}(k)}{\mathrm{d}\ln k} = 1 - 4\epsilon_H + 2\eta_H = 1 - 6\epsilon_V + 2\eta_V}\,. \tag{3.77}$$

Exact scale invariance corresponds to $n_S = 1$. The measured value is $n_S = 0.968 \pm 0.006$ [51].

Primordial quantum fluctuations excite also the graviton and lead to primordial gravitational waves. The quantity of interest for tensor perturbations is

$$h_{ij}(\tau, \mathbf{x}) = \frac{1}{(2\pi)^{3/2}} \int \mathrm{d}^3k \left(\hat{h}^+_\mathbf{k} \epsilon^+_{ij}(\mathbf{k}) + \hat{h}^\times_\mathbf{k} \epsilon^\times_{ij}(\mathbf{k})\right) . \tag{3.78}$$

Gravitational waves have two polarizations ϵ^+_{ij} and $\epsilon^\times_{ij}$. Then, the canonically normalized field is defined as

$$\hat{v}^{+/\times}_\mathbf{k} = z\hat{h}^{+/\times}_\mathbf{k} = a\hat{h}^{+/\times}_\mathbf{k}\,, \tag{3.79}$$

with $z = a$. Thus, we simply have

$$\frac{z''}{z} = \frac{a''}{a} = (aH)^2(2 - \epsilon_H) = \frac{2 - \epsilon_H}{\tau^2(1 - \epsilon_H)^2} = \frac{2 + 3\epsilon_H}{\tau^2} + \mathcal{O}(2)\,. \tag{3.80}$$

The tensor power spectrum is then given by

$$\mathcal{P}_h(k) := 4\mathcal{P}_h^{+/\times}(k) = \frac{4}{a^2}\frac{k^3}{2\pi^2}|v_k(\tau)|^2 = 2\frac{H^2}{\pi^2}\left(\frac{k}{aH}\right)^{3-2\nu_T} = 2\frac{H^2}{\pi}\bigg|_{k=aH}\,, \tag{3.81}$$

where we used

$$\nu_T^2 = \tau^2\frac{a''}{a} + \frac{1}{4} = \frac{9}{4} + 3\epsilon_H \quad \Rightarrow \quad \nu_T = \frac{3}{2} + \epsilon_H + \mathcal{O}(2)\,. \tag{3.82}$$

For tensors, the deviation from scale invariance is usually described in terms of the tensor spectral index

$$\boxed{n_T := \frac{\mathrm{d}\ln\mathcal{P}_h(k)}{\mathrm{d}\ln k} = 3 - 2\nu_T = -2\epsilon_H = -2\epsilon_V}\,, \tag{3.83}$$

where now $n_T = 0$ corresponds to exact scale invariance. Another useful quantity is the tensor-to-scalar ratio r, defined as

$$\boxed{r = \frac{\mathcal{P}_\mathcal{R}}{\mathcal{P}_h} = 16\epsilon_H = 16\epsilon_V}\,. \tag{3.84}$$

At first order in slow roll, we have the so-called consistency relation

$$r = -8n_T\,. \tag{3.85}$$

Finally, if the spectral indices $n_S(k)$ and $n_T(k)$ are scale dependent, we quantify this effect by the running of the spectral indices

$$\alpha_S := \frac{\mathrm{d}n_S}{\mathrm{d}\ln k} \quad \text{and} \quad \alpha_T := \frac{\mathrm{d}n_T}{\mathrm{d}\ln k}\,. \tag{3.86}$$

3.2.4 Higher-order Techniques

While the above derivations for the expressions of the scalar and tensor power spectra (Eqs. (3.91) and (3.81)) are quite simple, they are not very precise. The reason for that is that the high and low-frequency solutions of the Mukhanov-Sasaki equation (Eqs. (3.73) and (3.74)) are extrapolated to the intermediate regime of the horizon crossing ($k = aH$) where they were not meant to be applied. In the near future, experiments are expected to measure the inflationary observables with increasing accuracy (the CORE satellite will be able to lower the detection limit of the tensor-to-scalar ratio down to 10^{-3} [52]). This means the theoretical predictions must also be on par.

A possible strategy in this direction would be to improve the matching of the short and long wavelength solutions by seeking a solution in the intermediate region $k \sim aH$ and then match this solution against the other two. To gain a better insight into this situation, let us write z''/z and a''/a again in the exact forms

$$\frac{z''}{z} = 2a^2H^2\left(1+\epsilon_H-\frac{3}{2}\eta_H+\frac{1}{2}\eta_H^2-\frac{1}{2}\epsilon_H\eta_H+\frac{1}{2}\frac{1}{H}\dot{\epsilon}_H-\frac{1}{2}\frac{1}{H}\dot{\eta}_H\right), \tag{3.87}$$

$$\frac{a''}{a} = 2a^2H^2\left(1-\frac{1}{2}\epsilon_H\right). \tag{3.88}$$

The derivatives of the first two slow-roll parameters ϵ_H and η_H are given by

$$\frac{\dot{\epsilon}_H}{H} = \epsilon_H^2-2\epsilon_H\eta_H, \tag{3.89}$$

$$\frac{\dot{\eta}_H}{H} = \epsilon_H\eta_H-\zeta_H^2, \tag{3.90}$$

where $\zeta_H^2 \sim \mathcal{O}\left(\epsilon_H^2, \eta_H^2, \epsilon_H\eta_H\right)$. We can see that they are of second order in the slow-roll parameters. Since in the leading order slow-roll approximation the slow-roll parameters are assumed to be small, the derivatives of ϵ_H and η_H are approximately zero and are therefore treated as constant. Using $\tau \simeq -(1+\epsilon_H)/aH$ and the small argument approximation for the Hankel functions, Stewart and Lyth [53] computed the first-order slow-roll corrections to the scalar power spectrum, which reads

$$\mathcal{P}_\mathcal{R}(k) \simeq \left[1+(4\alpha-2)\epsilon_H-2\alpha\eta_H\right]\left(\frac{H}{2\pi}\right)^2\left(\frac{H}{\dot{\phi}}\right)^2\Bigg|_{k=aH} \tag{3.91}$$

where $\alpha \equiv (2-\ln 2-\gamma) \simeq 0.729637$ and $\gamma \simeq 0.577216$ is the Euler-Mascheroni constant [54].

At next-to-leading order, the slow-roll parameters cannot be treated as constant and the Hankel solution is no longer valid. Stewart and Gong [55] have proposed an alternative approach, still within the slow-roll approximation. Instead of replacing z''/z in Eq. (3.87) with a constant divided by τ^2 as is usually done in the original slow-roll approximation, they choose the ansatz $z = \tau^{-1}f(\ln\tau)$. The Mukhanov-Sasaki equation now contains an additional term that can be treated as a homogeneity. Then, the solution for v_k can be found using Green's method. The integral in the expression for v_k can then be perturbatively expanded up to any order in slow-roll parameters. We will present this method in detail in Chapter 9 where we will compute higher-order corrections to the inflationary observables in the context of scalar-tensor theories. We refer the Reader to [54, 56–72] for various extensions and applications of this method and to [49, 73–85] for other related methods.

3.2.5 Example: chaotic inflation from a polynomial potential

As an application of the previously derived results, let us consider single-field inflation from a polynomial potential and see what predictions for the observables we can obtain. The potential is given by

$$V(\phi) = b_n \phi^n \,. \tag{3.92}$$

The first two PSRPs defined in Eqs.(3.19)–(3.20) are easily computed to be

$$\epsilon_V = \frac{n^2}{2}\frac{1}{\phi^2}\,, \tag{3.93}$$

$$\eta_V = n\,(n-1)\,\frac{1}{\phi^2}\,. \tag{3.94}$$

In the first-order slow-roll approximation, inflation ends when $\epsilon_H \simeq \epsilon_V = 1$. We can solve this equation to obtain the value of the scalar field at the end of inflation

$$\phi_{\rm end} = \frac{n}{\sqrt{2}}\,. \tag{3.95}$$

The observables are usually computed at the time when the modes of interest crossed the horizon. This time corresponds to around 50–60 e-folds before the end of inflation. Using the e-fold integral (3.26) we find

$$N = \frac{\phi_i^2}{2n} - \frac{n}{4}\,. \tag{3.96}$$

We can invert this relation and express the value of the field ϕ_i as a function of the number of e-folds N. Then, using (3.77) we find for the scalar spectral index

$$n_S = 1 - \frac{2n+4}{4N+1}\,, \tag{3.97}$$

while from (3.84) the tensor-to-scalar ratio is

$$r = \frac{16n}{4N+1}\,. \tag{3.98}$$

Let us now consider $N = 60$ and take the quadratic potential $V = \frac{1}{2}m^2\phi^2$. We find

$$n_S \simeq 0.97\,, \qquad r \simeq 0.13\,. \tag{3.99}$$

Similarly, for the quartic potential $V = \frac{1}{4}\lambda\phi^4$ we find

$$n_S \simeq 0.95\,, \qquad r \simeq 0.26\,. \tag{3.100}$$

Comparing these values with the latest results from the Planck Collaboration (Fig. 3.3), we see that both models are essentially ruled out since they predict a tensor-to-scalar ratio which is too large.

3.3 Scalar-Tensor Theories

Over the years a vast plethora of inflationary models have been proposed, originating from diverse physics frameworks. Recently, the increasing sensitivity of the experiments, and in particular

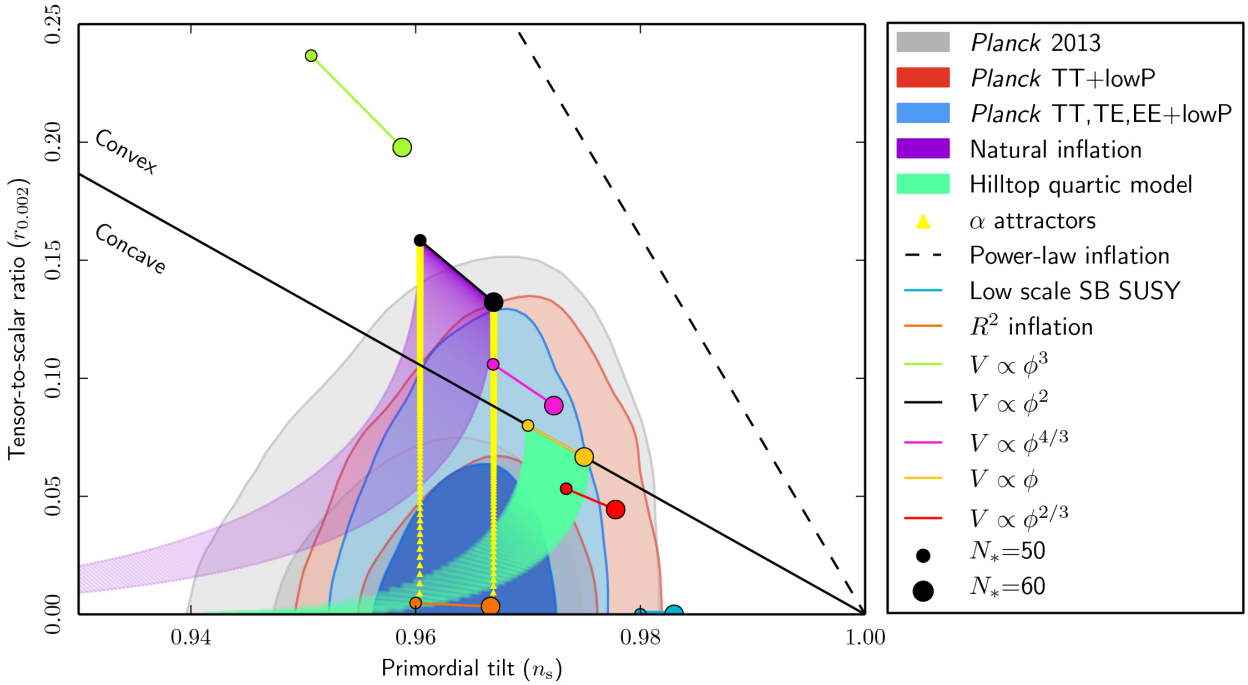

Figure 3.3: Marginalized joint 68% and 95% CL regions for n_S and r at $k = 0.002\text{Mpc}^1$ from Planck 2015 [51] compared to the theoretical predictions of selected inflationary models.

measurements from the Planck and BICEP2/Keck Collaborations [1, 51], have put stringent constraints on many of these models. As we saw in the previous section, the simplest models, where a single scalar field is minimally coupled to gravity, seem to be disfavored[4]. On the other hand, slightly more involved models such as the Starobinsky model [87–92], nonminimal Higgs inflation [42, 93–113], or the so-called α–attractors [114–126] give predictions for the observables that lie inside the sweet spot of the measurements. A common feature of these models is that they can be formulated in terms of a nonminimal coupling function $A(\Phi)$ between the inflaton Φ and the scalar curvature R. Such nonminimal coupling is expected to be generated at the quantum level of the theory even if it is absent in the classical action [127]. These nonminimally coupled theories belong to a general class of gravity theories termed *scalar-tensor (ST) theories* [2]. Other examples of such theories include, among others, the $f(R)$ models [128–135], scale-invariant models [136–155] and nonminimal inflationary models [91, 127, 156–169].

Scalar-tensor theories are usually formulated in either the *Jordan frame (JF)* or the *Einstein frame (EF)*. In the JF the Planck mass is a dynamical quantity that depends on the value of the scalar field, whose self-interactions are described by a potential. Furthermore, the scalar field is minimally coupled to the metric, and the matter part of the action is just the standard one. In the EF the gravitational action has the standard Einstein-Hilbert form plus a scalar field described by an effective potential. Moreover, the scalar appears in the matter sector of the action through the rescaling factor which multiplies the metric tensor. The two frames are mathematically equivalent at the classical level[5] since one can always switch between them by applying a conformal transformation of the metric and a field redefinition, collectively referred to as *frame transformation*. Nevertheless, the physical equivalence of the frames with respect to the physical predictions has become a matter of a long-standing debate [174–193].

[4] See however [86].

[5] See also [170–173] for considerations on the quantum equivalence of the frames.

3.3.1 General action functional

The most general action for scalar-tensor theories has the form [178]

$$S = \int \mathrm{d}^4x\sqrt{-g}\left\{\frac{1}{2}\mathcal{A}(\Phi)R - \frac{1}{2}\mathcal{B}(\Phi)g^{\mu\nu}\left(\nabla_\mu\Phi\right)\left(\nabla_\nu\Phi\right) - \mathcal{V}(\Phi)\right\} + S_m\left[e^{2\sigma(\Phi)}g_{\mu\nu}, \chi\right], \tag{3.101}$$

where in the first term g is the metric determinant, R denotes the Ricci scalar associated with the metric $g_{\mu\nu}$ and $\mathcal{V}(\Phi)$ is the scalar potential. In the second term, S_m stands for the matter part of the action. Furthermore, the four functions $\mathcal{A}(\Phi)$, $\mathcal{B}(\Phi)$, $\mathcal{V}(\Phi)$ and $\sigma(\Phi)$ are arbitrary dimensionless functions of the scalar field Φ that completely characterize a model, and we call them *model functions*. Throughout, we normalize Φ in terms of the reduced Planck mass, $M_{\rm Pl}/(8\pi G)^{1/2} \equiv 1$.

By considering a rescaling of the metric

$$g_{\mu\nu} = e^{2\bar{\gamma}(\bar{\Phi})}\bar{g}_{\mu\nu} \tag{3.102}$$

and a redefinition of the field

$$\Phi = \bar{f}(\bar{\Phi}) \tag{3.103}$$

one can easily verify that the action (3.101) is invariant up to a boundary term, if the model functions transform according to the following relations:

$$\bar{\mathcal{A}}(\bar{\Phi}) = e^{2\bar{\gamma}(\bar{\Phi})}\mathcal{A}\left(\bar{f}(\bar{\Phi})\right), \tag{3.104}$$

$$\bar{\mathcal{B}}(\bar{\Phi}) = e^{2\bar{\gamma}(\bar{\Phi})}\left[(\bar{f}')^2\mathcal{B}\left(\bar{f}(\bar{\Phi})\right) - 6(\bar{\gamma}')^2\mathcal{A}\left(\bar{f}(\bar{\Phi})\right) - 6\bar{\gamma}'\bar{f}'\mathcal{A}'\right], \tag{3.105}$$

$$\bar{\mathcal{V}}(\bar{\Phi}) = e^{4\bar{\gamma}(\bar{\Phi})}\mathcal{V}\left(\bar{f}(\bar{\Phi})\right), \tag{3.106}$$

$$\bar{\sigma}(\bar{\Phi}) = \sigma\left(\bar{f}(\bar{\Phi})\right) + \bar{\gamma}(\bar{\Phi}), \tag{3.107}$$

where a prime indicates differentiation with respect to the argument of the function, e.g. $\bar{\gamma}' := \mathrm{d}\bar{\gamma}(\bar{\Phi})/\mathrm{d}\bar{\Phi}$ and $\mathcal{A}' := \mathrm{d}\mathcal{A}(\Phi)/\mathrm{d}\Phi$, and an overbar denotes quantities which are given in terms of the conformal metric $\bar{g}_{\mu\nu}$.

Now, using the transformations (3.102)-(3.103) one can fix two out of the four arbitrary functions $\{\mathcal{A}, \mathcal{B}, \mathcal{V}, \sigma\}$. Different choices for these functions correspond to different *parametrizations*. For example, the choice

$$\mathcal{A} = F(\phi), \quad \mathcal{B} = 1, \quad \mathcal{V} = \mathcal{V}(\phi), \quad \sigma = 0, \tag{3.108}$$

corresponds to the JF in the Boisseau-Esposito-Farèse-Polarski-Starobinski parametrization [194, 195],

$$S = \frac{1}{2}\int d^4x\sqrt{-g}\left[F(\phi)R - \nabla^\rho\phi\nabla_\rho\phi - 2\mathcal{V}(\phi)\right] + S_m\left(g_{\mu\nu}, \chi\right). \tag{3.109}$$

The choice

$$\mathcal{A} = \Psi, \quad \mathcal{B} = \frac{\omega(\Psi)}{\Psi}, \quad \mathcal{V} = \mathcal{V}(\Psi), \quad \sigma = 0, \tag{3.110}$$

corresponds to the JF in the Brans-Dicke-Bergmann-Wagoner parametrization [196–198],

$$S = \frac{1}{2}\int d^4x\sqrt{-g}\left[\Psi R - \frac{\omega(\Psi)}{\Psi}\nabla^\rho\Psi\nabla_\rho\Psi - 2\mathcal{V}(\Psi)\right] + S_m\left(g_{\mu\nu}, \chi\right). \tag{3.111}$$

Table 3.1: Transformations between frames and parametrizations.

	JF BDBW (Ψ)	JF BEPS (ϕ)	EF canonical (φ)
JF BDBW (Ψ)	Identity	$F(\phi) = \Psi$ $(\frac{d\phi}{d\Psi})^2 = \frac{\omega(\Psi)}{\Psi}$ $(\frac{dF}{d\phi})^2 = \frac{\Psi}{\omega(\Psi)}$	$\alpha(\varphi) = -\frac{1}{2}\ln\Psi$ $(\frac{d\varphi}{d\Psi})^2 = \frac{2\omega(\Psi)+3}{4\Psi^2}$ $(\frac{d\alpha}{d\varphi})^2 = \frac{1}{2\omega(\Psi)+3}$
JF BEPS (ϕ)	$\Psi = F(\phi)$ $\frac{d\Psi}{d\phi} = \frac{dF}{d\phi}$ $\omega(\Psi) = F(\phi)\frac{1}{(\frac{dF}{d\phi})^2}$	Identity	$\alpha(\varphi) = -\frac{1}{2}\ln F(\phi)$ $(\frac{d\varphi}{d\phi})^2 = \frac{3}{4}(\frac{d\ln F(\phi)}{d\phi})^2 + \frac{1}{2F(\phi)}$
EF can (φ)	$\Psi = e^{-2\alpha(\varphi)}$ $(\frac{d\Psi}{d\varphi})^2 = 4e^{-4\alpha(\varphi)}(\frac{d\alpha}{d\varphi})^2$ $\omega(\Psi) = \frac{1}{2}\left(\frac{1}{(\frac{d\alpha}{d\varphi})^2} - 3\right)$	$F(\phi) = e^{-2\alpha(\varphi)}$ $\left(\frac{d\phi}{d\varphi}\right)^2 = 2e^{-2\alpha(\varphi)}\left(1 - 3\left(\frac{d\alpha}{d\varphi}\right)^2\right)$ $(\frac{dF}{d\phi})^2 = \frac{2e^{-2\alpha(\varphi)}\left(\frac{d\alpha}{d\varphi}\right)^2}{1-3\left(\frac{d\alpha}{d\varphi}\right)^2}$	Identity

Finally, the choice

$$\mathcal{A} = 1, \quad \mathcal{B} = 2, \quad \mathcal{V} = \mathcal{V}(\varphi), \quad \sigma = \sigma(\varphi), \tag{3.112}$$

represents the EF in the canonical parametrization [196–199]

$$S = \frac{1}{2}\int d^4x\sqrt{-g}\left[R - 2g^{\mu\nu}\,\nabla_\mu\varphi\nabla_\nu\varphi - 2\,\mathcal{V}(\varphi)\right] + S_m\left(e^{2\sigma(\varphi)}g_{\mu\nu}, \chi\right). \tag{3.113}$$

The transformations between these frames and parametrizations are shown in Table 3.1.

3.3.2 The Frame Controversy

Generally, when studying scalar-tensor theories, authors adhere to three viewpoints regarding which frame is best suited to describe the physical world (see [2] for a nice discussion on the topic):

1. the Jordan frame is physical while the Einstein one is unphysical
2. the Einstein frame is physical while the Jordan one is unphysical
3. the Jordan and Einstein frames are physically equivalent

Here the term "physical" indicates a theory that is theoretically consistent and makes predictions for the values of some observables which can, at least in principle, be measured by macroscopic experiments [176].

Proponents of the first viewpoint dismiss the Einstein frame as it lacks the physical motivation of the Jordan frame. Non-minimally coupled Lagrangians arise in many extended theories of gravity and string theories. In the Jordan frame, massive particles follow time-like geodesics and the Weak Equivalence Principle is satisfied. In the Einstein frame, on the other hand, the coupling of the scalar field to matter acts as a fifth force and the particles deviate from geodesic motion. At the quantum level, however, even the Jordan frame seems to violate the Equivalence Principle [200]. This means that the Equivalence Principle is not sufficient to discriminate between conformally related frames[6].

Proponents of the second viewpoint purport that the Jordan frame leads to a negative definite or indefinite kinetic energy for the scalar field, while the energy density is positive definite in the Einstein frame. This means that the theory in the Jordan frame does not have a stable ground state and that the system decays into a lower energy state *ad infinitum* (violation of the weak energy condition). The weak energy condition is satisfied if $T_{ab}t^a t^b \geq 0$ for all time-like vectors t^a or, for the fluid $T_{ab} = (\rho + P)\, u_a u_b + P g_{ab}$, we have $\rho \geq 0$ and $\rho + P \geq 0$. However, as pointed out in [178], there is no physical observable that corresponds to the sign of $T_{ab}t^a t^b$ for all time-like vectors t^a. Therefore, there is no inconsistency between the two frames that can be measured.

Proponents of the third viewpoint conform to Dicke's view [199] who claims that the two frames are equivalent, as long as the units of mass, length, time, and all quantities derived from them scale with appropriate powers of the conformal factor in the Einstein frame. In this sense, the two conformally related frames are just different *representations* of the same theory, analogous to different gauges of a gauge theory.

A way to circumvent the frame issue altogether is to do calculations with frame-independent quantities and express the cosmological observables in a manifestly invariant way (see Refs. [201–207]). We will explore this approach in the context of scalar-tensor theories when we study higher-order corrections to the inflationary observables in Chapter 9.

3.3.3 Equations of motion

The equations of motion can be obtained by varying the action (3.101) while considering $g^{\mu\nu}$, Φ and χ to be the dynamical fields. The variation takes the form

$$\begin{aligned}\delta S = \frac{1}{2}\int \mathrm{d}^4x\sqrt{-g}\left\{E^{(g)}_{\mu\nu}\delta g^{\mu\nu} + E^{(\Phi)}\delta\Phi + 2\mathrm{e}^{4\sigma}E^{(\chi)}\delta\chi\right\} \\ + \frac{1}{2}\int \mathrm{d}^4x\,\partial_\sigma\left(\sqrt{-g}\left[\mathscr{B}^{\rho}_{(g)} + \mathscr{B}^{\sigma}_{(\Phi)} + 2\mathrm{e}^{4\sigma}\mathscr{B}^{\rho}_{(\chi)}\right]\right)\,,\end{aligned} \tag{3.114}$$

where

$$\sqrt{-g}\,\mathscr{B}^{\rho}_{(g)} = \sqrt{-g}\left\{\mathcal{A}g_{\mu\nu}g^{\rho\lambda}\nabla_\lambda\delta g^{\mu\nu} - \mathcal{A}\nabla_\mu\delta g^{\rho\mu} - g^{\rho\lambda}\left(\nabla_\lambda\mathcal{A}\right)g_{\mu\nu}\,\delta g^{\mu\nu} + \left(\nabla_\mu\mathcal{A}\right)\delta g^{\mu\rho}\right\}\,, \tag{3.115}$$

$$\sqrt{-g}\,\mathscr{B}^{\rho}_{(\Phi)} = -\sqrt{-g}\,2\mathcal{B}g^{\rho\mu}\left(\nabla_\mu\Phi\right)\delta\Phi \tag{3.116}$$

and $\sqrt{-g}\,\mathrm{e}^{4\sigma}\mathscr{B}^{\rho}_{(\chi)}$ are the boundary terms arising from varying the action with respect to the metric tensor $g^{\mu\nu}$, the scalar field Φ, and the matter fields respectively. The boundary terms do not give

[6] In Ref. [170] the authors calculate the one-loop divergences in both frames and find that they coincide on shell but not off shell.

a contribution to the equations of motion, but we have nevertheless presented them here for completeness. Using the least action principle $\delta S = 0$, we arrive at the following equations of motion:

$$\begin{aligned} E^{(g)}_{\mu\nu} :=& \mathcal{A}\left(R_{\mu\nu} - \frac{1}{2}g_{\mu\nu}R\right) + \left(\frac{1}{2}\mathcal{B} + \mathcal{A}''\right) g_{\mu\nu}g^{\rho\sigma}\nabla_\rho\Phi\nabla_\sigma\Phi - \left(\mathcal{B} + \mathcal{A}''\right)\nabla_\mu\Phi\nabla_\nu\Phi \\ &+ \mathcal{A}'\left(g_{\mu\nu}\Box\Phi - \nabla_\mu\nabla_\nu\Phi\right) + g_{\mu\nu}\mathcal{V} - T_{\mu\nu} = 0\,, \end{aligned} \tag{3.117}$$

$$E^{(\Phi)} := R\mathcal{A}' + \mathcal{B}'g^{\mu\nu}\nabla_\mu\Phi\nabla_\nu\Phi + 2\mathcal{B}\Box\Phi - 2\mathcal{V}' + 2\sigma' T = 0\,, \tag{3.118}$$

$$E^{(\chi)}_A := E^{(\chi)}_A\left[\mathrm{e}^{2\sigma}g_{\mu\nu}, \chi^C\right] = 0\,. \tag{3.119}$$

Here, the matter energy-momentum tensor is

$$T_{\mu\nu} \equiv -\frac{2}{\sqrt{-g}}\frac{\delta S_{\mathrm{m}}}{\delta g^{\mu\nu}}\,, \tag{3.120}$$

while $T := g^{\mu\nu}T_{\mu\nu}$ is its trace and $\Box := g^{\mu\nu}\nabla_\mu\nabla_\nu$. In this thesis, we will not be interested in the equations of motion for the matter fields χ. Nevertheless, we have included them here in order to make it clear that matter fields "feel" the geometry determined by $\hat{g}_{\mu\nu} := \mathrm{e}^{2\alpha}g_{\mu\nu}$. This means that freely falling material objects follow the corresponding geodesics. Therefore, if we perform an experiment in order to measure the geometry determined by $g_{\mu\nu}$ using reference objects built out of the matter fields, we must also make use of the relevant correction factors.

The Ricci scalar in (3.117) can be eliminated by making use of a contraction with the metric, viz.,

$$g^{\mu\nu}E^{(g)}_{\mu\nu} := -\mathcal{A}R + \mathcal{B}g^{\mu\nu}\nabla_\mu\Phi\nabla_\nu\Phi + 3\mathcal{A}''g^{\mu\nu}\nabla_\mu\Phi\nabla_\nu\Phi + 3\mathcal{A}'\Box\Phi + 4\mathcal{V} - T = 0\,. \tag{3.121}$$

In this way, we can obtain an equation of motion that describes the propagation of the scalar field Φ and does not contain the second derivatives of the metric tensor $g_{\mu\nu}$. We find

$$\frac{2\mathcal{A}\mathcal{B}+3\left(\mathcal{A}'\right)^2}{\mathcal{A}}\Box\Phi + \frac{\left(2\mathcal{A}\mathcal{B}+3\left(\mathcal{A}'\right)^2\right)'}{2\mathcal{A}}g^{\mu\nu}\nabla_\mu\Phi\nabla_\nu\Phi - \frac{2\left(\mathcal{A}\mathcal{V}'-2\mathcal{V}\mathcal{A}'\right)}{\mathcal{A}} + \frac{2\mathcal{A}\sigma'-\mathcal{A}'}{\mathcal{A}}T = 0\,. \tag{3.122}$$

Finally, combining (3.118) and the covariant divergence of the tensor equation (3.117) results in

$$E^{(c)}_\nu := \nabla^\mu E^{(g)}_{\mu\nu} + \frac{1}{2}E^{(\Phi)}\nabla_\nu\Phi = -\nabla^\mu T_{\mu\nu} + \sigma' T\nabla_\nu\Phi = 0\,, \tag{3.123}$$

which is the well known continuity equation.

In the case of a FLRW metric, Eqs. (3.117), (3.122) and (3.123) become

$$H^2 = -\frac{\mathcal{A}'}{\mathcal{A}}H\dot{\Phi} + \frac{\mathcal{B}}{6\mathcal{A}}\dot{\Phi}^2 + \frac{1}{3\mathcal{A}}\mathcal{V} + \frac{1}{3\mathcal{A}}\rho - \frac{\mathcal{K}}{a^2}\,, \tag{3.124}$$

$$2\dot{H}+3H^2 = -2\frac{\mathcal{A}'}{\mathcal{A}}H\dot{\Phi} - \left(\frac{\mathcal{B}}{2\mathcal{A}} + \frac{\mathcal{A}''}{\mathcal{A}}\right)\dot{\Phi}^2 - \frac{\mathcal{A}'}{\mathcal{A}}\ddot{\Phi} + \frac{1}{\mathcal{A}}\mathcal{V} - \frac{1}{\mathcal{A}}P - \frac{\mathcal{K}}{a^2}\,, \tag{3.125}$$

$$\ddot{\Phi} = -3H\dot{\Phi} - \frac{1}{2}\frac{\left(2\mathcal{A}\mathcal{B}+3(\mathcal{A}')^2\right)'}{\left(2\mathcal{A}\mathcal{B}+3(\mathcal{A}')^2\right)}\dot{\Phi}^2 - 2\frac{\mathcal{A}\mathcal{V}'-2\mathcal{V}\mathcal{A}'}{2\mathcal{A}\mathcal{B}+3(\mathcal{A}')^2} - \frac{\left(2\mathcal{A}\sigma'-\mathcal{A}'\right)}{2\mathcal{A}\mathcal{B}+3(\mathcal{A}')^2}\left(\rho - 3P\right)\,, \tag{3.126}$$

$$\dot{\rho} = -3H\left(\rho + P\right) + \sigma'\left(\rho - 3P\right)\dot{\Phi}\,. \tag{3.127}$$

Note that for $\mathcal{A} = $ const. and $\sigma = 0$ the above equations reduce to the corresponding ones derived in Chapter 2 for the case of a minimally coupled scalar field, as expected.

3.3.4 Inflationary Observables

Perturbations in the context of scalar-tensor theories were originally studied by Hwang et al. [208–215]. They can be treated in the same way as in the minimal case. The comoving curvature perturbation $\mathcal{R}$ and the two polarizations of the gravitational waves satisfy in Fourier space the following equations [216]:

$$\frac{1}{a^3 Q_{\mathcal{R}}}\frac{d}{dt}\left(a^3 Q_{\mathcal{R}}\dot{\mathcal{R}}\right) + \frac{k^2\mathcal{R}}{a^2} = 0\,, \tag{3.128}$$

$$\frac{1}{a^3 Q_T}\frac{d}{dt}\left(a^3 Q_T\dot{h}_{+,\times}\right) + \frac{k^2 h_{+,\times}}{a^2} = 0\,, \tag{3.129}$$

where the quantities $Q_{\mathcal{R}}$ and Q_T are given by

$$Q_{\mathcal{R}} = \frac{\mathcal{B}\dot{\Phi}^2 + \frac{3\dot{\mathcal{A}}^2}{2\mathcal{A}}}{\left(H + \frac{\dot{\mathcal{A}}}{2\mathcal{A}}\right)^2} =: \frac{\dot{\Phi}^2}{H^2}Z_{\mathcal{R}}\,, \qquad Q_T = \mathcal{A} =: Z_T\,. \tag{3.130}$$

Here, we have also defined $Z_{\mathcal{R}}$ and Z_T as

$$Z_{\mathcal{R}} := \frac{k + \frac{3\dot{f}^2}{2f\dot{\varphi}^2}}{\left(1 + \frac{\dot{f}}{2Hf}\right)^2}\,, \qquad Z_T := \frac{f}{M_{\rm Pl}^2}\,. \tag{3.131}$$

Note that in the Einstein frame in the canonical parametrization with $\mathcal{A} = 1$ $(= M_{\rm Pl})$ and $\mathcal{B} = 1$, we have $Z_{\mathcal{R}} = Z_T = 1$. Next, further defining

$$z_{\mathcal{R}} := a\sqrt{Q_{\mathcal{R}}}\,, \qquad v_{\mathcal{R}} := z_{\mathcal{R}}\mathcal{R}\,, \tag{3.132}$$

and

$$z_T := a\sqrt{Q_T}\,, \qquad v_T := z_T h_{+,\times}\,, \tag{3.133}$$

the Mukhanov-Sasaki equations (3.128) and (3.129) can be written as

$$\frac{d^2 v_{\mathcal{R},k}}{d\tau^2} + \left(k^2 - \frac{1}{z_{\mathcal{R}}}\frac{d^2 z_{\mathcal{R}}}{d\tau^2}\right)v_{\mathcal{R},k} = 0\,, \tag{3.134}$$

$$\frac{d^2 v_{T,k}}{d\tau^2} + \left(k^2 - \frac{1}{z_T}\frac{d^2 z_T}{d\tau^2}\right)v_{T,k} = 0\,. \tag{3.135}$$

These are usually solved in the de Sitter limit $\tau = -1/(aH)$ and one finally obtains for the scalar and tensor spectral indices, as well as the tensor-to-scalar ratio [2, 211, 215]

$$n_S = 1 + 2\left(2\epsilon_1 - \epsilon_2 + \epsilon_3 - \epsilon_4\right)\,, \tag{3.136}$$

$$n_T = 2\left(\epsilon_1 - \epsilon_3\right)\,, \tag{3.137}$$

$$r = -16\left(\epsilon_1 - \epsilon_3\right)\,, \tag{3.138}$$

with

$$\epsilon_1 := \frac{\dot{H}}{H^2} = -\epsilon_H\,, \tag{3.139}$$

$$\epsilon_2 := \frac{\ddot{\Phi}}{H\dot{\Phi}} = -\eta_H\,, \tag{3.140}$$

$$\epsilon_3 := \frac{\dot{\mathcal{A}}}{2H\mathcal{A}}\,, \tag{3.141}$$

$$\epsilon_4 := \frac{\dot{E}}{2HE}\,, \tag{3.142}$$

where

$$E = \mathcal{A}\left[\mathcal{B} + \frac{3\left(\dot{\mathcal{A}}\right)^2}{2\mathcal{A}\left(\dot{\Phi}\right)^2}\right]\,. \tag{3.143}$$

Note that the first order consistency relation $n_T = -8r$ holds true in the case of scalar-tensor theories as well.

Chapter 4

The Standard Model of Particle Physics and Beyond

The Standard Model (SM) of particle physics [217–219] is a renormalizable quantum field theory that describes all known elementary particles and their gauge interactions (excluding gravity). For over forty years it has passed every experimental test. The discovery [220, 221] of the Higgs boson [222–225] in 2012 by LHC at CERN, unveiled the last missing piece of the puzzle.

The SM is based on the symmetry group $G_{\rm SM} = SU(3)_C \times SU(2)_L \times U(1)_Y$. The $SU(3)_C$ group is associated with the theory of quantum chromodynamics (QCD), a non-Abelian gauge theory which describes the strong interactions between quarks and gluons, while $SU(2)_L \times U(1)_Y$ describes the electroweak (EW) interactions between quarks, leptons, electroweak gauge bosons ($W^{1,2,3}$ and B) and the Higgs boson. By means of the Higgs mechanism (to be detailed below), the EW gauge symmetry gets spontaneously broken into the electromagnetic $U(1)_{\rm EM}$ around the 100 GeV scale. In this way, fermions obtain their masses through Yukawa interactions with the Higgs, while Higgs-kinetic terms lead to new massive eigenstates for three of the electroweak gauge bosons (now denoted as $W^{\pm}$ and Z), while one eigenstate remains massless and is identified with the photon γ (or the A gauge field).

Quarks are fundamental constituents of matter of spin-1/2 but are never found in isolation in Nature due to their asymptotic freedom at low energies. They are thus confined to form hadrons (composed of three quarks) such as protons and neutrons and also mesons (composed of a quark and an anti-quark) such as pions and kaons. There are six types of quarks, also known as flavors: up, down, charm, strange, top, bottom, arranged into three generations or families due to their quantum numbers under the SM gauge group. Gluons have spin-1 and are the force carriers of the strong interactions. They are what “glues" quarks together into composite particles.

Apart from quarks, matter also consists of leptons which have spin-1/2 too but are color-neutral (or transform as singlets) under $SU(3)_C$. Just as quarks, they are categorized into three families, with the electron and its corresponding neutrino making up the first. The electron, muon and tau are electrically charged, while neutrinos are not. Neutrinos are also massless in the SM. Nevertheless, oscillations between them suggest [226–233] that they indeed have masses, albeit small. This is the first indication that the SM needs to be extended.

All of the particles of the SM and their quantum numbers under the $G_{\rm SM}$ and $U(1)_{\rm EM}$ are collectively shown in Table 4.1.

Table 4.1: Properties of the elementary particles of the Standard Model [234].

name	symbol	spin	charge	T_3	dim $[G_{\text{SM}}]$	mass
electron R	e^-	$1/2$	-1	0	$(1,1,-1)$	0.511 MeV
electron L	e^-	$1/2$	-1	$-1/2$	$(1,2,-1/2)$	0.511 MeV
e-neutrino L	ν_e	$1/2$	0	$+1/2$	$(1,2,-1/2)$	< 2 eV
muon R	μ	$1/2$	-1	0	$(1,1,-1)$	105.66 MeV
muon L	μ	$1/2$	-1	$-1/2$	$(1,2,-1/2)$	105.66 MeV
μ-neutrino L	ν_μ	$1/2$	0	$+1/2$	$(1,2,-1/2)$	< 0.19 MeV
tau R	τ	$1/2$	-1	0	$(1,1,-1)$	1776.86 MeV
tau L	τ	$1/2$	-1	$-1/2$	$(1,2,-1/2)$	1776.86 MeV
τ-neutrino L	ν_τ	$1/2$	0	$+1/2$	$(1,1,-1/2)$	< 18.2 MeV
down-quark R	d	$1/2$	$-1/3$	0	$(3,1,-1/3)$	4.7 MeV
down-quark L	d	$1/2$	$-1/3$	$-1/2$	$(3,2,1/6)$	4.7 MeV
up-quark R	u	$1/2$	$2/3$	0	$(3,1,2/3)$	2.2 MeV
up-quark L	u	$1/2$	$2/3$	$+1/2$	$(3,2,1/6)$	2.2 MeV
strange-quark R	s	$1/2$	$-1/3$	0	$(3,1,-1/3)$	94.6 MeV
strange-quark L	s	$1/2$	$-1/3$	$-1/2$	$(3,2,1/6)$	94.6 MeV
charm-quark R	c	$1/2$	$2/3$	0	$(3,1,2/3)$	1.28 GeV
charm-quark L	c	$1/2$	$2/3$	$+1/2$	$(3,2,1/6)$	1.28 GeV
bottom-quark R	b	$1/2$	$-1/3$	0	$(3,1,-1/3)$	4.18 GeV
bottom-quark L	b	$1/2$	$-1/3$	$-1/2$	$(3,1,1/6)$	4.18 GeV
top-quark R	t	$1/2$	$2/3$	0	$(3,1,2/3)$	173.1 GeV
top-quark L	t	$1/2$	$2/3$	$+1/2$	$(3,1,1/6)$	173.1 GeV
gluons	G^α_μ	1	0	0	$(8,1,0)$	0
photon	γ	1	0			$< 10^{-18}$ eV
W^+-boson	W^+	1	$+1$			80.385 GeV
W^--boson	W^-	1	-1			80.385 GeV
Z-boson	Z^0	1	0			91.1876 GeV
Higgs boson	h	0	0			125.09 GeV

4.1 The Standard Model Lagrangian

The SM Lagrangian can be schematically split into different parts: the gauge sector $\mathcal{L}_G$, the fermion sector $\mathcal{L}_F$, the Higgs sector $\mathcal{L}_H$, and the Yukawa sector $\mathcal{L}_Y$[1]. We have

$$\mathcal{L}_{\text{SM}} = \mathcal{L}_G + \mathcal{L}_F + \mathcal{L}_H + \mathcal{L}_Y \,. \tag{4.1}$$

Gauge sector

The first term in the right-hand side of (4.1) is the kinetic term of the gauge fields of the $SU(3)_C \times SU(2)_L \times U(1)_Y$ gauge symmetry

$$\mathcal{L}_G = -\frac{1}{4}\sum_{A=1}^{8} G^{A,\mu\nu} G_{A,\mu\nu} - \frac{1}{4}\sum_{a=1}^{3} W^{a,\mu\nu} W_{a,\mu\nu} - \frac{1}{4} B^{\mu\nu} B_{\mu\nu} \,, \tag{4.2}$$

[1] We have omitted the gauge-fixing and ghost sectors for simplicity.

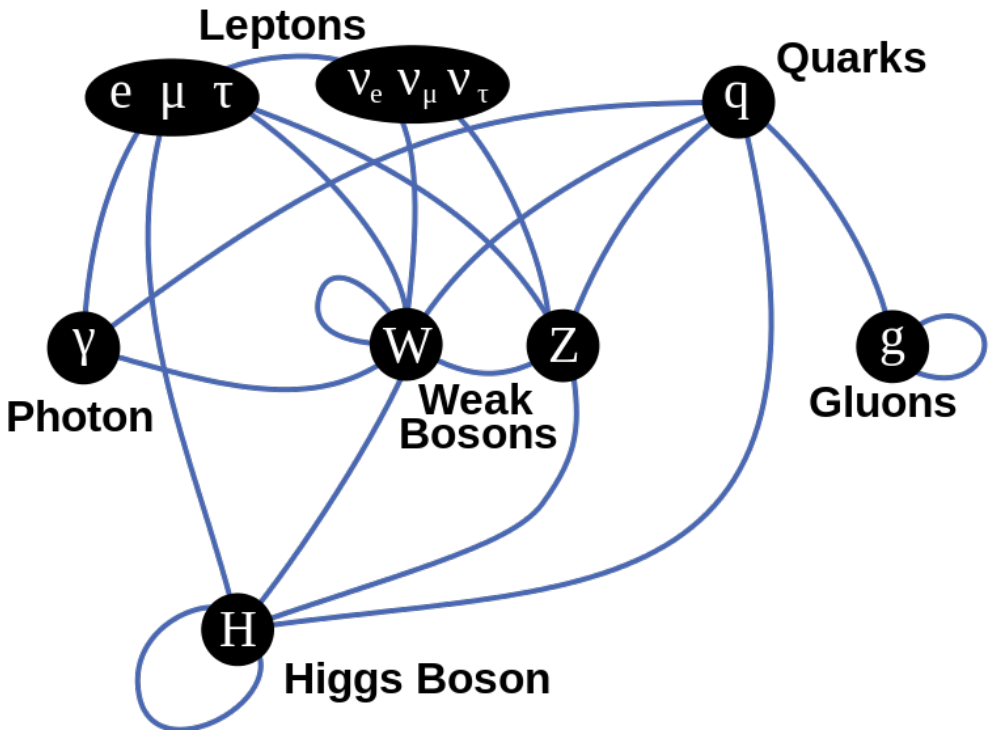

Figure 4.1: A schematic representation of the interactions between the Standard Model particles at tree level.

where $G^{A,\mu\nu}$, $W^{a,\mu\nu}$, and $B^{\mu\nu}$ are the field tensors of the corresponding gauge fields

$$SU(3): \quad G^{A,\mu\nu} = \partial^\mu G^{A,\nu} - \partial_\nu G^{A,\mu} + g_3 f^{ABC} G^{B,\mu} G^{C,\nu}\,, \tag{4.3}$$

$$SU(2): \quad W^{a,\mu\nu} = \partial^\mu W^{a,\nu} - \partial_\nu W^{a,\mu} + g_2 \epsilon^{abc} W^{b,\mu} W^{c,\nu}\,, \tag{4.4}$$

$$U(1): \quad B^{\mu\nu} = \partial^\mu B^\nu - \partial^\nu B^\mu\,. \tag{4.5}$$

g_3, g_2 and $g_1 := \sqrt{\frac{5}{3}} g_Y$ are the gauge coupling constants of $SU(3)_C$, $SU(2)_L$ and $U(1)_Y$, respectively. f^{ABC} and ϵ^{abc} are the totally antisymmetric structure constants of $SU(3)$ and $SU(2)$, respectively. They are defined by the commutation relations between the group generators t^a and T^A, with $a = 1\ldots3$ and $A = 1\ldots8$,

$$SU(2): \quad \left[t^a, t^b\right] = i\epsilon^{abc} t^c\,, \tag{4.6}$$

$$SU(3): \quad \left[T^A, T^B\right] = i f^{ABC} T^C\,, \tag{4.7}$$

where the $SU(2)$ generators are related to the Pauli matrices as $t^a = \sigma^a/2$ and the $SU(3)$ generators are related to the Gell-Mann matrices as $T^A = \lambda^A/2$.

Fermion sector

The fermion sector of the SM Lagrangian contains the fermions and the gauge bosons by means of the gauge covariant derivative. A striking feature of the weak interactions, discovered in the 1950s, is that they violate parity. Therefore, the charged weak gauge bosons only couple to quarks and leptons with left-handed chirality. Then, under weak isospin $SU(2)$ the left-handed particles

transform as doublets, whereas the right-handed ones transform as singlets

$$L_L = \begin{pmatrix} \nu_{e\,L} \\ e_L \end{pmatrix}, \quad Q_L = \begin{pmatrix} u_L \\ d_L \end{pmatrix}, \quad L_{R,e} = e_R\,, \quad Q_{R,u} = u_R\,, \quad Q_{R,d} = d_R\,. \tag{4.8}$$

The Lagrangian term reads

$$\mathcal{L}_F = Q^\dagger_{L_i} i\bar{\sigma}_\mu D^\mu Q_{L_i} + u^\dagger_{R_i} i\sigma_\mu D^\mu u_{R_i} + d^\dagger_{R_i} i\sigma_\mu D^\mu d_{R_i} + L^\dagger_{L_i} i\bar{\sigma}_\mu D^\mu L_{L_i} + e^\dagger_{R_i} i\sigma_\mu D^\mu e_{R_i}\,, \tag{4.9}$$

where $\sigma_\mu = (\mathbb{1}, \sigma_i)$ and $\bar{\sigma} = (\mathbb{1}, -\sigma_i)$. Also, the flavour index $i = 1 \ldots 3$ runs through the three families of quarks and leptons and we have omitted the colour indices for brevity. The covariant derivative is given by

$$D^\mu = \partial^\mu - ig_3\theta_S G^{\mu,A} T^A - ig_2\theta_W W^{\mu,a} t^a - ig_Y Y B^\mu\,, \tag{4.10}$$

where $\theta_S = 0, 1$ for singlets or triplets of $SU(3)_C$ and $\theta_W = 0, 1$ for singlets or doublets of $SU(2)_L$. Moreover, Y is the weak hypercharge, which along with the third component of weak isospin T_3 give the electric charge Q as

$$Q = T_3 + Y\,. \tag{4.11}$$

Higgs sector

The Higgs part of the Lagrangian contains all the terms that generate the spontaneous symmetry breaking (SSB) of $SU(2)_L \times U(1)_Y$ down to $U(1)_{\text{EM}}$ that results in some of the gauge bosons and chiral fermions acquiring their masses. In order for SSB to occur, we introduce a complex scalar doublet H, known as the *Higgs field*, which acquires a non-zero vacuum expectation value (VEV)

$$\langle 0|H|0\rangle =: \langle H\rangle = \frac{1}{\sqrt{2}} \begin{pmatrix} 0 \\ v_h \end{pmatrix}. \tag{4.12}$$

The Higgs Lagrangian has the form

$$\mathcal{L}_H = \left(D^\mu H\right)^\dagger \left(D_\mu H\right) - V\left(H\right), \tag{4.13}$$

with the covariant derivative $D^\mu = \partial^\mu - ig_2 W^{\mu,a} t^a - ig_Y Y_h B^\mu$. The Higgs potential $V(H)$ has the form

$$V\left(H\right) = -\mu_h^2 H^\dagger H + \lambda_h \left(H^\dagger H\right)^2, \tag{4.14}$$

where μ_h^2 is the Higgs mass term and λ_h is the Higgs self-coupling. For $\mu_h^2 > 0$ and $\lambda > 0$ the Higgs potential has a non-trivial minimum, $v_h = \sqrt{\frac{\mu_h^2}{\lambda_h}}$, which breaks the symmetry. Then we can study the theory around the symmetry-breaking minimum. The Higgs doublet becomes

$$H = \begin{pmatrix} \phi^+ \\ \phi^0 = \frac{1}{\sqrt{2}}\left(v_h + h + i\chi\right), \end{pmatrix} \tag{4.15}$$

where ϕ^+ and ϕ^0 are complex fields containing 4 degrees of freedom in total. In the unitary gauge,

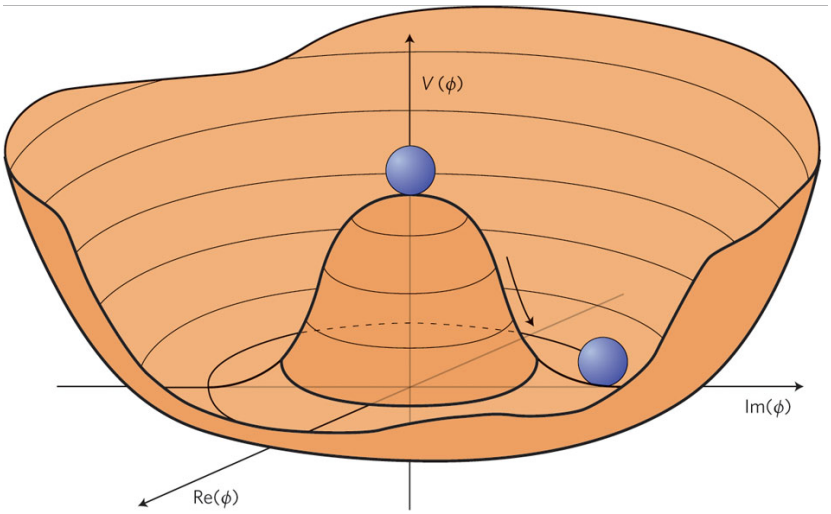

Figure 4.2: Shape of the Higgs potential that leads to spontaneous symmetry breaking. Credit: [235]

the Higgs potential (4.13) contains the terms

$$V \supset \mu_h^2 h^2 + \lambda_h v_h h^3 + \frac{1}{4}\lambda_h h^4 \tag{4.16}$$

$$= \frac{1}{2}M_h^2 h^2 + \sqrt{\frac{\lambda_h}{2}} M_h h^3 + \frac{1}{4}\lambda_h h^4 \,, \tag{4.17}$$

where we introduced the Higgs boson mass

$$M_h^2 := 2\mu_h^2 = 2\lambda_h v_h^2 \,. \tag{4.18}$$

Moving on, the term relevant for the gauge boson masses is successively written as

$$\begin{aligned}
\mathcal{L}_{H,\text{bilinear}} &= \frac{1}{8}\left| \begin{pmatrix} g_2 W_\mu^3 + g_1 B_\mu & g_2\sqrt{2}W_\mu^+ \\ g_2\sqrt{2}W_\mu^- & -g_2 W_\mu^3 + g_Y B_\mu \end{pmatrix} \begin{pmatrix} 0 \\ v_h \end{pmatrix} \right|^2 \\
&= \frac{g_2^2 v_h^2}{4} W_\mu^+ W^{\mu -} + \frac{v_h^2}{8} \begin{pmatrix} W_\mu^3 & B_\mu \end{pmatrix} \begin{pmatrix} g_2^2 & -g_2 g_Y \\ -g_2 g_Y & g_Y^2 \end{pmatrix} \begin{pmatrix} W^{3,\mu} \\ B^\mu \end{pmatrix} \\
&= \frac{g_2^2 v_h^2}{4} W_\mu^+ W^{\mu -} + \frac{v_h^2}{8} \begin{pmatrix} Z_\mu & A_\mu \end{pmatrix} \begin{pmatrix} g_2^2 + g_Y^2 & 0 \\ 0 & 0 \end{pmatrix} \begin{pmatrix} Z^\mu \\ A^\mu \end{pmatrix} ,
\end{aligned} \tag{4.19}$$

where we defined $W_\mu^\pm = \frac{1}{\sqrt{2}}\left(W_\mu^1 \mp i W_\mu^2\right)$. In the last line above we performed a diagonalization of the mass matrix of the eigenstates Z_μ and A_μ

$$\begin{pmatrix} Z_\mu \\ A_\mu \end{pmatrix} = \begin{pmatrix} \cos\theta_W & -\sin\theta_W \\ \sin\theta_W & \cos\theta_W \end{pmatrix} \begin{pmatrix} W_\mu^3 \\ B_\mu \end{pmatrix} , \tag{4.20}$$

with the help of the Weinberg angle θ_W given by

$$\cos\theta_W = \frac{g_2}{\sqrt{g_2^2 + g_Y^2}} \quad \text{and} \quad \sin\theta_W = \frac{g_Y}{\sqrt{g_2^2 + g_Y^2}} \,. \tag{4.21}$$

From (4.19) we can read off the masses of the electroweak gauge bosons

$$M_W^2 = \frac{1}{4} g_2^2 v_h^2 , \quad M_Z^2 = \frac{1}{4} \left(g_2^2 + g_Y^2 \right) v_h^2 , \quad \text{and} \quad M_A = 0 . \tag{4.22}$$

The massless field A_μ is identified with the photon. Note that we started with four massless gauge bosons (each containing two degrees of freedom) and we ended up with one massless gauge boson and three massive ones (each containing three degrees of freedom). The three new degrees of freedom correspond to the three would-be Goldstone bosons of the Higgs doublet which were “eaten away" by the gauge bosons.

Yukawa sector

Mass terms for the fermions are generated by coupling the Higgs doublet with left-handed and right-handed fermion fields in gauge-invariant combinations. The terms allowed by gauge and Lorentz invariance are

$$\mathcal{L}_Y = - \sum_{i=1}^{3} Y_{ij}^u Q_{L_i}^\dagger \left(i \sigma_2 H^* \right) u_{R_j} - \sum_{i=1}^{3} Y_{ij}^d Q_{L_i}^\dagger H d_{R_j} - \sum_{i=1}^{3} Y_{ij}^e L_{L_i}^\dagger H e_{R_j} + \text{H.c.} , \tag{4.23}$$

where the Yukawa matrices $Y_{ij}^{u,d,e}$ are 3×3 complex-valued matrices. We can diagonalize them and define the real mass eigenstates through unitary transformations

$$Y_{\text{diag}}^u = V_L^u Y^u V_L^{u\dagger} , \quad Y_{\text{diag}}^d = V_L^d Y^d V_L^{d\dagger} , \quad Y_{\text{diag}}^e = V_L^e Y^e V_L^{e\dagger} . \tag{4.24}$$

Then, by expanding the Higgs field around its VEV we obtain the mass matrices

$$M_u = \frac{v_h}{\sqrt{2}} Y_{\text{diag}}^u = \text{diag} \left(M_u, M_c, M_t \right) \tag{4.25}$$

$$M_d = \frac{v_h}{\sqrt{2}} Y_{\text{diag}}^d = \text{diag} \left(M_d, M_s, M_b \right) \tag{4.26}$$

$$M_e = \frac{v_h}{\sqrt{2}} Y_{\text{diag}}^e = \text{diag} \left(M_e, M_\mu, M_\tau \right) \tag{4.27}$$

Note that in (4.23), neutrinos have no right-handed components and therefore remain massless.

Electroweak Precision Observables

The predictions of the Standard Model Lagrangian have been probed with very high accuracy in particle accelerators such as LEP and TEVATRON, and most recently LHC. For the electroweak sector, in particular, one needs only three input parameters in order to compare the theoretical predictions of the SM with the experimental data: the mass of the Z boson determined by LEP1 [236], the fine-structure constant α_{em} extracted from measurements of the anomalous magnetic moment of the electron (see [237] and references therein), and the Fermi constant G_F determined from the muon lifetime [238]:

$$M_Z = 91.1876 \pm 0.0021 \, \text{GeV} , \tag{4.28}$$

$$\alpha_{\text{em}}^{-1} = 137.035999139(31) , \tag{4.29}$$

$$G_F = 1.1663787(6) \times 10^{-5} \, \text{GeV}^{-2} . \tag{4.30}$$

Using these three inputs, one can predict with high precision all the other observables of the electroweak sector. One could also use them to parametrize and constrain new Physics effects via the so-called “oblique parameters" introduced in [239–242].

Let us write the vacuum polarization amplitudes of the EW gauge fields, i.e. the quadratic part of the effective Lagrangian, after EW symmetry breaking as

$$\mathcal{L}^{(2)}_{\text{eff}} = -\frac{1}{2}W^3\Pi_{33}(q^2)W^3 - \frac{1}{2}B\Pi_{00}(q^2)B - W^3\Pi_{30}(q^2)B - W^+\Pi_{WW}(q^2)W^-\,, \tag{4.31}$$

where the Lorentz indices have been contracted with $q_\mu q_\nu/q^2 - g_{\mu\nu}$. Since this is an effective low-energy action, it does not explicitly depend on any high-energy completion of the SM. The functions Π_{ij}, however, obtain corrections from loops involving both the SM and possibly new Physics degrees of freedom. Expanding the polarization amplitudes in (4.31) for small momenta up to $\mathcal{O}(q^2)$, one ends up with 8 independent quantities $\Pi(0)$ and $\Pi'(0)$. Specifically, $\Pi'_{WW}(0)$ and $\Pi'_{00}(0)$ fix the value of the coupling constants g_2 and g_Y. Also, $\Pi_{ZZ}(0)$ fixes the VEV v_h through the mass of the Z boson. Furthermore, for the photon to be massless, we need $\Pi_{\gamma\gamma}(0) = \Pi_{\gamma Z}(0) = 0$. The rest three independent physical quantities are paremetrized as

$$\hat{S} = \frac{g_2}{g_Y}\Pi'_{30}(0) = \frac{\alpha_{\text{em}}}{4\sin^2\theta_W}S\,, \tag{4.32}$$

$$\hat{T} = \frac{\Pi_{33}(0) - \Pi_{WW}(0)}{M_W^2} = \alpha_{\text{em}}T\,, \tag{4.33}$$

$$\hat{U} = \Pi'_{33}(0) - \Pi'_{WW}(0)\,. \tag{4.34}$$

The parameter T essentially describes the difference between the new Physics contributions of neutral and charged current processes at low energies while S (and U) measure new Physics contributions to neutral (charged) current processes at different energy scales. The measured values for the STU parameters are [243]

$$S = -0.03 \pm 0.10\,, \tag{4.35}$$

$$T = 0.01 \pm 0.12\,, \quad \text{where} \quad M_h = 125.5 \pm 0.4\,\text{GeV}\,, \tag{4.36}$$

$$U = 0.05 \pm 0.10\,, \tag{4.37}$$

and are in excellent agreement with the SM values of zero.

4.2 Shortcomings of the Standard Model

Since its inception, the SM has been remarkably successful. Numerous experiments have validated its predictions for over forty years. Nevertheless, there are some phenomena that cannot be explained by it. Also, the SM has a few theoretical inconsistencies of its own. These considerations have led to the development of physics beyond the Standard Model (BSM). After the discovery of the Higgs boson in 2012, the LHC has now shifted its focus into energy scales where BSM effects could lie. In this section, we briefly review the shortcomings of the SM. Afterwards, we will try to present viable solutions for some of these problems.

From an *experimental* point of view, the SM does not account for:

- Dark matter (DM)

Almost 85% of matter in the Universe is in a form that does not radiate. It is therefore assumed to be electrically neutral and also stable so that it could have survived until today. Interestingly, none of the particles of the SM can account for DM, which means we need to extend it in order to provide a Particle Physics description for DM. We will discuss DM in detail in Chapter 5.

- Neutrino masses

  In the SM, neutrinos are exactly massless. This is due to the fact that the SM contains only left-handed neutrinos. Nevertheless, experiments have observed neutrinos change flavours, which implies that they mix and therefore have non-zero masses.

- Matter-antimatter asymmetry

  The Universe appears to be populated mostly by matter[2]. Nevertheless, the SM predicts that matter and antimatter should have been copiously produced during the Big Bang.

From a *theoretical* point of view, the following problems arise in the SM:

- Strong CP problem

  QCD seems to preserve charge-conjugation and parity (CP-symmetry) even though there is no explicit reason as to why it should. The theory is usually extended with the introduction of a CP-violating term known as the θ term. This parameter, however, is constrained by experiments to be very small ($\theta \ll 10^{-9}$). A well-motivated solution to the strong CP-problem is the introduction of a Peccei-Quinn global $U(1)$ symmetry which treats the θ parameter as a dynamical field. The potential of this field then has a minimum at $\theta = 0$ which is the CP-conserving point.

- Gauge unification

  In quantum field theory, all coupling parameters depend on the energy scale at which they are measured. The measured values of the three SM gauge couplings and the terms contained in their respective renormalization group equations, suggest that the values of the couplings come close at energy scales of around 10^{16} GeV. At this energy scale, then, it is hypothesized that the three forces merge into a single force and a Grand Unified Theory (GUT) encompasses the SM. The simplest GUT contains an $SU(5)$ gauge group which breaks down to G_{SM} with the help of new heavy fields.

- Vacuum stability

  The measured value of the Higgs boson mass ($M_h = 125.09 \pm 0.24$ GeV), in conjunction with the mass of the top quark ($M_t = 173.34 \pm 0.76$ GeV) have created a new problem for the SM. When one tries to solve the renormalization group equations (RGEs) of the couplings of the SM, then one finds that the Higgs self-coupling λ_h runs to negative values above energies of $\sim 10^{10}$ GeV. This signals a possible unboundedness of the Higgs potential and a vacuum instability as a result. We will look more closely into this problem in Section 4.4.

- Hierarchy problem

  The mass parameter μ_h^2 in the Higgs potential (4.14) is the only dimensionful parameter in the SM. It has the dimension of (mass)^2 and it sets the electroweak scale at around 100 GeV. This parameter is not protected by any symmetry and may in principle receive a contribution from radiative corrections. These radiative corrections are generally proportional to the energy scale Λ_{NP} where new physics is assumed to be at work or to the ultraviolet cutoff scale Λ_{UV}

[2]Trace amounts of antimatter are only naturally produced by collisions of cosmic rays or in astrophysical sources (or from lightning strikes!).

up to where the SM is valid. Naturally, then, one would expect the measured value of the Higgs mass to be much higher, around $\Lambda_{\rm NP}$ or $\Lambda_{\rm UV}$, unless there is an incredible fine-tuning cancellation between the quadratic radiative corrections and the bare mass. We will look more closely into this problem in Section 4.3.

- Gravity

  While not exactly a problem of the SM in itself, we would ideally want the SM to also incorporate gravity. As it stands, however, the general theory of relativity is non-renormalizable and we cannot employ the usual prescriptions of quantum field theory to describe it. Intensive efforts towards a theory of quantum gravity have resulted in string theory and loop quantum gravity. Nevertheless, these theories are still far from even being verifiable.

Next, let us take a closer look at some of the above problems since they will be of interest to us in this thesis.

4.3 Vacuum Stability

The observed mass of the Higgs boson has allowed us to determine the last free parameter in the SM, namely the Higgs self-coupling,

$$\lambda_h = M_h^2/2v_h^2 \simeq 0.13\,. \tag{4.38}$$

The Higgs self-coupling is not in fact constant, but evolves with energy just like any other coupling in a quantum field theory, due to loop corrections. We can then use the renormalization group equations (RGEs) to evolve the SM couplings and determine up to what scale the theory is valid. Quantum gravity is expected to come into play around $M_{\rm Pl}$, but any theoretical inconsistency before that would be an indication that new Physics effects should be considered.

For the SM to be valid up to the Planck scale, it should not have any Landau poles and the Higgs potential should be stable. A coupling develops a Landau pole when it becomes infinite at a finite energy scale. In such a case, either the theory completely changes form similar to what happens when QCD confines, or we need new Physics to tame the uncontrollable growth of the coupling. For the Higgs potential to be absolutely stable, the electroweak vacuum should be its global minimum. We can write the SM potential as

$$V(h) = -\frac{\mu_h^2}{2}h^2 + \frac{\lambda_h(h)}{4}h^4\,, \tag{4.39}$$

where we have now included a field dependence in the Higgs self-coupling, in order to take into account its running when we go to large field values. The Higgs potential is said to be stable or bounded from below as long as $\lambda_h(h) > 0$ for large field values. The one-loop RGE for λ_h in the $\overline{\rm MS}$ scheme has the form

$$(4\pi)^2\frac{{\rm d}\lambda_h}{{\rm d}\ln\mu} = -6y_t^4 + 24\lambda_h^2 + \lambda_h\left(12y_t^2 - \frac{9}{5}g_1^2 - 9g_2^2\right) + \frac{27}{200}g_1^4 + \frac{9}{20}g_1^2g_2^2 + \frac{9}{8}g_2^4\,, \tag{4.40}$$

where μ is the renormalization scale. It turns out that the large value of the top Yukawa coupling y_t and the negative sign that comes with it (since it is a fermion), force λ_h to become smaller with energy until it crosses zero at $\sim 10^{10}$ and then becomes negative. The evolution of the SM couplings up to very high energies is shown in Figure 4.4. If gravity does not introduce any new particle

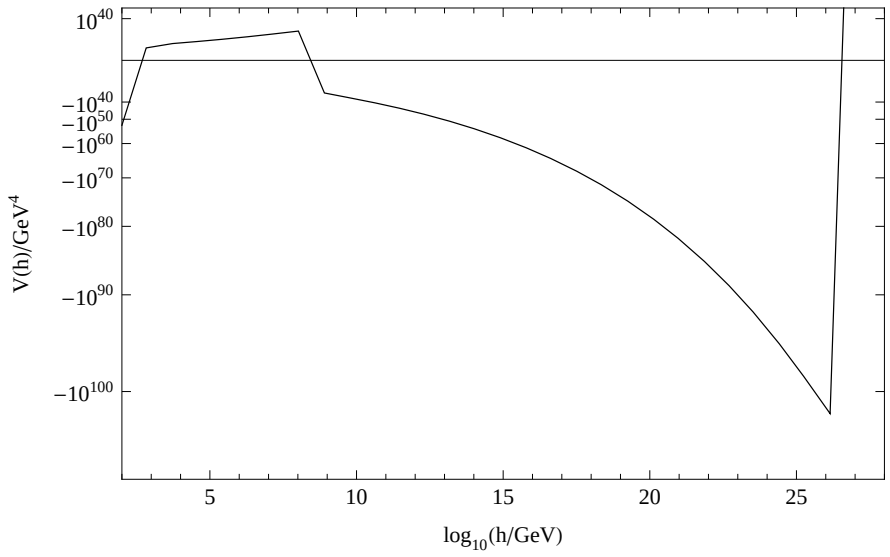

Figure 4.3: The SM Higgs effective potential as a function of the Higgs field strength, Eq. (4.39). The global minimum at $\sim 10^{26}$ GeV is caused by λ_h running positive (from low to high energy) at this scale (see Figure 4.4). The local minimum at the electroweak scale is generated by the negative Higgs mass parameter. Credit: [139]

thresholds, then the $U(1)$ gauge coupling develops a Landau pole above 10^{35} GeV and the Higgs potential has a new global minimum at 10^{26} GeV (see Figure 4.3).

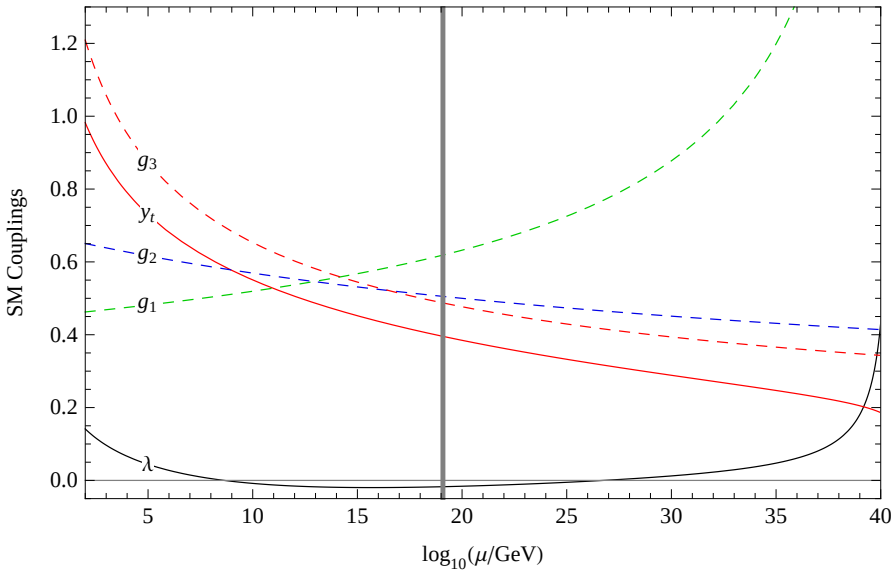

Figure 4.4: Running of the gauge couplings, the top Yukawa and the Higgs self-coupling in the Standard Model. Credit: [139]

The fact that λ_h becomes negative at higher energies signals a possible instability for the SM vacuum and poses a great problem since at any moment the SM vacuum could transition through a quantum tunnelling effect to the lower state of the high-energy minimum with potentially catastrophic results for the Universe. Luckily, due to the interplay between the Higgs boson and top quark masses, the SM vacuum is actually in a near-critical condition, at the border between stability and metastability (see Figure 4.5). Absolute stability would be achieved if the Higgs were a little

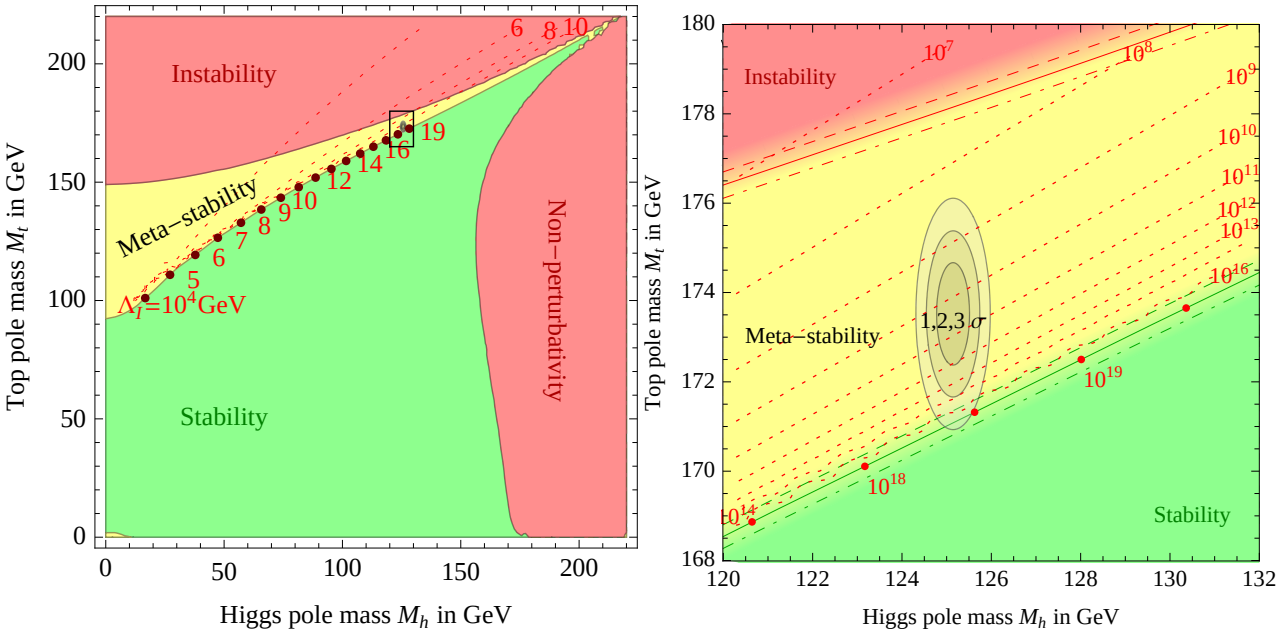

Figure 4.5: Left: SM phase diagram in terms of Higgs and top pole masses. The plane is divided into regions of absolute stability, meta-stability, instability of the SM vacuum, and non-perturbativity of the Higgs quartic coupling. The top Yukawa coupling becomes non-perturbative for $M_t > 230$ GeV. The dotted contour-lines show the instability scale Λ_I in GeV. **Right**: Zoom in the region of the preferred experimental range of M_h and M_t. Credit: [4]

heavier [4]

$$M_h > (129.1 \pm 1.5)\,\text{GeV} \qquad \text{(stability condition)}, \tag{4.41}$$

or the top quark were a little lighter

$$M_t < (171.53 \pm 0.42)\,\text{GeV} \qquad \text{(stability condition)}. \tag{4.42}$$

Furthermore, careful studies [3,4,244–251] of the vacuum stability issue have shown that the probability of vacuum decay to have happened in the past is very small, while the lifetime of the vacuum exceeds by many orders of magnitude the age of the Universe (see Figure 4.6). In any case, from a theoretical perspective, we would prefer the electroweak vacuum to be absolutely stable. This can be easily achieved if we introduce new scalar fields to the SM that couple with the Higgs. Then, the RGE of λ_h would receive a positive contribution from the new portal couplings, and depending on their values, λ_h could be made to remain positive for all higher field values.

4.4 Hierarchy Problem

Over the last decades, the hierarchy or naturalness problem has been the main driving force for the construction of theories beyond the Standard Model. In 1978, Susskind showed [252] that the mass of a scalar field is very sensitive to any higher energy scales in the theory due to large quantum corrections. These corrections would tend to drive the mass of the scalar field up to the highest energy scale in the theory. In the SM, the only scalar is the Higgs field. As we will see next, any physical states will give a threshold correction to the Higgs mass proportional to their own mass scale, a fact that is independent of any regularization and renormalization scheme.

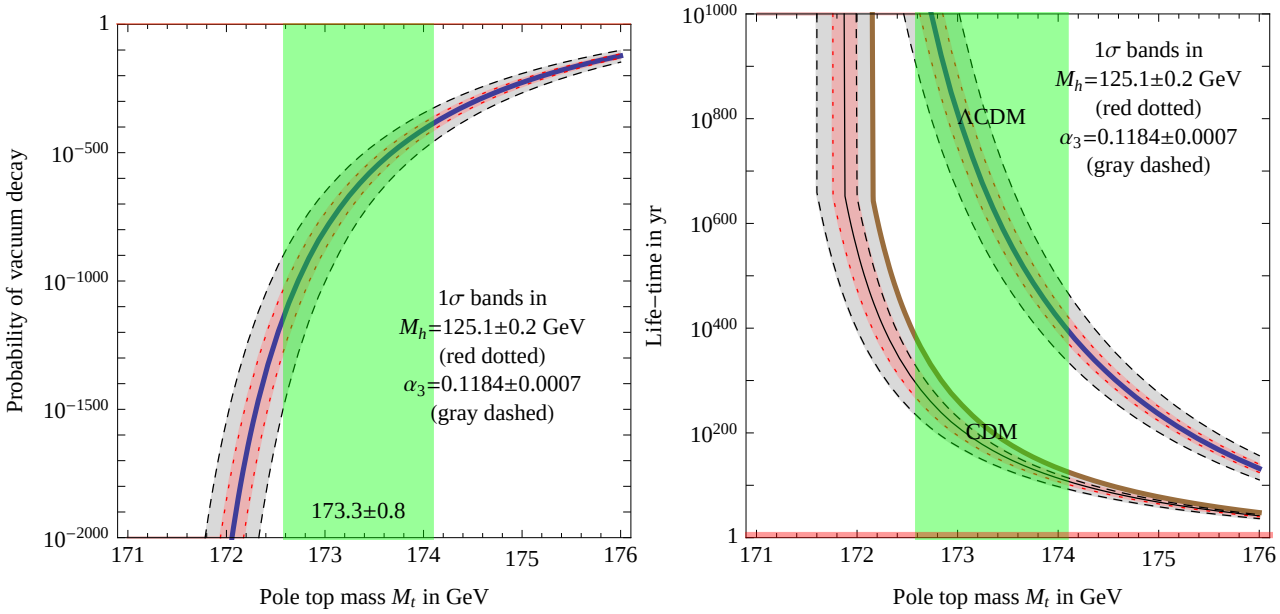

Figure 4.6: Left: The probability that electroweak vacuum decay happened in our past light-cone, taking into account the expansion of the universe. **Right**: The life-time of the electroweak vacuum, with two different assumptions for future cosmology: universes dominated by the cosmological constant (ΛCDM) or by dark matter (CDM). Credit: [4]

Let us start by considering the contributions of fermion loops to the two-point function of the SM Higgs field. Using a cutoff scale Λ in order to regularize the loop integral, the corrections to the Higgs mass are given by

$$\Delta M_h^2 \approx \frac{-y_t^4}{4\pi^2}\left(\Lambda^2 + M_t^2 \ln\left(\frac{\Lambda^2}{M_t^2}\right) - M_t^2\right), \tag{4.43}$$

where we only included the top quark since it is the heaviest of the fermions and contributes the most in the above expression. We can see that as the cutoff scale Λ grows, so do the corrections which means they are quadratically divergent. The renormalized Higgs mass is given by the sum of the bare mass M_0 and the corrections,

$$M_h^2 = M_0^2 + \Delta M_h^2 \approx M_0^2 - \frac{y_t^2}{8\pi^2}\Lambda^2 . \tag{4.44}$$

The measured mass of the Higgs is $M_h = 125\,\text{GeV}$. Suppose now that we interpret Λ as a physical scale and choose it to be the Planck scale $M_{\text{Pl}} \approx 10^{19}\,\text{GeV}$. We would then need an enormous amount of fine-tuning between M_0, y_t, and Λ in order to achieve the observed Higgs mass. It is thus unnatural for the Higgs mass to be around the electroweak scale. This is known as the *naturalness problem* and is an effect of the *hierarchy problem* where there is a vast hierarchy between the electroweak and another scale (e.g. right-handed neutrino scale, GUT, or Planck scale) and a large amount of fine-tuning is required in order to absorb the threshold corrections to the bare Higgs mass term.

Suppose now that we use dimensional regularization in order to calculate the quantum corrections to the Higgs mass. We find

$$\delta M_h^2 \approx \frac{-y_t^2 M_t^2}{4\pi^2}\left(\frac{2}{\epsilon} - \gamma_E + \ln(4\pi) - \ln\frac{M_t^2}{\mu^2}\right). \tag{4.45}$$

The right-hand side is still divergent, but the $1/\epsilon$ pole corresponds to a logarithmic divergence as opposed to the quadratic divergence we saw in the cutoff regularization scheme. Physics, nevertheless, should be independent of regularization and subtraction schemes. We will then define the hierarchy problem in terms of real physical threshold effects and not in terms of quadratic divergences [253]. In both the cutoff and dimensional regularization schemes, the threshold contribution is that of the top mass, M_t^2. The effect of the top quark does not require much fine-tuning since the top mass is close to that of the Higgs, but new heavier particles could potentially give large contributions. Consider for example that we couple the Higgs to a new massive particle with coupling y and mass M. Then, the threshold contribution would be proportional to y^2M^2 and we say that the theory has a hierarchy problem if $y^2M^2 \gg M_h^2$.

We can understand the same phenomenon also in the context of the renormalization group. Suppose again that a single fermion with mass M couples to the Higgs with a Yukawa coupling y. Then, the RGE for the Higgs mass would have the form

$$(4\pi)^2 \frac{\partial M_h^2}{\partial \ln \mu} = -16M^2y^2 + 2\lambda_h M_h^2 \,. \tag{4.46}$$

Running from a scale μ_0 to a scale μ_1 with $M \gg M_h$ would induce a change in Higgs mass of the order of

$$\delta M_h^2 \approx -\frac{16}{(4\pi)^2} y^2 M^2 \ln \frac{\mu_1}{\mu_0} \,. \tag{4.47}$$

We see again that for scales that are significantly separated we need a large amount of fine-tuning in order to achieve $M_h \ll M$.

The hierarchy problem is a problem that only the Higgs has in the SM. Scalar fields are additively renormalized, as opposed to fermion fields which are renormalized in a multiplicative way. For example, the one-loop correction to the fermion mass, M_f, is found to be

$$\delta M_f \propto M_f \ln \left(\frac{\Lambda}{M_f} \right) . \tag{4.48}$$

We see that the mass correction is proportional to the mass itself and there is no fine-tuning involved. In the limit $M_f \to 0$, the corrections are also zero which means quantum corrections would not generate a mass term if $M_f = 0$ initially. In this limit, the fermion mass is protected by the chiral symmetry which serves as a "custodial symmetry". According to 't Hooft, a quantity in nature should be small if the underlying theory becomes more symmetric as that quantity goes to zero [5]. A similar situation arises for spin-1 particles. The quantum corrections to the gauge boson masses are proportional to the gauge boson mass themselves, which are protected by the gauge symmetry that also serves as a custodial symmetry.

For spin-0 particles such as the Higgs, there is no established custodial symmetry in the SM that can protect its mass from large radiative corrections (with the exception of the non-trivial *conformal symmetry* or *scale invariance* which we will discuss in detail later on). We should therefore search for a new symmetry that will serve as a custodial symmetry for the scalar particles and the Higgs in particular.

In supersymmetric theories, scalars and fermions are connected by supersymmetry. The chiral symmetry that protects the fermions now also protects the scalars. Let us consider again the one-loop contributions to the Higgs mass. There is now an extra contribution from the top superpartner, the stop $\tilde{t}$. We find (for the up-type Higgs H_u)

$$\delta M_{H_u}^2 \simeq -\frac{6y_t^2}{16\pi^2}\Lambda^2 + \frac{6y_t^2}{16\pi^2}\Lambda^2 - \frac{3y_t^2}{4\pi^2} M_{\tilde{t}}^2 \ln \left(\frac{\Lambda}{M_{\tilde{t}}} \right) . \tag{4.49}$$

The first two terms explicitly cancel out and we are left with threshold contributions from new heavy states which are at most logarithmically sensitive to the cutoff. Therefore, as long as supersymmetry is softly broken not too far away from the electroweak scale, the hierarchy problem seizes to exist. Unfortunately, LHC has not, as of the writing of this thesis, discovered any supersymmetric particles, which has cast a shadow of doubt on the physical manifestation of the beautiful idea of supersymmetry.

Another option is that of a global symmetry. The Higgs is then considered to be a pseudo-Nambu–Goldstone boson (pNGB) of a spontaneously broken global symmetry, while its mass is protected by a shift symmetry (see [254] for a review). This idea has resulted in the little Higgs model (see [255–257] for some reviews) and its extensions [258–260] and in the twin Higgs model [261, 262]. In such scenarios, a top partner is usually introduced around the TeV scale. The radiative contribution to the Higgs mass has the form

$$\delta M_h^2 \simeq -\frac{6y_t^2}{16\pi^2}\Lambda^2 + \frac{6y_t^2}{16\pi^2}\Lambda^2 - \frac{3y_t^2}{4\pi^2}M_T^2 \ln\left(\frac{\Lambda}{M_T}\right), \tag{4.50}$$

where M_T is the energy scale associated with the top partner T. As in the supersymmetric case, the quadratic divergences cancel and we are only left with a logarithmically divergent part.

There have been other well-motivated solutions for the hierarchy problem. Most of them predict new particles around the TeV scale so that they are not very fine-tuned. This is convenient, in the sense that dark matter is also thought to reside around the TeV scale. In Chapter 6 we will consider classical scale invariance as a possible solution to the hierarchy problem.

4.5 Right-handed Neutrinos and Type-I Seesaw

Numerous solar, atmospheric, reactor, and accelerator (anti-)neutrino experiments (see [226–233] for example) have established that neutrinos produced in a well-defined flavour eigenstate can be detected, after propagating a macroscopic distance, as a different flavour eigenstate. This is evidence that neutrinos have nonzero mass and they mix among themselves, much like quarks. As a consequence, we must find a way to explain these observations by going beyond the Standard Model (see [263–265] for some reviews). The simplest way of generating mass for the neutrinos is to add three right-handed neutrinos N_R to the SM. This is similar to the way the rest of the SM fermions obtain their masses. The relevant Lagrangian term has the form

$$\mathcal{L}_N = -Y_\nu^{ij}\bar{L}_i\, i\sigma_2 H^* N_j\,. \tag{4.51}$$

We are now able to write down a neutrino mass term. Notice the Yukawa couplings Y_ν^{ij} in (4.51) which couples the Higgs doublet with the left and right-handed neutrinos. Such a Yukawa coupling could in principle deteriorate the vacuum stability problem since it would appear in the RGE of the Higgs self-coupling λ_h. Nevertheless, since neutrinos are many orders of magnitude lighter than the top quark, we can completely ignore these Yukawa couplings in regards to the evolution of λ_h.

We can in principle also add another term for the right-handed neutrinos which breaks lepton number. Then, the neutrino part of the Lagrangian is augmented to

$$-\mathcal{L}_N = Y_\nu^{ij}\bar{L}_i\, i\sigma_2 H^* N_j + \text{H.c.} + \frac{1}{2}\bar{N}_i^c M_R N_j\,. \tag{4.52}$$

The last term is a Majorana term and M_R is a 3×3 mass matrix which sets the scale of the right-handed neutrinos. It is usually assumed to be much larger than the electroweak scale, $M_R \gg$

v_h. Employing then the type-I seesaw mechanism we can obtain the masses of the left-handed neutrinos, given by

$$m_\nu = v_h^2 Y_\nu^T M_R^{-1} Y_\nu \,. \tag{4.53}$$

In order to obtain the estimated mass $m_\nu = \mathcal{O}(0.1\,\text{eV})$ one usually assumes a Yukawa coupling Y_ν of order unity and a seesaw scale of $M_R = \mathcal{O}(10^{14}\,\text{GeV})$. Note, however, that Y_ν can be naturally much smaller, which could bring the seesaw scale closer to the electroweak scale, avoiding in such a way an unnatural hierarchy between the scales. We will be concerned again with right-handed neutrinos in the context of classical scale invariance in Chapter 7.

Chapter 5

Dark Matter

As we discussed in Chapter 2, dark matter (DM) comprises around 85% of the matter content of the Universe [1]. It is of paramount importance then to understand how DM came to be and what it is composed of.

In this chapter, we begin by outlining the main evidence supporting the existence of DM. Then, in Section 5.2 we briefly review the properties of some of the most popular DM candidates. In Section 5.3, we focus on the WIMP paradigm and its various aspects. Finally, in Section 5.4 we briefly review the status of the ongoing DM searches.

5.1 Evidence for Dark Matter

The first evidence for the presence of DM came from F. Zwicky in 1933 [266]. He was studying the movement of galaxies in the Coma Cluster by measuring their velocities, when he noticed that the mass-to-light ratio was $\sim$ 400 times what one would expect if all the mass was made up of stars like our Sun. He named the missing matter "dark matter", but his findings were largely ignored at the time.

5.1.1 Galactic rotation curves

Around the 1970s, astronomers who were studying the rotation curves of galaxies, *i.e.* the circular velocities of stars and gas as a function of the distance from the galactic center, found that the rotation velocities do not decrease with distance as one would expect from Kepler's Second Law, but instead remain nearly constant beyond the galactic disk. This behaviour is shown in Fig. 5.1. From standard Newtonian gravity, the stars' circular velocity is expected to be

$$v(r) = \sqrt{\frac{GM(r)}{r}}\,, \tag{5.1}$$

where $M(r)$ is the mass enclosed inside the sphere with radius r and G is the gravitational constant. Beyond the optical disc, assuming all mass is concentrated inside the disc, Gauss' Law tells us that M should remain constant and the velocity should be falling as $v \propto r^{-1/2}$. Nevertheless, since the velocity is observed to be almost constant beyond the Galactic disk, there must be a non-luminous halo with

$$\rho(r) \propto \frac{M(r)}{r^3} \sim \frac{1}{r^2}\,. \tag{5.2}$$

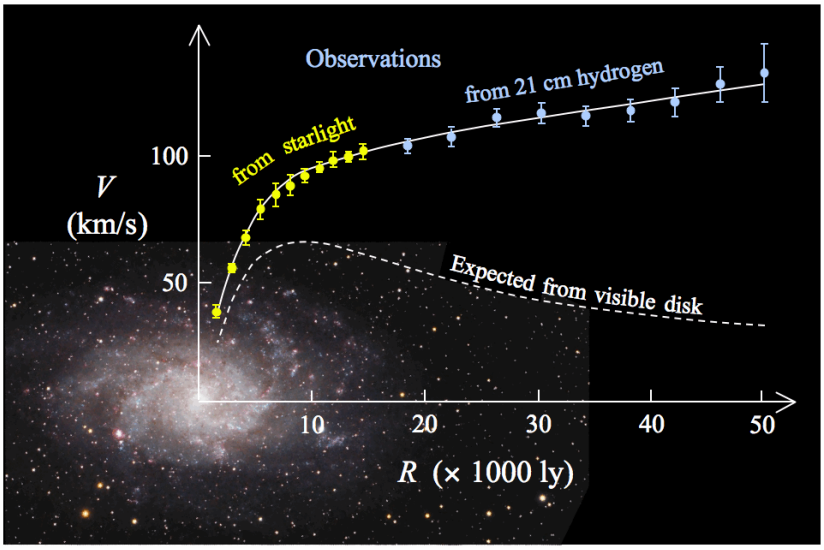

Figure 5.1: Rotation curve of spiral galaxy M 33 (yellow and blue points with error bars) and the predicted one from the distribution of the visible matter (white line). The discrepancy between the two curves can be accounted for by adding a dark matter halo surrounding the galaxy. Credit: [267]

5.1.2 Gravitational lensing

The existence of DM is also inferred by gravitational lensing effects. Since DM interacts gravitationally, its mass distorts spacetime causing the bending of light coming from behind sources (for a review see, *e.g.*, [268]). This effect is most easily observed when light passes through a very massive and/or dense object, such as the central region of a galaxy or a galaxy cluster. These objects act as astrophysical lenses that bend and magnify the light coming from galaxies far behind them (an example is shown in Fig. 5.2). This effect is commonly known as strong lensing. The distribution of mass in the lens can be determined by the size and shape of the image and then be compared with the visible mass.

Figure 5.2: An example of gravitational lensing. Faraway galaxies are distorted and magnified as their light is bent by the gravitational field of a dark matter halo. Source: NASA/ESA

Perhaps the most spectacular piece of evidence in favour of DM comes from the Bullet Cluster [269, 270]. It consists of two cluster galaxies which have undergone a head-on collision. The trajectories followed by its components were dictated by their individual properties. First, the stars contained in the galaxies, observable in visible light, were mostly unaffected by the collision and

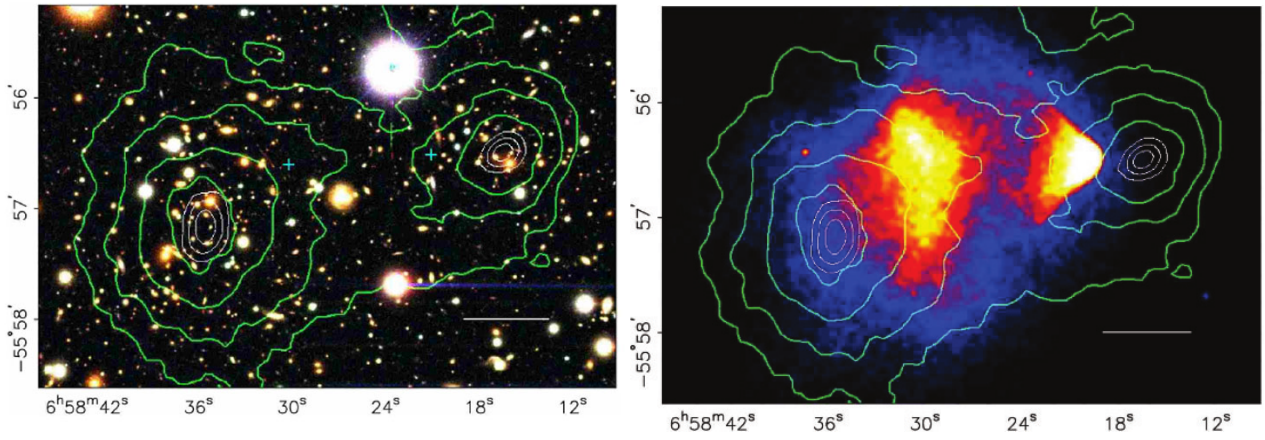

Figure 5.3: Shown on the left is a color image from the Magellan images of the Bullet Cluster. On the right is the same image from Deep Chandra with the X-ray brightness of the gas component is coded in yellow, red and blue colours. The distribution of the gravitating mass, obtained from weak lensing reconstruction, is shown in both images by green contours. Credit: [270]

passed right through, only slightly slowing down due to gravitational interactions. Second, the hot gas clouds, observed through their X-ray emission, interact electromagnetically and caused the gases of both clusters to slow much more than the stars. The third component, dark matter, passed through the interaction region and its distribution was inferred indirectly by the gravitational lensing of background objects. This was the first observation of a system where the dark matter and the baryonic component have been separated from each other and it shows that dark matter is a separate form of matter which is, at least mostly, collisionless.

5.1.3 CMB radiation

Last but not least, the most precise prediction for the DM density is coming from the CMB spectrum. The power spectrum of temperature anisotropies, when expanded in terms of spherical harmonics, depends on cosmological parameters that can be determined by applying statistical methods. The best fit to the power spectrum as observed by Planck [51] is a flat ΛCDM model, with baryonic and dark matter density

$$\Omega_b h^2 = 0.02226 \pm 0.00023\,, \tag{5.3}$$
$$\Omega_{\rm DM} h^2 = 0.1186 \pm 0.0020\,, \tag{5.4}$$

where $h = H_0 / \left(100 \text{ km Mpc}^{-1}\, s^{-1}\right) = 0.678 \pm 0.009$ is the reduced Hubble parameter, with H_0 denoting the Hubble constant today.

5.1.4 General remarks on dark matter

As of yet, little is known about the nature of DM as a particle. Nevertheless, any candidate for (most of) the DM must be consistent with the following observationally-motivated constraints:

1. *Relic abundance.* The DM relic abundance needs to reproduce the observed cold dark matter density of (5.4).

2. *Neutral.* The DM should be electromagnetically neutral since there has been no detection of irregular light emission.
3. *Stable.* Since the presence of DM is ascertained today, this implies that the corresponding particle(s) must be cosmologically stable or have a lifetime greater than the age of the Universe. At the theoretical level, in order to achieve stable DM, one usually assumes there is a stabilizing symmetry such as a Z_2 under which the DM species is odd while the SM particles are even.
4. *Cold/Warm and non-relativistic today.* The DM particle should be non-relativistic at matter-radiation equality to form structures in the early Universe in agreement with the observations. Hot DM is relativistic, cold DM is non-relativistic and warm DM starts to behave as non-relativistic at a temperature of a few keV. Cold or warm DM are able to reproduce the current observations, contrary to hot DM. Cosmological simulations point to the mass of DM being above $\sim \mathcal{O}\,(1 - 10\,\mathrm{keV})$ [271–273].
5. *Non-baryonic.* If DM was baryonic then it would radiate and thus contribute to the baryonic component measured from the CMB anisotropies. Furthermore, baryonic DM would be concentrated near the center of galaxies instead of forming the spherical halos around galaxies we observe.

5.2 Dark matter candidates

Let us now briefly review some of the most studied DM candidates.

- *MACHOs.* Massive (astrophysical) compact halo objects (MACHOs) is the simplest possible solution to the DM problem: dark or very faint bodies are notoriously difficult to detect, and the galaxy may in principle be filled with a large population of this kind. The most attractive MACHO candidate is that of a population of planet-sized objects that can be baryonic in nature. These objects can in principle be detected through microlensing effects, that is, when a MACHO passes through the line of sight of a distant star, distorting its image [274]. Experiments like the MACHO Project [275], EROS [276], OGLE [277, 278], and POINT-AGAPE [279] observed millions of stars for $5 - 10$ years and found $\mathcal{O}(10)$ events each. However, the expected number would be 3 to 5 times larger if MACHOs were to comprise all of the missing mass of galaxies. Therefore, MACHOs can at most account for 20% of the missing mass.
- *PBH.* Primordial black holes are a hypothetical type of black holes that formed before the era of nucleosynthesis due to the gravitational collapse of important density fluctuations. They were first put forward as DM candidates in the 1970s [280–282]. Since then, various experiments [275, 276, 283–290] have constrained a vast region of the mass parameter space between 5×10^{14} g and 10^{40} g. Primordial black holes lighter than 5×10^{14} g would have evaporated due to Hawking radiation [291], while MACHOs heavier than 10^{40} g are ruled out by the dynamics of the galactic disk [292].

  After the observation by LIGO [293] of gravitational waves originating from the merger of two black holes with mass $\sim 30\ M_\odot \simeq 6 \times 10^{34}$ g, there has been a renewed interest in PBH as DM [294–299]. In the future, gravitational wave astronomy will be able to constrain the properties of other exotic particles formed by new dark sector particles, whether these are related to DM or not [300].
- *SM neutrinos.* Neutrinos have been advocated as a solution to the DM problem for a long time. In the early Universe, they were in thermal equilibrium with the rest of the SM particles, until

they decoupled when the temperature dropped below $\sim 1 - 10\,\text{MeV}$. Their relic abundance is computed to be

$$\Omega_\nu h^2 = \sum_{i=1}^{3} \frac{m_{\nu_i}}{93\,\text{eV}}\,. \tag{5.5}$$

The current lower limit on the neutrino masses is $\sum m_\nu < 0.23\,\text{eV}$ [1], which means neutrinos cannot constitute 100% of the dark matter. Furthermore, being relativistic during decoupling, neutrinos would act as hot DM, erasing fluctuations at scales lower than their free-streaming length, $40\,\text{Mpc} \times (m_\nu/30\,\text{eV})$ [301]. This would mean that galaxies formed top-down, that is, large structures formed first, which is at odds with observations.

- *Axions.* As we saw in Chapter 4, axions were proposed by Peccei and Quinn (PQ) [302,303] as a solution to the strong CP problem (see [304] for a review). After PQ symmetry breaking in the very early Universe, the axion field is practically massless and its spatial inhomogeneities are wiped out fast over distances of order the size of the causal horizon H^{-1}. Later, at a temperature of order a GeV, the temperature-dependent mass of the axion becomes of order the expansion rate, $m_A(T) \simeq 3H(T)$, and the axion field begins to oscillate around the minimum of its effective potential. This oscillation of the classical axion field corresponds to a coherent state of numerous, extremely non-relativistic axions and can thus constitute a cold dark matter candidate [305–307]. Experiments have constrained the available mass parameter range, see for example [308], but axions still remain viable DM candidates.

- *Sterile neutrinos.* As proposed by Dodelson and Widrow [309], right-handed (sterile) neutrinos, apart from providing mass to the active neutrinos via a seesaw mechanism (see Section 4.5), could also serve the role of dark matter. A sterile neutrino could be warm or moderately cold depending on the cosmological production mechanism, for example, produced by oscillations between active and sterile neutrinos. Such a candidate could describe the low-scale structure observations better than cold dark matter candidates (see, e.g., [310,311]). The most favorable mass range for sterile neutrino DM is around the keV scale. For example, in the neutrino minimal Standard Model (νMSM), three sterile neutrinos are added to the SM. In order to account for DM, one of them is at the keV scale. The other two are generally heavier and can account for the observed light neutrino masses via a seesaw mechanism. Furthermore, if they are nearly degenerate and have masses in the range $150\,\text{MeV} - 100\,\text{GeV}$, oscillation-induced leptogenesis can lead to baryogenesis. Thus, sterile neutrinos can also serve as a solution to the baryon asymmetry problem. For various models on keV sterile neutrino DM see [312] and for more details see the white paper [313].

- *MOND.* Despite all the model-building efforts and various types of candidates for DM, experiments have still not found any evidence for the particle nature of DM. It could well be the case that, starting at galactic scales, Newtonian gravity behaves in a different way as to what is observed at shorter scales, and as a result the effect of DM could be mimicked. In this vein, Milgrom proposed in 1983 the idea of "modified Newtonian dynamics" (MOND) [314]. The essential part of this theory is the relation

$$\tilde{\mu}\left(\frac{|\mathbf{a}|}{a_0}\right)\mathbf{a} = -\nabla\Phi_N\,, \qquad \text{with} \quad \begin{cases} \tilde{\mu} \sim 1 & \text{for} \quad x \gg 1 \\ \tilde{\mu} \sim x & \text{for} \quad x \ll 1\,, \end{cases} \tag{5.6}$$

where $\mathbf{a}$ is the acceleration of a particle, $-\nabla\Phi_N$ the conventional Newtonian gravitational field and $a_0 \sim 10^{-10} m\,s^{-2}$ is a natural constant. The usual Newtonian dynamics is reproduced when the function $\tilde{\mu}$ is unity. The advantage of the above relation is that it can reproduce very well the galactic rotation curves and the relation between the total baryonic mass to the asymptotic rotation velocity for spiral galaxies (encoded in the so-called Tully-Fisher relation).

There have been attempts at incorporating MOND into more complete theories. Most notably, in the non-relativistic regime, Eq. (5.6) can be derived with a variational principle starting from the so-called aquadratic Lagrangian (AQUAL) [315]. There is also a complete relativistic formulation of MOND in the context of the tensor-vector-scalar theory (TeVeS) [316]. For reviews on these approaches see Refs. [317, 318].

Despite their successes, MOND and its generalizations fail to adequately account the observed properties of galaxy clusters (and particularly the bullet cluster) and also no satisfactory cosmological model has been constructed from the theory. For more details regarding the shortcomings of MOND theories, see [319, 320]. Finally, the accurate measurement of the speed of gravitational waves compared to the speed of light from the GW170817 signal has ruled out many modified gravity theories which had been advocated as solutions to the dark energy problem [321].

- *WIMPs.* Weakly interacting massive particles (WIMPs) are by far the most studied DM candidates. They can arise naturally in many well-motivated SM extensions. Furthermore, the thermal freeze-out mechanism seems to be able to provide the DM relic abundance for reasonable ranges of WIMP mass and annihilation cross section. Thermal WIMPs also have the advantage of being testable by experiments. A WIMP is usually considered to be a particle with mass in the range from around 2 GeV up to around 100 TeV. The lower value comes from the so-called Lee-Weinberg bound [322] while the upper value is a rough estimate obtained by unitarity considerations [323]. In most cases, WIMPs interact weakly with the known particles. This renders them phenomenologically attractive since they could lie within the reach of current searches, including the LHC. In this thesis, we will only be concerned with WIMP DM candidates. In the next section we will present the WIMP paradigm in more detail, while Section 5.4 will be devoted to DM direct/indirect detection and collider searches.

5.3 The WIMP paradigm

The relic abundance of WIMPs is usually determined through the mechanism of thermal freeze-out which will be detailed in the following. After the end of inflation and the assumed subsequent reheating, all particles are in thermal equilibrium, while the Universe continues to expand. As the temperature continues to drop, so does the interaction rate $\Gamma_{\rm DM}$ of the DM species. Nevertheless, thermal equilibrium cannot be maintained and, once $\Gamma_{\rm DM}$ becomes smaller than the expansion rate H of the Universe, a DM number density "freeze-out" occurs and dark matter particles decouple from the rest of the light degrees of freedom that remain thermalized. Thus, the DM relic abundance survives to the present epoch having the value that we observe today.

In this section, we first briefly review the derivation of the Boltzmann equations in an expanding Universe. Then, employing the mechanism of thermal freeze-out for the simplest case of one WIMP species, we obtain semi-analytical results for the DM relic density. After that, we review some of the most studied WIMP candidates and focus on the case of vector DM. This type of WIMP arises in extensions of the SM with new gauge symmetries. As we will see, new gauge symmetries have the advantage of containing intrinsic discrete symmetries that can automatically stabilize the extra gauge bosons, resulting in naturally stable DM candidates.

5.3.1 Boltzmann equations

Let us consider a generic particle X_a whose number density evolution is governed by the Boltzmann equation

$$\boxed{\frac{\mathrm{d}n_a}{\mathrm{d}t} + 3Hn_a = \mathcal{C}_a}\,, \tag{5.7}$$

where H is the usual Hubble parameter and $\mathcal{C}_a$ is the collision operator for the reactions that change the number of X_a particles. The second term on the left-hand side of (5.7) accounts for the dilution effect of the expansion of the Universe. If the X_a particles have no interactions then the right-hand side is zero and we simply have $n_a a^3 = \text{const}$, where a is the scale factor.

In this thesis we will only consider $2 \to 2$ processes, for which the collision operator can be written as

$$\mathcal{C}_a = \sum_{b,c,d} \mathcal{C}_{ab\to cd}\,, \tag{5.8}$$

where the sum runs over all the possible reactions $ab \to cd$. For a single reaction, the collision operator is given by

$$\begin{aligned}\mathcal{C}_{ab\to cd} = -\int (2\pi)^4 \delta^4\left(p_a + p_b - p_c - p_d\right) \mathrm{d}\Pi_a \mathrm{d}\Pi_b \mathrm{d}\Pi_c \mathrm{d}\Pi_d \\ \left[|\mathcal{M}_{ab\to cd}|^2 f_a f_b - |\mathcal{M}_{cd\to ab}|^2 f_c f_d\right]\,,\end{aligned} \tag{5.9}$$

with f_i being the phase space distribution for the particle i. The Lorentz invariant phase space (LIPS) is defined as

$$\mathrm{d}\Pi_i := g_i \frac{\mathrm{d}^3 p_i}{2E_i (2\pi)^3}\,, \tag{5.10}$$

where g_i is the number of the internal degrees of freedom of the particle i. Assuming CP (or T) invariance, there is an equality between the two matrix elements $\mathcal{M}_{ab\to cd} = \mathcal{M}_{cd\to ab}$, and we can rewrite

$$\mathcal{C}_{ab\to cd} = -\int (2\pi)^4 \delta^4\left(p_a + p_b - p_c - p_d\right) \mathrm{d}\Pi_a \mathrm{d}\Pi_b \mathrm{d}\Pi_c \mathrm{d}\Pi_d |\mathcal{M}_{ab\to cd}|^2 \left[f_a f_b - f_c f_d\right]\,. \tag{5.11}$$

Let us also assume kinetic equilibrium during freeze-out. Then, we have

$$f_i\left(E,t\right) = \frac{n_i(t)}{n_i^{\mathrm{eq}}(t)} f_i^{\mathrm{eq}}\left(E,t\right)\,, \tag{5.12}$$

with the equilibrium number density given as

$$n_i^{\mathrm{eq}} = g_i \int \frac{\mathrm{d}^3 p}{(2\pi)^3} f_i^{\mathrm{eq}}(\mathbf{p})\,, \tag{5.13}$$

where $f_i^{\mathrm{eq}}(\mathbf{p})$ is the thermal distribution for the species at thermal equilibrium. Energy conservation implies that

$$f_a^{\mathrm{eq}} f_b^{\mathrm{eq}} = \exp\left[-\left(E_a + E_b\right)/T\right] = \exp\left[-\left(E_c + E_d\right)/T\right] = f_c^{\mathrm{eq}} f_d^{\mathrm{eq}}\,. \tag{5.14}$$

Then, performing the integrals over the momenta, we obtain

$$\mathcal{C}_{ab\to cd} = -\left\langle \sigma v_r \right\rangle_{ab\to cd} \left[n_a n_b - \frac{n_a^{\mathrm{eq}} n_b^{\mathrm{eq}}}{n_c^{\mathrm{eq}} n_d^{\mathrm{eq}}} n_c n_d\right] = -\left\langle \sigma v_r \right\rangle_{cd\to ab} \left[\frac{n_c^{\mathrm{eq}} n_d^{\mathrm{eq}}}{n_a^{\mathrm{eq}} n_b^{\mathrm{eq}}} n_a n_b - n_c n_d\right]\,, \tag{5.15}$$

where σ is the total cross section for that particular process, v_r is the relative velocity between two DM particles, and $\langle \sigma v_r \rangle_{ab\to cd}$ denotes the thermal average

$$\langle \sigma v_r \rangle_{ab\to cd} := \frac{\int \mathrm{d}^3 p_a \mathrm{d}^3 p_b \, \sigma\left(\mathbf{p}_a, \mathbf{p}_b\right)_{ab\to cd} v_r \, e^{-E_a/T} e^{-E_b/T}}{\int \mathrm{d}^3 p_a \mathrm{d}^3 p_b e^{-E_a/T} e^{-E_b/T}} \,. \tag{5.16}$$

Equation (5.15) contains two equivalent expressions for the collision operator describing the reaction $ab \to cd$. The first form contains the thermally averaged cross section for that particular reaction, while the second form involves the thermally averaged cross section for the opposite reaction $cd \to ab$.

5.3.2 Thermal Averaging

Let us now compute $\langle \sigma v_r \rangle_{ab\to cd}$ in an efficient manner. The first step is to compute the squared transition matrix element $|\mathcal{M}|^2$ (summed over final spins and averaged over initial polarizations) and express it in terms of the Mandelstam variables s, t, u. Note that

$$t - u = -\frac{(m_a^2 - m_b^2)(m_c^2 - m_d^2)}{s} + 4 p_a(s) p_c(s) \cos\theta_{\mathrm{CM}} \,, \tag{5.17}$$

where θ_{CM} is the scattering angle in the center-of-mass frame and $p_i(s)$ is the magnitude of the 3-momentum of particle i, given by

$$p_{\mathrm{in}} := p_a(s) = p_b(s) = \left[\frac{s}{4} - \frac{m_a^2 + m_b^2}{2} + \frac{(m_a^2 - m_b^2)^2}{4s}\right]^{1/2} , \tag{5.18}$$

$$p_{\mathrm{out}} := p_c(s) = p_d(s) = \left[\frac{s}{4} - \frac{m_c^2 + m_d^2}{2} + \frac{(m_c^2 - m_d^2)^2}{4s}\right]^{1/2} . \tag{5.19}$$

The sum of the Mandelstam variables gives $s + t + u = m_1^2 + m_2^2 + m_3^2 + m_4^2$, which allows us to write

$$t = \tfrac{1}{2}[m_a^2 + m_b^2 + m_c^2 + m_d^2 - s + (t-u)] \,, \tag{5.20}$$

$$u = \tfrac{1}{2}[m_a^2 + m_b^2 + m_c^2 + m_d^2 - s - (t-u)] \,. \tag{5.21}$$

Then, using Eqs. (5.17)–(5.21) we can write $|\mathcal{M}|^2$ as a function of s and $\cos\theta_{\mathrm{CM}}$.

Next, we wish to derive a simple formula for the thermal average in (5.16) by reducing the integral from 6 dimensions to 1. Following [324, 325], for the denominator we have

$$\int \mathrm{d}^3 p_i \, e^{-E_i/T} = 4\pi^2 T m_a^2 \, K_2\left(\frac{m_a}{T}\right) , \tag{5.22}$$

where K_2 is the modified Bessel functions of the second kind of order 2. Moving to the numerator, we can first rewrite the volume element as

$$\mathrm{d}^3\mathbf{p}_a \mathrm{d}^3\mathbf{p}_b = 4\pi |\mathbf{p}_a| E_a \mathrm{d}E_a \, 4\pi |\mathbf{p}_b| E_b \mathrm{d}E_b \, \frac{1}{2} \mathrm{d}\cos\theta \,, \tag{5.23}$$

where θ is the angle between $\mathbf{p}_a$ and $\mathbf{p}_b$. After changing the integration variables from E_a, E_b, θ to E_+, E_- and s,

$$\begin{aligned} E_+ &= E_a + E_b && (5.24)\\ E_- &= E_a - E_b && (5.25)\\ s &= m_a^2 + m_b^2 + 2E_aE_b - 2|\mathbf{p}_a||\mathbf{p}_b|\cos\theta\,, && (5.26)\end{aligned}$$

the volume element becomes

$$\frac{\mathrm{d}^3\mathbf{p}_a}{(2\pi)^3 2E_a}\frac{\mathrm{d}^3\mathbf{p}_b}{(2\pi)^3 2E_b} = \frac{1}{(2\pi)^4}\frac{dE_+dE_-ds}{8}\,, \tag{5.27}$$

and the initial integration region

$$\{E_a \geq m_a, E_b \geq m_b, |\cos\theta| \leq 1\} \tag{5.28}$$

transforms into

$$\begin{aligned} & s \geq (m_a + m_b)^2, && (5.29)\\ & E_+ \geq \sqrt{s}, && (5.30)\\ & \left| E_- - E_+\frac{m_b^2 - m_a^2}{s}\right| \leq 2p_{ab}\sqrt{\frac{E_+^2 - s}{s}}\,. && (5.31)\end{aligned}$$

Integrating over E_- gives us

$$\int \mathrm{d}E_- = 4p_{ab}\sqrt{\frac{E_+^2 - s}{s}} \tag{5.32}$$

and the volume element takes the form

$$\frac{\mathrm{d}^3\mathbf{p}_a}{(2\pi)^3 2E_a}\frac{\mathrm{d}^3\mathbf{p}_b}{(2\pi)^3 2E_b} = \frac{1}{(2\pi)^4}\frac{p_{ab}}{2}\sqrt{\frac{E_+^2 - s}{s}}dE_+ds\,. \tag{5.33}$$

Finally, performing the E_+ integration and collecting everything together the thermal average takes the simple form [326]

$$\boxed{\langle\sigma_{ab\to cd}v_r\rangle = \frac{1}{2m_a^2m_b^2TK_2(m_a/T)K_2(m_b/T)}\int_{(m_a+m_b)^2}^{\infty} dsK_1(\sqrt{s}/T)p_{\mathrm{in}}(s)w(s)}\,, \tag{5.34}$$

where K_1 is the Bessel function of the second kind of order 1 and $w := E_aE_b\sigma_{ab\to cd}v_r$. The cross section for a given process $a + b \to c + d$ is

$$\sigma_{ab\to cd}v_r = \frac{1}{1+\delta_{cd}}\frac{p_{\mathrm{out}}(s)}{32\pi s p_{\mathrm{in}}(s)}\int d\cos\theta\,|\mathcal{M}_{ab\to cd}|^2\,. \tag{5.35}$$

Finally, employing the asymptotic expansion $K_n(x) = (2x/\pi)^{-1/2}e^{-x}[1 + (4n^2-1)/(8x) + \ldots]$ of the Bessel functions, changing the integration variable from s to $y = (s^{1/2} - m_1 - m_2)/T$, and then expanding in powers of T, we find

$$\begin{aligned}\langle\sigma v_{\mathrm{r}}\rangle &= \frac{w(s_0)}{m_1m_2} - \frac{3(m_1+m_2)}{2m_1m_2}\left[\frac{w(s_0)}{m_1m_2} - 2w'(s_0)\right]T + \mathcal{O}(T^2)\\ &= \frac{1}{m_1m_2}\left[1 - \frac{3(m_1+m_2)T}{2m_1m_2}\right]w(s)\big|_{s\to(m_1+m_2)^2+3(m_1+m_2)T} + \mathcal{O}(T^2)\,, && (5.36)\end{aligned}$$

where $s_0 = (m_1 + m_2)^2$.

5.3.3 Freeze-out Mechanism

Having obtained a compact formula for the thermally averaged annihilation cross section times the relative velocity, we now move on to examine the evolution of the number density of DM and how it can be related to the observed relic density through the mechanism of thermal freeze-out.

Let us focus on the simplest case: one single DM particle X with mass M_X, kept in thermal equilibrium through the annihilation reaction $XX \to \phi_{\rm SM}\phi_{\rm SM}$. The number density evolution of the X particles is described by the Boltzmann equation which reads

$$\boxed{\frac{\mathrm{d}n_X}{\mathrm{d}t} + 3Hn_X = -\langle\sigma v_r\rangle\left(n_X^2 - n_X^{\mathrm{eq}\,2}\right)}\,. \tag{5.37}$$

All the other SM species are assumed to be in thermal equilibrium, which means we have to solve only the above Boltzmann equation and not a coupled set of them.

For numerical purposes, it proves useful to rewrite (5.37) in terms of dimensionless quantities. Employing the comoving density $Y_X = n_X/\mathbf{s}$ (cf. Eq. (2.62)) and using the temperature as a time variable through $x := M_X/T$ the Boltzmann equation is transformed into

$$\boxed{\frac{\mathrm{d}Y_X}{\mathrm{d}x} = -\frac{\mathbf{s}\,(x=1)\,\langle\sigma v_r\rangle}{H\,(x=1)}\frac{1}{x^2}\left[Y_X^2 - Y_X^{\mathrm{eq}\,2}\right]}\,, \tag{5.38}$$

where H and $\mathbf{s}$ are evaluated at $T = M_X$.

The above equation is a particular form of Riccati equation for which there is no closed solution. In this regard, various numerical codes/tools have been developed [327–333] that are able to numerically solve the Boltzmann equation(s) for a given model and compute the relic density. Nevertheless, for the simple case under consideration here, it is possible to obtain a semi-analytical solution which is accurate up to a 10% factor. In this approach, the Boltzmann equation is solved in two opposite regimes. Remember that the evolution of DM depends on how the annihilation rate compares with the expansion rate. At very early times, when the Universe was hot and dense, the annihilation processes were very efficient since $\Gamma \gg H$ and the X particles were kept in thermal equilibrium ($Y_X \simeq Y_X^{\mathrm{eq}}$). At late times, after the temperature has dropped below the mass M_X and $\Gamma \ll H$, the DM particles can no longer interact with each other fast enough compared to the expansion rate of the Universe, and consequently fall out of equilibrium. This behaviour is illustrated in Fig. 5.4. In summary,

$$Y(x \lesssim x_f) \simeq Y_{\mathrm{eq}}(x) \quad \text{and} \quad Y(x \gtrsim x_f) \simeq Y_{\mathrm{eq}}(x_f)\,, \tag{5.39}$$

where x_f is the freeze-out point which physically corresponds to the time when the expansion rate of the Universe takes over the annihilation rate. The three main types of dark matter are usually distinguished according to their freeze-out temperature: hot dark matter with $x_f \ll 3$, cold dark matter with $x_f \gg 3$, and warm dark matter with the intermediate value $x_f \sim 3$.

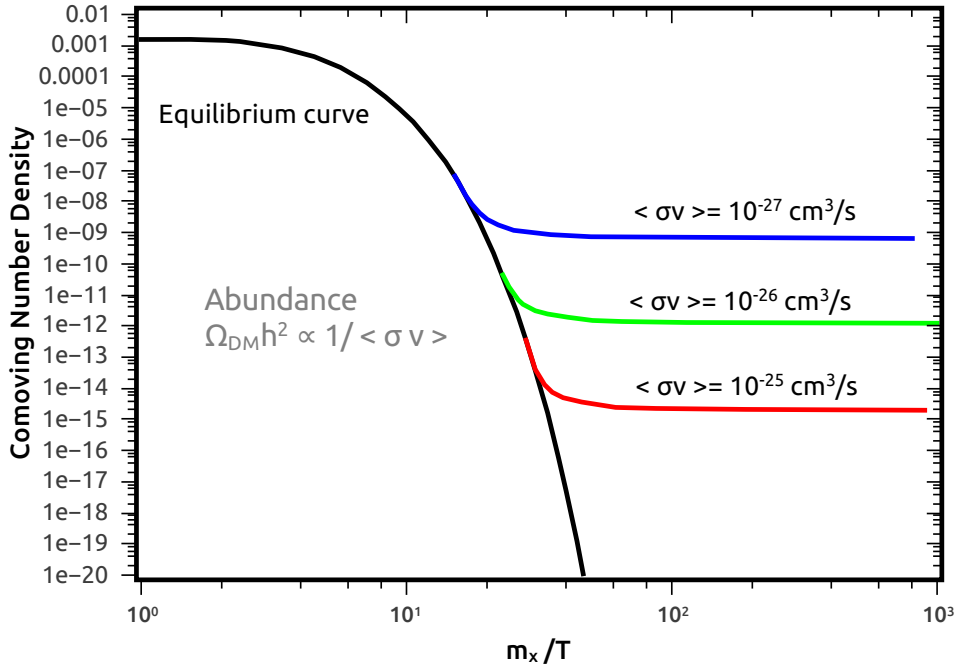

Figure 5.4: The evolution of the comoving number density as a function of the ratio M_X/T in the context of the freeze-out mechanism. Notice that the size of the annihilation cross section determines the DM abundance since $\Omega_{\rm DM} \propto 1/\langle\sigma v_r\rangle$. Credit: [334]

Coming back to the Boltzmann equation, let us further define the variable $\Delta_X := Y_X - Y_X^{\rm eq}$ and rewrite the differential equation as

$$\frac{{\rm d}\Delta_X}{{\rm d}x} = -\frac{{\rm d}Y_X^{\rm eq}}{{\rm d}x} - \frac{Z}{x^2}\left[\Delta_X^2 + 2\Delta_X Y_X^{\rm eq}\right], \qquad Z := \frac{s\,(x=1)\,\langle\sigma v_r\rangle}{H\,(x=1)}\,. \tag{5.40}$$

Before freeze-out, the number density can be well approximated by the equilibrium density. We may thus impose ${\rm d}\Delta_X/{\rm d}x = 0$ and solve for Δ_X, which gives

$$\Delta_X = -\frac{x^2}{Z\left[\Delta_X + 2Y_X^{\rm eq}\right]}\frac{{\rm d}Y_X^{\rm eq}}{{\rm d}x}, \qquad x \leq x_f\,. \tag{5.41}$$

After freeze-out, $Y_X^{\rm eq}$ is irrelevant, and we have

$$Y_X \simeq \Delta_X = -\left(\int_{x_f}^{x} {\rm d}x \frac{Z}{x^2}\right)^{-1}, \qquad x \geq x_f\,. \tag{5.42}$$

The last thing we need is the freeze-out value x_f. Since it is defined as the time when Y_X ceases to track $Y_X^{\rm eq}$, we may write

$$\Delta_X(x_f) = cY_X^{\rm eq}(x_f) \quad \Rightarrow \quad x_f \simeq \ln\left[0.038c\,(c+2)\,g\frac{\langle\sigma v_r\rangle\, M_X M_{\rm Pl}}{g_*^{1/2}x_f^{1/2}}\right], \tag{5.43}$$

where c is a constant of order one and we use the early time solution. The value of x_f is obtained by solving the above equation iteratively. With x_f at our disposal, we can finally determine the relic

density today

$$\boxed{\Omega_X h^2 = \frac{1.07 \times 10^9 \text{GeV}^{-1}}{g_*^{1/2} M_{\text{Pl}} J(x_f)}, \qquad J(x_f) = \int_{x_f}^{\infty} \mathrm{d}x \frac{\langle \sigma v_r \rangle}{x^2}}. \tag{5.44}$$

What is astonishing here is that for typical weak-scale pair annihilation cross sections ($\sigma \sim G_F^2 T^2$, with G_F the Fermi constant), for a typical freeze-out temperature ($T \sim M_X/20$), and for EW-scale masses ($M_X \sim \mu_{\text{EW}} \sim 200\,\text{GeV}$), the thermal relic density matches the observed cosmological density [1] ($\Omega_{\text{DM}} h^2 \approx 0.12$). This fact has been dubbed the *WIMP miracle*.

5.3.4 WIMP Candidates

At this point, let us briefly review some WIMPs that have either withstood the test of time or that have recently attracted attention.

- *Lightest supersymmetric particle (LSP).* One of the most appealing features of the supersymmetric extensions of the SM is that, among the plethora of new particles, the LSP can be stable due to an R-parity symmetry and thus serve the role of dark matter. For technical reasons, supersymmetric models require two Higgs doublets. The neutral supersymmetric particles are then

$$\text{Spin } 3/2 \text{ Fermion:} \quad \text{Gravitino } \tilde{G} \tag{5.45}$$

$$\text{Spin } 1/2 \text{ Fermions:} \quad \tilde{B},\ \tilde{W},\ \tilde{H}_u,\ \tilde{H}_d \ \rightarrow \ \text{Neutralinos } \chi_1,\ \chi_2,\ \chi_3,\ \chi_4 \tag{5.46}$$

$$\text{Spin } 0 \text{ Bosons:} \quad \text{Sneutrinos } \tilde{\nu}_e,\ \tilde{\nu}_\mu,\ \tilde{\nu}_\tau\,. \tag{5.47}$$

  The gravitino is sometimes called a super-WIMP since its interaction rate is very weak compared to that of other supersymmetric DM candidates [335–339]. It can be hot, warm, or cold DM, depending on its mass and production mechanism. Sneutrinos are not very good DM candidates since they are underabundant (if they exist) and thus cannot constitute all of dark matter (see however [340–342]). The most successful supersymmetric particle that can play the role of WIMP dark matter is the lightest among the neutralinos, usually denoted as $\chi := \chi_1$ [343,344] (see also [345–348]). It is characterized by a mass range from about 2 GeV to 10^4 GeV and has viable detection prospects.

- *Two Higgs doublet models (2HDM).* In this family of SM extensions, the Higgs sector is augmented with the addition of another Higgs doublet which gives rise to new charged and neutral Higgs bosons [349] (see [350] for a review). Among these models, the simplest is the inert doublet model (IDM) where a Z_2 symmetry is imposed, under which all the SM fields are even while the new Higgs doublet is odd [351–354]. Then, the lightest of the extra neutral states H^0 or A^0 can constitute dark matter. Since these states couple to the SM Higgs boson, this scenario could give possible signals from spin-independent scattering in direct detections experiments.

- *Little Higgs.* As we saw in Section 4.4, little Higgs models are advocated as a solution to the naturalness problem. After the global symmetry gets broken, there remains a Z_2 symmetry often called T-parity [355–357] under which the new heavy fields are odd while the SM fields are even. Then, the lightest of these extra fields is stable and can constitute dark matter.

- *The twin Higgs models.* In this class of models, a copy of the SM is introduced. The Higgs sector respects a global $SU(4)$ symmetry which is broken at the one-loop level by radiative

corrections. A discrete Z_2 symmetry between the two sectors ensures equality of their couplings. Then a WIMP DM candidate can arise from the twin sector [358–361]. The coupling of twin DM to the SM Higgs can result in a spin-independent cross section that direct detection experiments can search for.

- *Scalar dark matter.* Perhaps the simplest model that can provide a DM candidate is that of the SM extended with a real singlet scalar field S [362–364]. The essential couplings are just its bare mass term and a portal coupling to the SM Higgs field,

$$V = \frac{1}{2}\mu_S^2 S^2 + \frac{1}{2}\lambda_{hs} S^2 |H|^2 \,. \tag{5.48}$$

  The portal coupling λ_{hs} can also help in the stabilization of the vacuum. By imposing the Z_2 symmetry $S \to -S$, the singlet scalar is rendered absolutely stable and can constitute dark matter (see [365, 366] for recent phenomenological analyses).

- *Fermionic dark matter.* Dirac or Majorana fermions can also play the role of dark matter. Charging the fermions under a new global $U(1)$ results in no mixing with the SM fermions. Then, employing the machinery of effective field theory, non-renormalizable dimension-5 and dimension-6 operators connect the dark and visible sectors [367–371]. The model can be made renormalizable with the addition of a real singlet scalar field [372–375] (see also [376–378]).

- *Vector dark matter (VDM).* Last but not least, enlarging the gauge group of the SM can provide for new DM candidates in the form of the extra gauge bosons [379–427]. As we will promptly see, the main advantage of these models is that the new gauge symmetries contain intrinsic discrete symmetries that automatically render the vector bosons stable. There is therefore no need to put by hand any stabilizing symmetry. Since vector dark matter will be of interest to us in this thesis, in the next subsection we will review how these intrinsic symmetries arise in the $U(1)$ and $SU(N)$ gauge groups.

5.3.5 Stabilizing Symmetries from new Gauge Groups

In this subsection we will closely follow the analysis of [401] and see how stabilizing symmetries can arise from the breaking of new Abelian and non-Abelian gauge groups.

$U(1)$ case

The simplest way to enlarge the gauge structure of the SM is to introduce a new Abelian gauge sector. For the $U(1)$ to get broken, a single charged scalar Φ that obtains a VEV $\langle\Phi\rangle = v_\phi/\sqrt{2}$ suffices. Then, the Lagrangian of the hidden sector has the form

$$\mathcal{L}_{\text{hidden}} = -\frac{1}{4}F_{\mu\nu}F^{\mu\nu} + (D_\mu\Phi)^\dagger D^\mu\Phi - V(\Phi) \,, \tag{5.49}$$

where $F_{\mu\nu}$ is the field strength tensor of the gauge field X_μ, $V(\phi)$ is the scalar potential and we take the charge of Φ to be $+1/2$. The imaginary part of Φ becomes the longitudinal component of the gauge field which acquires the mass $M_X = g_X v_\phi/2$, where g_X is the gauge coupling. Denoting with ϕ the real part of the singlet and normalizing it canonically, $\Phi = (\phi + v_\phi)/\sqrt{2}$, the gauge-scalar part of the Lagrangian becomes

$$\Delta\mathcal{L}_{\text{s-g}} = \frac{g_X^2}{4} v_\phi \phi \; X_\mu X^\mu + \frac{g_X^2}{8}\phi^2 \; A_\mu A^\mu \,. \tag{5.50}$$

The system is invariant under the Z_2 symmetry

$$X_\mu \to -X_\mu \,, \tag{5.51}$$

which is essentially a charge conjugation symmetry. It acts on the scalar field as $\Phi \to \Phi^*$ and is preserved by both the Lagrangian and the vacuum. Due to this Z_2 symmetry the massive gauge field is stable and can therefore play the role of dark matter.

$SU(2)$ case

We can easily extend the above considerations to the $SU(2)$ case. The scalar field Φ now becomes a doublet and the hidden Lagrangian has the form

$$\mathcal{L}_{\text{hidden}} = -\frac{1}{4}F^a_{\mu\nu}F^{a\,\mu\nu} + (D_\mu\Phi)^\dagger D^\mu\Phi - V(\Phi)\,, \tag{5.52}$$

with $a = 1, 2, 3$. In the unitary gauge, the scalar field obtains the form

$$\Phi = \frac{1}{\sqrt{2}}\begin{pmatrix} 0 \\ \phi + v_\phi \end{pmatrix} \tag{5.53}$$

and the three gauge bosons obtain equal masses, $M_{X^1} = M_{X^2} = M_{X^3} =: M_X = g_X v_\phi/2$. After symmetry breaking, the scalar-gauge and gauge-gauge field interactions have the form

$$\begin{aligned}
\Delta\mathcal{L}_{\text{s-g}} &= \frac{g_X^2}{4}v_\phi\phi\; X^a_\mu X^{a\,\mu} + \frac{g_X^2}{8}\phi^2\; X^a_\mu X^{a\,\mu}\,, \\
\Delta\mathcal{L}_{\text{g-g}} &= -g_X\epsilon^{abc}(\partial_\mu X^a_\nu)X^{\mu\,b}X^{\nu\,c} - \frac{g_X^2}{4}\left((X^a_\mu X^{\mu\,a})^2 - X^a_\mu X^a_\nu\; X^{\mu\,b}X^{\nu\,b}\right)\,.
\end{aligned} \tag{5.54}$$

This system possesses a $Z_2 \times Z_2'$ symmetry

$$\begin{aligned}
Z_2 &: \;\; X^1_\mu \to -X^1_\mu \;\;,\;\; X^2_\mu \to -X^2_\mu\,, \\
Z_2' &: \;\; X^1_\mu \to -X^1_\mu \;\;,\;\; X^3_\mu \to -X^3_\mu\,.
\end{aligned} \tag{5.55}$$

This means all three X^a_μ fields are stable and can constitute dark matter.

$SU(N)$ case

Let us now extend the above analysis to the $SU(N)$ case and see how the $Z_2 \times Z_2'$ parity arises. We can break $SU(N)$ completely by the VEVs of $N-1$ fields Φ_i in the fundamental representation. Without loss of generality, we may gauge–transform those fields and write them as

$$\Phi_1 = \begin{pmatrix} 0 \\ 0 \\ \dots \\ 0 \\ \phi_1 \end{pmatrix} \;\;,\;\; \Phi_2 = \begin{pmatrix} 0 \\ 0 \\ \dots \\ \phi_2^{(1)} \\ \phi_2^{(2)} e^{i\rho_2} \end{pmatrix} \;\;,\;\; \dots \;\;,\;\; \Phi_{N-1} = \begin{pmatrix} 0 \\ \phi_{N-1}^{(1)} \\ \dots \\ \phi_{N-1}^{(N-2)} e^{i\rho_{N-1}^{(N-3)}} \\ \phi_{N-1}^{(N-1)} e^{i\rho_{N-1}^{(N-2)}} \end{pmatrix}\,, \tag{5.56}$$

where $\phi_i^{(j)}$ and $\rho_i^{(j)}$ are real.

We identify the transformation properties of the gauge fields with those of the corresponding $SU(N)$ generators. We can choose the basis of the $N(N-1)$ off–diagonal generators $T^{ab}, \tilde{T}^{ab}$ as

$$\begin{aligned}(T^{ab})_{ij} &= \delta_{ia}\delta_{jb} + \delta_{ib}\delta_{ja}\ ,\\ (\tilde{T}^{ab})_{ij} &= -i\delta_{ia}\delta_{jb} + i\delta_{ib}\delta_{ja}\ ,\end{aligned} \tag{5.57}$$

where $a = 1, ..., N-1$ and $b = 2, ..., N$. Denoting the Cartan generators by H^α, there is a Z_2 that acts as

$$T^{ab} \to -T^{ab}\ ,\ \ \tilde{T}^{ab} \to \tilde{T}^{ab}\ ,\ \ H^\alpha \to -H^\alpha\ , \tag{5.58}$$

and can be associated with complex conjugation of the group elements. This Z_2 is a known outer automorphism of $SU(N)$.

We can define another Z_2 by reflecting the off–diagonal generators containing nonzero elements in the first row:

$$\begin{aligned}&T^{1a} \to -T^{1a}\ ,\ \ \tilde{T}^{1a} \to -\tilde{T}^{1a}\ ,\\ &T^{bc} \to T^{bc}\ \ \ ,\ \ \tilde{T}^{bc} \to \tilde{T}^{bc}\ \ \ (b, c \geq 2),\\ &H^\alpha \to H^\alpha\ .\end{aligned} \tag{5.59}$$

This Z_2 corresponds to the group transformation with

$$U = e^{\frac{i\pi}{N}}\ \mathrm{diag}(-1, 1, ..., 1)\ . \tag{5.60}$$

Therefore, it is identified as an inner automorphism. Let us now focus on the upper left $SU(2)$ block

$$T^{12},\ \ \tilde{T}^{12},\ \ H^1 = \mathrm{diag}(1, -1, 0, ..., 0)\ . \tag{5.61}$$

The gauge fields X_μ^{1-3} associated with this block transform under these two parities the same way as the $SU(2)$ gauge fields did under $Z_2 \times Z_2'$ in (5.55).

Note that these symmetries are preserved by gauge interactions with scalars. The first Z_2 acts on scalar fields by reflecting the complex phases. The *CP* invariance of the Lagrangian guarantees this symmetry, which is also preserved by the vacuum. The second Z_2 corresponds to a gauge transformation. It acts in a multiplicative way on vectors of the form $(0, a_1, ..., a_{N-1})$ by introducing an overall constant phase that cancels in all the Lagrangian terms. Therefore, it also holds in the broken phase as well.

Now, as long as the ϕ_i contain a zero first component, the interaction vertices have only an even number of T^{1a} and $\tilde{T}^{1a}$. The gauge fields corresponding to $a > 2$ are heavier than those with $a = 2$. They thus decay to the lighter fields by virtue of the vertices involving $T^{12}T^{1k}$ $(k > 2)$. In this way, only the final $SU(2)$ remains stable. Therefore, DM is composed mostly of the aforementioned X_μ^{1-3} gauge fields whose stability is enforced by $Z_2 \times Z_2'$.

5.4 Dark Matter Searches

Let us close this chapter on dark matter by briefly reviewing its experimental status. The main WIMP search strategies generally fall in three big categories:

- *Direct detection* searches aim at probing the scattering cross section of WIMPs off nuclei, by seeking for nuclear recoil in some target material in a low-background underground detector.

- *Indirect detection* experiments look for the byproducts of WIMP annihilations against the expected background at galactic and extragalactic scales, using Earth-based telescopes or satellites.
- *Collider* searches may be able to infer the existence of electrically neutral particles, such as WIMPs, through missing energy signatures in QCD jets and photons, originating from proton-proton (LHC) or electron-positron (ILC) collisions.

In Fig. 5.5 we show a pictorial summary of the WIMP searches.

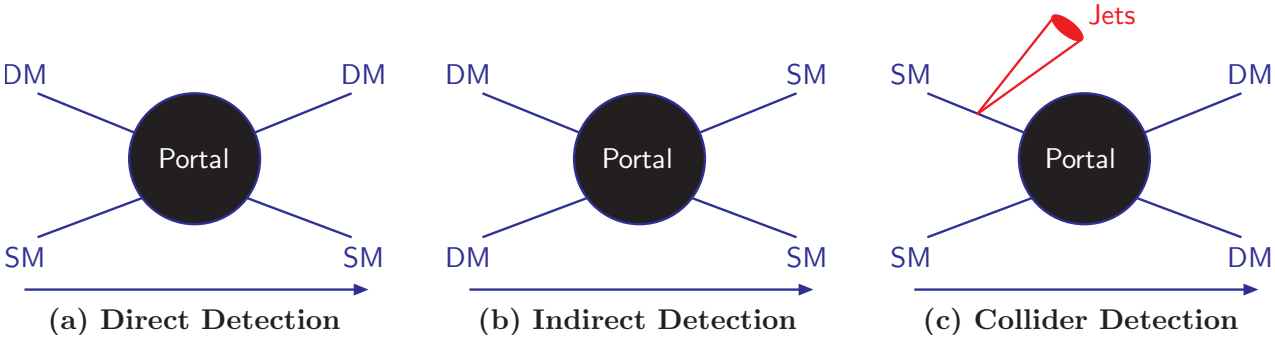

Figure 5.5: Illustration of the DM interactions with SM particles for the three main categories of DM searches. Credit: [334]

5.4.1 Direct detection

Over the last few years, intense activity and impressive progress has taken place in the direction of directly detecting dark matter. A plethora of experiments [428–457] looking for elastic scatterings of DM particles off nuclei have set strong bounds on WIMP interactions.

The WIMP-nuclei differential scattering rate can be written as

$$\frac{\mathrm{d}R}{\mathrm{d}E_R} = \frac{\rho_0}{m_{\mathcal{N}} M_X} \int_{v_{\min}}^{v_{\mathrm{esc}}} \mathrm{d}^3\vec{v}\, v f_E(\vec{v},t) \frac{\mathrm{d}\sigma}{\mathrm{d}E_R}\,, \tag{5.62}$$

where E_R is the nuclear recoil energy, ρ_0 is the local WIMP density in the galactic halo ($\rho_0 = 0.3\,\mathrm{GeV/cm^3}$) [458–464], $m_{\mathcal{N}}$ is the nucleus mass and M_X the WIMP mass. $\vec{v}$ is the velocity of the DM particle relative to Earth and $f_E(\vec{v},t)$ is the WIMP velocity distribution in the Earth frame. The minimum WIMP velocity required to produce a detectable event at energy E_R is $v_{\min} = \sqrt{m_{\mathcal{N}} E_R/(2\mu_{\mathrm{red}}^2)}$, while v_{esc} is the velocity for which the WIMP escapes the Milky Way gravitational potential. Moreover, $\mu_{\mathrm{red}} = m_{\mathcal{N}} M_X/(m_{\mathcal{N}} + M_X)$ is the WIMP-nucleus reduced mass and $\mathrm{d}R/\mathrm{d}E$ is the WIMP-nucleus differential cross section. The latter can be written as

$$\frac{d\sigma}{dE} = \frac{m_N}{2\mu_{\mathrm{red}}^2 v^2}\left(\sigma_{SI} F_{SI}^2(\mathcal{N}, E_R) + \sigma_{SD} F_{SD}^2(\mathcal{N}, E_R)\right), \tag{5.63}$$

where F_{SI} and F_{SD} are the nuclear form factors that depend on the recoil energy [346, 465–467]. σ_{SI} and σ_{SD} are the *spin-independent* and *spin-dependent* cross sections in the zero momentum transfer

limit, given by

$$\sigma_{SI} = \frac{4\mu_{\rm red}^2}{\pi}\left[Zf_p + (A-Z)\,f_n\right]^2 , \tag{5.64}$$

$$\sigma_{SD} = \frac{32\mu_{\rm red}^2}{\pi}G_F^2\frac{J+1}{J}\left[a_p\left\langle S_p\right\rangle + a_n\left\langle S_n\right\rangle\right]^2 , \tag{5.65}$$

where J is the total spin of the nucleus, A and Z are the number of nucleons and protons, and f_p, f_n and a_p, a_n are the spin-dependent and spin-independent WIMP couplings to protons and neutrons, respectively. For a given model these can be calculated using the corresponding effective Lagrangian. The terms in brackets $\langle S_{p,n}\rangle = \langle\mathcal{N}|S_{p,n}|\mathcal{N}\rangle$ are the expectation values of the spin content of the proton and neutron in the nucleus.

Most experiments are more sensitive to spin-independent interactions. This is attributed to the $A^2 \sim 10^4$ enhancement (assuming $f_n = f_p = 1$) of the spin-independent scattering rate and also to the fact that experiments containing nuclei with non-zero spin are difficult to scale up. In this thesis, we will only consider models with scalar mediators between the DM particles and the quarks in the nuclei. Therefore, we will only employ the spin-independent cross section (5.64) in our calculations. Plugging (5.63) into (5.62), one may then compare the predicted number of recoil events with data, and derive bounds on σ_{SI} (or σ_{SD}).

Over the last few years various hints for a DM signal have surfaced from experiments such as DAMA/LIBRA [468, 469], CoGent [429, 430, 470, 471] and CDMS-II [436], but these come into conflict with the null results of numerous other experiments [438, 439, 441, 443, 446–453, 453, 472–479]. The current strongest exclusion limit in the plane of spin-independent DM-nucleon cross section has been placed by the XENON1T experiment [479] for large DM masses; a (null) result also corroborated by LUX [441] and PandaX-II [478]. The next generation of DM direct detection experiments includes LZ [480, 481], DarkSide-20k [435], DARWIN [481], and SuperCDMS [482] (see Fig. 5.6). Hopefully, one or more of these experiments will be able to directly detect dark matter in the near future.

5.4.2 Indirect detection

The nature of dark matter could potentially be inferred by astrophysical signals containing excesses of high-energy gamma-rays, neutrinos or anti-matter (positrons, anti-protons and anti-deuterium), produced by DM annihilations or decays. Since the annihilation rate of DM is proportional to the number density squared, the obvious targets for studies are nearby regions where DM densities are expected to be enhanced. In other words, the same annihilation processes that determined the DM relic abundance in the early Universe will also take place today in galactic regions with higher DM concentration. The most promising messengers for indirect DM detection are photons and neutrinos which propagate almost unperturbed through the galaxy. On the other hand, charged particles originating in the DM halo undergo many processes (such as bremsstrahlung, inverse Compton scattering with CMB photons, etc.) that disturb their propagation until the point of detection. The most competitive current searches come from Earth-based telescopes such as H.E.S.S. and CTA, or satellites such as AMS and Fermi-LAT [485–499]. Over the past few years, several potential signals have appeared in indirect DM searches. All of these, however, are either controversial and come into conflict with each other, or can be explained away by other astrophysical phenomena. For a recent review on the status of indirect DM searches see [500].

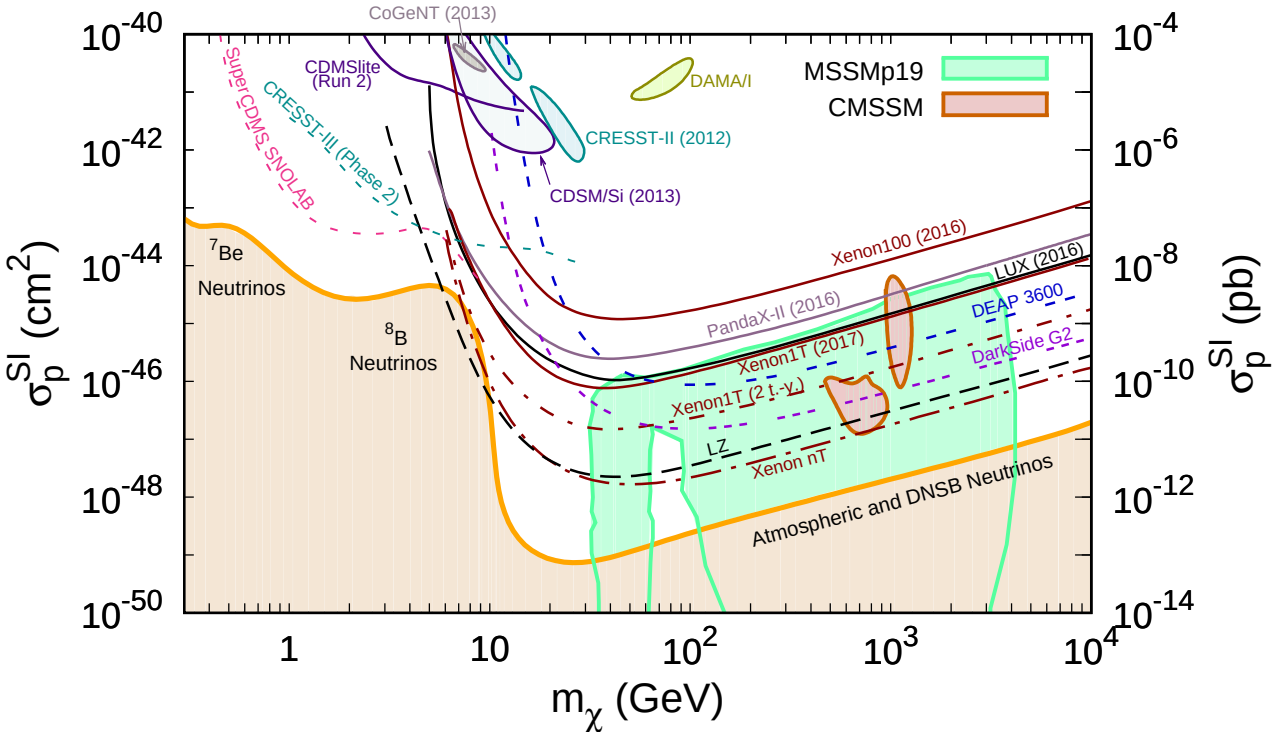

Figure 5.6: Current and future limits on DM direct detection spin-independent cross section as a function of the DM mass. The shaded area below the orange line on the bottom corresponds to the irreducible neutrino background [483]. Credit: [484]

5.4.3 Collider searches

Particle accelerators such as the currently operating LHC and the proposed International Linear Collider (ILC) [501] could in principle provide us with information on particle dark matter via the detection of mono-jet or mono-photon signals arising from XXj and $XX\gamma$ production. In order to disentangle a DM signal, experimentalists must select events with large missing energy [502] thus reducing the SM background. However, missing energy only confirms the presence of a neutral and stable particle[1] and cannot be used to uniquely ascertain the presence of DM in a signal event. Nevertheless, data obtained by colliders in conjunction with direct and indirect searches may be useful and help us refine information on the properties of DM, such as its mass and couplings. For more detailed reviews see, e.g., [503, 504].

[1] Stable in the context of the LHC, not necessarily cosmologically stable.

Chapter 6

Classical Scale Invariance

After this lengthy introduction, we are finally ready to examine the main topic of this thesis, namely, *classical scale invariance* (CSI). This symmetry was originally advocated as a solution to the hierarchy problem [6], but we will see that it can also serve as a framework for the construction of minimal extensions of the Standard Model that are able to provide solutions to its shortcomings.

In the next section, we will begin by conjecturing that the dimensionality of spacetime is the reason behind the appearance of only (super-)renormalizable operators in the SM Lagrangian. Then, in Section 6.2 we will argue that classical scale invariance is responsible for this fact and briefly review the main features of the symmetry. In Section 6.3 we will see how a scale can be radiatively generated due to the running of the coupling constants by reviewing the famous Coleman-Weinberg mechanism. We will also see how the electroweak scale can be made stable against radiative corrections from higher scales. After that, we will generalize the Coleman-Weinberg mechanism to the case of multiple scalar fields in Section 6.4. In Section 6.5, we will present an example of a CSI model and proceed to discuss the main features of the various CSI models found in the literature. Finally, in Section 6.6, we will see how the Planck scale can be dynamically generated in a CSI manner by the VEV of a scalar field that can also drive inflation.

6.1 Renormalizability of Effective Field Theories

In the Wilsonian approach [505, 506], the Lagrangian is written as a sum of local operators

$$\mathcal{L} = \sum_i \rho_i M_i^{d_i-4} \mathcal{O}_i, \tag{6.1}$$

and is defined on a sphere in Euclidean momentum space with radius M. Renormalizability is then seen as a consequence of the scaling of operators. A theory can be redefined at a lower momentum scale $M' = M/N$, if one first integrates out the high-energy modes of the fields in the operators $\mathcal{O}_i$ with Euclidean momenta larger than M/N. Then, the radius of validity is rescaled to a sphere of radius M which leads to the new operator coefficients

$$\rho_i \to \rho_i / N^{d_i-4}\,. \tag{6.2}$$

In four dimensions, operators are classified into three categories:

1. Relevant operators ($d < 4$):

$$\phi^\dagger\phi\,,\ \bar{\psi}\psi\,,\ \phi^3 \tag{6.3}$$

2. Marginal operators ($d = 4$):

$$(\partial^\mu \phi)^\dagger (\partial_\mu \phi) \ , \ \bar{\psi} i \not{D} \psi \ , \ F_{\mu\nu} F^{\mu\nu} \ , \ \bar{\psi}\psi\phi \ , \ \left(\phi^\dagger \phi\right)^2 \tag{6.4}$$

3. Irrelevant operators ($d > 4$):

$$\bar{\psi}\psi\phi^\dagger\phi \ , \ (\bar{\psi}\psi)^2 \ , \ (D^\mu \phi)^\dagger (D_\mu \phi) \left(\phi^\dagger \phi\right) \ , \ \left(\phi^\dagger \phi\right)^3 \tag{6.5}$$

The irrelevant or non-renormalizable operators have a negative power-law dependence on the renormalization scale. Therefore, they do not appear naturally in the low-energy theory. The relevant or super-renormalizable operators, such as the mass term of a scalar field, have a positive power-law dependence on the renormalization scale. Therefore, the appearance of such terms with a coefficient that is much smaller than the cut-off scale is deemed unnatural. Finally, marginal or renormalizable operators come with dimensionless coupling constants.

If we regard the SM as an effective field theory in the Wilsonian picture then we face two choices:

- The first possibility is that the cutoff scale of the theory is given by the scale of the only relevant operator, i.e. the Higgs mass. This means new physics such as Supersymmetry must appear around the electroweak scale. If that were the case, however, dimension 6 (and higher) operators would induce rapid proton decay since they would be suppressed only by the low new physics scale. Of course, this cut-off scale could be concealed from experiments by a symmetry such as R-parity.
- The second possibility is that the cut-off scale is much larger than the EW scale. Then, the non-renormalizable operators are naturally absent. But then extreme fine-tuning would be needed to explain why the Higgs mass is so much smaller than this scale, which leads to the naturalness problem.

The above suggest that we cannot successfully apply the Wilsonian picture to the SM. But how else can we explain the size of the Higgs mass and the absence of higher-order operators?

6.2 Classical scale invariance

In the SM Lagrangian all operators are renormalizable and the coupling constants are dimensionless, with the exception of the Higgs mass parameter. Despite decades of precision flavour physics, the SM has displayed no evidence for the existence of non-renormalizable interactions. Also, the fact that the proton appears to be stable suggests that there are no generic higher-order operators up to the scale of 10^{16} GeV.

How can we then make sense of the fact that Nature would only allow renormalizable interactions to exist at the fundamental level? An interesting possibility which we explore in this thesis is that the fundamental theory is scale invariant at the classical level. Then, in four dimensions only operators of mass-dimension $d = 4$ are allowed. Any operator of dimension $d \neq 4$ would have a dimensionfull coupling constant which sets a unique scale in the theory and breaks the classical scale invariance.

We may parallelize this property to the Copernican principle in cosmology, which states that no point in space is unique, or to the invariance of physics with respect to any chosen reference frame. In Cosmology, while the Universe appears isotropic and homogeneous at large scales, we saw in Chapter 3 that quantum fluctuations have generated structure. Similarly, classical scale symmetry

prompts us to demand that no momentum scale be unique at the classical level. Then, as we will see in the next section, quantum effects break the tree-level scale invariance due to the running of the coupling constants which results in the interactions of particles to appear different at different energy scales.

Coming back to the Higgs mass term, if classical scale invariance is a fundamental property of Nature, then this operator is not allowed in a fundamental theory. We must therefore look for a mechanism to generate this term dynamically (see Section 6.3). But before that, let us examine classical scale invariance in more detail.

We start by considering a simple model with one real scalar field $\phi(x)$. The Lagrangian that describes this model is

$$\mathcal{L} \;=\; \frac{1}{2}\partial_\mu\phi(x)\partial^\mu\phi(x) \;+\; \frac{1}{2}m^2\phi^2(x) \;-\; \lambda\phi^4(x)\,. \tag{6.6}$$

Under a scale transformation, the coordinates transform as

$$x \to x' = \exp(\epsilon)x\,, \tag{6.7}$$

while the scalar field transforms as

$$\phi(x) \;\to\; \phi'(x) \;=\; \sigma\phi(\sigma x)\,, \tag{6.8}$$

where $\sigma = e^\epsilon > 0$. In general, a scale transformation is defined as $\phi(x) \to \phi'(x) = e^{\epsilon a}\phi(e^\epsilon x)$, where a is the scaling dimension of the field $\phi(x)$. In the free theory scalars have scaling dimension $d_\phi = 1$, while fermions have $d_\psi = 3/2$. Now, under the scale transformation (6.8) the classical action

$$S[\phi(x)] \;=\; \int d^4x\; \mathcal{L}[\,\partial_\mu\phi(x), \phi(x)] \tag{6.9}$$

transforms as

$$\begin{aligned} S[\sigma\phi(\sigma x)] = & \int_{-\infty}^{\infty} d^4x \left[\sigma^2\frac{1}{2}\partial_{x\mu}\phi(\sigma x)\partial_x^\mu\phi(\sigma x) \;+\; \frac{1}{2}m^2\sigma^2\phi^2(\sigma x) \;-\; \lambda\sigma^4\phi^4(\sigma x)\right] \\ = & \int_{\sigma(-\infty)}^{\sigma(\infty)} d^4(\sigma x) \left[\frac{1}{2}\partial_{(\sigma x)\mu}\phi(\sigma x)\partial^\mu_{(\sigma x)}\phi(\sigma x) \;+\; \frac{1}{2}\sigma^{-2}m^2\phi^2(\sigma x) \;-\; \lambda\phi^4(\sigma x)\right]. \end{aligned} \tag{6.10}$$

Clearly, for the transformed action $S[\sigma\phi(\sigma x)]$ to be equal to the original one $S[\phi(x)]$, the dimensionful parameter m^2 has to vanish. In other words, the absence of a mass term results in a scale-invariant theory.

Invariance of the theory under scale transformations will lead to a conserved Noether current Θ_μ. We can find an expression for this current by making use of the fact that the symmetric energy-momentum tensor may be defined as

$$T^{\mu\nu} = 2\frac{\delta}{\delta g_{\mu\nu}}\int \mathrm{d}^4x\mathcal{L}\,. \tag{6.11}$$

Then, under scale transformations $\delta g_{\mu\nu} \propto g_{\mu\nu}$, this yields

$$\partial_\mu\Theta^\mu = \delta S \propto \delta g_{\mu\nu}T^{\mu\nu} \propto g_{\mu\nu}T^{\mu\nu} = T^\mu_\mu\,. \tag{6.12}$$

We see that the trace of the energy-momentum tensor gives the conservation of the scaling or dilatation current. When $T^\mu_\mu = 0$, the theory is said to be scale invariant.

So far, the analysis has been performed at tree level. We could include quantum corrections by considering the running of the coupling constants of the theory with energy. A scale transformation acts as $g \to g + \epsilon\beta(g)$, where $\beta(g)$ is the usual β-function. Including one-loop corrections, we find

$$\partial_\mu \Theta^\mu = T^\mu_{\ \mu} = \delta\mathcal{L} = \beta(g)\frac{\partial}{\partial g}\mathcal{L}\,. \tag{6.13}$$

If the β-functions vanish, then the quantum theory is scale invariant. Alternatively, if the Lagrangian is scale-invariant but $\beta(g) \neq 0$, then scale invariance is broken and the theory is *classically scale invariant*. The breaking of scale invariance is only due to the logarithmic running of coupling constants and the scales might be generated in a dynamical way. We can therefore either view classical scale invariance as softly broken scale invariance or adopt Hill's conjecture and view it as a classical symmetry which becomes exact in the classical limit of $\hbar \to 0$ [507]. When performing calculations in CSI theories one should not use a cut-off regulator since that would break scale invariance [6]. Instead, one should use a regularization scheme that does not introduce the UV scale explicitly, such as dimensional regularization. We will see that models endowed with classical scale invariance can address the hierarchy problem and also provide solutions to various problems of the SM (and Cosmology).

The symmetry group of a scale-invariant field theory in d dimensions is

$$ISO(d-1,1) \rtimes \mathbb{R}^+\,, \tag{6.14}$$

where $ISO(d-1,1)$ is the Poincaré group (in Minkowski space) and $\mathbb{R}^+$ is generated by dilatations. Lorentz transformations are invariant under dilatations, while the momentum generators carry charge 1. It is possible to extend the group of scale transformations to the conformal group

$$SO(d,2)\,, \tag{6.15}$$

by including special conformal transformations. Of course, conformal theories are scale invariant. In $d = 4$, the converse statement also seems to hold, see e.g. [508]. For this reason, in the literature classical scale invariance is sometimes referred to as classical conformal invariance.

Another related model-building approach is to consider theories with an exact quantum scale invariance of the UV theory [509–512]. If the full quantum theory, including gravity, respects scale invariance which is broken spontaneously, the Higgs mass would be protected from radiative corrections by an exact dilatational symmetry. This solution to the hierarchy problem is similar to Supersymmetry.

6.3 Coleman-Weinberg Mechanism

In their seminal paper in 1973 [7], S. Coleman and E. Weinberg developed a mechanism for the dynamical generation of scale in a classically massless theory. In this Section we will see how radiative corrections can dynamically generate nonzero vacuum expectation values and masses. Following [7], we first review the effective action and potential. Then, we calculate the effective potential for a classically massless $U(1)$ theory.

6.3.1 Effective Action and Potential

In order to study the spontaneous symmetry breaking at the quantum level we define the effective action and potential. We do this in the path integral representation of quantum field theory. The

vacuum-to-vacuum transition amplitude for a scalar field ϕ, described by a Lagrangian $\mathcal{L}$, in the presence of an external source $J(x)$, is given by

$$Z[J] = \int \mathcal{D}\phi \exp\left[i \int \mathrm{d}^4x \mathcal{L}[\phi] + J\phi\right] . \tag{6.16}$$

$Z[J]$ is called the generating functional of the Green's function. From $Z[J]$, we can define the energy functional $W[J]$ as

$$e^{iW[J]} = Z[J] = \langle \Omega | \Omega \rangle_J . \tag{6.17}$$

The energy functional corresponds to the vacuum energy in the presence of the source, and it is analogous to the Helmholtz free energy in a condensed matter system. Let us now define the mean or "classical" field ϕ_{cl} as

$$\phi_{\mathrm{cl}} = \frac{\delta W[J]}{\delta J(x)} = \frac{\langle \Omega | \phi(x) | \Omega \rangle_J}{\langle \Omega | \Omega \rangle_J} \tag{6.18}$$

The classical field is a function of spacetime and a functional of the source. The effective action $\Gamma[\phi_{\mathrm{cl}}]$ is obtained by a Legendre transform of the energy functional, namely,

$$\Gamma[\phi_{\mathrm{cl}}] = W[J] - \int \mathrm{d}^4x J(x)\phi(x) . \tag{6.19}$$

We can expand the effective action as a series of one-particle-irreducible connected Green's functions Γ_i

$$\Gamma = \sum_n \frac{1}{n!} \int \mathrm{d}^4x_1 \ldots \mathrm{d}^4x_n \Gamma^{(n)}(x_1, \ldots, x_n)\, \phi_{\mathrm{cl}}(x_1) \ldots \phi_{\mathrm{cl}}(x_n) . \tag{6.20}$$

We can also expand the effective action in powers of momentum

$$\Gamma = \int \mathrm{d}^4x \left[-V(\phi_{\mathrm{cl}}) + \frac{1}{2} \left(\partial_\mu \phi_{\mathrm{cl}}\right)^2 Z(\phi_{\mathrm{cl}}) + \ldots \right] , \tag{6.21}$$

where $V(\phi_{\mathrm{cl}})$ is the effective potential which at tree level is equal to the normal scalar potential. Varying (6.19) with respect to the classical field, we find

$$\frac{\delta \Gamma[\phi_{\mathrm{cl}}]}{\delta \phi_{\mathrm{cl}}} = -J(x) . \tag{6.22}$$

Spontaneous symmetry breaking occurs if ϕ_{cl} develops a nonzero vacuum expectation value. This can easily happen when the source is switched off, whereby

$$\left. \frac{\delta \Gamma[\phi_{\mathrm{cl}}]}{\delta \phi_{\mathrm{cl}}} \right|_{\phi_{\mathrm{cl}} \neq 0} = 0 . \tag{6.23}$$

From (6.21), we can see that, if we consider the vacuum state to be translationally invariant then the above condition reduces to

$$\left. \frac{\delta V(\phi_{\mathrm{cl}})}{\delta \phi_{\mathrm{cl}}} \right|_{\phi_{\mathrm{cl}} \neq 0} = 0 . \tag{6.24}$$

The above shows that the effective potential is a very useful tool for studying the symmetry breaking properties of a theory. By studying the minima of the effective potential we gain insight into the structure of the vacuum. It is then interesting to explore whether radiative corrections change the qualitative nature of the extrema of the classical potential.

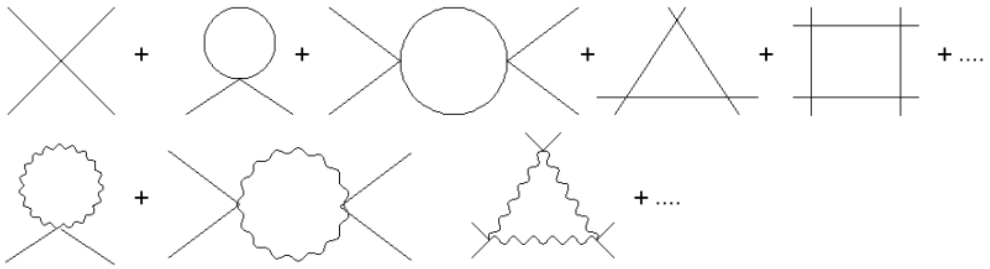

Figure 6.1: Feynman diagrams for the one-loop effective potential of scalar QED, including scalar and gauge boson loops.

6.3.2 One-loop effective potential for classically massless $U(1)$

Let us now employ the above formalism to study spontaneous symmetry breaking in a classically massless $U(1)$ theory, where we also introduce a complex scalar field. At tree level, the $U(1)$ symmetry is unbroken since the potential only has one minimum at the origin of field space. By including radiative corrections, we want to examine whether the $U(1)$ symmetry gets broken. The Lagrangian of the theory has the form

$$\mathcal{L} = \left(D_\mu \Phi\right)^\dagger \left(D^\mu \Phi\right) + \frac{1}{4} F^{\mu\nu} F_{\mu\nu} - \frac{\lambda}{4!} |\Phi|^4 , \tag{6.25}$$

where the complex scalar is given by $\Phi = \left(\phi_1 + i\phi_2\right)/\sqrt{2}$ and the covariant derivative by $D_\mu = \partial_\mu - ie_{\rm CW} A_\mu$, with $e_{\rm CW}$ being the gauge coupling. $F^{\mu\nu}$ is the normal field strength tensor and due to gauge invariance the effective potential depends only on $\phi_{\rm cl}^2 = \phi_1^2 + \phi_2^2$.

Next, we will calculate the effective potential following [7] and using a cut-off regularization scheme with a cut-off Λ. Nevertheless, one can obtain the same results by using dimensional regularization and the $\overline{\rm MS}$ subtraction scheme. The interactions contained in Eqs. (6.20) and (6.21) are shown as Feynman diagrams in Fig. 6.1. We are interested in all 1PI diagrams with vanishing momentum on the external lines. Then, calculating and summing up these Feynman diagrams, we can calculate the effective potential. We obtain

$$V = \frac{1}{4!}\lambda\phi_{\rm cl}^4 - \frac{1}{2}B\phi_{\rm cl}^2 - \frac{1}{4!}C\phi_{\rm cl}^4 + \frac{1}{2}\int \frac{{\rm d}^4k}{(2\pi)^4} \ln\left(1 + \frac{\lambda\phi_{\rm cl}^2}{2k^2}\right) + \frac{3}{2}\int \frac{{\rm d}^4k}{(2\pi)^4} \ln\left(1 + \frac{e_{\rm CW}^2\phi_{\rm cl}^2}{k^2}\right) , \tag{6.26}$$

where B and C are counter-terms that are needed for normalization. The UV divergent integral may be evaluated using a cut-off regularization with cut-off Λ. We obtain

$$\begin{aligned} V = {} & \frac{1}{4!}\lambda\phi_{\rm cl}^4 - \frac{1}{2}B\phi_{\rm cl}^2 - \frac{1}{4!}C\phi_{\rm cl}^4 + \frac{\Lambda^2\phi_{\rm cl}^2}{64\pi^2}\left(\lambda + 6e_{\rm CW}^2\right) \\ & + \frac{\lambda^2\phi_{\rm cl}^4}{256\pi^2}\left(\ln\frac{\lambda\phi_{\rm cl}^2}{2\Lambda^2} - \frac{1}{2}\right) + \frac{3\lambda^2\phi_{\rm cl}^4}{64\pi^2}\left(\ln\frac{e_{\rm CW}^2\phi_{\rm cl}^2}{\Lambda^2} - \frac{1}{2}\right) . \end{aligned} \tag{6.27}$$

In order to remove the divergences, we need to renormalize the theory. This can be achieved by imposing the following renormalization conditions:

$$\frac{{\rm d}^2V}{{\rm d}\phi_{\rm cl}^2} = 0 , \qquad \left.\frac{{\rm d}^4V}{{\rm d}\phi_{\rm cl}^4}\right|_M = \lambda . \tag{6.28}$$

The first condition characterizes a classically massless theory, while the second condition defines the quartic coupling constant at an arbitrary renormalization scale M. Applying these conditions on Eq. (6.27), we obtain an expression for the one-loop effective potential

$$V = \frac{1}{4!}\lambda\phi_{\rm cl}^4 + \left(\frac{\lambda^2}{256\pi^2} + \frac{3e_{\rm CW}^4}{64\pi^2}\right)\phi_{\rm cl}^4\left(\ln\frac{\phi_{\rm cl}^2}{M^2} - \frac{25}{6}\right). \tag{6.29}$$

Let us now investigate the minima of the effective potential to determine if it admits spontaneous symmetry breaking. Consider first the case of the pure scalar ϕ^4 theory with $e_{\rm CW} = 0$. Then, the effective potential has the form

$$V = \frac{1}{4!}\lambda\phi_{\rm cl}^4 + \frac{\lambda^2}{256\pi^2}\phi_{\rm cl}^4\left(\ln\frac{\phi_{\rm cl}^2}{M^2} - \frac{25}{6}\right). \tag{6.30}$$

For the above potential, a minimum away from the origin can be achieved for a non-zero $\phi_{\rm cl}$ if

$$\lambda\ln\frac{\phi_{\rm cl}^2}{M^2} \sim -\frac{32}{3}\pi^2. \tag{6.31}$$

Such a value is outside the validity of perturbation theory since each higher order is expected to be accompanied with a factor of $\lambda\ln\phi_{\rm cl}/M^2$; we must therefore view this minimum as spurious. Of course, this result was to be expected since the only way to obtain a minimum at non-zero values of $\phi_{\rm cl}$ is to balance the λ-term with the λ^2-term.

Moving on to scalar QED, symmetry breaking at perturbative couplings may now occur naturally since we can balance λ against $e_{\rm CW}^4$. It is the interactions of the scalar field with the gauge bosons that will dynamically break the symmetry. Since $\lambda \sim e_{\rm CW}^4$ is small, we will drop the λ^2 term. Keeping the λ and $e_{\rm CW}^4$ terms results in the following effective potential:

$$V = \frac{1}{4!}\lambda\phi_{\rm cl}^4 + \frac{3e_{\rm CW}^4}{64\pi^2}\phi_{\rm cl}^4\left(\ln\frac{\phi_{\rm cl}^2}{M^2} - \frac{25}{6}\right). \tag{6.32}$$

Choosing the renormalization scale at the VEV of the scalar field, $M = \langle\phi\rangle$, we find that there is a minimum for a non-zero value of $\phi_{\rm cl}$ when

$$\lambda = \frac{33}{8\pi}e_{\rm CW}^4. \tag{6.33}$$

With this relationship between the coupling constants at our disposal, we obtain a final expression for the effective potential

$$\boxed{V = \frac{3e_{\rm CW}^4}{64\pi^2}\phi_{\rm cl}^4\left(\ln\frac{\phi_{\rm cl}^2}{\langle\phi\rangle^2} - \frac{1}{2}\right)}. \tag{6.34}$$

One can see that this potential only depends on $e_{\rm CW}$ and $\langle\phi\rangle$, not on λ. In essence, we have exchanged a dimensionless coupling constant, λ, for a dimensionful parameter, $\langle\phi\rangle$. This phenomenon is known as *dimensional transmutation*. By employing the Coleman-Weinberg mechanism, we have generated a scale, $\langle\phi\rangle$, from a theory with no input mass scales! Finally, it is easy to calculate the masses of the particles in the theory. There is one massive vector boson with mass

$$M_A^2 = e_{\rm CW}^2\langle\phi\rangle^2, \tag{6.35}$$

and one massive scalar boson with mass

$$M_\phi^2 = \frac{\mathrm{d}^2 V}{\mathrm{d}\phi^2} = \frac{3e_{\mathrm{CW}}^4}{8\pi^2}\langle\phi\rangle^2 \,. \tag{6.36}$$

Notice that the scalar boson mass is parametrically suppressed with respect to the gauge boson mass.

6.3.3 Coleman-Weinberg mechanism and renormalization group running

One could argue that Eq. (6.33) implies a careful matching of the coupling constants since only when this equation holds we get a non-zero VEV for ϕ_{cl}. This would seem like a strange coincidence or an indication of fine-tuning. However, there is no fine-tuning involved in this relationship at all. In order to understand why that is the case, let us study the renormalization group running of the couplings contained in the theory described above. The β-functions of the relevant couplings have the form [7]

$$\beta_{e_{\mathrm{CW}}} = \frac{\mathrm{d}e_{\mathrm{CW}}}{\mathrm{d}t} = \frac{e_{\mathrm{CW}}^3}{48\pi^2} \,, \tag{6.37}$$

$$\beta_\lambda = \frac{\mathrm{d}\lambda}{\mathrm{d}t} = \frac{1}{4\pi^2}\left(\frac{5}{6}\lambda^2 - 3e_{\mathrm{CW}}^2\lambda + 9e_{\mathrm{CW}}^4\right) \,, \tag{6.38}$$

where $t = \ln\frac{\mu}{M_0}$. Let us entertain a situation where at a high energy scale, M_0, the couplings have the arbitrary values $e_{\mathrm{CW}}(M_0) = e_0$ and $\lambda(M_0) = \lambda_0$, and then we evolve them down to lower energies. Notice that β_λ is positive and that the value of λ will decrease as energy decreases. When at some point λ becomes small, the e^4-term dominates, and the coupling will continue to decrease until it eventually becomes negative. At some energy scale M_c, the value of λ will be such that

$$\lambda(M_c) = \frac{33}{8\pi}e_{\mathrm{CW}}^4(M_c) \,. \tag{6.39}$$

This is exactly the energy scale where symmetry breaking occurs. It is the positive β-function that drives λ negative and induces spontaneous symmetry breaking. In other words, the RG running of the couplings triggers symmetry breaking which dynamically generates scales via dimensional transmutation.

6.3.4 Bardeen's Argument on the Hierarchy Problem

In 1995, Bardeen proposed [6] that classical scale invariance could address the hierarchy problem. In Chapter 4, we saw how the hierarchy problem can be best thought of in terms of physical threshold effects of massive particles and not in terms of quadratic divergences. In the proposed CSI models there is only one scale, which is radiatively generated. Then, all masses in the theory are parametrically related to the generated scale. Therefore, as long as this dynamically generated scale is near the EW scale, a CSI theory does not have a hierarchy problem. Nevertheless, classical scale invariance does not protect the Higgs mass from new large scales that can appear in quantum gravity, for example. The smallness of the cosmological constant, however, suggests that gravity does not feel the presence of vacuum expectation values of quantum fields, and similarly the smallness of the Higgs mass suggests that quantum fields do not feel the presence of the scale of gravity. It is thus possible that the UV theory of gravity does not affect low-energy physics.

In the SM, there are two typical scales: the QCD and the EW scales. The QCD scale $\Lambda_{\rm QCD}$ is dynamically generated at a low scale where the strong gauge coupling α_s diverges. The QCD scale, then, is related to a UV scale $\Lambda_{\rm UV}$ through

$$\Lambda_{\rm QCD} = \Lambda_{\rm UV} \exp\left(-\frac{2\pi}{b_0 \alpha_s(\Lambda_{\rm UV})}\right) , \tag{6.40}$$

where b_0 is the coefficient of the β_s function $\beta_s = d\alpha_s/dt = -(b_0/2\pi)\alpha_s^2$. Since the one-loop β_s function is proportional to $\hbar$, the small QCD scale $\sim \Lambda_{\rm UV} \exp(-c/\hbar)$ is generated in a non-perturbative way and is also stable against radiative corrections of higher-energy scales. This is the famous mechanism of dimensional transmutation in QCD. The dimensionless parameter α_s has been traded with the dimensionful scale $\Lambda_{\rm QCD}$.

Classically scale-invariant theories generate scale in a similar way. Integrating the RGE of the gauge coupling $e_{\rm CW}$ (6.37) and setting the RG scale $M = v_\phi$, one finds [513]

$$v_\phi \;=\; \Lambda_{UV} \exp\left[-24\pi^2 \left(\frac{1}{e^2_{\rm CW}(v_\phi)} - \frac{1}{e^2_\phi(\Lambda_{UV})}\right)\right] \;\simeq\; \Lambda_{UV} \exp\left[\frac{-24\pi^2}{e^2_{\rm CW}(v_\phi)}\right] . \tag{6.41}$$

We see that the VEV v_ϕ is generated at a scale which is exponentially suppressed with respect to the UV cut-off scale Λ_{UV}. The exponential smallness of the ratio $v_\phi/\Lambda_{UV} \ll 1$ is guaranteed by the perturbativity of the coupling constant $e^2_{\rm CW}$ in the vacuum of the theory. Therefore, as long as quantum gravity or any other UV physics do not destabilize the Higgs mass, the scales of the theory will be naturally generated at scales exponentially smaller than the UV cut-off, and no fine-tuning will be needed. This addresses the naturalness problem.

6.4 Gildener-Weinberg Approach

In the previous section we reviewed the Coleman-Weinberg mechanism which is only applicable in the case when there is only one scalar field in the theory. In Chapters 7 and 8 we will be interested with classically scale-invariant models containing multiple scalar fields. To this end, we need to employ the method of E. Gildener and S. Weinberg (GW) [514] which generalizes the CW mechanism in the case of multiple scalar fields. In this section, we provide a brief review of the GW formalism following closely Ref. [515].

Let us begin by considering a renormalizable gauge field theory with a set of n real scalar fields ϕ_i and $(i = 1, 2, \ldots, n)$. We may collect ϕ_i and its n components in an n-dimensional multiplet scalar field $\mathbf{\Phi}$. Then, the tree-level scale-invariant potential is generally given by

$$V_0(\mathbf{\Phi}) = \frac{1}{4!} f_{ijkl}\, \phi_i \phi_j \phi_k \phi_l \,, \tag{6.42}$$

where f_{ijkl} is fully symmetric in all its indices and stands for the quartic coupling of the potential. Summation over repeated indices is implied.

We now need to find a direction $\mathbf{n}$ along which the potential has a non-trivial continuous local minimum in the multi-dimensional field space and then perform a perturbative analysis around this direction. There are three conditions that must be satisfied along the direction $\mathbf{n}$: **flat**, **stationary** and **non-negative definite**. For the flat condition, one has $V_0(\mathbf{\Phi}) = 0$ everywhere along the ray $\mathbf{\Phi}^{\rm flat} = \varphi \mathbf{n}$, where φ is the radial distance from the origin in the field space. We may also write this

condition as

$$\min_{N_i N_i = 1} V_0(\mathbf{N}) = \min_{N_i N_i = 1} f_{ijkl}(\mu) N_i N_j N_k N_l = 0\,. \tag{6.43}$$

We suppose this constraint is met for a particular unit vector $\mathbf{N} = \mathbf{n}$ with $\mathbf{\Phi} = \varphi\mathbf{N}$ and for a particular renormalization group scale $\mu = \Lambda$.

The next step is to ensure that the flat direction $\mathbf{\Phi}^{\text{flat}} = \varphi\mathbf{n}$ represents a stationary line. We have

$$\left.\frac{\partial V_0(\mathbf{N})}{\partial N_i}\right|_{\mathbf{N}=\mathbf{n}} = 0\,, \qquad (\text{equivalent to} \quad \nabla V_0(\mathbf{\Phi})|_{\mathbf{\Phi}=\varphi\mathbf{n}}) \tag{6.44}$$

which can be written explicitly as

$$f_{ijkl}(\Lambda) n_j n_k n_l = 0\,. \tag{6.45}$$

Note that Eq. (6.45) imposes only a single constraint on the coupling f_{ijkl}. This means we are not allowed to choose a renormalization scale to make all the couplings f_{ijkl} vanish.

Finally, in order to ensure that the stationary line is a local minimum rather than a local maximum, we consider the Hessian matrix, defined as

$$(\mathbf{P})_{ij} := \left.\frac{\partial^2 V_0(\mathbf{N})}{\partial N_i \partial N_j}\right|_{\mathbf{N}=\mathbf{n}} = \frac{1}{2} f_{ijkl} n_k n_l \tag{6.46}$$

and demand that it be non-negative definite, i.e.the $n \times n$-dimensional matrix $\mathbf{P}$ has either vanishing or positive eigenvalues.

Now that we have a well-defined ray with a local minimum, let us study how quantum corrections come into play. Since the tree-level potential $V_0(\mathbf{N})$ vanishes along the flat direction $\mathbf{\Phi}^{\text{flat}}$, we expect the full potential of the theory to be dominated by the one-loop effective potential, $V_1(\mathbf{\Phi})$. Adding higher-order contributions will generate a small curvature in the radial direction $\mathbf{\Phi}^{\text{flat}} = \varphi\mathbf{n}$, leading to a minimum along the ray where $\varphi = v_\varphi$. This reminds us of the CW mechanism where radiative symmetry breaking generates a nontrivial minimum. Furthermore, higher-order corrections will also produce a small shift $\delta\mathbf{\Phi} = v_\varphi \delta\mathbf{n}$ in a direction perpendicular to the flat direction $\mathbf{n}$, i.e. $\mathbf{n} \cdot \delta\mathbf{n}$. The stationary condition (6.44) may then be extended to the full effective potential containing the one-loop contribution. We have

$$\nabla \left(V_0(\mathbf{\Phi}) + V_1(\mathbf{\Phi})\right)|_{\mathbf{\Phi}=v_\varphi(\mathbf{n}+\delta\mathbf{n})} = 0\,. \tag{6.47}$$

We can expand this expression to the first-loop order by treating $\delta\mathbf{\Phi}$ as a one-loop order parameter. We thus obtain

$$v_\varphi^2 \mathbf{P} \cdot \delta\mathbf{\Phi} + \nabla V_1(\mathbf{\Phi})|_{\mathbf{\Phi}=v_\varphi\mathbf{n}} = 0\,. \tag{6.48}$$

The first term above can be eliminated by contracting the expression from the left with $\mathbf{n}$ since $\mathbf{n} \cdot \mathbf{P} = 0$ by virtue of (6.44) and (6.45). We thus obtain the minimization condition along the radial direction:

$$\mathbf{n} \cdot \nabla V_1(\mathbf{\Phi})|_{\mathbf{\Phi}=v_\varphi\mathbf{n}} = \left.\frac{\partial V_1(\varphi\mathbf{n})}{\mathrm{d}\varphi}\right|_{\varphi=v_\varphi} = 0\,. \tag{6.49}$$

Along the flat direction $\mathbf{\Phi}^{\text{flat}} = \varphi\mathbf{n}$, the one-loop effective potential can be written as

$$V_1(\varphi\mathbf{n}) = A(\mathbf{n})\varphi^4 + B(\mathbf{n})\varphi^4 \ln\frac{\varphi^2}{\Lambda^2}\,, \tag{6.50}$$

where A, B are $\mathbf{n}$-dependent dimensionless constants. They are given in the $\overline{\text{MS}}$ scheme as

$$A = \frac{1}{64\pi^2 v_\varphi^4}\left\{\text{Tr}\left[M_S^4\left(-\frac{3}{2}+\ln\frac{M_S^2}{v_\varphi^2}\right)\right]+3\,\text{Tr}\left[M_V^4\left(-\frac{3}{2}+\ln\frac{M_V^2}{v_\varphi^2}\right)\right] -4\,\text{Tr}\left[-\frac{3}{2}+\ln\frac{M_F^2}{v_\varphi^2}\right]\right\}, \tag{6.51}$$

$$B = \frac{1}{64\pi^2 v_\varphi^4}\left(\text{Tr}\,M_S^4+3\,\text{Tr}\,M_V^4-4\,\text{Tr}\,M_F^4\right), \tag{6.52}$$

where M_S, M_V and M_F correspond to tree-level scalar, vector and fermion mass matrices respectively[1]. Minimizing (6.54) with the help of (6.49) we find

$$\Lambda = v_\varphi \exp\left(\frac{A}{2B}+\frac{1}{4}\right), \tag{6.53}$$

which is a generalized version of the dimensional transmutation phenomenon we encountered in the CW mechanism. Using this expression, we may rewrite the one-loop effective potential as

$$\boxed{V_1(\varphi\mathbf{n}) = B(\mathbf{n})\varphi^4\left(\ln\frac{\varphi^2}{v_\varphi^2}-\frac{1}{2}\right)}. \tag{6.54}$$

For infinitely large values of φ in any field direction $\mathbf{N}$ the one-loop effective potential is bounded from below if $B > 0$.

Now, let us consider the masses of the scalar bosons of the theory when the one-loop corrections are taken into account. The mass matrix is given by

$$\left(M_0^2+\delta M^2\right)_{ij} = \left.\frac{\partial^2\left(V_0(\mathbf{\Phi})+V_1(\mathbf{\Phi})\right)}{\partial\Phi_i\partial\Phi_j}\right|_{\mathbf{\Phi}=v_\varphi(\mathbf{n}+\delta\mathbf{n})}. \tag{6.55}$$

Expanding to first order we find

$$\left(\delta M^2\right)_{ij} = \left.\frac{\partial^2 V_1(\mathbf{\Phi})}{\partial\Phi_i\partial\Phi_j}\right|_{\mathbf{\Phi}=v_\varphi\mathbf{n}} + v_\varphi f_{ijkl}n_k\delta\Phi_l\,. \tag{6.56}$$

Contracting the above expression with n_i and n_j, we are finally able to obtain the scalon mass:

$$M_s^2 = n_i n_j\left(\delta M^2\right)_{ij} = n_i n_j\left.\frac{\partial^2 V_1(\mathbf{\Phi})}{\partial\Phi_i\partial\Phi_j}\right|_{\mathbf{\Phi}=v_\varphi\mathbf{n}} = \left.\frac{\partial^2 V_1(\varphi\mathbf{n})}{\partial\varphi^2}\right|_{\varphi=v_\varphi\mathbf{n}} = 8Bv_\varphi^2 \tag{6.57}$$

where we have used (6.54) and (6.53) to arrive at the last equality in (6.57). We refer to the field s as the pseudo-Goldstone boson of the anomalously broken scale invariance, because it is massless at tree level when scale invariance is valid, but acquires non-zero mass at the one-loop level once scale invariance is broken by quantum corrections.

The mass eigenvalues for the remaining massive scalar states of the theory can be easily determined as long as $\left(\delta M^2\right)_{ij}$ remains a small effect compared to the tree-level mass matrix $\left(M_0^2\right)_{ij}$.

[1] See [147] for a model that contains tensor masses. Also, note that the internal degrees of freedom for Majorana fermions are half of those of the Dirac fermions. In such a case, the pre-factor -4 in front of the trace should be replaced with -2.

Then, their masses are obtained via:

$$M_H^2 = \tilde{n}_i \tilde{n}_j \left. \frac{\partial^2 V_0(\mathbf{\Phi})}{\partial \Phi_i \partial \Phi_j} \right|_{\mathbf{\Phi}=v_\varphi \mathbf{n}} = \tilde{\mathbf{n}} \cdot \mathbf{P} \cdot \tilde{\mathbf{n}} \,, \tag{6.58}$$

where the massive scalar directions are defined similarly to $\mathbf{\Phi}^{\text{flat}}$ as $\mathbf{\Phi}^H = \varphi \tilde{\mathbf{n}}$, with $\tilde{\mathbf{n}}$ being a generic unit vector perpendicular to $\mathbf{n}$. Finally, Goldstone bosons remain massless as long as $V_1(\mathbf{\Phi})$ respects the same global symmetries as $V_0(\mathbf{\Phi})$.

6.5 Classically scale-invariant extensions of the Standard Model

At this point, let us present as an example a simple CSI model studied in Ref. [516] which employs the GW formalism of the CW mechanism. The SM gauge symmetry is extended by a $U(1)_X$ gauge symmetry with doubly X-charged scalar Φ and singly X-charged Majorana fermion N, both singlets under the SM gauge group. The scalar potential is given by

$$V(H,\Phi) = \frac{\lambda_H}{2}(H^\dagger H)^2 + \frac{\lambda_\Phi}{2}(\Phi^\dagger \Phi)^2 + \lambda_P (H^\dagger H)(\Phi^\dagger \Phi) \,, \tag{6.59}$$

while the extra Yukawa term is

$$\mathcal{L}_y = -\frac{y}{2} \Phi \bar{N} N \,, \tag{6.60}$$

Assume that both the Higgs doublet H and the complex singlet Φ acquire VEVs

$$H = \begin{pmatrix} H^+ \\ \frac{1}{\sqrt{2}}(v_H + h' + iG) \end{pmatrix} \,, \qquad \Phi = \frac{1}{\sqrt{2}}(v_\Phi + \phi' + iJ) \,. \tag{6.61}$$

Then, the scalar potential (6.59) has a flat direction when the couplings satisfy

$$\lambda_H(\Lambda)\lambda_\Phi(\Lambda) - \lambda_P^2(\Lambda) = 0 \,. \tag{6.62}$$

Employing this constraint, we find that the VEVs are related as

$$\frac{v_H^2}{v_\Phi^2} = -\frac{\lambda_P}{\lambda_H} \,. \tag{6.63}$$

Since the scalars mix, we need to perform a diagonalization of the scalar mass matrix in order to obtain the physical masses. Using an orthogonal rotation on the scalar mass eigenstates

$$\begin{pmatrix} h \\ \phi \end{pmatrix} = \begin{pmatrix} \cos\theta & -\sin\theta \\ \sin\theta & \cos\theta \end{pmatrix} \begin{pmatrix} h' \\ \phi' \end{pmatrix} \,, \tag{6.64}$$

with mixing angle θ given by

$$\sin^2\theta = -\frac{\lambda_P}{\lambda_H - \lambda_P} \,, \tag{6.65}$$

we find the tree-level masses of the scalars to be

$$m_h^2 = (\lambda_H - \lambda_P) v_H^2 \,, \qquad m_\phi^2 = 0 \,. \tag{6.66}$$

Note that one eigenvalue is zero at tree level since it corresponds to the pseudo-Goldstone boson of the broken classical scale invariance. Furthermore, the gauge boson and fermion masses are

$$m_X^2 = 4g_X^2 v_\Phi^2 \,, \qquad m_N = \frac{y}{\sqrt{2}} v_\Phi \,. \tag{6.67}$$

Next, let us consider the one-loop corrected potential along the flat direction, given by

$$V_1(r) = Ar^4 + Br^4 \ln\left(\frac{r^2}{\Lambda^2}\right) \,, \tag{6.68}$$

with the radial field r is defined as

$$\begin{pmatrix} v_H + h' \\ v_\Phi + \phi' \end{pmatrix} = r \begin{pmatrix} n_h \\ n_\phi \end{pmatrix} \,. \tag{6.69}$$

The fields n_h, n_ϕ satisfy the constraint $n_h^2 + n_\phi^2 = 1$, with their VEVs being $\sin\theta$ and $\cos\theta$, respectively. Moreover, the coefficients A and B in this model have the form

$$\begin{aligned} A = \frac{1}{64\pi^2 v_r^4}\Bigg\{ & m_h^4 \left(-\frac{3}{2} + \log\frac{m_h^2}{v_r^2}\right) + 6m_W^4 \left(-\frac{5}{6} + \log\frac{m_W^2}{v_r^2}\right) \\ & + 3m_Z^4 \left(-\frac{5}{6} + \log\frac{m_Z^2}{v_r^2}\right) + 3m_X^4 \left(-\frac{5}{6} + \log\frac{m_X^2}{v_r^2}\right) \\ & - 12m_t^4 \left(-1 + \log\frac{m_t^2}{v_r^2}\right) - 2m_N^4 \left(-1 + \log\frac{m_N^2}{v_r^2}\right)\Bigg\} \,, \end{aligned} \tag{6.70}$$

$$B = \frac{1}{64\pi^2 v_r^4}\left(m_H^4 + 6m_W^4 + 3m_Z^4 + 3m_X^4 - 12m_t^4 - 2m_N^4\right) \,, \tag{6.71}$$

with v_r being the VEV of the field r. The mass of the pseudo-Goldstone boson of broken scale invariance, also referred to as the *scalon*, now receives a one-loop mass correction of the form

$$m_\phi^2 = \frac{\partial^2 V_1}{\partial r^2}\Big|_{r=v_r} = 8Bv_r^2 \,. \tag{6.72}$$

Going back to the tree-level potential (6.59), in the mass eigenstate basis it reads

$$\begin{aligned} V(h,\phi) = {} & \frac{1}{2}m_h^2 h^2 + \frac{1}{2}\sqrt{1 - \frac{\lambda_P}{\lambda_H}}(\lambda_P + \lambda_H) v_H h^3 + \frac{1}{8}\frac{(\lambda_H + \lambda_P)^2}{\lambda_P} h^4 \\ & + \sqrt{-\lambda_P(\lambda_H - \lambda_P)}\, v_H h^2 \phi + \frac{1}{2}\sqrt{\frac{-\lambda_P}{\lambda_H}}(\lambda_H + \lambda_P) h^3 \phi - \frac{1}{2}\lambda_P h^2 \phi^2 \,. \end{aligned} \tag{6.73}$$

Note that due to the dimensional transmutation condition (6.63), in (6.73) quartic terms contain no more than two scalon (ϕ) fields, and in cubic terms no more than one [517, 518]. This point can be understood from the fact that the flat direction of the tree-level potential defined by the VEV of the unit vector field (n_h, n_ϕ) is also an eigenvector of the mass matrix with zero eigenvalue. This is a general feature of the GW formalism which sets it apart from the standard CW mechanism and has serious phenomenological implications as we will see in Chapters 7 and 8.

At this point, let us briefly discuss the different CSI models that have been proposed in the literature. All CSI extensions of the Standard Model start with the SM Lagrangian but without the Higgs

mass term. New field content and potentially extra gauge symmetries are then added in order to generate scales dynamically. The generation of scale is then transmitted to the Higgs and triggers electroweak symmetry breaking. For example, the authors of [138, 139, 144, 147, 424, 515, 518–555] extended only the scalar sector, while the authors of [137, 253, 404, 409, 410, 412–414, 417, 513, 516, 517, 544, 556–585] extended the gauge sector as well with Abelian or non-Abelian gauge symmetries (either weakly or strongly coupled). Some of these models have the appealing feature that they also predict stable and weakly interacting massive particles which can be viable candidates for dark matter. Furthermore, new scalars which couple to the Higgs contribute through their portal couplings positively to the RGE of the Higgs self-coupling and can therefore potentially solve the vacuum stability problem. Some of these models are also able to generate masses for the SM neutrinos.

6.6 Dynamical generation of the Planck scale

The Coleman-Weinberg mechanism could also be responsible for the dynamical generation of the Planck scale. Recently, there have been some attempts to consider gravity in a CSI framework [110, 138, 143–147, 149, 151–155, 169, 548, 586–599]. The underlying idea is to think of the Planck mass $M_{\rm Pl}$ as the VEV of a scalar field, ϕ, that is non-minimally coupled to gravity. In these theories, the Einstein-Hilbert term $M_{\rm Pl}R$ is replaced by $\xi\phi^2 R$, where ξ is the non-minimal coupling, and we obtain a scalar-tensor theory for gravity (see Section 3.3). If a VEV is dynamically generated for ϕ, then $v_\phi = M_{\rm Pl}/\sqrt{\xi}$, and we obtain the standard GR Lagrangian. The Higgs could communicate with ϕ through a portal coupling $\lambda_{h\phi}$. This would induce a Higgs mass of

$$M_h^2 = \lambda_{h\phi}\frac{M_{\rm Pl}^2}{\xi}\,. \tag{6.74}$$

Of course, in order to get the observed value for the Higgs mass an extremely small value of $\lambda_{h\phi}$ is required. Such a value for $\lambda_{h\phi}$ could be considered natural since it is multiplicatively renormalized.

The scalar field ϕ is interesting from the point of view that it can also drive inflation. The relevant action is Eq. (3.109), which we reproduce here for the convenience of the Reader

$$S = \frac{1}{2}\int d^4x\sqrt{-g}\left[F(\phi)R - \nabla^\rho\phi\nabla_\rho\phi - 2\mathcal{V}(\phi)\right] + S_m\left(g_{\mu\nu},\chi\right)\,, \tag{6.75}$$

with $F(\phi) = \xi\phi^2$ and $\mathcal{V}(\phi) = \frac{1}{4}\lambda_\phi(\phi)\phi^4$. In order to avoid problems related to the eternal inflation, we must assume that

$$\mathcal{V}(v_\phi)_{\rm eff} = 0\,, \tag{6.76}$$

where $\mathcal{V}(\phi)_{\rm eff}$ is the one-loop effective potential of the inflaton. It can be shown that the above condition results in

$$\frac{1}{4}\beta_{\lambda_\phi}(v_\phi) + \lambda_\phi(v_\phi) = 0, \tag{6.77}$$

where β_{λ_ϕ} is the β-function of the running quartic inflaton self-coupling λ_ϕ. We will examine a model based on CSI inflation in Chapter 9.

Chapter 7

Dark matter and neutrino masses from a classically scale-invariant multi-Higgs portal

7.1 Introduction

The work presented in this chapter was done in collaboration with Prof. Kyriakos Tamvakis and has been published in Physical Review D [414].

In this chapter, we construct a classically scale-invariant $SU(2)_X$ extension of the Standard Model that satisfies perturbativity and stability up to the Planck scale and also incorporates RH neutrinos and vector dark matter, while the Higgs sector consists of three scalar fields. The symmetry breaking occurs in the dark sector via the Coleman-Weinberg mechanism and is then communicated to the electroweak and neutrino sectors. The DM consists of the three extra gauge bosons, whose interactions, apart from annihilations, also include semiannihilations.

In the next section, we present the model and analyze the stability of the tree-level potential. We proceed to obtain possible flat directions, setting up the model for the study of symmetry breaking through the Coleman-Weinberg mechanism. We compute the one-loop effective potential and the resulting scalar masses. Subsequently, in Sec. 7.3, we undertake a phenomenological analysis of the model. We identify one of the predicted scalar states with the observed Higgs boson. Then, we find benchmark sets of values for a minimal subset of the free parameters of the model that correctly reproduce the Higgs boson mass. After that, we scan over the rest of the parameters and obtain masses for the dark gauge bosons, the right-handed neutrinos and one of the scalar bosons, all the while checking that the stability and perturbativity constraints are satisfied. In Sec. 7.4, for the same set of benchmark values, we calculate the dark matter relic density and constrain the masses of the dark gauge bosons from both the observed relic density and the limits set by direct detection experiments.

7.2 The model

In this section we present the model and study its properties. Employing the Coleman-Weinberg mechanism [7] in the Gildener-Weinberg [600] formalism we minimize the tree-level potential and find the flat direction between the VEVs of the scalar fields. Then we obtain the tree-level masses of the scalars, one of which (we call it *darkon*) turns out to be massless due to the flat direction. Including the one-loop potential, we find that radiative corrections become dominant along the flat

direction and lift the darkon's mass to values that can be even higher than the masses of the other scalars.

7.2.1 The tree-level scalar potential

In order to address the open issues discussed in the Introduction we consider the Standard Model in a classically scale invariant (CSI) framework and extend the gauge group with an additional $SU(2)_X$ symmetry [409, 410]. In addition to the new gauge bosons, the dark sector contains a SM-singlet scalar $SU(2)_X$ isodoublet Φ. Aiming at the problem of neutrino mass generation, we also introduce a real scalar σ, singlet under both the SM and dark gauge groups. Right-handed neutrinos are also included in the standard fashion as total fermionic singlets. The tree-level scalar potential, in terms of the SM Higgs field H and the new scalars Φ, σ, has the form

$$V_0 \;=\; \lambda_h (H^\dagger H)^2 + \lambda_\phi (\Phi^\dagger \Phi)^2 + \frac{\lambda_\sigma}{4}\sigma^4 - \lambda_{h\phi}(H^\dagger H)(\Phi^\dagger\Phi) - \frac{\lambda_{\phi\sigma}}{2}(\Phi^\dagger\Phi)\sigma^2 + \frac{\lambda_{h\sigma}}{2}(H^\dagger H)\sigma^2, \quad (7.1)$$

where we included all possible couplings among scalars and have introduced negative signs for the portal couplings $\lambda_{h\phi}$ and $\lambda_{\phi\sigma}$. Models having all mixing scalar couplings positive, i.e. both the portals to the dark sector $\lambda_{h\phi}$, $\lambda_{\phi\sigma}$ and the observable sector Higgs mixing $\lambda_{h\sigma}$, do not lead to a symmetry breaking flat direction and are not of interest. It is then reasonable to examine models with the portal to the dark sector being negative. Taking the observable mixing $\lambda_{h\sigma}$ also negative is not necessarily interesting because it allows for a flat direction independent of the dark sector. Therefore, we restrict the possible breaking patterns making the above choice of signs which is sufficient for our purposes.

In addition to the scalar potential, the Lagrangian has the following extra Yukawa terms:

$$-\mathcal{L}_N = Y_\nu^{ij}\bar{L}_i\, i\sigma_2 H^* N_j + \text{H.c.} + Y_\sigma^{ij}\bar{N}_i^c N_j \sigma, \quad (7.2)$$

where Y_ν^{ij} is the Dirac neutrino Yukawa matrix which couples the left-handed lepton doublet L_i to the SM Higgs doublet H and the right-handed neutrino N_j and Y_σ^{ij} is the right-handed Majorana neutrino Yukawa matrix which will be assumed diagonal.

Considering the unitary gauge and the symmetry breaking pattern $SU(2)_L \times U(1)_Y \times SU(2)_X \to SU(2)_L \times U(1)_Y \to U(1)_{em}$, we may replace the scalar doublets by

$$H = \frac{1}{\sqrt{2}}\begin{pmatrix} 0 \\ h \end{pmatrix}, \quad \Phi = \frac{1}{\sqrt{2}}\begin{pmatrix} 0 \\ \phi \end{pmatrix}. \quad (7.3)$$

Then, the tree-level potential takes the form

$$V_0(h,\phi,\sigma) = \frac{\lambda_h}{4}h^4 + \frac{\lambda_\phi}{4}\phi^4 + \frac{\lambda_\sigma}{4}\sigma^4 - \frac{\lambda_{h\phi}}{4}h^2\phi^2 - \frac{\lambda_{\phi\sigma}}{4}\phi^2\sigma^2 + \frac{\lambda_{h\sigma}}{4}h^2\sigma^2. \quad (7.4)$$

The scalar potential is bounded from below if the matrix

$$\mathcal{A} \;=\; \frac{1}{8}\begin{pmatrix} 2\lambda_h & -\lambda_{h\phi} & \lambda_{h\sigma} \\ -\lambda_{h\phi} & 2\lambda_\phi & -\lambda_{\phi\sigma} \\ \lambda_{h\sigma} & -\lambda_{\phi\sigma} & 2\lambda_\sigma \end{pmatrix} \quad (7.5)$$

is *copositive*, i.e. such that $\eta_a \mathcal{A}_{ab} \eta_b$ is positive for non-negative vectors in the basis (h^2, ϕ^2, σ^2). It can be shown [601–605] that this is equivalent to the conditions

$$\lambda_h \geq 0, \lambda_\phi \geq 0, \lambda_\sigma \geq 0\,, \tag{7.6}$$

$$\frac{\lambda_{h\phi}}{2\sqrt{\lambda_h \lambda_\phi}} \leq 1, \quad \frac{-\lambda_{h\sigma}}{2\sqrt{\lambda_h \lambda_\sigma}} \leq 1, \quad \frac{\lambda_{\phi\sigma}}{2\sqrt{\lambda_\phi \lambda_\sigma}} \leq 1\,, \tag{7.7}$$

$$\left[2\left(1-\frac{\lambda_{h\phi}}{2\sqrt{\lambda_h\lambda_\phi}}\right)\left(1+\frac{\lambda_{h\sigma}}{2\sqrt{\lambda_h\lambda_\sigma}}\right)\left(1-\frac{\lambda_{\phi\sigma}}{2\sqrt{\lambda_\phi\lambda_\sigma}}\right)\right]^{1/2} \geq -1+\frac{\lambda_{\phi\sigma}}{2\sqrt{\lambda_\phi\lambda_\sigma}}+\frac{\lambda_{h\phi}}{2\sqrt{\lambda_h\lambda_\phi}}-\frac{\lambda_{h\sigma}}{2\sqrt{\lambda_h\lambda_\sigma}}\,. \tag{7.8}$$

Note that the last condition is equivalent to *either* of the following statements:

$$\frac{\lambda_{h\phi}}{2\sqrt{\lambda_h\lambda_\phi}}-\frac{\lambda_{h\sigma}}{2\sqrt{\lambda_h\lambda_\sigma}}+\frac{\lambda_{\phi\sigma}}{2\sqrt{\lambda_\phi\lambda_\sigma}} \leq 1\,, \tag{7.9}$$

$$\det \mathcal{A} = \lambda_h\lambda_\phi\lambda_\sigma - \tfrac{1}{4}\left(\lambda_{h\phi}^2\lambda_\sigma + \lambda_{h\sigma}^2\lambda_\phi + \lambda_{\phi\sigma}^2\lambda_h\right) + \tfrac{1}{4}\lambda_{h\phi}\lambda_{h\sigma}\lambda_{\phi\sigma} \geq 0\,. \tag{7.10}$$

Therefore, vacuum stability requires the validity of the above conditions to hold at all energies up to M_P. In order to study the flat directions of the tree-level potential we may parametrize the scalar fields as

$$h = \varphi N_1, \quad \phi = \varphi N_2, \quad \sigma = \varphi N_3, \tag{7.11}$$

with N_i a unit vector in the three-dimensional field space. Then, the tree-level potential attains the form

$$V_0 = \frac{\varphi^4}{4}\left[\lambda_h N_1^4 + \lambda_\phi N_2^4 + \lambda_\sigma N_3^4 - \lambda_{h\phi} N_1^2 N_2^2 + \lambda_{h\sigma} N_1^2 N_3^2 - \lambda_{\phi\sigma} N_2^2 N_3^2\right]\,. \tag{7.12}$$

The condition for an extremum along a particular direction $N_i = n_i$ is [600]

$$\left.\frac{\partial V_0}{\partial N_i}\right|_{\mathbf{n}} = V_0(\mathbf{n}) = 0\,. \tag{7.13}$$

Then, the equations giving the symmetry breaking direction are

$$2\lambda_h n_1^2 = \lambda_{h\phi} n_2^2 - \lambda_{h\sigma} n_3^2\,, \tag{7.14}$$

$$2\lambda_\phi n_2^2 = \lambda_{h\phi} n_1^2 + \lambda_{\phi\sigma} n_3^2\,, \tag{7.15}$$

$$2\lambda_\sigma n_3^2 = \lambda_{\phi\sigma} n_2^2 - \lambda_{h\sigma} n_1^2\,, \tag{7.16}$$

$$\lambda_h n_1^4 + \lambda_\phi n_2^4 + \lambda_\sigma n_3^4 - \lambda_{h\phi} n_1^2 n_2^2 - \lambda_{\phi\sigma} n_2^2 n_3^2 + \lambda_{h\sigma} n_1^2 n_3^2 = 0. \tag{7.17}$$

The solution of these equations in terms of the scalar couplings is

$$n_1^2 = \frac{4\lambda_\sigma\lambda_\phi - \lambda_{\phi\sigma}^2}{2\lambda_\sigma\left(2\lambda_\phi+\lambda_{h\phi}\right)+\lambda_{\phi\sigma}\left(\lambda_{h\phi}-\lambda_{\phi\sigma}\right)-\lambda_{h\sigma}\left(2\lambda_\phi+\lambda_{\phi\sigma}\right)}\,, \tag{7.18}$$

$$n_2^2 = \frac{2\lambda_\sigma\lambda_{h\phi} - \lambda_{h\sigma}\lambda_{\phi\sigma}}{2\lambda_\sigma\left(2\lambda_\phi+\lambda_{h\phi}\right)+\lambda_{\phi\sigma}\left(\lambda_{h\phi}-\lambda_{\phi\sigma}\right)-\lambda_{h\sigma}\left(2\lambda_\phi+\lambda_{\phi\sigma}\right)}\,, \tag{7.19}$$

$$n_3^2 = \frac{\lambda_{h\phi}\lambda_{\phi\sigma} - 2\lambda_\phi\lambda_{h\sigma}}{2\lambda_\sigma\left(2\lambda_\phi+\lambda_{h\phi}\right)+\lambda_{\phi\sigma}\left(\lambda_{h\phi}-\lambda_{\phi\sigma}\right)-\lambda_{h\sigma}\left(2\lambda_\phi+\lambda_{\phi\sigma}\right)}\,. \tag{7.20}$$

Note that $n_1^2 + n_2^2 + n_3^2 = 1$.

7.2.2 The scalar masses

Assuming spontaneous breaking of the gauge and the scale symmetry via the Coleman-Weinberg mechanism, we can write the shifted scalar fields as

$$h \;=\; (\varphi + v)\, n_1, \quad \phi \;=\; (\varphi + v)\, n_2, \quad \sigma \;=\; (\varphi + v)\, n_3. \tag{7.21}$$

The individual VEVs are

$$\langle h \rangle \;\equiv\; v_h = v\, n_1, \;\langle \phi \rangle \;\equiv\; v_\phi = v n_2, \;\langle \sigma \rangle \;\equiv\; v_\sigma = v n_3\,. \tag{7.22}$$

From the shifted tree-level potential we can read off the scalar mass matrix

$$\mathcal{M}_0^2 = v^2 \begin{pmatrix} 2\lambda_h n_1^2 & -n_1 n_2 \lambda_{h\phi} & +n_1 n_3 \lambda_{h\sigma} \\ -n_1 n_2 \lambda_{h\phi} & 2\lambda_\phi n_2^2 & -n_2 n_3 \lambda_{\phi\sigma} \\ +n_1 n_3 \lambda_{h\sigma} & -n_2 n_3 \lambda_{\phi\sigma} & 2\lambda_\sigma n_3^2 \end{pmatrix} \tag{7.23}$$

in the (h, ϕ, σ) basis. We can now set up the diagonalization of the mass matrix (7.23) by introducing a general rotation in terms of three parametric angles,

$$\mathcal{R}\, \mathcal{M}_0^2\, \mathcal{R}^{-1} \;=\; \mathcal{M}_d^2\,, \tag{7.24}$$

with the rotation matrix $\mathcal{R}^{-1}$ given by

$$\mathcal{R}^{-1} \;=\; \begin{pmatrix} \cos\alpha\cos\beta & \sin\alpha & \cos\alpha\sin\beta \\ -\cos\beta\cos\gamma\sin\alpha + \sin\beta\sin\gamma & \cos\alpha\cos\gamma & -\cos\gamma\sin\alpha\sin\beta - \cos\beta\sin\gamma \\ -\cos\gamma\sin\beta - \cos\beta\sin\alpha\sin\gamma & \cos\alpha\sin\gamma & \cos\beta\cos\gamma - \sin\alpha\sin\beta\sin\gamma \end{pmatrix} \tag{7.25}$$

and

$$\begin{pmatrix} h \\ \phi \\ \sigma \end{pmatrix} = \begin{pmatrix} . & . & . \\ . & \mathcal{R}^{-1} & . \\ . & . & . \end{pmatrix} \begin{pmatrix} h_1 \\ h_2 \\ h_3 \end{pmatrix}. \tag{7.26}$$

Next, we choose two of the above three angles in the rotation matrix to parametrize the total vev v direction according to

$$v_h \;=\; v \sin\alpha = v n_1\,, \tag{7.27}$$

$$v_\phi \;=\; v \cos\alpha\cos\gamma = v n_2\,, \tag{7.28}$$

$$v_\sigma \;=\; v \cos\alpha\sin\gamma = v n_3\,. \tag{7.29}$$

Then, $\mathcal{M}_d^2$ is diagonal, provided that the following relations are satisfied:

$$\tan^2\alpha \;=\; \frac{v_h^2}{v_\phi^2 + v_\sigma^2} = \frac{4\lambda_\phi\lambda_\sigma - \lambda_{\phi\sigma}^2}{2\left(\lambda_\sigma\lambda_{h\phi} - \lambda_\phi\lambda_{h\sigma}\right) + \lambda_{\phi\sigma}\left(\lambda_{h\phi} - \lambda_{h\sigma}\right)}\,, \tag{7.30}$$

$$\tan^2\gamma \;=\; \frac{v_\sigma^2}{v_\phi^2} = \frac{2\lambda_h\lambda_{\phi\sigma} - \lambda_{h\phi}\lambda_{h\sigma}}{4\lambda_h\lambda_\sigma - \lambda_{h\sigma}^2}\,, \tag{7.31}$$

$$\tan 2\beta \;=\; \frac{v_h v_\phi v_\sigma v\left(\lambda_{h\sigma} + \lambda_{h\phi}\right)}{\left(\lambda_\phi + \lambda_\sigma + \lambda_{\phi\sigma}\right) v_\phi^2 v_\sigma^2 - \lambda_h v_h^2 v^2}\,. \tag{7.32}$$

The resulting mass eigenvalues are

$$\begin{aligned} M_{h_1}^2/2 =& \lambda_h v_h^2 \cos^2\alpha\cos^2\beta + \lambda_\phi v_\phi^2 \left(\cos\beta\cos\gamma\sin\alpha - \sin\beta\sin\gamma\right)^2 \\ &+\lambda_\sigma v_\sigma^2 \left(\cos\gamma\sin\beta + \cos\beta\sin\alpha\sin\gamma\right)^2 \\ &+\lambda_{h\phi} v_h v_\phi \cos\alpha\cos\beta\left(\cos\beta\cos\gamma\sin\alpha - \sin\beta\sin\gamma\right) \\ &-\lambda_{\phi\sigma} v_\phi v_\sigma \left(\cos\beta\cos\gamma\sin\alpha - \sin\beta\sin\gamma\right)\left(\cos\gamma\sin\beta + \cos\beta\sin\alpha\sin\gamma\right) \\ &-\lambda_{h\sigma} v_h v_\sigma \cos\alpha\cos\beta\left(\cos\gamma\sin\beta + \cos\beta\sin\alpha\sin\gamma\right) \end{aligned} , \tag{7.33}$$

$$M_{h_2}^2 = 0\,, \tag{7.34}$$

$$\begin{aligned} M_{h_3}^2/2 =& \lambda_h v_h^2 \cos^2\alpha\sin^2\beta + \lambda_\phi v_\phi^2 \left(\sin\beta\cos\gamma\sin\alpha + \cos\beta\sin\gamma\right)^2 \\ &+\lambda_\sigma v_\sigma^2 \left(\cos\gamma\cos\beta - \sin\beta\sin\alpha\sin\gamma\right)^2 \\ &+\lambda_{h\phi} v_h v_\phi \cos\alpha\sin\beta\left(\sin\beta\cos\gamma\sin\alpha + \cos\beta\sin\gamma\right) \\ &+\lambda_{\phi\sigma} v_\phi v_\sigma \left(\sin\beta\cos\gamma\sin\alpha + \cos\beta\sin\gamma\right)\left(\cos\gamma\cos\beta - \sin\beta\sin\alpha\sin\gamma\right) \\ &+\lambda_{h\sigma} v_h v_\sigma \cos\alpha\sin\beta\left(\cos\gamma\cos\beta - \sin\beta\sin\alpha\sin\gamma\right)\,. \end{aligned} \tag{7.35}$$

As expected, one of these masses turns out to be zero at tree level. Regarding the rest, M_{h_1} and M_{h_3} are ultimately functions of the overall vev v and the scalar couplings. Since their exact, analytic expressions are not necessary, we leave them as they stand.

7.2.3 Neutrinos

One of the defining properties of the present model is that it incorporates the appropriate structure for massive Majorana neutrinos. Right-handed neutrinos in three families are introduced as singlets of both the Standard Model and the $SU(2)_X$ dark sector. They obtain their mass as a result of broken scale invariance through their coupling to the singlet σ that mediates between the two sectors and obtains a nonzero vev. The Yukawa terms (7.2) that give rise to neutrino masses are

$$\frac{Y_\nu^{ij}}{\sqrt{2}} v_h \nu_i\, i\sigma_2 N_j + \text{H.c.} + Y_\sigma^{ij} v_\sigma \bar{N}_i^{\,c} N_j\,. \tag{7.36}$$

The neutrino mass matrix, being of the seesaw type, can lead to the desired scale of $\mathcal{O}(0.1\ \text{eV})$ for the left-handed neutrino masses. Thus, in a $(\nu_s,\ N_i^c)$ basis, we have

$$\begin{pmatrix} 0 & \frac{Y_\nu^{ij}}{\sqrt{2}} v_h \\ \frac{Y_\nu^{ij}}{\sqrt{2}} v_h & Y_\sigma^{ij} v_\sigma \end{pmatrix}. \tag{7.37}$$

Assuming $Y_\nu^{ij}\, v_h$ to be no more than the lightest charged lepton mass, namely $\mathcal{O}(10^{-4}\ \text{GeV})$, and taking characteristic values $v_\sigma \sim \mathcal{O}(1\ \text{TeV})$ and $Y_\sigma \sim \mathcal{O}(0.1)$, we have $Y_\nu\, v_h \ll Y_\sigma\, v_\sigma$ and we arrive at approximate eigenvalues

$$M_N \approx Y_\sigma^{ij} v_\sigma, \quad m_\nu \approx \frac{v_h^2}{4 v_\sigma}\, Y_\nu^{(ik)} \left(Y_\sigma^{-1}\right)^{(k\ell)} Y_\nu^{(\ell j)}, \tag{7.38}$$

with $M_N \sim \mathcal{O}(100\ \text{GeV})$ and $m_\nu \sim \mathcal{O}(0.1\ \text{eV})$. As we will see next, the right-handed neutrino mass scale is related to the masses of the rest of the particles and cannot take arbitrary values.

7.2.4 The one-loop potential

Now, let us consider the full one-loop potential. Following the Gildener-Weinberg approach [600], along the minimum flat direction at the scale Λ the one-loop effective potential has the form (cf. Section 6.4)

$$V_1(\mathbf{n}\varphi) = A\varphi^4 + B\varphi^4 \log\frac{\varphi^2}{\Lambda^2}. \tag{7.39}$$

The coefficients A and B are dimensionless parameters and are given in the $\overline{MS}$ scheme by

$$\begin{aligned} A = \frac{1}{64\pi^2 v^4}\Bigg[&\sum_{i=1,3} M_{h_i}^4\left(-\frac{3}{2}+\log\frac{M_i^2}{v^2}\right) + 6M_W^4\left(-\frac{5}{6}+\log\frac{M_W^2}{v^2}\right) + 3M_Z^4\left(-\frac{5}{6}+\log\frac{M_Z^2}{v^2}\right) \\ &+9M_X^4\left(-\frac{5}{6}+\log\frac{M_X^2}{v^2}\right) - 12M_t^4\left(-1+\log\frac{M_t^2}{v^2}\right) - 2\sum_{i=1}^{3} M_{N_i}^4\left(-1+\log\frac{M_{N_i}^2}{v^2}\right)\Bigg], \end{aligned} \tag{7.40}$$

$$B = \frac{1}{64\pi^2 v^4}\left(\sum_{i=1,3} M_{h_i}^4 + 6M_W^4 + 3M_Z^4 + 9M_X^4 - 12M_t^4 - 2\sum_{i=1}^{3} M_{N_i}^4\right). \tag{7.41}$$

The minimization condition (6.49) gives

$$\log\left(\frac{v}{\Lambda}\right) = -\frac{1}{4} - \frac{A}{2B}. \tag{7.42}$$

Thus the one-loop effective potential becomes

$$V_1(\mathbf{n}\varphi) = B\varphi^4\left[\log\frac{\varphi^2}{v^2} - \frac{1}{2}\right]. \tag{7.43}$$

The pseudo-Goldstone boson (darkon) mass is now shifted from zero to

$$M_{h_2}^2 = \left.\frac{\partial^2 V_1(\mathbf{n}\varphi)}{\partial\varphi^2}\right|_{\varphi=v} = \frac{1}{8\pi^2 v^2}\left(M_{h_1}^4 + M_{h_3}^4 + 6M_W^4 + 3M_Z^4 + 9M_X^4 - 12M_t^4 - 6M_N^4\right), \tag{7.44}$$

where we have assumed for simplicity that all right-handed neutrinos are degenerate in mass. Note that the right-handed neutrino contribution to (7.44), as fermionic, enters with a minus sign. As a result, M_N cannot be too large. In what follows we shall identify the state h_1 with the observed Higgs of 125.09 GeV and choose a higher value for the h_3 mass. The h_2 state, although massless at tree level, can have any mass with respect to the other scalars due to the sizable one-loop correction. Note that radiative corrections to the tree-level masses of h_1 and h_3 are small enough to ignore to a first approximation.

7.3 Phenomenological analysis

In this section we present an analysis of the phenomenological viability of the model, taking into account theoretical and experimental constraints. Our procedure in broad terms will be as follows:

First, we choose values from a subset of the free parameters of the model (i.e. v_ϕ, v_σ and some of the scalar couplings), appropriate to fix the mass M_{h_1} to the experimental value of 125.09 GeV. Then the M_{h_3} mass is automatically obtained. In order to calculate the darkon mass M_{h_2} we scan over the two remaining unknown masses M_X and M_N in (7.44), while checking that the stability and perturbativity conditions are satisfied. Finally, we calculate the total decay rates of all the scalar bosons and compare the one corresponding to the Higgs boson with the bounds set by LHC.

7.3.1 Theoretical constraints

The tree-level potential (7.4) and the one-loop effective potential (7.43) have to be bounded from below for the vacuum to be stable. For this to be valid, the stability conditions (8.7)-(7.10) need to hold for all energies up to the Planck scale ($M_{\rm P} = 1.22 \times 10^{19}$ GeV) as well as the positivity condition $B > 0$ has to be satisfied. The latter translates to

$$M_{h_3}^4 + 9M_X^4 - 6M_N^4 > 12M_t^4 - 6M_W^4 - 3M_Z^4 - M_{h_1}^4\,, \tag{7.45}$$

or

$$M_{h_3}^4 + 9M_X^4 - 6M_N^4 > (317.26\ \text{GeV})^4\,, \tag{7.46}$$

where we used the values $M_t = 173.34$ GeV [606], $M_W = 80.384$ GeV and $M_Z = 91.1876$ GeV. The above inequality implies that the masses of the extra gauge bosons M_X have to be in general larger than the masses of the right-handed neutrinos M_N, unless the scalar boson mass M_{h_3} is considerably larger than the right-hand side of (7.46).

Another constraint arises from the requirement that the model must remain perturbative all the way up to $M_{\rm P}$. This can be achieved by demanding that all couplings are bounded,

$$\text{all couplings} < 2\,\pi. \tag{7.47}$$

To determine how the couplings of the model vary with energy, we need to solve the renormalization group equations (RGEs). We present the two-loop gauge and one-loop Yukawa and scalar RGEs below (however in our numerical analysis we use the full two-loop RGEs for all the couplings, computed using Refs. [607–613]):

$$\beta_{g_1} = \frac{41}{10}g_1^3 + \frac{1}{(4\pi)^2}\frac{1}{50}g_1^3\Big(199g_1^2 + 135g_2^2 + 440g_3^2 - 85y_t^2\Big)\,, \tag{7.48}$$

$$\beta_{g_2} = -\frac{19}{6}g_2^3 + \frac{1}{(4\pi)^2}\frac{1}{30}g_2^3\Big(27g_1^2 + 175g_2^2 + 360g_3^2 - 45y_t^2\Big)\,, \tag{7.49}$$

$$\beta_{g_3} = -7g_3^3 + \frac{1}{(4\pi)^2}\frac{1}{10}g_3^3\Big(11g_1^2 + 45g_2^2 - 260g_3^2 - 20y_t^2\Big)\,, \tag{7.50}$$

$$\beta_{g_X} = -\frac{43}{6}g_X^3 - \frac{1}{(4\pi)^2}\frac{259}{6}g_X^5\,, \tag{7.51}$$

$$\beta_{y_t} = y_t\left(\frac{9}{2}y_t^2 - \frac{17}{20}g_1^2 - \frac{9}{4}g_2^2 - 8g_3^2\right)\,, \tag{7.52}$$

$$\beta_{Y_\sigma} = 4\,Y_\sigma\,\text{Tr}\Big(Y_\sigma Y_\sigma^*\Big) + 12\,Y_\sigma Y_\sigma^* Y_\sigma\,, \tag{7.53}$$

$$\beta_{\lambda_h} = -6y_t^4 + 24\lambda_h^2 + \lambda_h\left(12y_t^2 - \frac{9}{5}g_1^2 - 9g_2^2\right) + \frac{27}{200}g_1^4 + \frac{9}{20}g_1^2g_2^2 + \frac{9}{8}g_2^4 + 2\lambda_{h\phi}^2 + \frac{1}{2}\lambda_{h\sigma}^2\,, \tag{7.54}$$

$$\beta_{\lambda_\phi} = \frac{9}{8}g_X^4 - 9g_X^2\lambda_\phi + 24\lambda_\phi^2 + 2\lambda_{h\phi}^2 + \frac{1}{2}\lambda_{\phi\sigma}^2\,, \tag{7.55}$$

$$\beta_{\lambda_\sigma} = -64\text{Tr}\Big(Y_\sigma Y_\sigma^* Y_\sigma Y_\sigma^*\Big) + 16\lambda_\sigma\text{Tr}\Big(Y_\sigma Y_\sigma^*\Big) + 18\lambda_\sigma^2 + 2\lambda_{h\sigma}^2 + 2\lambda_{\phi\sigma}^2\,, \tag{7.56}$$

$$\beta_{\lambda_{h\phi}} = \lambda_{h\phi}\left(6y_t^2 + 12\lambda_h + 12\lambda_\phi - 4\lambda_{h\phi} - \frac{9}{10}g_1^2 - \frac{9}{2}g_2^2 - \frac{9}{2}g_X^2\right) + \lambda_{h\sigma}\lambda_{\phi\sigma}\,, \tag{7.57}$$

$$\beta_{\lambda_{\phi\sigma}} = \lambda_{\phi\sigma}\left(8\mathrm{Tr}\left(Y_\sigma Y_\sigma^*\right) + 12\lambda_\phi + 6\lambda_\sigma - 4\lambda_{\phi\sigma} - \frac{9}{2}g_X^2\right) + 4\lambda_{h\sigma}\lambda_{h\phi}\,, \tag{7.58}$$

$$\beta_{\lambda_{h\sigma}} = \lambda_{h\sigma}\left(6y_t^2 + 8\mathrm{Tr}\left(Y_\sigma Y_\sigma^*\right) + 12\lambda_h + 6\lambda_\sigma + 4\lambda_{h\sigma} - \frac{9}{10}g_1^2 - \frac{9}{2}g_2^2\right) + 4\lambda_{h\phi}\lambda_{\phi\sigma}\,, \tag{7.59}$$

where we defined $\beta_\kappa \equiv (4\pi)^2 \frac{d\kappa}{d\ln\mu}$.

In order to solve the RGEs we have to specify the boundary conditions for the couplings. For the SM gauge couplings and the top quark Yukawa coupling we use the NNLO values at M_t [4, 571]:

$$g_1(\mu = M_t) = \sqrt{\frac{5}{3}}\left(0.35830 + 0.00011\left(\frac{M_t}{\mathrm{GeV}} - 173.34\right) - 0.00020\left(\frac{M_W - 80.384\,\mathrm{GeV}}{0.014\,\mathrm{GeV}}\right)\right), \tag{7.60}$$

$$g_2(\mu = M_t) = 0.64779 + 0.00004\left(\frac{M_t}{\mathrm{GeV}} - 173.34\right) + 0.00011\left(\frac{M_W - 80.384\,\mathrm{GeV}}{0.014\,\mathrm{GeV}}\right), \tag{7.61}$$

$$g_3(\mu = M_t) = 1.1666 + 0.00314\left(\frac{\alpha_s(M_Z) - 0.1184}{0.0007}\right) - 0.00046\left(\frac{M_t}{\mathrm{GeV}} - 173.34\right), \tag{7.62}$$

$$y_t(\mu = M_t) = 0.93690 + 0.00556\left(\frac{M_t}{\mathrm{GeV}} - 173.34\right) - 0.00042\left(\frac{\alpha_s(M_Z) - 0.1184}{0.0007}\right). \tag{7.63}$$

In our numerical analysis we use as inputs the central values $\alpha_s(M_Z) = 0.1184$, $M_W = 80.384$ GeV and $M_t = 173.34$ GeV. For the right-handed neutrino Yukawa coupling Y_σ and dark gauge coupling g_X we define $Y_\sigma(M_N) = M_N/v_\sigma$ and $g_X(M_X) = 2\,M_X/v_\phi$ respectively. Finally, to define the scalar couplings λ_i, we consider their values at the renormalization scale Λ determined by (7.42), where the one-loop effective potential is minimized [518].

A few comments are in order regarding the behavior of the running couplings. First of all, the $SU(2)_X$ gauge coupling g_X decreases at higher energies, being asymptotically free, in a similar fashion to the $SU(2)_L$ gauge coupling g_2. On the other hand, the RGE of the right-handed neutrino Yukawa coupling Y_σ has a positive sign and forces Y_σ to increase with energy until it potentially reaches a Landau pole. As it turns out, this can be avoided if $Y_\sigma(M_N) \lesssim 0.35$. The Higgs self-coupling λ_h generally behaves like the corresponding one in the SM. There, λ_h drops fast at increasing energy due to the large negative contribution from the top Yukawa coupling y_t, crosses zero at some point and then becomes nearly constant up to the Planck scale. Nevertheless, in our case, we have the freedom to choose a starting value for λ_h such that it remains positive inside the whole energy range under consideration. The self-coupling of the singlet scalar λ_σ depends highly on Y_σ and it too can reach a Landau pole unless $Y_\sigma(M_N) \lesssim 0.31$. Therefore Y_σ is further constrained. Now, the dark scalar self-coupling λ_ϕ generally increases with energy, driven mainly by the first term in (7.55). A Landau pole is avoided if we have $g_X(M_X) \lesssim 2.51$. Finally, the scalar portal couplings $(\lambda_{h\phi}, \lambda_{\phi\sigma}, \lambda_{h\sigma})$ are mainly multiplicatively renormalized and, as it turns out, they do not run much if we choose initial values that are small enough.

The model contains many free parameters, therefore we need to restrict or fix most of them. The initial eight dimensionless free parameters[1] λ_h, λ_ϕ, λ_σ, $\lambda_{h\phi}$, $\lambda_{h\sigma}$, $\lambda_{\phi\sigma}$, g_X, Y_σ are reduced to six after imposing the experimental values on v_h and M_{h_1}. Whether we use the dimensionless scalar

[1] We have assumed that the neutrino Dirac Yukawa coupling takes up values in the neighborhood of the corresponding electron Yukawa coupling.

couplings or, alternatively, the vevs through the minimization conditions (7.14)-(7.16) as input parameters, is a matter of choice. A six-dimensional parameter space is not easily managed in its full generality. So, we propose to proceed in the following way: We leave g_X and Y_σ free and list characteristic (benchmark) values for the scalar couplings (at Λ) and the vevs v_σ and v_ϕ that reproduce the measured Higgs mass $M_{h_1} = 125.09$ GeV. These are shown in Table 7.1 where we also show the value for the mass of h_3 that we obtain.

Set	v_h[GeV]	v_ϕ[GeV]	v_σ[GeV]	$\lambda_h(\Lambda)$	$\lambda_\phi(\Lambda)$	$\lambda_\sigma(\Lambda)$	$\lambda_{h\phi}(\Lambda)$	$\lambda_{\phi\sigma}(\Lambda)$	$\lambda_{h\sigma}(\Lambda)$	M_{h_3}[GeV]
A	246	2112	770	0.1276	0.004	0.2257	0.0036	0.06	0.001	550.62
B	246	3245	1470	0.1285	0.0005	0.0122	0.0015	0.005	0.0001	251.93
C	246	4513	2181	0.1287	0.0035	0.0642	0.001	0.03	0.001	868.15

Table 7.1: Benchmark sets of values for the model parameters able to reproduce the observed Higgs boson mass $M_{h_1} = 125.09$ GeV.

Not all these sets are compatible with the stability of the potential. For example, with the values in set B the stability condition (7.10) is violated. Choosing the first set of values (A), we scan over the remaining two free parameters g_X and Y_σ and obtain the darkon mass M_{h_2} contours shown in Fig. 7.1, while checking that the stability conditions (8.7)-(7.10) are satisfied, that the one-loop potential is bounded from below (7.46) and that all the couplings remain perturbative up to the Planck scale (7.47).

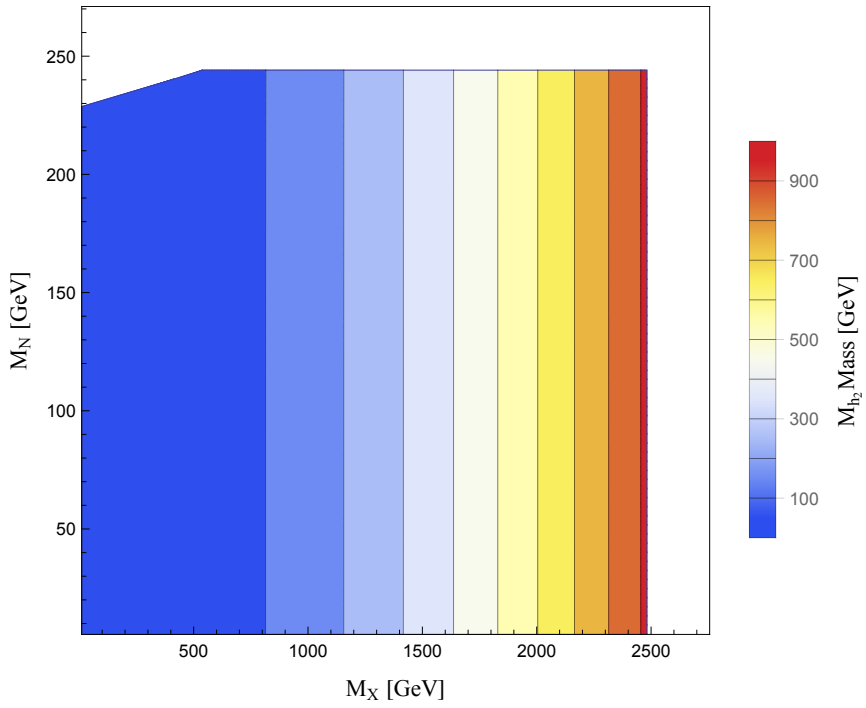

Figure 7.1: Parameter space scan in the plane (g_X, Y_σ), taking into account constraints from stability and perturbativity. The color coding signifies the mass of the darkon M_{h_2}.

We also present the running of the scalar couplings in Fig. 7.2, again for the values of set A in Table 7.1 and indicative values for g_X and Y_σ corresponding to $M_X = 725$ GeV and $M_N = 240$ GeV.

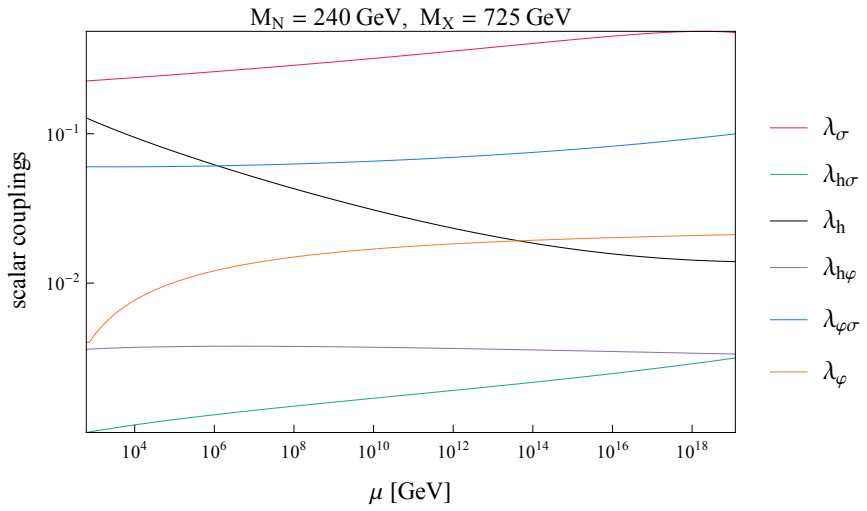

Figure 7.2: The RG evolution of the scalar couplings at two-loop order for $M_N = 240$ GeV and $M_X = 725$ GeV.

7.3.2 Experimental constraints

The three scalar fields of the present model all develop a vev and mix through the portal terms in the scalar potential (7.4). Moreover, the corresponding mass eigenstates interact with the SM electroweak sector, as well as with the $SU(2)_X$ gauge fields and the right-handed neutrinos. The strength of these interactions is suppressed by the corresponding entries in the rotation matrix $\mathcal{R}$ (7.25). In order to study possible signatures of the extra scalars at the LHC and future colliders, we may construct an effective Lagrangian that contains all the interactions between the scalars and the rest of the fields:

$$\begin{aligned}\mathcal{L}_{\text{eff}}^{h_i} = \mathcal{R}_{i1} h_i \Bigg(& \frac{2M_W^2}{v_h} W_\mu^+ W^{-\mu} + \frac{M_Z^2}{v_h} Z_\mu Z^\mu - \frac{M_t}{v_h} \bar{t}t - \frac{M_b}{v_h} \bar{b}b \\ & - \frac{M_c}{v_h} \bar{c}c - \frac{M_\tau}{v_h} \bar{\tau}\tau + \frac{\alpha_s}{12\pi v_h} G^a_{\mu\nu} G^{a\mu\nu} + \frac{\alpha}{\pi v_h} A_{\mu\nu} A^{\mu\nu} \Bigg) \\ & + \mathcal{R}_{i2} h_i \frac{3M_X}{v_\phi} X^a_\mu X^{a\mu} - \mathcal{R}_{i3} h_i \frac{M_N}{v_\sigma} \overline{N} N + V^h_{ijk} h_i h_j h_k \,,\end{aligned} \tag{7.64}$$

with V^h_{ijk} given by

$$\begin{aligned} V^h_{ijk} = {} & \mathcal{R}_{i1} \left[\lambda_{h\phi} \mathcal{R}_{j2} \left(v_h \mathcal{R}_{k2} + v_\phi \mathcal{R}_{k1} \right) - \lambda_{h\sigma} \mathcal{R}_{j3} \left(v_h \mathcal{R}_{k3} + v_\sigma \mathcal{R}_{k1} \right) \right. \\ & \left. + \mathcal{R}_{j1} \left(-6\lambda_h v_h \mathcal{R}_{k1} + \lambda_{h\phi} v_\phi \mathcal{R}_{k2} - \lambda_{h\sigma} v_\sigma \mathcal{R}_{k3} \right) \right] \\ & + \mathcal{R}_{i2} \left[\lambda_{h\phi} \mathcal{R}_{j1} \left(v_h \mathcal{R}_{k2} + v_\phi \mathcal{R}_{k1} \right) - \lambda_{\phi\sigma} \mathcal{R}_{j3} \left(v_\phi \mathcal{R}_{k3} + v_\sigma \mathcal{R}_{k2} \right) \right. \\ & \left. + \mathcal{R}_{j2} \left(-6\lambda_\phi v_\phi \mathcal{R}_{k2} + \lambda_{h\phi} v_h \mathcal{R}_{k1} - \lambda_{\phi\sigma} v_\sigma \mathcal{R}_{k3} \right) \right] \\ & + \mathcal{R}_{i3} \left[-\lambda_{h\sigma} \mathcal{R}_{j1} \left(v_h \mathcal{R}_{k3} + v_\sigma \mathcal{R}_{k1} \right) + \lambda_{\phi\sigma} \mathcal{R}_{j2} \left(v_\phi \mathcal{R}_{k3} + v_\sigma \mathcal{R}_{k2} \right) \right. \\ & \left. + \mathcal{R}_{j3} \left(-6\lambda_\sigma v_\sigma \mathcal{R}_{k3} - \lambda_{h\sigma} v_h \mathcal{R}_{k1} + \lambda_{\phi\sigma} v_\phi \mathcal{R}_{k2} \right) \right] , \end{aligned} \tag{7.65}$$

where i, j, k take the values $1, 2, 3$. Note that all scalar vertices containing two or more h_2's are zero due to the Gildener-Weinberg conditions (7.13) and the particular parametrization of the vevs (7.29) (see also [534]). Thus, the decay rates for the decays $h_i \to h_2 h_2$ are zero at tree level. In addition, for all benchmark sets in Table 7.1, the decay $h_1 \to h_3 h_3$ is kinematically forbidden. Therefore, in the current framework there are not any lighter scalars that h_1 can decay to.

Next, let us consider the total decay widths of all scalars in relation to the corresponding SM Higgs total decay width with the same mass $\Gamma^{\rm tot}_{h_i}\left(M_h = M_{h_i}\right)$:

$$\begin{aligned}\Gamma^{\rm tot}_{h_i} &= \mathcal{R}^2_{i1}\left[{\rm BR}^{\rm SM}_{WW}+{\rm BR}^{\rm SM}_{ZZ}+{\rm BR}^{\rm SM}_{gg}+{\rm BR}^{\rm SM}_{\gamma\gamma}+{\rm BR}^{\rm SM}_{Z\gamma}+{\rm BR}^{\rm SM}_{\bar{t}t}+{\rm BR}^{\rm SM}_{\bar{b}b}+{\rm BR}^{\rm SM}_{\bar{c}c}+{\rm BR}^{\rm SM}_{\bar{\tau}\tau}\right]\times\Gamma^{\rm SM}_h\left(M_h=M_{h_i}\right)\\ &+ \Gamma\left(h_i\to XX\right)+\Gamma\left(h_i\to\overline{N}N\right)+\Gamma\left(h_i\to h_jh_k\right)\,,\end{aligned} \tag{7.66}$$

where $BR^{\rm SM}_{\chi\chi}$ are the branching ratios of the SM Higgs decays into quarks, leptons or gauge bosons. The rest of the decay rates in (7.66) are given by

$$\Gamma\left(h_i\to XX\right) = \frac{3\,M^3_{h_i}}{32\pi v^2_\phi}\sqrt{1-\frac{4M^2_X}{M^2_{h_i}}}\left(1-4\,\frac{M^2_X}{M^2_{h_i}}+12\,\frac{M^4_X}{M^4_{h_i}}\right)\left|\mathcal{R}_{i2}\right|^2\,, \tag{7.67}$$

$$\Gamma\left(h_i\to\overline{N}N\right) = \frac{3\,M^2_N\,M_{h_i}}{8\pi v^2_\sigma}\left(1-\frac{4M^2_N}{M^2_{h_i}}\right)^{3/2}\left|\mathcal{R}_{i3}\right|^2\,, \tag{7.68}$$

$$\Gamma\left(h_i\to h_jh_k\right) = \frac{1}{16\pi}\,\frac{1}{\left(1+\delta_{jk}\right)M_{h_i}}\sqrt{1-\frac{2(M^2_{h_j}+M^2_{h_k})}{M^2_{h_i}}+\frac{(M^2_{h_j}-M^2_{h_k})^2}{M^4_{h_i}}}\left|V^h_{ijk}\right|^2\,. \tag{7.69}$$

Using (7.66), the total decay width $\Gamma^{\rm tot}_{h_1}$ of a SM Higgs-like scalar h_1 is given as

$$\Gamma^{\rm tot}_{h_1} = \cos^2\alpha\cos^2\beta\,\Gamma^{\rm SM}_{h_1}+\Gamma^{\rm inv}_{h_1}, \tag{7.70}$$

where $\Gamma^{\rm SM}_{h_1}$ denotes the total decay width of the SM Higgs with mass $M_{h_1}=125.09$ GeV and $\Gamma^{\rm inv}_{h_1}$ is the invisible decay width of the Higgs boson to non-SM states that are kinematically allowed. Namely, only when $M_X, M_N \lesssim 62.5$ GeV we may have

$$\Gamma^{\rm inv}_{h_1} = \Gamma\left(h_1\to XX\right)+\Gamma\left(h_1\to\overline{N}N\right)\,. \tag{7.71}$$

For completeness, we present in Table 7.2 the branching ratios of a SM Higgs with mass $M_{h_1}=125.1$ GeV.

Decay mode	Branching ratio
$b\bar{b}$	0.575
W^+W^-	0.216
gg	0.0856
$\tau^+\tau^-$	0.0630
$c\bar{c}$	0.0290
Z^0Z^0	0.0267
$\gamma\gamma$	2.28×10^{-3}
γZ^0	1.55×10^{-3}

Table 7.2: Branching ratios for a SM Higgs boson with $M_h=125.1\,\text{GeV}$, for which $\Gamma^{\rm SM}_h = 4.08\times10^{-3}\,\text{GeV}$ [614]. We did not include the rest of the decay modes because their branching ratios are negligible.

In order to clarify the deviation of h_1 from the SM Higgs, we construct the *signal strength parameter* μ_{h_1} which can be written as

$$\mu_{h_1} = \frac{\sigma\left(pp\to h_1\right)}{\sigma^{\rm SM}\left(pp\to h\right)}\,\frac{\text{BR}\left(h_1\to\chi\chi\right)}{\text{BR}^{\rm SM}\left(h\to\chi\chi\right)} \tag{7.72}$$

where σ, BR are the production cross section and branching ratio of h_1 and $\sigma^{\rm SM}$, BR$^{\rm SM}$ the corresponding quantities for the SM Higgs. Using (7.70) and $\sigma\left(pp \to h_1\right) = \cos^2\alpha\cos^2\beta\,\sigma^{\rm SM}\left(pp \to h\right)$, the expression (7.72) becomes

$$\mu_{h_1} = \cos^4\alpha\cos^4\beta\,\frac{\Gamma^{\rm SM}_{h_1}}{\Gamma^{\rm tot}_{h_1}}. \tag{7.73}$$

However, due to the smallness of $\mathcal{R}^2_{12}$ and $\mathcal{R}^2_{13}$, the invisible decay width $\Gamma^{\rm inv}_{h_1}$ is highly suppressed relative to the total decay width $\Gamma^{\rm tot}_{h_1}$ and (7.73) simplifies to

$$\mu_{h_1} \simeq \cos^2\alpha\cos^2\beta. \tag{7.74}$$

When the Higgs signal strengths from ATLAS and CMS [615–617] are combined [618], one obtains the constraint

$$\mu_{h_1} > 0.81, \quad @\,95\%\ \text{C.L.}, \tag{7.75}$$

which translates to

$$\mathcal{R}_{11} = \cos\alpha\cos\beta > 0.9. \tag{7.76}$$

Using the benchmark values of the first set of Table 7.1 we obtain

$$\mathcal{R}_{11} = 0.994, \tag{7.77}$$

which lies comfortably within the allowed range. Thus, the state h_1 behaves mostly like the SM Higgs boson and is at the moment indistinguishable from it. Run II of the LHC may be able to provide a check for the scalar sector of the model if a universal deviation for the SM Higgs couplings is established and if new scalar states are discovered.

7.4 Dark matter analysis

7.4.1 Boltzmann equation and relic density

As stated in the Introduction, the rationale behind introducing the hidden or dark $SU(2)_X$ gauge sector is twofold. First, when the new sector is spontaneously broken by means of the Coleman-Weinberg mechanism, the electroweak scale is dynamically generated through the Higgs portal. Second, since the $SU(2)_X$ gauge symmetry is completely broken by the vev v_ϕ of the scalar complex doublet Φ, the three dark gauge bosons X^a acquire equal masses $M_X = \frac{1}{2}g_X v_\phi$ and become stable due to an intrinsic $Z_2 \times Z_2'$ discrete symmetry, thus rendering themselves potential WIMP dark matter candidates. $SU(2)_X$ vector dark matter has been studied in [379, 381–385, 400, 401, 404–408] and in the context of classical scale invariance in [409–411, 413].

Next, we calculate $\Omega_{\rm DM}$, following Refs. [322, 325, 619]. We start with the Boltzmann equation which describes the evolution of the number density n of a given particle species over time. The dark vector bosons X^a can both annihilate and semiannihilate [620–622], the relevant processes being listed in Figs. 7.3–7.5.

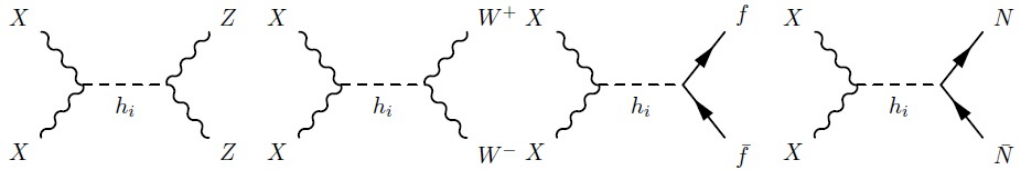

Figure 7.3: Feynman diagrams for DM annihilation to gauge bosons and fermions.

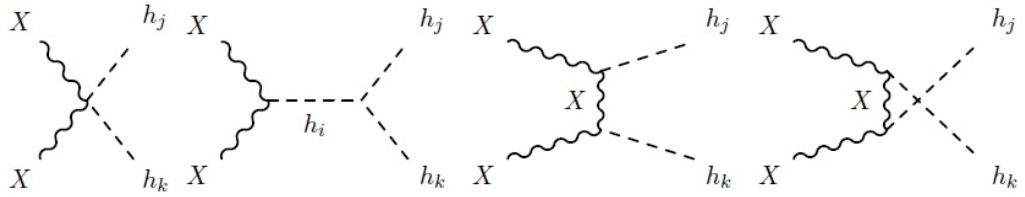

Figure 7.4: Feynman diagrams for DM annihilation to scalars.

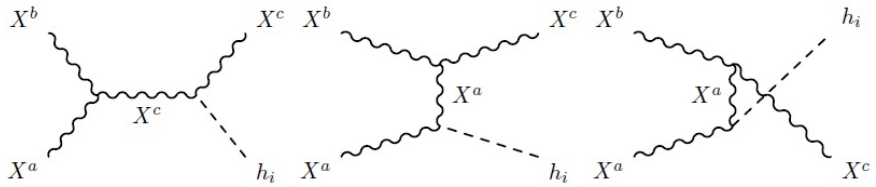

Figure 7.5: Feynman diagrams for DM semiannihilation.

The corresponding Boltzmann equation has the form [411]

$$\frac{dn}{dt} + 3\,H\,n = -\frac{\langle\sigma v\rangle_a}{3}\left(n^2 - n_{eq}^2\right) - \frac{2\,\langle\sigma v\rangle_s}{3}\,n\left(n - n_{eq}\right), \tag{7.78}$$

where H is the Hubble expansion parameter, n_{eq} is the number density during equilibrium and $\langle\sigma v\rangle$ is the thermally averaged cross section of the DM particles times their relative velocity, with the subscripts a and s denoting annihilation and semiannihilation respectively. The thermally averaged cross section times velocity is given in the nonrelativistic approximation by [623]

$$\langle\sigma v\rangle \simeq \frac{1}{M_X^2}\left[w(s) - \frac{3}{2x}\left(2w(s) - w'(s)\right)\right]\Bigg|_{s=4M_X^2}, \tag{7.79}$$

with the quantity $w(s)$ defined as

$$w(s) = \frac{1}{4}\left(1 - \frac{\delta_{jk}}{2}\right)\beta\left(s, m_j, m_k\right)\int\frac{d(\cos\theta)}{2}\sum|\mathcal{M}\left(X\,X \to \text{all}\right)|^2, \tag{7.80}$$

where $\sum|\mathcal{M}|^2$ stands for the matrix element squared of all possible channels, averaging over initial polarizations and summing over final spins, $\beta\left(s, m_j, m_k\right)$ is the final-state Lorentz invariant phase space $\beta\left(s, m_j, m_k\right) = \frac{1}{8\pi}[1 - (m_j + m_k)^2/s]^{1/2}[1 - (m_j - m_k)^2/s]^{1/2}$ and s denotes the usual Mandelstam variable $s = (p_1 + p_2)^2 = 2\left(M_X^2 + E_1E_2 - p_1p_2\cos\theta\right)$. Finally, the prime stands for differentiation with respect to $s/(4M_X^2)$ and x is defined as $x \equiv M_X/T$. The relevant individual cross sections necessary for the determination of the total annihilation and semiannihilation cross sections are too lengthy to write down. However, these can be found from an analogous calculation

in the appendix of Ref. [399]. In Fig. 7.6 we present these cross sections with respect to the dark matter mass M_X for a fixed right-handed neutrino mass at $M_N = 240$ GeV.

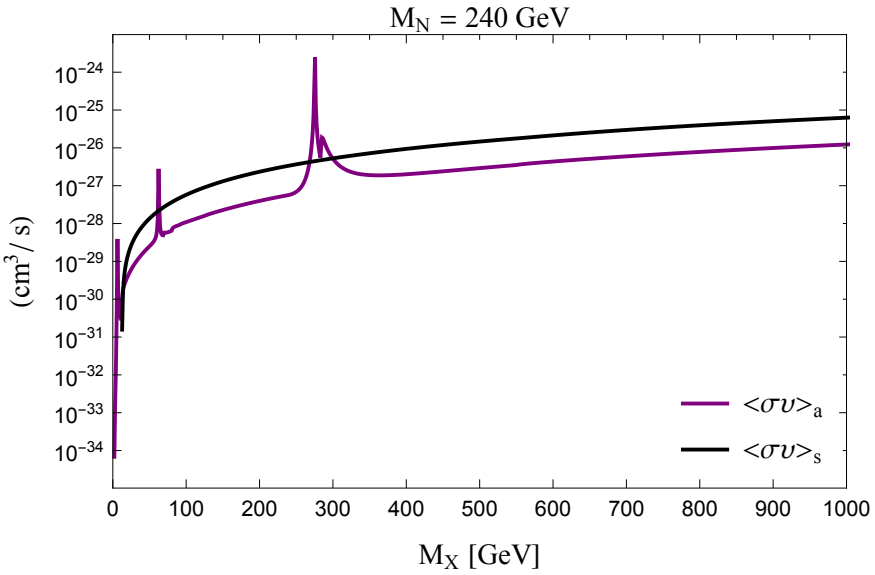

Figure 7.6: This plot shows the thermally averaged total annihilation (purple solid line) and semiannihilation (black solid line) cross sections times relative velocity with respect to the dark matter mass M_X. The peaks correspond to the poles of the scalar propagators.

We observe that the thermally averaged semiannihilation cross section is almost an order of magnitude larger than the thermally averaged annihilation cross section. Also, we see two peaks for $\langle\sigma v\rangle_a$ that correspond to $M_X = M_{h_1}/2$ and $M_X = M_{h_3}/2$ (for set A in Table 7.1) and arise due to the form of the scalar propagators at $s = 4M_X^2$:

$$\Pi_{h_i} = \frac{i}{4M_X^2 - M_{h_i}^2 + iM_{h_i}\Gamma_{h_i}^{\rm tot}}, \tag{7.81}$$

with $\Gamma_{h_i}^{\rm tot}$ given in (7.66). There is no peak for the darkon h_2 because its mass varies since it depends on M_X.

Returning to the Boltzmann equation (7.78), it is useful to express it in terms of the comoving volume $Y = n/\mathbf{s}$, $Y_{eq} = n_{eq}/\mathbf{s}$, where $\mathbf{s}$ is the entropy density, as

$$\frac{dY}{dx} = -\frac{Z_a}{3x^2}\left(Y^2 - Y_{eq}^2\right) - \frac{2Z_s}{3x^2}\left(Y^2 - Y\,Y_{eq}\right), \qquad Z_{a,s} \equiv \frac{\mathbf{s}\,(x=1)}{H\,(x=1)}\,\langle\sigma v\rangle_{a,s}\,. \tag{7.82}$$

The entropy density is given by $\mathbf{s} = \frac{2\pi^2 g_*}{45}\frac{M_X^3}{x^3}$ and the Hubble parameter is given by $H = \sqrt{\frac{4\pi^3 g_*}{45}}\frac{M_X^2}{M_{\rm P}}$, in terms of the effective number of relativistic degrees of freedom g_* at the time of freeze-out $(x = x_f)$. In order to solve (7.82) we may consider the two extreme regions $x \ll x_f$ and $x \gg x_f$, whereupon, defining $\Delta = Y - Y_{eq}$ [322] we obtain

$$\Delta = -Y_{eq}'\,\frac{3x^2}{2\,(Z_a + Z_s)}, \quad \text{when} \quad x \ll x_f, \tag{7.83}$$

$$\Delta' = -\frac{\Delta^2}{3x^2}\,(Z_a + 2Z_s)\,, \quad \text{when} \quad x \gg x_f, \tag{7.84}$$

where the prime now denotes d/dx. Moreover, if we define $\Delta(x_f) = c\,Y_{eq}(x_f)$, with c being a

constant of order one, we can match the solutions of (7.83) and (7.84) and obtain an expression for the freeze-out point which can be solved iteratively [322]:

$$x_f = \ln\left\{0.038\,\frac{3M_X M_P}{\sqrt{g_*(T_f)x_f}}\left[\,c\,(c+2)\,\langle\sigma v\rangle_a + 2\,c\,(c+1)\,\langle\sigma v\rangle_s\,\right]\right\}. \tag{7.85}$$

We find typical values between $x_f \approx 25-26$ and for the DM mass range that we consider in our numerical analysis we use $g_* = 86.25$. Also, for the constant c we use $c = 1/2$ [624]. The present day relic abundance is obtained by integrating (7.84) from $x = x_f$ to $x = \infty$:

$$Y_\infty^{-1} = \int_{x_f}^{\infty} \frac{Z_a + 2Z_s}{3x^2} dx\,. \tag{7.86}$$

Then, using the mass density of the DM particles today, $\rho_\infty = M_X \mathbf{s}_\infty Y_\infty$ and the critical density $\rho_c = 3H^2(\infty)M_P/(8\pi) = 1.054\times 10^{-5}\,h^2\,\mathrm{cm}^{-3}$, we finally obtain the dark matter relic density

$$\Omega_X h^2 = \frac{\rho_\infty}{\rho_c}\,h^2 = 3\times\frac{1.07\times 10^9\ \mathrm{GeV}^{-1}}{\sqrt{g_*}\,M_P\,J(x_f)}, \qquad J(x_f) = \int_{x_f}^{\infty} dx\,\frac{\langle\sigma v\rangle_a + 2\,\langle\sigma v\rangle_s}{x^2}, \tag{7.87}$$

where we used $\mathbf{s}_\infty = 2891.2\ \mathrm{cm}^{-3}$ for the present day entropy density and $h = 0.673$ for the Hubble scale factor [243].

The measured value for the DM relic density is $\Omega_{\rm DM}h^2 \pm 1\sigma = 0.1187 \pm 0.0017$ [243], which is a combination of the results from Planck+WP+highL+BAO. In Fig. 7.7 we scan again the parameter space of (g_X, Y_σ), but this time we also include the points where the DM relic density is saturated within 3σ (black region). We observe that the DM mass is constrained to be between $M_X \sim 710-740$ GeV.

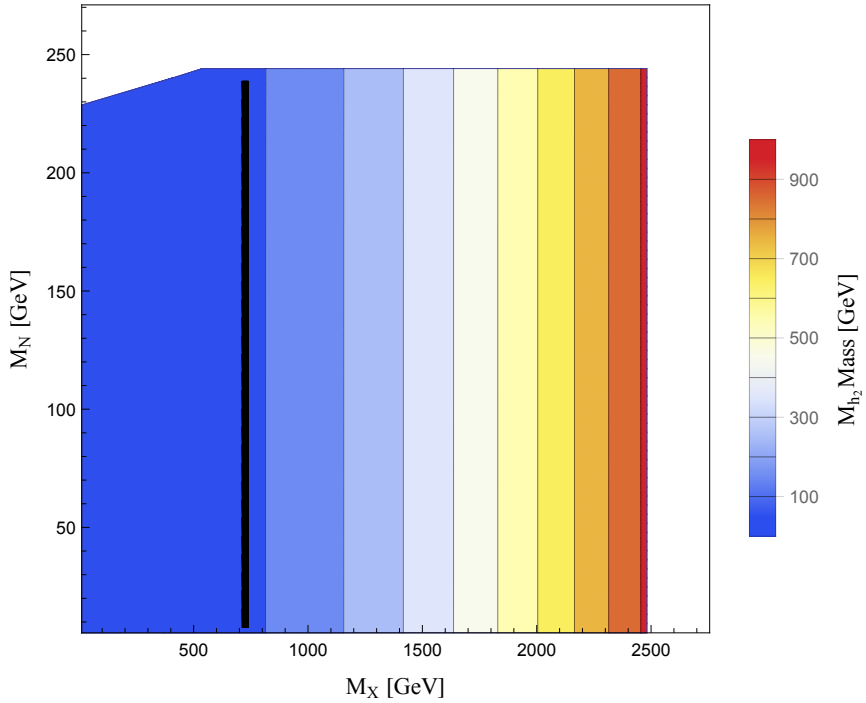

Figure 7.7: This plot is the same with Fig. 7.1 but we also calculated the points where the dark gauge bosons can saturate the observed DM relic density at 3σ (black band).

7.4.2 Dark matter direct detection

In recent years, numerous experiments have been set up aiming at directly detecting WIMP dark matter. So far these searches have not been fruitful in actually detecting dark matter. However, with each new experiment pushing the limits of sensitivity, DM detection could be just around the corner.

In the present model, the DM candidate X can in principle interact with the nucleons through the t-channel exchange of scalar bosons h_i. The relevant Feynman diagram is presented in Fig. 7.8.

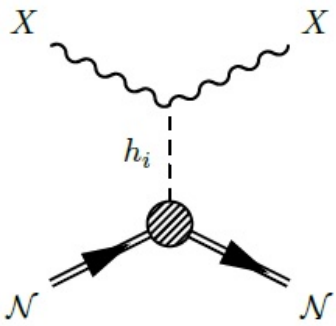

Figure 7.8: Feynman diagram for DM-nucleon elastic scattering.

This interaction is expressed through the following effective Hamiltonian in the limit of small momentum exchange between the DM particle and the nucleon:

$$H_{\text{eff}} = \frac{2M_X^2}{v_\phi} X_\mu X^\mu \left[\sum_i \frac{\mathcal{R}_{i2}\mathcal{R}_{1i}}{M_{h_i}^2}\right] \frac{m_q}{v_h}\bar{q}q\,, \tag{7.88}$$

where $\mathcal{R}_{i2}$ and $\mathcal{R}_{1i}$ are the rotation matrix elements from (7.25). The nucleonic matrix element can be parametrized as $\left\langle \mathcal{N}\middle|\sum_q m_q\bar{q}q\middle|\mathcal{N}\right\rangle = f_{\mathcal{N}} m_{\mathcal{N}}$, where $m_{\mathcal{N}} = \left(m_p + m_n\right)/2 = 0.939$ GeV is the average nucleon mass and $f_{\mathcal{N}} = 0.303$ [365, 400] is the nucleon form factor (see also [625–627]). The spin independent dark matter elastic scattering off a nucleon cross section then has the form

$$\sigma_{SI} = \frac{\mu_{\text{red}}^2}{\pi v_h^2 v_\phi^2}\left| f_{\mathcal{N}} M_X m_{\mathcal{N}} \sum_i \frac{\mathcal{R}_{i2}\mathcal{R}_{1i}}{M_{h_i}^2}\right|^2, \tag{7.89}$$

where $\mu_{\text{red}} = M_X m_{\mathcal{N}}/\left(M_X + m_{\mathcal{N}}\right)$ is the DM-nucleon reduced mass, just $\mu_{red} \approx m_{\mathcal{N}}$ in our case.

Employing (7.89), we evaluate the spin independent cross section for various M_X and M_N masses and then, using the experimental results from LUX (2013) [628] and the projected limits from XENON 1T [450], we construct the plot shown in Fig. 7.9.

We find that relatively low M_X masses are excluded by LUX (2013). Nevertheless, masses above circa 700 GeV, such as those suitable for the saturation of the measured relic density (cf. Fig. 7.7), are favored for detection by XENON 1T.

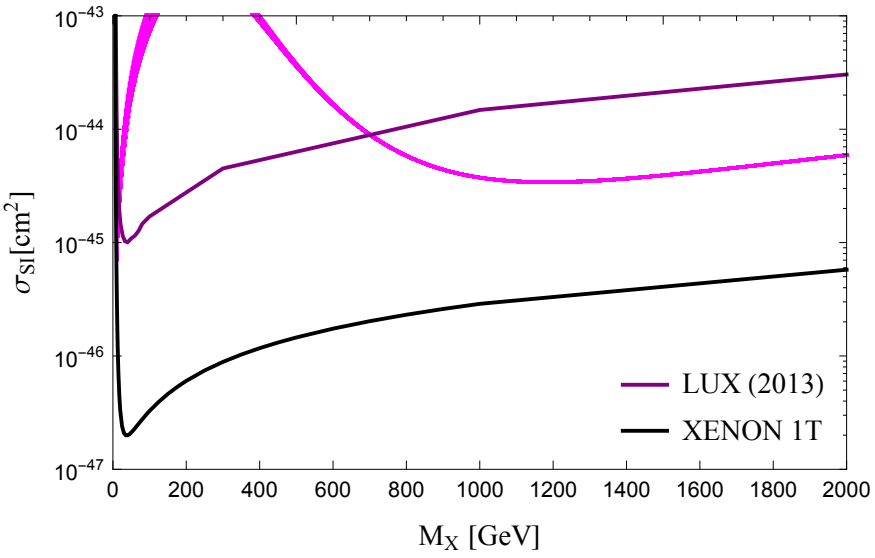

Figure 7.9: The plot shows the DM-nucleon cross section as a function of the DM mass for varying M_N masses respecting the stability and perturbativity constraints discussed in Sec. 7.3.1 (magenta band). The purple solid line corresponds to the experimental limits from LUX (2013) and the black solid line corresponds to the anticipated results for XENON 1T.

Chapter 8

Dark matter from a classically scale-invariant $SU(3)_X$

8.1 Introduction

The work presented in this chapter was done in collaboration with Prof. Kyriakos Tamvakis and has been published in Physical Review D [418].

In this chapter, we propose a CSI extension of the SM where a new $SU(3)_X$ gauge symmetry can provide massive gauge fields that can account for the observed DM relic density. The hidden sector will be broken completely by two scalar triplets. These will have portal couplings with the Higgs field and will help in the stabilization of the potential. The scalar sector will consist of three Higgs-like particles, one of which will be massless at tree level but will nevertheless acquire a nonzero mass once we consider the full one-loop scalar potential. All eight of the extra gauge bosons will become massive, while the three lightest will be stable due to their parities under an intrinsic $Z_2 \times Z_2'$ discrete symmetry of $SU(3)_X$. These three dark gauge bosons will be our DM candidates. Because of the rich structure of the extra gauge group, the computation of the DM relic density will include various types of processes apart from DM annihilations, such as semiannihilations, coannihilations, and DM conversions.

The layout of this chapter is the following: In the next section we present the model and calculate the masses of the new fields. In Sec. 8.3 we impose various theoretical and experimental constraints on the model. Then, in Sec. 8.4 we give a detailed analysis of the system of Boltzmann equations that need to be solved in order to obtain the DM relic abundance, and we also focus on the role of coannihilations and DM conversion processes. Furthermore, we examine the direct detection prospects of the DM candidates.

8.2 The Model

We begin with a CSI version of the Standard Model and consider an $SU(3)_X$ extension of its gauge symmetry in order to accommodate the presence of dark matter. The non-CSI version of this model was recently considered in Ref. [401]. The breaking of the gauge symmetry $SU(3)_C \times SU(2)_L \times U(1)_Y \times SU(3)_X \to SU(3)_C \times U(1)_{em}$ is achieved through the Coleman-Weinberg mechanism [7]. In addition to the new $SU(3)_X$ gauge bosons, referred to as “dark" gauge bosons, the model contains a pair of complex scalars $\Phi_1(1,1,0;3)$ and $\Phi_2(1,1,0;3)$ transforming as singlets under the Standard Model gauge group and as triplets under $SU(3)_X$, referred to as “dark" scalars. In this section we explore the scalar and gauge sectors of the model. First, we present the tree-level potential. Employing the Gildener-Weinberg formalism [600], we minimize the tree-level potential at a

definite energy scale which defines a flat direction among the scalar fields. Then, we compute the tree-level scalar and dark gauge boson masses. One of the scalar bosons turns out to be massless at tree level and corresponds to the pseudo–Nambu-Goldstone boson (pNGB) of broken scale symmetry. Finally, we present the one-loop effective potential which becomes dominant along the flat direction and greatly lifts the mass of the pNGB.

8.2.1 Tree-level potential

The most general renormalizable and scale-invariant tree-level scalar potential involving the standard Higgs doublet H and the dark triplets Φ_1, Φ_2 is

$$\begin{aligned} V_0 \;=\; & \lambda_h (H^\dagger H)^2 \;+\; \lambda_1 (\Phi_1^\dagger \Phi_1)^2 + \lambda_2 (\Phi_2^\dagger \Phi_2)^2 - \lambda_3 (\Phi_1^\dagger \Phi_1)(\Phi_2^\dagger \Phi_2) + \lambda_4 (\Phi_1^\dagger \Phi_2)(\Phi_2^\dagger \Phi_1) \\ & + \left[\frac{\lambda_5}{2} (\Phi_1^\dagger \Phi_2)^2 + \lambda_6 (\Phi_1^\dagger \Phi_1)(\Phi_1^\dagger \Phi_2) + \lambda_7 (\Phi_2^\dagger \Phi_2)(\Phi_1^\dagger \Phi_2) + \text{H.c.} \right] - \lambda_{h1} (H^\dagger H)(\Phi_1^\dagger \Phi_1) \\ & + \;\lambda_{h2} (H^\dagger H)(\Phi_2^\dagger \Phi_2) \;- \left(\lambda_{h12} (H^\dagger H)(\Phi_1^\dagger \Phi_2) + \text{H.c.} \right), \end{aligned} \tag{8.1}$$

where all appearing coupling constants are taken to be real and positive. Notice that we have assumed negative signs for the λ_{h1} and λ_3 portal couplings as the basic seed of symmetry breaking. Out of the 12 degrees of freedom included in Φ_1, Φ_2, 8 are Higgsed away. Using gauge freedom and removing 5 of them from Φ_1 and 3 from Φ_2, we end up in the unitary gauge with Φ_1 containing 1 and Φ_2 3 real degrees of freedom

$$\Phi_1 \;=\; \frac{1}{\sqrt{2}} \begin{pmatrix} 0 \\ \\ 0 \\ \\ v_1 + \phi_1 \end{pmatrix}, \qquad \Phi_2 \;=\; \frac{1}{\sqrt{2}} \begin{pmatrix} 0 \\ \\ v_2 + \phi_2 \\ \\ (v_3 + \phi_3) + i(v_4 + \phi_4) \end{pmatrix}. \tag{8.2}$$

Assuming CP invariance implies that all vacuum expectation values (VEVs) are real and $v_4 = 0$. The extra $SU(3)_X$ can be completely broken if at least two of the remaining VEVs are nonzero, so we further assume $v_3 = 0$ for simplicity. The standard Higgs will correspond to 1 real degree of freedom

$$H \;=\; \frac{1}{\sqrt{2}} \begin{pmatrix} 0 \\ \\ v_h + h \end{pmatrix}. \tag{8.3}$$

The scalar potential is further simplified if we impose invariance of the potential under the discrete symmetry

$$\Phi_2 \;\to\; -\Phi_2, \tag{8.4}$$

which implies

$$\lambda_6 = \lambda_7 = \lambda_{h12} = 0. \tag{8.5}$$

Omitting the VEVs for the moment, the resulting potential is

$$\begin{aligned} V_0 \;=\; & \frac{\lambda_h}{4} h^4 + \frac{\lambda_1}{4} \phi_1^4 + \frac{\lambda_2}{4} \phi_2^4 - \frac{\lambda_{h1}}{4} h^2 \phi_1^2 + \frac{\lambda_{h2}}{4} h^2 \phi_2^2 - \frac{\lambda_3}{4} \phi_1^2 \phi_2^2 \\ & + \frac{\lambda_2}{4} (\phi_3^2 + \phi_4^2)^2 + \left(\frac{\lambda_2}{2} \phi_2^2 + \frac{\lambda_3}{4} \phi_1^2 + \frac{\lambda_4}{4} \phi_1^2 + \frac{\lambda_{h2}}{4} h^2 \right) (\phi_3^2 + \phi_4^2) + \frac{\lambda_5}{4} \phi_1^2 \left(\phi_3^2 - \phi_4^2 \right). \end{aligned} \tag{8.6}$$

The above potential is bounded from below if the following conditions [148, 604, 605] are satisfied for all energies up to the Planck scale[1]:

$$\lambda_h \geq 0,\, \lambda_1 \geq 0,\, \lambda_2 \geq 0, \tag{8.7}$$

$$2\sqrt{\lambda_h\lambda_1} - \lambda_{h1} \geq 0, \quad 2\sqrt{\lambda_h\lambda_2} + \lambda_{h2} \geq 0, \quad 2\sqrt{\lambda_1\lambda_2} - \lambda_3 \geq 0, \tag{8.8}$$

$$4\lambda_h\lambda_1\lambda_2 - \left(\lambda_{h1}^2\lambda_2 + \lambda_{h2}^2\lambda_1 + \lambda_3^2\lambda_h\right) + \lambda_{h1}\lambda_{h2}\lambda_3 \geq 0. \tag{8.9}$$

8.2.2 Scalar masses

Gauge symmetry breaking to $SU(3)_C \times U(1)_{em}$ can arise through the nonzero VEVs v_h, v_1, v_2. Since the tree-level potential does not contain any dimensionful parameters, this can only occur via the Coleman-Weinberg mechanism [7]. Having multiple scalars, we will make use of the Gildener-Weinberg approach [600] in order to minimize the potential. The tree-level potential is minimized at a particular renormalization scale $\mu = \Lambda$ which defines the flat direction among the VEVs. The corresponding equations read [600]

$$\lambda_h(\Lambda)\, v_h^4 + \lambda_1(\Lambda)\, v_1^4 + \lambda_2(\Lambda)\, v_2^4 - \lambda_3(\Lambda)\, v_1^2 v_2^2 - \lambda_{h1}(\Lambda)\, v_h^2 v_1^2 + \lambda_{h2}(\Lambda)\, v_h^2 v_2^2 = 0, \tag{8.10}$$
$$2\lambda_h(\Lambda)\, v_h^2 - \lambda_{h1}(\Lambda)\, v_1^2 + \lambda_{h2}(\Lambda)\, v_2^2 = 0, \tag{8.11}$$
$$2\lambda_1(\Lambda)\, v_1^2 - \lambda_3(\Lambda)\, v_2^2 - \lambda_{h1}(\Lambda)\, v_h^2 = 0, \tag{8.12}$$
$$2\lambda_2(\Lambda)\, v_2^2 - \lambda_3(\Lambda)\, v_1^2 + \lambda_{h2}(\Lambda)\, v_h^2 = 0. \tag{8.13}$$

Along the flat direction, the shifted scalar fields may be written as

$$h = (\varphi + v)\, n_h, \quad \phi_1 = (\varphi + v)\, n_1, \quad \phi_2 = (\varphi + v)\, n_2, \tag{8.14}$$

where $\varphi^2 = h^2 + \phi_1^2 + \phi_2^2$ and the overall VEV v is $v^2 = v_h^2 + v_1^2 + v_2^2$, with $n_h^2 + n_1^2 + n_2^2 = 1$.

The mass matrix of the three scalar fields that participate in the symmetry breaking can be read off from the shifted tree-level potential to be

$$\mathcal{M}_0^2 = v^2 \begin{pmatrix} 2\lambda_h n_h^2 & -n_h n_1 \lambda_{h1} & n_h n_2 \lambda_{h2} \\ -n_h n_1 \lambda_{h1} & 2\lambda_1 n_1^2 & -n_1 n_2 \lambda_3 \\ n_h n_2 \lambda_{h2} & -n_1 n_2 \lambda_3 & 2\lambda_2 n_2^2 \end{pmatrix} \tag{8.15}$$

in the (h, ϕ_1, ϕ_2) basis. Next, we may consider a general rotation

$$\mathcal{R}\, \mathcal{M}_0^2\, \mathcal{R}^{-1} = \mathcal{M}_d^2 \implies \begin{pmatrix} h \\ \phi_1 \\ \phi_2 \end{pmatrix} = \mathcal{R}^{-1} \begin{pmatrix} h_1 \\ h_2 \\ h_3 \end{pmatrix}, \tag{8.16}$$

[1] In fact, a more rigorous treatment shows that we must replace λ_3 with $\lambda_3 + \min[0, \lambda_4 + \lambda_5, \lambda_4 - \lambda_5]$ in the stability conditions (8.7)–(8.9). However, we shall assume $\lambda_4 + \lambda_5 > 0$ and $\lambda_4 - \lambda_5 > 0$, resulting in positive masses for the fields ϕ_3 and ϕ_4 [cf. (8.27)–(8.28)]. Therefore $\min[0, \lambda_4 + \lambda_5, \lambda_4 - \lambda_5] = 0$.

in terms of the rotation matrix $\mathcal{R}^{-1}$ given by

$$\mathcal{R}^{-1} = \begin{pmatrix} \cos\alpha\cos\beta & \sin\alpha & \cos\alpha\sin\beta \\ -\cos\beta\cos\gamma\sin\alpha + \sin\beta\sin\gamma & \cos\alpha\cos\gamma & -\cos\gamma\sin\alpha\sin\beta - \cos\beta\sin\gamma \\ -\cos\gamma\sin\beta - \cos\beta\sin\alpha\sin\gamma & \cos\alpha\sin\gamma & \cos\beta\cos\gamma - \sin\alpha\sin\beta\sin\gamma \end{pmatrix}. \quad (8.17)$$

Two of these rotation angles may be chosen to be related to the flat direction through

$$\begin{aligned} n_h &= \sin\alpha, \\ n_1 &= \cos\alpha\cos\gamma, \\ n_2 &= \cos\alpha\sin\gamma. \end{aligned} \quad (8.18)$$

Then, $\mathcal{M}_d^2$ is diagonal, provided that the following relation is satisfied:

$$\tan 2\beta = \frac{v_h v_1 v_2 v\,(\lambda_{h2} + \lambda_{h1})}{(\lambda_1 + \lambda_2 + \lambda_3)\,v_1^2 v_2^2 - \lambda_h v_h^2 v^2}\,. \quad (8.19)$$

The resulting tree-level masses include a zero eigenvalue, namely, $M_{h_2} = 0$, which corresponds to the pNGB of broken scale invariance. Of course, this mass will be strongly lifted at the one-loop level. The other two eigenvalues M_{h_1}, M_{h_3} are given by complicated expressions in terms of the overall VEV, the angles, and the scalar couplings. In addition to the above three scalar states there are also the scalar fields ϕ_3, ϕ_4, which we did not include in the above analysis. These fields do not receive a VEV but obtain tree-level masses as soon as the gauge symmetry breaking is established. As we will see in Sec. 8.2.4, radiative corrections will strongly affect only the flat direction defined by h_2, while the masses of ϕ_3, ϕ_4, h_1, h_3 will stay close to their tree-level values.

8.2.3 Dark gauge boson masses

The $SU(3)_X$ gauge fields enter the Lagrangian through the kinetic terms

$$\mathcal{L}_X = -\frac{1}{2}\,\mathrm{tr}\{X_{\mu\nu}X^{\mu\nu}\} + |D_\mu\Phi_1|^2 + |D_\mu\Phi_2|^2, \quad (8.20)$$

where the field strength tensor is defined as $X_{\mu\nu} = \partial_\mu X_\nu - \partial_\nu X_\mu + i g_X \left[X_\mu, X_\nu\right]$ and the covariant derivative of Φ_i has the form $D_\mu\Phi_i = \partial_\mu\Phi_i + i g_X X_\mu \Phi_i$.

Following Ref. [401], we consider the discrete symmetry $Z_2 \times Z_2'$ of the $SU(3)$ generators in the Gell-Mann basis, where the first Z_2 corresponds to a gauge transformation, while the second Z_2' is identified with complex conjugation. The parities of the gauge fields X_μ and the scalar fields Φ_i under $Z_2 \times Z_2'$ are summarized in Table 8.1. This discrete symmetry is important for the identification of dark matter since the lightest fields with nontrivial discrete signatures will not be able to decay to Standard Model matter.

Fields	$Z_2 \times Z_2'$
h, ϕ_1, ϕ_2, ϕ_3, X_μ^7	$(+,+)$
X_μ^2, X_μ^5	$(-,+)$
X_μ^1, X_μ^4	$(-,-)$
ϕ_4, X_μ^3, X_μ^6, X_μ^8	$(+,-)$

Table 8.1: Gauge and scalar fields parities under $Z_2 \times Z_2'$.

For the particular choice of nonzero $v_{1,2}$ and $v_{3,4} = 0$, there is only one mixing term, $X^3_\mu X^{\mu 8}$, among the dark gauge fields. The gauge boson mass matrix has the form

$$\mathcal{M}^2_X = \frac{g_X^2}{4}\begin{pmatrix} v_2^2 & 0 & 0 & 0 & 0 & 0 & 0 & 0 \\ 0 & v_2^2 & 0 & 0 & 0 & 0 & 0 & 0 \\ 0 & 0 & v_2^2 & 0 & 0 & 0 & 0 & -\frac{v_2^2}{\sqrt{3}} \\ 0 & 0 & 0 & v_1^2 & 0 & 0 & 0 & 0 \\ 0 & 0 & 0 & 0 & v_1^2 & 0 & 0 & 0 \\ 0 & 0 & 0 & 0 & 0 & v_1^2+v_2^2 & 0 & 0 \\ 0 & 0 & 0 & 0 & 0 & 0 & v_1^2+v_2^2 & 0 \\ 0 & 0 & -\frac{v_2^2}{\sqrt{3}} & 0 & 0 & 0 & 0 & \left(4v_1^2+v_2^2\right)/3 \end{pmatrix}. \tag{8.21}$$

Defining the gauge boson mass eigenstates as

$$\begin{pmatrix} X^{3'}_\mu \\ X^{8'}_\mu \end{pmatrix} = \begin{pmatrix} \cos\delta & \sin\delta \\ -\sin\delta & \cos\delta \end{pmatrix}\begin{pmatrix} X^3_\mu \\ X^8_\mu \end{pmatrix}, \tag{8.22}$$

with the mixing angle given by

$$\tan 2\delta = \frac{\sqrt{3}v_2^2}{2v_1^2 - v_2^2}, \implies \tan\delta = \frac{-2v_1^2 + v_2^2 \pm 2\sqrt{v_1^4 - v_1^2v_2^2 + v_2^4}}{\sqrt{3}v_2^2}, \tag{8.23}$$

we obtain the masses shown in Table 8.2. In the following, we keep only the " + " solution in (8.23) corresponding to $\tan\delta$ being small and positive for $v_1^2 \gg v_2^2$.

Gauge fields	Mass^2
X^1_μ	$\frac{1}{4}g_X^2v_2^2$
X^2_μ	$\frac{1}{4}g_X^2v_2^2$
$X^{3'}_\mu$	$\frac{1}{4}g_X^2v_2^2\left(1-\frac{\tan\delta}{\sqrt{3}}\right)$
X^4_μ	$\frac{1}{4}g_X^2v_1^2$
X^5_μ	$\frac{1}{4}g_X^2v_1^2$
X^6_μ	$\frac{1}{4}g_X^2\left(v_1^2+v_2^2\right)$
X^7_μ	$\frac{1}{4}g_X^2\left(v_1^2+v_2^2\right)$
$X^{8'}_\mu$	$\frac{1}{3}g_X^2v_1^2\left(1-\frac{\tan\delta}{\sqrt{3}}\right)^{-1}$

Table 8.2: Dark gauge boson masses.

In addition to the above gauge boson mass terms, the scalar kinetic terms also give a scalar/gauge-boson mixing

$$ig_X X^a_\mu(\partial^\mu\Phi_i)^\dagger T^a\Phi_i + H.c. = g_X\frac{v_2}{2}\left(\partial^\mu\phi_4\, X^6_\mu - \partial^\mu\phi_3 X^7_\mu\right). \tag{8.24}$$

This leads to a redefinition of the two scalar and gauge fields involved according to

$$\tilde{X}^6_\mu = X^6_\mu + \frac{2}{g_X}\frac{v_2}{v_1^2+v_2^2}\partial_\mu\phi_4, \quad \tilde{X}^7_\mu = X^7_\mu - \frac{2}{g_X}\frac{v_2}{v_1^2+v_2^2}\partial_\mu\phi_3, \tag{8.25}$$

$$\tilde{\phi}_3 = \frac{v_1}{\sqrt{v_1^2+v_2^2}}\phi_3, \qquad \tilde{\phi}_4 = \frac{v_1}{\sqrt{v_1^2+v_2^2}}\phi_4. \tag{8.26}$$

The normalized masses for X_6, X_7 are the ones entering in Table 8.2, while the resulting masses of the canonical scalar fields $\tilde{\phi}_3$, $\tilde{\phi}_4$ are

$$M^2_{\tilde{\phi}_3} = \frac{1}{2}(\lambda_4+\lambda_5)\left(v_1^2+v_2^2\right), \tag{8.27}$$

$$M^2_{\tilde{\phi}_4} = \frac{1}{2}(\lambda_4-\lambda_5)\left(v_1^2+v_2^2\right). \tag{8.28}$$

For $v_1^2 \gg v_2^2$, the mixing angle δ is small and positive [cf. (8.23)], while $X_\mu^{1,2}$ and $X_\mu^{3'}$ are nearly degenerate in mass and also the lightest of the eight dark gauge bosons. In addition, because of their parities under $Z_2 \times Z_2'$ (cf. Table 8.1), they are stable and can therefore constitute DM candidates. Note, however, that $\tilde{\phi}_4$ and $X_\mu^{3'}$ have the same parities under $Z_2 \times Z_2'$. This means that the decay process $X^{3'} \to \tilde{\phi}_4 + \text{SM}$ is possible if $M_{\tilde{\phi}_4} < M_{X^{3'}}$, and in that case $\tilde{\phi}_4$ can be a DM candidate instead of $X_\mu^{3'}$. However, in the following we will study the case $M_{\tilde{\phi}_4} > M_{X^{3'}}$ and relegate this alternative scenario to future work.

8.2.4 One-loop potential

The one-loop potential, along the flat direction, at a renormalization scale $\mu = \Lambda$ where the tree-level potential is minimized, takes the form

$$V_1(\mathbf{n}\varphi) = A\,\varphi^4 + B\,\varphi^4 \ln(\varphi^2/\Lambda^2), \tag{8.29}$$

where the dimensionless coefficients A, B are given (in the $\overline{MS}$ scheme) by

$$A = \frac{1}{64\pi^2 v^4}\left[\sum_{i=h_1,h_3,\tilde{\phi}_3,\tilde{\phi}_4} M_i^4\left(-\frac{3}{2}+\log\frac{M_i^2}{v^2}\right) + 6M_W^4\left(-\frac{5}{6}+\log\frac{M_W^2}{v^2}\right) + 3M_Z^4\left(-\frac{5}{6}+\log\frac{M_Z^2}{v^2}\right) + 3\sum_{i=1}^{8} M_{X^i}^4\left(-\frac{5}{6}+\log\frac{M_{X^i}^2}{v^2}\right) - 12M_t^4\left(-1+\log\frac{M_t^2}{v^2}\right)\right], \tag{8.30}$$

$$B = \frac{1}{64\pi^2 v^4}\left(\sum_{i=h_1,h_3,\tilde{\phi}_3,\tilde{\phi}_4} M_i^4 + 6M_W^4 + 3M_Z^4 + 3\sum_{i=1}^{8} M_{X^i}^4 - 12M_t^4\right). \tag{8.31}$$

Note that the model, with its present minimal field content, does not accommodate neutrino mass generation through a right-handed neutrino seesaw mechanism. Nevertheless, right-handed neutrinos can still be present and obtain their mass from a separate sector, the minimal example being a real scalar field that couples only to neutrinos. Of course, with the given symmetries of the model, if such a singlet exists, its couplings with the rest of the scalars cannot be forbidden *a priori*. Nevertheless, it could be assumed that these couplings are quite small, in which case they would not affect the analysis of the rest of the model.

Minimizing the one-loop effective potential, we obtain

$$V_1(\mathbf{n}\varphi) = B\,\varphi^4\left[\ln\left(\frac{\varphi^2}{v^2}\right) - \frac{1}{2}\right]. \tag{8.32}$$

An immediate consequence of the one-loop radiative corrections is to lift the pNGB mass to the nonzero value

$$M_{h_2}^2 = \left.\frac{\partial^2 V_1}{\partial \varphi^2}\right|_{\varphi=v} = \frac{1}{8\pi^2 v^2}\left(M_{h_1}^4 + M_{h_3}^4 + M_{\tilde{\phi}_3}^4 + M_{\tilde{\phi}_4}^4 + 6M_W^4 + 3M_Z^4 + 3\sum_{i=1}^{8} M_{X^i}^4 - 12M_t^4\right). \tag{8.33}$$

Finally, note that the one-loop corrections to the masses of $\tilde{\phi}_{3,4}$ are exactly zero, while the corrections to the masses of $h_{1,3}$ are very suppressed and can be safely ignored to a first approximation.[2]

8.3 Phenomenological analysis

In this section we study the phenomenological viability of the model. First we examine the interrelationship among the masses of the dark gauge bosons and scalars. Then, scanning over a range of values for the scalar couplings and the dark gauge coupling we find benchmark points that satisfy stability and perturbativity constraints, as well as bounds set by the first run of the LHC and measurements of the electroweak precision observables.

The Coleman-Weinberg mechanism is successfully realized if the mass of the dark scalar M_{h_2} [cf. (8.33)] turns out to be positive. For this to be true we must have $B > 0$ [cf. (8.32)], or

$$M_{h_3}^4 + M_{\tilde{\phi}_3}^4 + M_{\tilde{\phi}_4}^4 + 3\sum_{i=1}^{8} M_{X_i}^4 > (317.26\,\text{GeV})^4\,. \tag{8.34}$$

The scalar state h_1 (that we identify with the Higgs boson) has analogous couplings to the SM particles as a SM Higgs, but rescaled by the factor $\mathcal{R}_{11}$ from the rotation matrix (8.17),

$$g_{h_1\chi\chi} = \mathcal{R}_{11} g_{h\chi\chi}^{\text{SM}}, \tag{8.35}$$

with $\chi\chi$ denoting a pair of SM particles. Constructing the signal strength parameter for h_1 [414],

$$\mu_{h_1} = \frac{\sigma\,(pp \to h_1)}{\sigma^{\text{SM}}\,(pp \to h)} \frac{\text{BR}\,(h_1 \to \chi\chi)}{\text{BR}^{\text{SM}}\,(h \to \chi\chi)} \simeq \cos^2\alpha \cos^2\beta, \tag{8.36}$$

and employing the bound set by the first run of the LHC [615–618]:

$$\mu_{h_1} > 0.81, \quad @\,95\%\ \text{C.L.}, \tag{8.37}$$

we can constrain the matrix element $\mathcal{R}_{11}$ as

$$\mathcal{R}_{11} = \cos\alpha \cos\beta > 0.9\,, \tag{8.38}$$

meaning that the angles α, β cannot be too large.

Another experimental constraint arises from the measurements of the oblique parameters S, T, and U. Setting $U = 0$, we have [243]

$$S = 0.00 \pm 0.08, \qquad T = 0.05 \pm 0.07. \tag{8.39}$$

In this model, the above parameters are given by the formulas presented in Appendix A.

[2] See [528] for a complete treatment in a relevant CSI model.

We can further constrain the model by requiring the stability of the scalar potential and the perturbativity of the couplings as they evolve with the renormalization scale. To this end, we consider the scalar couplings (except λ_h) and the gauge coupling g_X and generate random values inside the intervals shown below,

$$\lambda_1,\, \lambda_2,\, \lambda_3,\, \lambda_{h1},\, \lambda_{h2},\, \lambda_4,\, \lambda_5 \;\in\; \left[10^{-6}, 1\right], \quad g_X \;\in\; [0,3]\,. \tag{8.40}$$

The scalar couplings are specified at the renormalization scale Λ where the tree-level potential is minimized, whereas the dark gauge coupling is defined at the scale of the lightest dark gauge boson $g_X(M_{X^{3'}})$.

Then, we calculate the VEVs v_1, v_2 and the Higgs self-coupling λ_h from the minimization conditions (8.10)–(8.13). At the first stage, we keep only the points that reproduce the measured Higgs mass $M_{h_1} = 125.09 \pm 0.24\,\text{GeV}$. Subsequently, we solve numerically the two-loop RGEs (cf. Appendix B) and keep only the values of the couplings that remain perturbative up to the Planck scale and also satisfy the vacuum stability conditions (8.7)–(8.9), as well as the bound set by LHC (8.38) and the constraints on the parameters S and T (8.39). We present five of these benchmark points in Table 8.3.

Most of these benchmark points (BPs) contain values for the dark VEVs for which $v_1^2 \gg v_2^2$. This results in the masses of the dark gauge bosons X_μ^1, X_μ^2, $X_\mu^{3'}$ being nearly degenerate, while the masses of the rest of the dark gauge bosons are well above them. Nonetheless, in BP2, we have also included the case $v_1 \simeq v_2$. In this case, the mass of $X_\mu^{3'}$ is fairly lower than the masses of X_μ^1 and X_μ^2, which are now close to the masses of X_μ^4 and X_μ^5, while the masses of X_μ^6 and X_μ^7 become nearly degenerate with the mass of $X_\mu^{8'}$. Therefore, in the case $v_1 \simeq v_2$, we have

$$M_{X^{3'}}^2 \simeq \frac{2}{3} M_{X^{1,2}}^2 \simeq \frac{2}{3} M_{X^{4,5}}^2 \simeq \frac{1}{3} M_{X^{6,7}}^2 \simeq \frac{1}{3} M_{X^{8'}}^2 . \tag{8.41}$$

As we will see in the next section, the case $v_1 \simeq v_2$ is distinct in its dark matter analysis.

Regarding the scalar bosons and the pNGB h_2 in particular, we observe that its mass depends highly on the values of the VEVs v_1, v_2 and the dark gauge coupling g_X, or equivalently on the masses of the dark gauge bosons and the rest of the scalars [cf. (8.33)]. For example, large values for the VEVs and g_X produce a large mass for h_2, as can be seen from BP4 in Table 8.3.

Finally, the dark gauge boson mass spectrum for both cases $v_1^2 \gg v_2^2$ and $v_1 \simeq v_2$ is shown schematically in Fig. 8.1.

8.4 Dark matter analysis

Recent astrophysical measurements [1] have corroborated the now well-established fact that $\sim 80\%$ of the nonrelativistic matter in the Universe is in a form that remains a mystery to us and cannot be explained by the known particles and forces. This “dark matter" (DM) could be constituted of scalar bosons, fermions, vector bosons, a combination of the above, or even something more exotic. Here we will focus on vector DM [379–411, 413–417].

Whatever the case may be, a DM candidate particle should be stabilized by some kind of symmetry, such that it may not decay to the SM particles. The simplest possibility of a stabilizing symmetry is that of a Z_2 discrete symmetry. A neutral and weakly interacting massive particle can be a DM candidate if it is the lightest Z_2 or Z_3-odd particle in a given model [629–634]. In order to

	BP1	BP2	BP3	BP4	BP5
$\lambda_1\,(\Lambda)$	0.00008	0.0112	0.0014	0.00017	0.00015
$\lambda_2\,(\Lambda)$	0.0706	0.01073	0.0689	0.12129	0.00126
$\lambda_{h1}\,(\Lambda)$	0.00292	0.0237	0.00282	0.0006	0.0016
$\lambda_{h2}\,(\Lambda)$	0.04116	0.00323	0.00031	0.00109	0.00344
$\lambda_3\,(\Lambda)$	0.00459	0.0211	0.0196	0.00911	0.00088
$\lambda_4\,(\Lambda)$	0.3104	0.3317	0.2878	0.3363	0.3564
$\lambda_5\,(\Lambda)$	0.0052	0.000003	0.000011	0.13762	0.00167
$\lambda_h\,(\Lambda)$	0.13811	0.13201	0.12804	0.12876	0.13295
g_X	1.25	0.88	0.81	2.01	0.29
v_h	246.22	246.22	246.22	246.22	246.22
v_1	3180.05	882.78	2365.61	5272.32	6610.41
v_2	557.43	869.86	891.70	1021.43	3898.50
M_{h_1}	125.07	125.02	125.17	125.08	125.14
M_{h_2}	588.86	97.82	189.80	2500.34	227.22
M_{h_3}	215.81	184.42	353.78	512.43	228.37
$M_{\tilde{\phi}_3}$	1282.51	504.70	958.99	2614.19	3247.10
$M_{\tilde{\phi}_4}$	1261.21	504.69	958.95	1692.65	3231.93
$M_{X^{1,2}}$	349.65	382.29	361.14	1028.25	560.84
$M_{X^{3'}}$	348.29	314.41	354.20	1023.32	531.48
$M_{X^{4,5}}$	1994.73	387.97	958.07	5307.55	950.98
$M_{X^{6,7}}$	2025.14	544.67	1023.88	5406.23	1104.05
$M_{X^{8'}}$	2312.35	544.70	1127.97	6158.13	1158.77
Λ	1747.67	407.03	834.25	4704.95	1838.82
$\Omega_X h^2$	0.0365	0.0670	0.1136	0.0952	6.19
$\sigma_{1,2}^{\text{eff}}$	2.2×10^{-45}	1.0×10^{-47}	1.5×10^{-47}	8.7×10^{-48}	0
σ_3^{eff}	1.2×10^{-44}	7.7×10^{-46}	2.8×10^{-46}	5.5×10^{-47}	1.5×10^{-46}

Table 8.3: Benchmark points for the model parameters that satisfy the stability and perturbativity constraints, as well as the bounds set by LHC and measurements of the oblique parameters. The VEVs, the masses, and Λ are in GeV units. For completeness, we have also included the values of the total relic density of $X^{1,2,3'}$ and their effective scattering cross sections off a nucleon (in cm^2 units) which we discuss in Secs. 8.4.1 and 8.4.2.

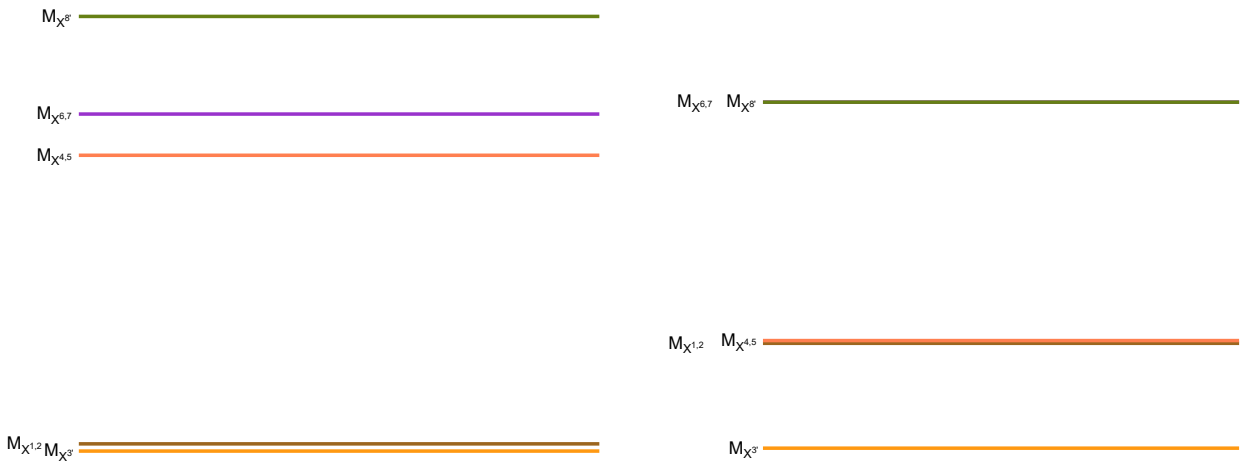

Figure 8.1: Mass spectra of dark gauge bosons for the cases $v_1^2 \gg v_2^2$ (left) and $v_1 \simeq v_2$ (right).

accommodate more DM candidates, one should consider a Z_N ($N \geq 4$) [621, 635–637] or a product of two or more Z_N's as the stabilizing symmetry [422, 638–643].

The intrinsic $Z_2 \times Z_2'$ symmetry of the dark sector of the model, not shared by the SM fields, singles out the particles with nontrivial signatures under this symmetry as a stable sector without any other symmetry requirements. The lightest of the dark gauge bosons then, are possible dark matter candidates. Under our assumptions, the lightest of them are the dark gauge bosons X_μ^1, X_μ^2 and $X_\mu^{3'}$.

The present model allows for various processes that are able to change the number density of dark matter particles. These are the following:

(a) *Annihilation into SM.* All dark gauge bosons interact with the scalars h_i ($i = 1, 2, 3$), which in turn communicate with the SM fields. Thus, the DM candidates $X_\mu^{1,2,3'}$ can annihilate to the SM particles through the Higgs portal.

(b) *Semiannihilation.* The non-Abelian nature of the extra gauge symmetry allows the processes $X^a X^b \to X^c h_i$ to occur. In this case, the final number of DM particles is one less than the initial number, as opposed to the case of annihilations where the number of DM particles is changed by two units. Semiannihilation processes are of great interest regarding DM phenomenology since they can dominate in much of the parameter space.

(c) *Coannihilation.* This kind of process has been thoroughly investigated in the context of supersymmetric DM models.[3] There, the lightest neutralino particle (LSP) is a DM candidate and can potentially coannihilate with the next-to-lightest supersymmetric particle (NLSP) if their respective masses are close enough. A similar situation arises in the dark sector of the model under consideration when $v_1 \simeq v_2$, since in that case the masses of the DM candidates X_μ^1 and X_μ^2 are close to those of X_μ^4 and X_μ^5 (cf. Fig. 8.1) and may in principle coannihilate with them through the processes $X^1 X^{4,5} \to X^{7,6} h_i$ and $X^2 X^{4,5} \to X^{6,7} h_i$. Notice, however, that we cannot employ the usual condition between the LSP and NLSP(s) number densities before, during, and after freeze-out, namely $n_i/n_j = n_i^{eq}/n_j^{eq}$, since its validity cannot be guaranteed when semiannihilations are also involved (see Ref. [620] for more details).

[3] See, for example, Ref. [644] and references therein.

(d) *DM conversion.* In multicomponent DM systems the various DM candidates have different masses in general. Then, if the relevant interactions are allowed, a DM species may be converted to another. In this model the three DM candidates $X_\mu^{1,2,3'}$ are nearly degenerate in mass, and such processes $\left(X^{1,2}X^{1,2} \to X^{3'}X^{3'}\right)$ are generally phase space suppressed. However, again in the limiting case $v_1 \simeq v_2$ the mass splitting of $X_\mu^{3'}$ with regard to X_μ^1 and X_μ^2 can have a significant effect in today's number density of these DM species.

8.4.1 Boltzmann equations and relic density

In order to determine the present day abundance of the DM species we need to solve a coupled set of Boltzmann equations involving the number densities of the dark sector particles. These equations can be written in a compact form as

$$\frac{dn_a}{dt} + 3H\, n_a = \mathcal{C}_a \qquad (a = 1, 2, 3')\,, \tag{8.42}$$

with H being the Hubble parameter and $\mathcal{C}_a = \sum_{bcd} \mathcal{C}_{ab\to cd}$ being the collision rate of all possible $2 \to 2$ processes for a given species that can change its number density. We can relate the collision rate of a reaction with its inverse by making use of the detailed balance equation

$$\mathcal{C}_{ab\to cd} = -\langle\sigma_{ab\to cd}v_r\rangle\left(n_a n_b - n_c n_d \frac{\bar{n}_a\bar{n}_b}{\bar{n}_c\bar{n}_d}\right) = +\langle\sigma_{cd\to ab}v_r\rangle\left(n_c n_d - n_a n_b \frac{\bar{n}_c\bar{n}_d}{\bar{n}_a\bar{n}_b}\right)\,, \tag{8.43}$$

where $\bar{n} \equiv n^{\rm eq}$ is the equilibrium number density and $\langle\sigma_{ab\to cd}v_r\rangle$ is the thermally averaged cross section times the relative velocity of the DM particles. It is given by the general formula [324–326]

$$\langle\sigma_{ab\to cd}v_r\rangle = \frac{1}{2m_a^2 m_b^2 T K_2(m_a/T) K_2(m_b/T)} \int_{(m_a+m_b)^2}^{\infty} ds K_1(\sqrt{s}/T)\, p_{\rm in}(s)\, w(s), \tag{8.44}$$

where $w(s) = E_a E_b \sigma_{ab\to cd} v_r$. The cross section for a given process $a + b \to c + d$ is

$$\sigma_{ab\to cd}v_r = \frac{1}{1+\delta_{cd}} \frac{p_{\rm out}(s)}{32\pi s\, p_{\rm in}(s)} \int d\cos\theta\, |\mathcal{M}_{ab\to cd}|^2\,, \tag{8.45}$$

with $|\mathcal{M}|^2$ denoting the spin summed and polarization averaged matrix element squared. In Eq. (8.44), $K_\nu(z)$ stands for the modified Bessel functions. The general expressions for the kinematical variables contained in (8.44) and (8.45) are provided in Appendix **??**.

We may now proceed to obtain the relic abundance of the DM candidates by solving numerically the set of Boltzmann equations. In order to write down the system of coupled equations, we need to identify the reactions which modify the number of X_μ^1, X_μ^2, and $X_\mu^{3'}$ particles. Since $M_{X_1} = M_{X_2} > M_{X_{3'}}$, the number densities satisfy $n_1 = n_2 \neq n_3$. It should also be clear that $\langle\sigma v_r\rangle_{11\to\chi\chi'} = \langle\sigma v_r\rangle_{22\to\chi\chi'} \neq \langle\sigma v_r\rangle_{33\to\chi\chi'}$, $\langle\sigma v_r\rangle_{12\to 3\chi} = \langle\sigma v_r\rangle_{21\to 3\chi} \neq \langle\sigma v_r\rangle_{13\to 2\chi} = \langle\sigma v_r\rangle_{31\to 2\chi} = \langle\sigma v_r\rangle_{23\to 1\chi} = \langle\sigma v_r\rangle_{32\to 1\chi}$, and $\langle\sigma v_r\rangle_{11\to 33} = \langle\sigma v_r\rangle_{22\to 33} \neq \langle\sigma v_r\rangle_{33\to 11} = \langle\sigma v_r\rangle_{33\to 22}$, where, for example, $\langle\sigma v_r\rangle_{12\to 3\chi}$ is short for $\langle\sigma v_r\rangle_{X_1X_2\to X_{3'}\chi}$, etc., and $\chi\chi'$ denotes SM SM and h_ih_j pairs when these are kinematically allowed.

The processes which modify the number of $X_\mu^{1,2}$ particles are

$$X^{1,2}X^{1,2} \to \chi\chi', \qquad X^{1,2}X^{2,1} \to X^{3',8'}h_i, \qquad X^{1,2}X^{3'} \to X^{2,1}h_i, \qquad X^{1,2}X^{1,2} \to X^{3'}X^{3'}\,, \tag{8.46}$$

whereas the ones which modify the number of $X^{3'}$ particles are

$$X^{3'}X^{3'} \to \chi\chi', \qquad X^{1,2}X^{3'} \to X^{2,1}h_i, \qquad X^{3'}h_i \to X^{1,2}X^{2,1}, \qquad X^{3'}X^{3'} \to X^{1,2}X^{1,2}\,. \tag{8.47}$$

The collision operators for the processes which modify the number of X^1_μ and X^2_μ particles are

$$\begin{aligned}
\mathcal{C}_{11\to\chi\chi'} &= -\langle\sigma v_r\rangle_{11\to\chi\chi'}\left[n_1^2-\overline{n}_1^2\right] = \mathcal{C}_{22\to\chi\chi'}\,,\\
\mathcal{C}_{12\to 3h_i} &= -\langle\sigma v_r\rangle_{12\to 3h_i}\left[n_1n_2-\overline{n}_1\overline{n}_2\frac{n_3}{\overline{n}_3}\right] = \mathcal{C}_{21\to 3h_i}\,,\\
\mathcal{C}_{12\to 8h_i} &= -\langle\sigma v_r\rangle_{12\to 8h_i}\left[n_1n_2-\overline{n}_1\overline{n}_2\right] = \mathcal{C}_{21\to 8h_i}\,,\\
\mathcal{C}_{13\to 2h_i} &= -\langle\sigma v_r\rangle_{13\to 2h_i}\left[n_1n_3-\overline{n}_1\overline{n}_3\frac{n_2}{\overline{n}_2}\right] = \mathcal{C}_{23\to 1h_i}\,,\\
\mathcal{C}_{11\to 33} &= -\langle\sigma v_r\rangle_{11\to 33}\left[n_1^2-n_3^2\frac{\overline{n}_1^2}{\overline{n}_3^2}\right] = \mathcal{C}_{22\to 33}\,,\\
\mathcal{C}_{1h_i\to 23} &= +\langle\sigma v_r\rangle_{23\to 1h_i}\left[n_2n_3-\overline{n}_2\overline{n}_3\frac{n_1}{\overline{n}_1}\right] = \mathcal{C}_{2h_i\to 13}\,,
\end{aligned} \tag{8.48}$$

whereas the ones which modify the number of $X^{3'}_\mu$ particles are

$$\begin{aligned}
\mathcal{C}_{33\to\chi\chi'} &= -\langle\sigma v_r\rangle_{33\to\chi\chi'}\left[n_3^2-\overline{n}_3^2\right]\,,\\
\mathcal{C}_{13\to 2h_i} &= -\langle\sigma v_r\rangle_{13\to 2h_i}\left[n_1n_3-\overline{n}_1\overline{n}_3\frac{n_2}{\overline{n}_2}\right] = \mathcal{C}_{23\to 1h_i}\,,\\
\mathcal{C}_{33\to 11} &= +\langle\sigma v_r\rangle_{11\to 33}\left[n_1^2-n_3^2\frac{\overline{n}_1^2}{\overline{n}_3^2}\right] = \mathcal{C}_{33\to 22}\,,\\
\mathcal{C}_{3h_i\to 12} &= +\langle\sigma v_r\rangle_{12\to 3h_i}\left[n_1n_2-\overline{n}_1\overline{n}_2\frac{n_3}{\overline{n}_3}\right]\,.
\end{aligned} \tag{8.49}$$

As discussed above, in the case $v_1 \simeq v_2$, the particles $X^{4,5}_\mu$ are thermally available to $X^{1,2}_\mu$ and may coannihilate with them. We therefore also have to include them in our analysis. The collision operators for the processes which change the number of $X^{4,5}_\mu$ particles are[4]

$$\begin{aligned}
\mathcal{C}_{44\to\chi\chi'} &= -\langle\sigma v_r\rangle_{44\to\chi\chi'}\left[n_4^2-\overline{n}_4^2\right] = \mathcal{C}_{55\to\chi\chi'}\,,\\
\mathcal{C}_{14\to 7h_i} &= -\langle\sigma v_r\rangle_{14\to 7h_i}\left[n_1n_4-\overline{n}_1\overline{n}_4\right] = \mathcal{C}_{15\to 6h_i} = \mathcal{C}_{24\to 6h_i} = \mathcal{C}_{25\to 7h_i}\,,\\
\mathcal{C}_{44\to 11} &= -\langle\sigma v_r\rangle_{44\to 11}\left[n_4^2-n_1^2\frac{\overline{n}_4^2}{\overline{n}_1^2}\right] = \mathcal{C}_{44\to 22} = \mathcal{C}_{55\to 11} = \mathcal{C}_{55\to 22}\,,\\
\mathcal{C}_{44\to 33} &= -\langle\sigma v_r\rangle_{44\to 33}\left[n_4^2-n_3^2\frac{\overline{n}_4^2}{\overline{n}_3^2}\right] = \mathcal{C}_{55\to 33}\,.
\end{aligned} \tag{8.50}$$

Next, let us define

$$Y_a \equiv \frac{n_a}{s}, \qquad x \equiv \frac{M_{X^{3'}}}{T}, \qquad \mathcal{Z}_{ab\to cd}(x) \equiv \frac{s(x=1)}{H(x=1)}\langle\sigma v_r\rangle_{ab\to cd}\,, \tag{8.51}$$

where $H = \sqrt{\frac{4\pi^3 g_\star}{45}}\frac{T^2}{M_{\rm Pl}}$, $g_\star \simeq g_{\star s}$ is the number of effective relativistic degrees of freedom, and $s = \frac{2\pi^2 g_{\star s}}{45}T^3$ is the entropy density. Then, we may finally write down the coupled set of Boltzmann

[4] Of course, these reactions also change the number of $X^{1,2,3'}_\mu$ particles. Also, we have assumed that the heavier dark gauge bosons $X^{6,7,8'}_\mu$ have already decayed to the lighter ones.

equations in dimensionless variables as

$$\begin{aligned}\frac{dY_1}{dx} = -\frac{1}{x^2}\Bigg\{ & \mathcal{Z}_{11\to\chi\chi'}\left[Y_1^2-\overline{Y}_1^2\right] + \mathcal{Z}_{12\to 3h_i}\left[Y_1Y_2-\overline{Y}_1\overline{Y}_2\frac{Y_3}{\overline{Y}_3}\right] \\ & + \mathcal{Z}_{12\to 8h_i}\left[Y_1Y_2-\overline{Y}_1\overline{Y}_2\right] + \mathcal{Z}_{13\to 2h_i}\left[Y_1Y_3-\overline{Y}_1\overline{Y}_3\frac{Y_2}{\overline{Y}_2}\right] \\ & - \mathcal{Z}_{23\to 1h_i}\left[Y_2Y_3-\overline{Y}_2\overline{Y}_3\frac{Y_1}{\overline{Y}_1}\right] + \mathcal{Z}_{11\to 33}\left[Y_1^2-Y_3^2\frac{\overline{Y}_1^2}{\overline{Y}_3^2}\right] \\ & - \mathcal{Z}_{44\to 11}\left[Y_4^2-Y_1^2\frac{\overline{Y}_4^2}{\overline{Y}_1^2}\right] - \mathcal{Z}_{55\to 11}\left[Y_5^2-Y_1^2\frac{\overline{Y}_5^2}{\overline{Y}_1^2}\right] \\ & + \mathcal{Z}_{14\to 7h_i}\left[Y_1Y_4-\overline{Y}_1\overline{Y}_4\right] + \mathcal{Z}_{15\to 6h_i}\left[Y_1Y_5-\overline{Y}_1\overline{Y}_5\right]\Bigg\}\,,\end{aligned} \tag{8.52}$$

$$\frac{dY_2}{dx} = \frac{dY_1}{dx}(1\leftrightarrow 2, 4\leftrightarrow 5, 7\leftrightarrow 6)\,, \tag{8.53}$$

$$\begin{aligned}\frac{dY_3}{dx} = -\frac{1}{x^2}\Bigg\{ & \mathcal{Z}_{33\to\chi\chi'}\left[Y_3^2-\overline{Y}_3^2\right] + \mathcal{Z}_{13\to 2h_i}\left[Y_1Y_3-\overline{Y}_1\overline{Y}_3\frac{Y_2}{\overline{Y}_2}\right] \\ & + \mathcal{Z}_{23\to 1h_i}\left[Y_2Y_3-\overline{Y}_2\overline{Y}_3\frac{Y_1}{\overline{Y}_1}\right] - \mathcal{Z}_{11\to 33}\left[Y_1^2-Y_3^2\frac{\overline{Y}_1^2}{\overline{Y}_3^2}\right] \\ & - \mathcal{Z}_{22\to 33}\left[Y_2^2-Y_3^2\frac{\overline{Y}_2^2}{\overline{Y}_3^2}\right] - \mathcal{Z}_{44\to 33}\left[Y_4^2-Y_3^2\frac{\overline{Y}_4^2}{\overline{Y}_3^2}\right] \\ & - \mathcal{Z}_{55\to 33}\left[Y_5^2-Y_3^2\frac{\overline{Y}_5^2}{\overline{Y}_3^2}\right] - 2\,\mathcal{Z}_{12\to 3h_i}\left[Y_1Y_2-\overline{Y}_1\overline{Y}_2\frac{Y_3}{\overline{Y}_3}\right]\Bigg\}\,.\end{aligned} \tag{8.54}$$

$$\begin{aligned}\frac{dY_4}{dx} = -\frac{1}{x^2}\Bigg\{ & \mathcal{Z}_{44\to\chi\chi'}\left[Y_4^2-\overline{Y}_4^2\right] + \mathcal{Z}_{44\to 11}\left[Y_4^2-Y_1^2\frac{\overline{Y}_4^2}{\overline{Y}_1^2}\right] \\ & + \mathcal{Z}_{44\to 22}\left[Y_4^2-Y_2^2\frac{\overline{Y}_4^2}{\overline{Y}_2^2}\right] + \mathcal{Z}_{44\to 33}\left[Y_4^2-Y_3^2\frac{\overline{Y}_4^2}{\overline{Y}_3^2}\right] \\ & + \mathcal{Z}_{14\to 7h_i}\left[Y_1Y_4-\overline{Y}_1\overline{Y}_4\right] + \mathcal{Z}_{24\to 6h_i}\left[Y_2Y_4-\overline{Y}_2\overline{Y}_4\right]\Bigg\}\,,\end{aligned} \tag{8.55}$$

$$\frac{dY_5}{dx} = \frac{dY_4}{dx}(4\leftrightarrow 5, 1\leftrightarrow 2, 7\leftrightarrow 6). \tag{8.56}$$

The equilibrium yields $\overline{Y}_a \equiv \frac{\overline{n}_a}{s}$ are given by

$$\overline{Y}_3 = \frac{\hat{g}_X}{g_{\star s}}\frac{45}{4\pi^4}x^2K_2(x)\,, \tag{8.57}$$

$$\overline{Y}_{1,2} = \frac{\hat{g}_X}{g_{\star s}}\frac{45}{4\pi^4}r_{1,2}^2x^2K_2(r_{1,2}x)\,, \tag{8.58}$$

$$\overline{Y}_{4,5} = \frac{\hat{g}_X}{g_{\star s}}\frac{45}{4\pi^4}r_{4,5}^2x^2K_2(r_{4,5}x)\,, \tag{8.59}$$

where we have defined $r_{1,2} \equiv \frac{M_{X^{1,2}}}{M_{X^{3'}}}$, $r_{4,5} \equiv \frac{M_{X^{4,5}}}{M_{X^{3'}}}$ and $\hat{g}_X = 3$ are the spin degrees of freedom of the dark gauge bosons. We have numerically solved this system using `Mathematica` and we have

also employed the packages `FeynArts/FormCalc` [645, 646] in order to produce analytic results for the various cross sections involved. Finally, we have obtained the total relic density of the $X^{1,2,3'}_\mu$ particles

$$\Omega_X h^2 = \Omega_{X^1} h^2 + \Omega_{X^2} h^2 + \Omega_{X^{3'}} h^2 \,, \tag{8.60}$$

where

$$\Omega_{X^a} h^2 = \frac{M_{X^a} s_0 Y^a(\infty)}{\rho_c / h^2} \,, \tag{8.61}$$

with $s_0 = 2890\ \text{cm}^{-3}$ and $\rho_c/h^2 = 1.05 \times 10^{-5}\,\text{GeV/cm}^3$. Equation (8.60) has to be compared with the measured DM relic density $\Omega_{\text{DM}} h^2 = 0.1197 \pm 0.0022$ [1]. Next, we further explore the cases $v_1^2 \gg v_2^2$ and $v_1 \simeq v_2$.

Case $v_1^2 \gg v_2^2$

In this case, as stated above, the masses of the DM candidates X^1, X^2, and $X^{3'}$ are nearly degenerate, while the masses of X^4 and X^5 are well above those of X^1 and X^2. Therefore, coannihilation effects play no significant role in the final relic density of $X^{1,2,3'}$. However, even though the mass splitting between $M_{X^1} = M_{X^2}$ and $M_{X^{3'}}$ is small, the DM conversion processes $X^{1,2}X^{1,2} \to X^{3'}X^{3'}$ can lower the number density of X^1 and X^2 and enhance that of $X^{3'}$, rendering $X^{3'}$ the predominant DM component.

To get a feeling of the effect of DM conversion, we set the parameters of the model according to BP1 of Table 8.3 and solve numerically the Boltzmann equations (8.52)–(8.54) (omitting the coannihilation terms), thus obtaining the solutions for the yields $Y_{1,2}$ and Y_3 with respect to $x = M_{X^{3'}}/T$.

In Fig. 8.2 we plot these solutions with the DM conversion processes switched on (left) and switched off (right). When the DM conversion is switched off, the final yields are closer together, with the separation attributed to the slightly different masses between $X^{1,2}$ and $X^{3'}$, as well as to the mixing between $X^{3'} - X^{8'}$ which results in more Feynman diagrams contributing to the annihilation processes $X^{3'}X^{3'} \to h_i h_j$ and the semiannihilation processes $X^{1,2}X^{2,1} \to X^{3'}h_i$.[5] On the other hand, the separation of the final yields is larger when the DM conversion processes are switched on, since more X^1 and X^2 particles have annihilated and have been converted to $X^{3'}$; a reaction that continues to occur to some extent even after freeze-out. In the case without DM conversion, the particles X^1, X^2, and $X^{3'}$ comprise 19%, 19%, and 62% of the total relic density respectively, while in the case with DM conversion they comprise 13%, 13%, and 74% of the total relic density, respectively.

In Fig. 8.3 we fix again the model parameters as in BP1, but this time we leave the extra gauge coupling g_X free and scan over it, ergo obtaining the total relic density $\Omega_X h^2$ of the DM candidates. We first observe a resonant dip around 110 GeV which corresponds to $M_{X^{3'}} \simeq M_{X^{1,2}} = M_{h_3}/2$. Then the relic density grows until $\sim 175\,\text{GeV}$ where the $t\bar{t}$ channel opens up. After that, there is a steep decrease around $M_{h_3} \simeq 215\,\text{GeV}$ where all the annihilation channels $X^aX^a \to h_3h_3$ and the semiannihilation channels $X^aX^b \to X^c h_3$ become kinematically available. This point crosses the observed DM relic density (blue band in Fig. 8.3) and corresponds to $g_X = 0.78$ (which also satisfies the constraints discussed in Sec. 8.3).

[5] In the non-CSI version of this model considered in Ref. [401], the authors performed their $SU(3)$ DM analysis under the simplified assumption that the rest of the dark sector particles do not contribute to DM annihilation. They also only included the couplings of the DM candidates to the two lightest scalar bosons h_1, h_2 and not the heavier $\mathcal{H}$ in their notation. Here, we include all possible couplings and Feynman diagrams relevant to the relic densities of $X^{1,2,3'}$.

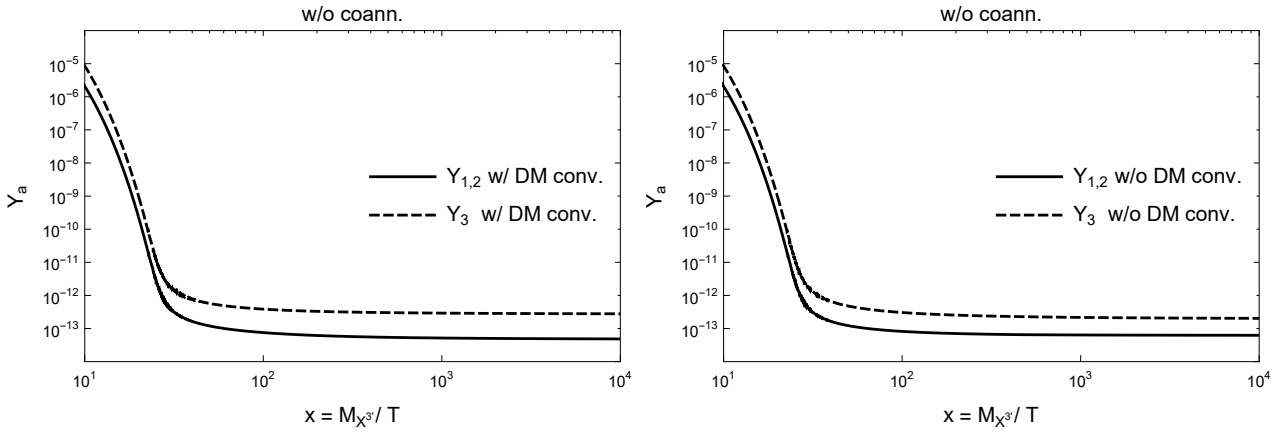

Figure 8.2: The yields $Y_{1,2}$ and Y_3 in terms of $x = M_{X^{3'}}/T$ for BP1. The right plot has been obtained neglecting the DM conversion terms in the Boltzmann equations. These terms are included in the left plot. The DM conversion process reduces the final number density of the X^1 and X^2 particles since some of them are converted to $X^{3'}$.

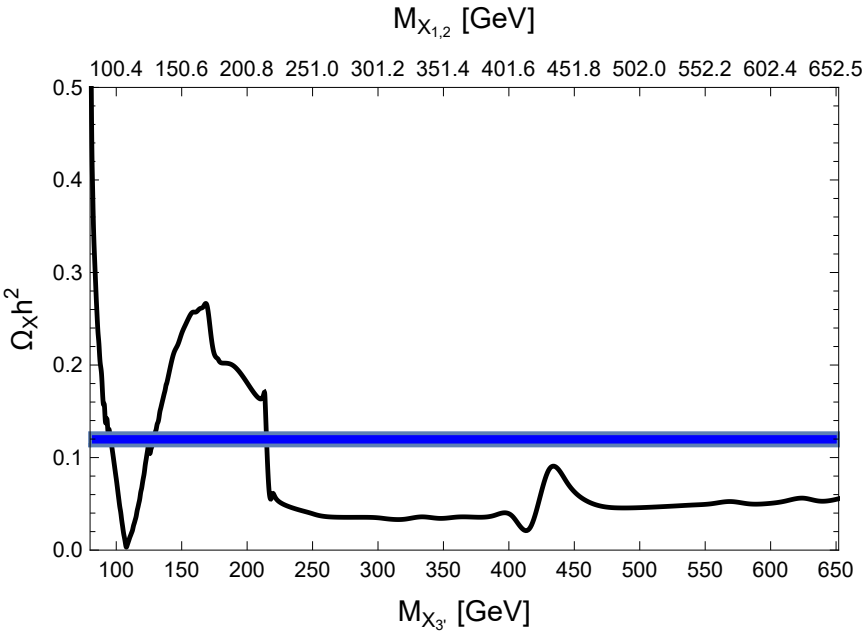

Figure 8.3: The total relic density of $X^{1,2}$ and $X^{3'}$ as a function of the dark gauge coupling g_X for BP1. The blue band corresponds to the observed DM relic density within 3σ.

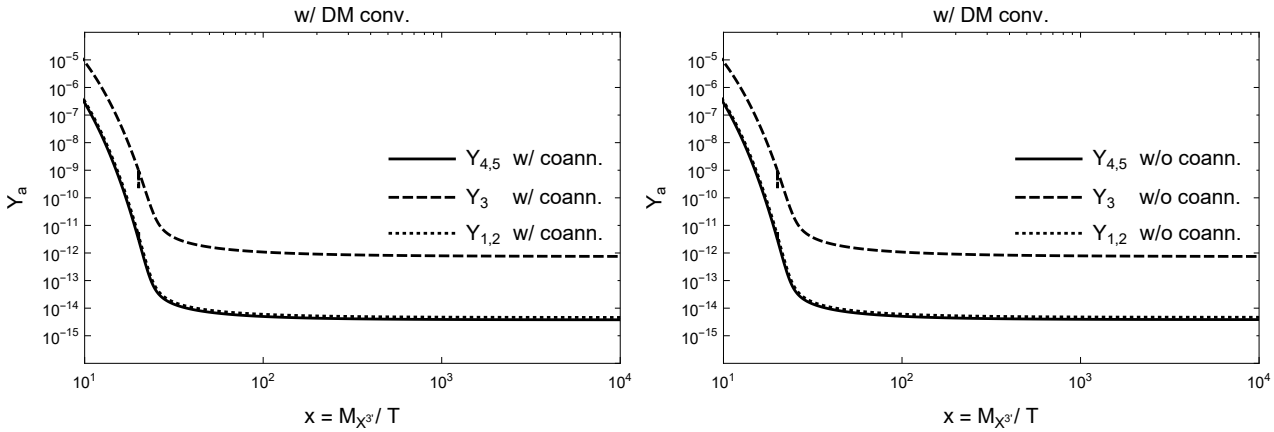

Figure 8.4: The yields $Y_{1,2}$, Y_3, and $Y_{4,5}$ in terms of $x = M_{X^{3'}}/T$ for BP2. The right plot has been obtained neglecting the coannihilation terms in the Boltzmann equations. These terms are included in the left plot. The difference is very small since most $X^{1,2}$ and $X^{4,5}$ particles are converted to $X^{3'}$.

Above M_{h_3}, one may expect that the relic density would decrease monotonically. This can be understood as follows: every vertex containing three dark gauge boson legs is proportional to g_X while every vertex containing two dark gauge bosons and one or two scalar bosons is proportional to g_X^2. Therefore, $\langle \sigma v_r \rangle \propto g_X^2$, or $\Omega_X h^2 \propto 1/g_X^2$. This indicates that the relic density should decrease as we increase g_X (and therefore $M_{X^{1,2,3'}}$). Nevertheless, the mass of the pNGB M_{h_2} depends on all the masses of the model [cf. (8.33)]. This means that as g_X grows, so do the dark gauge boson masses and consequently M_{h_2}. This effect tends to counterbalance the expected decrease of $\Omega_X h^2$. On the other hand, as g_X becomes smaller, the relic density of the DM candidates increases considerably and tends to overclose the Universe. For example, the small value of g_X from BP5 in Table 8.3 leads to $\Omega_X h^2 \simeq 6.2$, in which case $X^{1,2}$ are also completely depleted and $X^{3'}$ makes up 100% of the relic density. Furthermore, the dependence of M_{h_2} on g_X means that there can be only two resonant dips, corresponding to $M_{h_1}/2$ and $M_{h_3}/2$. This is in contrast to the non-CSI version of the model [401] where there should be three resonant dips, corresponding to $M_{h_1}/2$, $M_{h_2}/2$, $M_{h_3}/2$, since in that case M_{h_2} does not depend on g_X. As a result, the CSI version of the model that we consider is in general more constrained.

Case $v_1 \simeq v_2$

In this case, $X^{3'}$ is nearly 20% lighter than X^1 and X^2 [cf. (8.41)] while X^4 and X^5 are almost degenerate with the latter ones. Therefore, coannihilations between $X^{1,2}$ and $X^{4,5}$ may occur around the time of freeze-out and influence the relic density of these four particles. Since the semiannihilations $X^{1,2}X^{3'} \to X^{2,1}h_i$ are now phase-space suppressed, the Boltzmann equations governing the number densities of $X^{1,2}$ and $X^{4,5}$ are almost identical. We therefore expect their relic number densities to be very close. This is indeed the case as can be seen in Fig. 8.4.

There, we also distinguish between the cases when coannihilations are switched on (left) and switched off (right). The effect is clearly insignificant, and in both cases the DM candidates X^1, X^2, and $X^{3'}$ comprise approximately 1%, 1%, and 98% of the total relic density, respectively. The dominant phenomenon is DM conversion since most $X^{1,2}$ and $X^{4,5}$ have had enough time to annihilate to $X^{3'}$.

We display the importance of this effect in Fig. 8.5, where coannihilations are switched on, but this time we distinguish between the cases when DM conversion is switched on (left) and off (right).

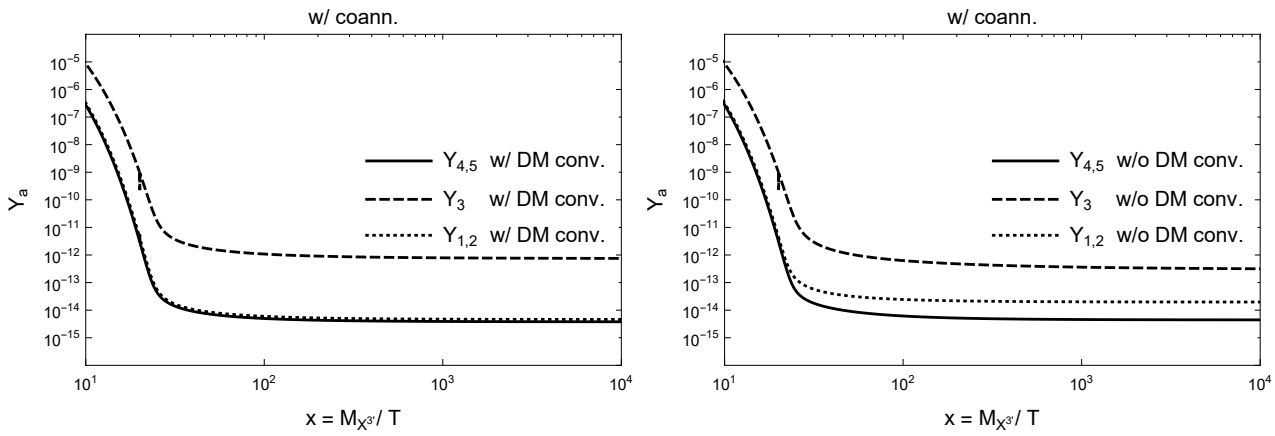

Figure 8.5: The yields $Y_{1,2}$, Y_3, and $Y_{4,5}$ in terms of $x = M_{X^{3'}}/T$ for BP2. The right plot has been obtained neglecting the DM conversion terms in the Boltzmann equations. These terms are included in the left plot. The DM conversion processes are significant since many $X^{1,2}$ particles are converted to $X^{3'}$.

With DM conversion switched on, the DM candidates X^1, X^2, and $X^{3'}$ comprise again 1%, 1%, and 98% of the total relic density. With DM conversion switched off, X^1, X^2, and $X^{3'}$ comprise around 7%, 7%, and 86% of the total relic density, respectively. Moreover, the total relic density is almost 2 times larger in the former case (DM conversion on) than in the latter case (DM conversion off). This can be attributed to the fact that without DM conversion freeze-out is delayed and more DM particles have time to annihilate to SM particles.

8.4.2 Direct detection

Maybe the best prospect for validating the WIMP DM paradigm is through the direct detection of DM particles at deep underground facilities. Many experiments are in progress, and hopefully we may soon get a glimpse of this dark world.

Interactions between the DM particles $X_\mu^{1,2,3'}$ and the nucleons N can be mediated through a t-channel exchange of the scalar bosons h_i. For the individual DM components, the corresponding spin-independent elastic scattering cross sections are

$$\sigma_{1,2}^{\mathrm{SI}} = \frac{f_N^2}{16\pi v_h^2} \frac{m_N^4}{\left(M_{X^{1,2}} + m_N\right)^2} \left| g_X^2 v_2 \sum_{i=1}^{3} \frac{\mathcal{R}_{i3}\mathcal{R}_{1i}}{M_{h_i}^2} \right|^2 , \tag{8.62}$$

$$\begin{aligned} \sigma_3^{\mathrm{SI}} = \frac{f_N^2}{16\pi v_h^2} \frac{m_N^4}{\left(M_{X^{3'}} + m_N\right)^2} \Bigg| & \frac{4}{3} g_X^2 v_1 \sin^2\delta \sum_{i=1}^{3} \frac{\mathcal{R}_{i2}\mathcal{R}_{1i}}{M_{h_i}^2} \\ & + \frac{1}{3} g_X^2 v_2 \left(\cos 2\delta + 2 - \sqrt{3}\sin 2\delta\right) \sum_{i=1}^{3} \frac{\mathcal{R}_{i3}\mathcal{R}_{1i}}{M_{h_i}^2} \Bigg|^2 , \end{aligned} \tag{8.63}$$

where $f_N \simeq 0.3$ [365,625–627,647–649] is the nucleon form factor and $m_N = 0.939\,\mathrm{GeV}$ is the average nucleon mass.

Since we have three DM candidates with different masses ($M_{X^1} = M_{X^2} > M_{X^{3'}}$), not all of them contribute equally to the local DM density which in direct detection experiments is assumed to be

composed of a single DM species. Nevertheless, we may assume that the contribution of each DM species to the local density is equal to the contribution of that particular species to the relic density and consequently construct the effective cross sections [639, 650, 651]

$$\sigma_a^{\rm eff} = \sigma_a^{\rm SI} \left(\frac{\Omega_{X^a} h^2}{\Omega_X h^2} \right). \tag{8.64}$$

For example, BP3 in Table 8.3 reproduces the observed DM relic density within 3σ, with X^1, X^2, and $X^{3'}$ comprising approximately 5%, 5%, and 90% of its total. The resulting effective cross sections are then

$$\begin{aligned} \sigma_{1,2}^{\rm eff} &= 1.46715 \times 10^{-47}\ {\rm cm}^2, \\ \sigma_3^{\rm eff} &= 2.77662 \times 10^{-46}\ {\rm cm}^2. \end{aligned}$$

Both of these numbers are well below the limits set by the LUX experiment [628], but are nevertheless within the reach of future experiments such as LZ [652] and XENON1T [653].

Chapter 9

Frame-dependence of higher-order inflationary observables in scalar-tensor theories

9.1 Introduction

The work presented in this chapter was done in collaboration with PhD student Thomas Pappas and Prof. Kyriakos Tamvakis and has been published in Physical Review D [654].

In this chapter, we compute the spectral indices up to third order in the slow-roll approximation in a general scalar-tensor theory in both the Einstein and Jordan frames, using quantities which are invariant under the conformal rescaling of the metric and transform as scalar functions under the reparametrization of the scalar field. The calculation is carried out by employing the Green's function method. We show that the frames are equivalent up to this order due to the underlying assumptions. Nevertheless, care must be taken when defining the number of e-folds.

In Section 9.2, we review the invariant formalism introduced in [205]. After presenting the three principal quantities which are invariant under a conformal transformation of the metric and a redefinition of the scalar field, we consider the slow-roll approximation in the two frames and define the corresponding *Hubble slow-roll* parameters (HSRPs). We also define a hierarchy of *potential slow-roll* parameters (PSRPs) which are frame independent. As shown in [655], this formalism proves to be attractive since many inflationary models can be classified according to the form of their invariant potentials. This provides an elegant explanation as to why vastly different models can produce the same predictions for the inflationary observables.

In Section 9.3, we adopt the Green's function method considered in [55] and calculate the spectral indices up to third order in the slow-roll parameters in both the JF and EF. Then, using the relations between the HSRPs we find that the two frames are equivalent. Furthermore, since the HSRPs can be related to the PSRPs, we express the spectral indices in terms of the PSRPs which are manifestly frame invariant.

In Section 9.4, we consider the nonminimal Coleman-Weinberg model developed in [148] and compare the predictions of the third order corrected expressions we obtained with the most commonly used first order results. Furthermore, even though the expressions for the observables that we obtain are frame invariant, the definition of the number of e-folds is not and this results to different predictions. To this end, we examine how the predictions change if the required 50–60 number of e-folds is taken in the Einstein or in the Jordan frame. Finally, we examine how the predicted values for the inflationary observables are affected by the end-of-inflation condition. The *exact* condition for inflation to end is when $\epsilon_H = 1$. The usual approach is to Taylor approximate

this condition with PSRPs. Most authors use only the first order approximation $\epsilon_H \approx \epsilon_V$ since this is indeed a good approximation for almost all of the inflationary epoch save for the last few e-folds before inflation ends when this approximation breaks down. Since we have obtained the third-order corrected expressions for the inflationary observables we also compare the results against three more end-of-inflation conditions, namely, the third-order Taylor approximation of the condition $\epsilon_H = 1$ with PSRPs, as well as against the Padé [1/1] and Padé [2/2] approximants [656]. All of these considerations prove to be relevant since the differences in the predictions that we obtain are within the accuracy of future experiments and may prove instrumental in ruling out various inflationary models.

9.2 Invariant formalism and slow-roll approximation

In this section, we consider the general action of a single scalar field that describes a wide class of scalar-tensor gravity theories. By using the frame and parametrization invariant formalism introduced in [203–206, 655] we write down the field equations of motion in terms of quantities that are invariant under conformal rescalings of the metric and redefinitions of the scalar field.

9.2.1 Invariants

Next, we follow [205] and consider three quantities which are invariant under a conformal rescaling of the metric and a reparametrization of the scalar field as a result of the transformation properties (3.104)-(3.107) of the model functions. These invariants are

$$\mathcal{I}_m(\Phi) \equiv \frac{e^{2\sigma(\Phi)}}{\mathcal{A}(\Phi)}, \tag{9.1}$$

$$\mathcal{I}_\mathcal{V}(\Phi) \equiv \frac{\mathcal{V}(\Phi)}{(\mathcal{A}(\Phi))^2}, \tag{9.2}$$

$$\mathcal{I}_\phi(\Phi) \equiv \int \left(\frac{2\mathcal{A}\mathcal{B} + 3(\mathcal{A}')^2}{4\mathcal{A}^2}\right)^{1/2} \mathrm{d}\Phi. \tag{9.3}$$

The first invariant, $\mathcal{I}_m(\Phi)$, is a quantity that characterizes the nonminimality of a theory. For constant $\mathcal{I}_m(\Phi)$ the scalar field is minimally coupled to gravity, and we are dealing with standard general relativity. On the other hand, if $\mathcal{I}_m'(\Phi) \not\equiv 0$, then this invariant is a dynamical function and the scalar field is nonminimally coupled to gravity, as is the case in the JF. The second invariant, $\mathcal{I}_\mathcal{V}(\Phi)$, contains the self-interactions of the scalar field and plays the role of an invariant potential. Finally, the third invariant, $\mathcal{I}_\phi(\Phi)$, measures the volume of the one-dimensional space of the scalar field and can be interpreted as the invariant propagating scalar degree of freedom.

The transformation properties of the model functions can also be used to define tensorial invariants, for example [205]

$$\hat{g}_{\mu\nu} \equiv \mathcal{A}(\Phi) g_{\mu\nu}. \tag{9.4}$$

The above choice is not unique since the tensor (9.4) does not change its transformation properties if it is multiplied by a scalar invariant, i.e.,

$$\bar{g}_{\mu\nu} \equiv e^{2\sigma(\Phi)} g_{\mu\nu} = \mathcal{I}_m \hat{g}_{\mu\nu} \tag{9.5}$$

is also invariant under the transformations (3.102) and (3.103).

In the following, a barred or a hatted variable will represent the quantity evaluated in the JF or EF, respectively. The relation between the time coordinate, the scale factor and the Hubble parameter in the two frames is [205]

$$\frac{\mathrm{d}}{\mathrm{d}\bar{t}} = \frac{1}{\sqrt{\mathcal{I}_m}}\frac{\mathrm{d}}{\mathrm{d}\hat{t}}, \quad \bar{a}(\bar{t}) = \sqrt{\mathcal{I}_m}\hat{a}(\hat{t}), \tag{9.6}$$

$$\bar{H} = \frac{1}{\sqrt{\mathcal{I}_m}}\left(\hat{H} + \frac{1}{2}\frac{\mathrm{d}\ln\mathcal{I}_m}{\mathrm{d}\hat{t}}\right). \tag{9.7}$$

An interesting and appealing feature of the invariant formalism, which was pointed out in [655], is that inflationary models with very different background physical motivations can be described by similar invariant potentials and thus lead to the same predictions for the inflationary observables. As an example, let us consider *induced gravity* inflation [657–663] and *Starobinsky* inflation [87–92, 664]. The former is described by the model functions

$$\mathcal{A}(\Phi) = \xi\Phi^2, \tag{9.8}$$
$$\mathcal{B}(\Phi) = 1, \tag{9.9}$$
$$\sigma(\Phi) = 0, \tag{9.10}$$
$$\mathcal{V}(\Phi) = \lambda\left(\Phi^2 - v^2\right)^2, \tag{9.11}$$

where ξ is the nonminimal coupling and v is the vacuum expectation value (VEV) of the scalar field Φ which induces the Planck mass scale,

$$1 = \xi v^2. \tag{9.12}$$

For Starobinsky inflation with $f(R) = R + bR^2$ one has [216]

$$\mathcal{A}(\Phi) = \Phi, \tag{9.13}$$
$$\mathcal{B}(\Phi) = 0, \tag{9.14}$$
$$\sigma(\Phi) = 0, \tag{9.15}$$
$$\mathcal{V}(\Phi) = \frac{b}{2}\left(\frac{\Phi - 1}{2b}\right)^2. \tag{9.16}$$

Next, following the recipe of [655] we can obtain the invariant potentials $\mathcal{I}_\mathcal{V}$ for the two models. As a first step, using (9.3) we calculate the form of the invariant fields

$$\text{Induced gravity:} \qquad \mathcal{I}_\phi = \sqrt{\frac{1+6\xi}{2\xi}}\ln\left(\frac{\Phi}{v_\Phi}\right), \tag{9.17}$$

$$\text{Starobinsky:} \qquad \mathcal{I}_\phi = \frac{\sqrt{3}}{2}\ln\Phi. \tag{9.18}$$

Afterwards, inverting the above relations we find $\Phi(\mathcal{I}_\phi)$ and then using (9.2) we calculate $\mathcal{I}_\mathcal{V}(\Phi(\mathcal{I}_\phi)) = \mathcal{I}_\mathcal{V}(\mathcal{I}_\phi)$ and obtain

$$\text{Induced gravity:} \qquad \mathcal{I}_\mathcal{V}(\mathcal{I}_\phi) = \frac{\lambda}{\xi^2}\left(1 - e^{-\sqrt{\frac{8\xi}{1+6\xi}}\mathcal{I}_\phi}\right)^2, \tag{9.19}$$

$$\text{Starobinsky:} \qquad \mathcal{I}_\mathcal{V}(\mathcal{I}_\phi) = \frac{1}{8\,b}\left(1 - e^{-\frac{2}{\sqrt{3}}\mathcal{I}_\phi}\right)^2. \tag{9.20}$$

The forms of the invariant potentials suggest that for large values of the nonminimal coupling

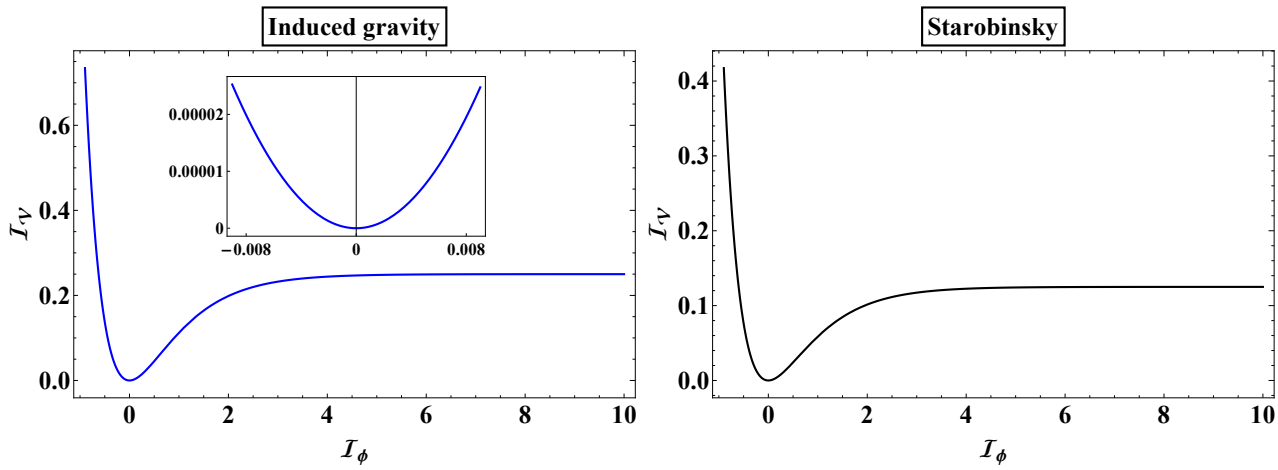

Figure 9.1: The normalized invariant inflationary potentials for induced gravity and Starobinsky models for $\xi = 2$. In the strong coupling limit the invariant potentials have a similar form and lead to the same predictions, while in the limit (9.21) induced gravity approaches the quadratic inflation attractor (inset in left plot).

($\xi \gtrsim 1$) the shape of the induced gravity invariant potential (9.19) coincides with its Starobinsky counterpart (9.20), a behavior depicted in Fig. 9.1. As a consequence, the two models yield identical predictions in the strong coupling regime. On the other hand, in the weak coupling limit induced gravity gives the same predictions with quadratic inflation [31]. Indeed, when

$$\mathcal{I}_\phi \ll \sqrt{\frac{1+6\xi}{8\xi}}\,, \tag{9.21}$$

the invariant potential for induced gravity becomes [116, 665]

$$\mathcal{I}_\mathcal{V} = M^2 \mathcal{I}_\phi^2, \quad \text{with} \quad M^2 = \frac{8\lambda}{\xi\,(1+6\xi)}\,. \tag{9.22}$$

Note in (9.21) that as ξ becomes smaller the allowed range for the field $\mathcal{I}_\phi$ in which induced gravity and quadratic inflation produce similar predictions becomes wider. As a consequence, only for small values of ξ the field $\mathcal{I}_\phi$ can produce the required 50-60 number of e-folds. This is why the induced gravity predictions reach the quadratic inflation attractor in the small coupling regime.

9.2.2 Slow-roll in the Jordan frame

Let us consider the slow rolling of the inflaton field in the JF. Taking the functional derivative of the action (3.101) with respect to the metric and the scalar field in the JF, we can write down the equations of motion in terms of the invariants as

$$\bar{H}^2 = \frac{1}{3}\left(\frac{\mathrm{d}\mathcal{I}_\phi}{\mathrm{d}\bar{t}}\right)^2 + \bar{H}\frac{\mathrm{d}\ln\mathcal{I}_m}{\mathrm{d}\bar{t}} - \frac{1}{4}\left(\frac{\mathrm{d}\ln\mathcal{I}_m}{\mathrm{d}\bar{t}}\right)^2 + \frac{1}{3}\frac{\mathcal{I}_\mathcal{V}}{\mathcal{I}_m}, \tag{9.23}$$

$$\frac{\mathrm{d}\bar{H}}{\mathrm{d}\bar{t}} = -\frac{1}{2}\bar{H}\frac{\mathrm{d}\ln\mathcal{I}_m}{\mathrm{d}\bar{t}} + \frac{1}{4}\left(\frac{\mathrm{d}\ln\mathcal{I}_m}{\mathrm{d}\bar{t}}\right)^2 - \left(\frac{\mathrm{d}\mathcal{I}_\phi}{\mathrm{d}\bar{t}}\right)^2 + \frac{1}{2}\frac{\mathrm{d}^2\ln\mathcal{I}_m}{\mathrm{d}\bar{t}^2}, \tag{9.24}$$

$$\frac{\mathrm{d}^2\mathcal{I}_\phi}{\mathrm{d}\bar{t}^2} = \left(-3\bar{H} + \frac{\mathrm{d}\ln\mathcal{I}_m}{\mathrm{d}\bar{t}}\right)\frac{\mathrm{d}\mathcal{I}_\phi}{\mathrm{d}\bar{t}} - \frac{1}{2\mathcal{I}_m}\frac{\mathrm{d}\mathcal{I}_\mathcal{V}}{\mathrm{d}\mathcal{I}_\phi}, \tag{9.25}$$

where we have neglected the contributions of the matter part of the action since we assume that the energy density and pressure of the scalar field dominate during the inflationary epoch.

The standard HSRPs in the JF have the form [205]

$$\bar{\epsilon}_0 \equiv -\frac{1}{\bar{H}^2}\frac{\mathrm{d}\bar{H}}{\mathrm{d}\bar{t}} = -\frac{\mathrm{d}\ln\bar{H}}{\mathrm{d}\ln\bar{a}}, \qquad \bar{\eta} \equiv -\left(\bar{H}\frac{\mathrm{d}\mathcal{I}_\phi}{\mathrm{d}\bar{t}}\right)^{-1}\frac{\mathrm{d}^2\mathcal{I}_\phi}{\mathrm{d}\bar{t}^2}. \tag{9.26}$$

Inflation in the JF occurs as long as $\bar{\epsilon}_0 < 1$, and slow rollover happens while $\bar{\epsilon}_0 \ll 1$. In the next section, we will be concerned with higher order corrections to the inflationary indices. As a result, we will need a series of slow-roll parameters which, following [205], we take to be

$$\bar{\kappa}_0 \equiv \frac{1}{\bar{H}^2}\left(\frac{\mathrm{d}\mathcal{I}_\phi}{\mathrm{d}\bar{t}}\right)^2 = \left(\frac{\mathrm{d}\mathcal{I}_\phi}{\mathrm{d}\ln\bar{a}}\right)^2, \tag{9.27}$$

$$\bar{\kappa}_1 \equiv \frac{1}{\bar{H}\bar{\kappa}_0}\frac{\mathrm{d}\bar{\kappa}_0}{\mathrm{d}\bar{t}} = \frac{\mathrm{d}\ln\bar{\kappa}_0}{\mathrm{d}\ln\bar{a}} = 2\left(-\bar{\eta}+\bar{\epsilon}_0\right), \tag{9.28}$$

$$\bar{\kappa}_{i+1} \equiv \frac{1}{\bar{H}\bar{\kappa}_i}\frac{\mathrm{d}\bar{\kappa}_i}{\mathrm{d}\bar{t}} = \frac{\mathrm{d}\ln\bar{\kappa}_i}{\mathrm{d}\ln\bar{a}}. \tag{9.29}$$

In the JF, it is also useful to consider a second series of slow-roll parameters involving the invariant $\mathcal{I}_m$ and thus related to the nonminimal coupling. This series has the form [205]

$$\bar{\lambda}_0 \equiv \frac{1}{2\bar{H}}\frac{\mathrm{d}\ln\mathcal{I}_m}{\mathrm{d}\bar{t}} = \frac{1}{2}\frac{\mathrm{d}\ln\mathcal{I}_m}{\mathrm{d}\ln\bar{a}}, \tag{9.30}$$

$$\bar{\lambda}_1 \equiv \frac{1}{\bar{H}\bar{\lambda}_0}\frac{\mathrm{d}\bar{\lambda}_0}{\mathrm{d}\bar{t}} = \frac{\mathrm{d}\ln\bar{\lambda}_0}{\mathrm{d}\ln\bar{a}}, \tag{9.31}$$

$$\bar{\lambda}_{i+1} \equiv \frac{1}{\bar{H}\bar{\lambda}_i}\frac{\mathrm{d}\bar{\lambda}_i}{\mathrm{d}\bar{t}} = \frac{\mathrm{d}\ln\bar{\lambda}_i}{\mathrm{d}\ln\bar{a}}. \tag{9.32}$$

Now, using the definitions of the slow-roll parameters (9.26)-(9.32) we can rewrite the system of the field equations (9.23)-(9.25) as

$$\mathcal{I}_\mathcal{V} = \bar{H}^2\mathcal{I}_m\left(3-\bar{\kappa}_0-6\bar{\lambda}_0+3\bar{\lambda}_0^2\right), \tag{9.33}$$

$$\bar{\kappa}_0 = \bar{\epsilon}_0-\bar{\lambda}_0\left(1+\bar{\epsilon}_0-\bar{\lambda}_0-\bar{\lambda}_1\right), \tag{9.34}$$

$$-\frac{1}{2\mathcal{I}_m}\frac{\mathrm{d}\mathcal{I}_\mathcal{V}}{\mathrm{d}\mathcal{I}_\phi} = \bar{H}\frac{\mathrm{d}\mathcal{I}_\phi}{\mathrm{d}\bar{t}}\left(3-\bar{\epsilon}_0+\frac{1}{2}\bar{\kappa}_1-2\bar{\lambda}_0\right). \tag{9.35}$$

In the slow-roll regime we must have [205]

$$|\bar{\kappa}_0| \ll 1, \quad |\bar{\kappa}_1| \ll 1, \quad |\bar{\lambda}_0| \ll 1, \quad |\bar{\lambda}_1| \ll 1, \tag{9.36}$$

and then the slow-rolling inflaton obeys the following approximate equations:

$$\mathcal{I}_\mathcal{V} \approx 3\bar{H}^2\mathcal{I}_m, \qquad 3\bar{H}\frac{\mathrm{d}\mathcal{I}_\phi}{\mathrm{d}\bar{t}} \approx -\frac{1}{2\mathcal{I}_m}\frac{\mathrm{d}\mathcal{I}_\mathcal{V}}{\mathrm{d}\mathcal{I}_\phi}. \tag{9.37}$$

9.2.3 Slow-roll in the Einstein frame

Analogously to the JF, the field equations in terms of the invariants in the EF have the form [205]

$$\hat{H}^2 = \frac{1}{3}\left[\left(\frac{\mathrm{d}\mathcal{I}_\phi}{\mathrm{d}\hat{t}}\right)^2 + \mathcal{I}_\mathcal{V}\right], \tag{9.38}$$

$$\frac{\mathrm{d}\hat{H}}{\mathrm{d}\hat{t}} = -\left(\frac{\mathrm{d}\mathcal{I}_\phi}{\mathrm{d}\hat{t}}\right)^2, \tag{9.39}$$

$$\frac{\mathrm{d}^2\mathcal{I}_\phi}{\mathrm{d}\hat{t}^2} = -3\hat{H}\frac{\mathrm{d}\mathcal{I}_\phi}{\mathrm{d}\hat{t}} - \frac{1}{2}\frac{\mathrm{d}\mathcal{I}_\mathcal{V}}{\mathrm{d}\mathcal{I}_\phi}. \tag{9.40}$$

The standard slow-roll parameters now are

$$\hat{\epsilon}_0 \equiv -\frac{1}{\hat{H}^2}\frac{\mathrm{d}\hat{H}}{\mathrm{d}\hat{t}} = -\frac{\mathrm{d}\ln\hat{H}}{\mathrm{d}\ln\hat{a}}, \qquad \hat{\eta} \equiv -\left(\hat{H}\frac{\mathrm{d}\mathcal{I}_\phi}{\mathrm{d}\hat{t}}\right)^{-1}\frac{\mathrm{d}^2\mathcal{I}_\phi}{\mathrm{d}\hat{t}^2}, \tag{9.41}$$

and again it will be useful to consider the following series of slow-roll parameters:

$$\hat{\kappa}_0 \equiv \frac{1}{\hat{H}^2}\left(\frac{\mathrm{d}\mathcal{I}_\phi}{\mathrm{d}\hat{t}}\right)^2 = \left(\frac{\mathrm{d}\mathcal{I}_\phi}{\mathrm{d}\ln\hat{a}}\right)^2, \tag{9.42}$$

$$\hat{\kappa}_1 \equiv \frac{1}{\hat{H}\hat{\kappa}_0}\frac{\mathrm{d}\hat{\kappa}_0}{\mathrm{d}\hat{t}} = \frac{\mathrm{d}\ln\hat{\kappa}_0}{\mathrm{d}\ln\hat{a}} = 2\left(-\hat{\eta} + \hat{\epsilon}_0\right), \tag{9.43}$$

$$\hat{\kappa}_{i+1} \equiv \frac{1}{\hat{H}\hat{\kappa}_i}\frac{\mathrm{d}\hat{\kappa}_i}{\mathrm{d}\hat{t}} = \frac{\mathrm{d}\ln\hat{\kappa}_i}{\mathrm{d}\ln\hat{a}}. \tag{9.44}$$

With the above definitions, the system (9.38)-(9.40) can be rewritten as

$$\mathcal{I}_\mathcal{V} = \hat{H}^2\left(3 - \hat{\kappa}_0\right), \tag{9.45}$$

$$\hat{\kappa}_0 = \hat{\epsilon}_0, \tag{9.46}$$

$$-\frac{1}{2}\frac{\mathrm{d}\mathcal{I}_\mathcal{V}}{\mathrm{d}\mathcal{I}_\phi} = \hat{H}\frac{\mathrm{d}\mathcal{I}_\phi}{\mathrm{d}\hat{t}}\left(3 - \hat{\epsilon}_0 + \frac{1}{2}\hat{\kappa}_1\right). \tag{9.47}$$

The slow-roll conditions are now simply

$$|\hat{\kappa}_0| \ll 1, \qquad |\hat{\kappa}_1| \ll 1, \tag{9.48}$$

and the approximate forms of the equations (9.45), (9.47) become

$$\mathcal{I}_\mathcal{V} \approx 3\hat{H}^2, \qquad 3\hat{H}\frac{\mathrm{d}\mathcal{I}_\phi}{\mathrm{d}\hat{t}} \approx -\frac{1}{2}\frac{\mathrm{d}\mathcal{I}_\mathcal{V}}{\mathrm{d}\mathcal{I}_\phi}. \tag{9.49}$$

In the next section, we will calculate the inflationary indices up to third order in the slow-roll parameters in both the EF and JF and then compare the results. It will prove useful to relate the EF

slow-roll parameters with the JF ones. This can be done using Eqs. (9.6), (9.7). We have

$$\hat{\kappa}_0 = \frac{\bar{\kappa}_0}{(1-\bar{\lambda}_0)^2}, \qquad \hat{\kappa}_1 = \frac{\bar{\kappa}_1}{1-\bar{\lambda}_0} + \frac{2\bar{\lambda}_0\bar{\lambda}_1}{(1-\bar{\lambda}_0)^2}, \tag{9.50}$$

$$\hat{\epsilon}_0 = \frac{\bar{\epsilon}_0 - \bar{\lambda}_0}{1-\bar{\lambda}_0} + \frac{\bar{\lambda}_0\bar{\lambda}_1}{(1-\bar{\lambda}_0)^2}. \tag{9.51}$$

9.2.4 Invariant potential slow-roll parameters

In the spirit of [32], we also define a hierarchy of slow-roll parameters in terms of the invariant inflaton potential. The standard potential slow-roll parameter ϵ_V assumes the form [205]

$$\epsilon_V = \frac{1}{4\mathcal{I}_\mathcal{V}^2}\left(\frac{\mathrm{d}\mathcal{I}_\mathcal{V}}{\mathrm{d}\mathcal{I}_\phi}\right)^2, \tag{9.52}$$

while η_V and higher-order parameters can be encoded in

$${}^n\beta_V \equiv \left(\frac{1}{2\mathcal{I}_\mathcal{V}}\right)^n \left(\frac{\mathrm{d}\mathcal{I}_\mathcal{V}}{\mathrm{d}\mathcal{I}_\phi}\right)^{n-1} \left(\frac{\mathrm{d}^{(n+1)}\mathcal{I}_\mathcal{V}}{\mathrm{d}\mathcal{I}_\phi^{(n+1)}}\right), \tag{9.53}$$

where ${}^n\beta_V$ is a parameter of order n in the slow-roll approximation. The first three parameters arising from this hierarchy are

$$\eta_V = \frac{1}{2\mathcal{I}_\mathcal{V}}\left(\frac{\mathrm{d}^2\mathcal{I}_\mathcal{V}}{\mathrm{d}\mathcal{I}_\phi^2}\right), \tag{9.54}$$

$$\zeta_V^2 = \frac{1}{4\mathcal{I}_\mathcal{V}^2}\left(\frac{\mathrm{d}\mathcal{I}_\mathcal{V}}{\mathrm{d}\mathcal{I}_\phi}\right)\left(\frac{\mathrm{d}^3\mathcal{I}_\mathcal{V}}{\mathrm{d}\mathcal{I}_\phi^3}\right), \tag{9.55}$$

$$\rho_V^3 = \frac{1}{8\mathcal{I}_\mathcal{V}^3}\left(\frac{\mathrm{d}^2\mathcal{I}_\mathcal{V}}{\mathrm{d}\mathcal{I}_\phi^2}\right)\left(\frac{\mathrm{d}^4\mathcal{I}_\mathcal{V}}{\mathrm{d}\mathcal{I}_\phi^4}\right). \tag{9.56}$$

Note that we have changed the symbols ξ and σ of [32] in order to avoid confusion with the non-minimal coupling and one of the model functions, respectively.

9.3 Higher-order spectral indices

In this section, we compute the tensor and scalar power spectra up to second-order corrections in the slow-roll approximation and the corresponding spectral indices in both the JF and EF using the invariant slow-roll parameters of Secs 9.2.2 and 9.2.3. We present the detailed calculation in the JF, and only give the final results for the EF since the calculation follows along the same lines with JF.

9.3.1 Jordan frame analysis

The evolution of linear (tensor and scalar) curvature cosmological perturbations in a flat FLRW background and in the presence of a scalar inflaton field is governed by the *Mukhanov-Sasaki equation*

(MSE) [46,47] which reads [209,210,212–215]

$$\frac{\mathrm{d}^2\nu}{\mathrm{d}\tau^2}+\left(k^2-\frac{1}{z}\frac{\mathrm{d}^2 z}{\mathrm{d}\tau^2}\right)\nu=0, \tag{9.57}$$

where k corresponds to the scale of the Fourier mode $\mathbf{k}$ of the gauge-invariant *comoving curvature perturbation* $\mathcal{R}_k$ [45]. Furthermore, the field ν (usually referred to as the *Mukhanov field*) is related to $\mathcal{R}_k$ via $\nu \equiv z\mathcal{R}_k$, where z is a parametrization-independent quantity that depends on both the background and the type of perturbations [205]. For tensor perturbations,

$$z=\frac{\bar{a}}{\sqrt{\mathcal{I}_m}}=\hat{a}, \tag{9.58}$$

while for scalar perturbations

$$z=\sqrt{\frac{2}{\mathcal{I}_m}}\frac{\bar{a}}{\bar{H}\left(1-\bar{\lambda}_0\right)}\frac{\mathrm{d}\mathcal{I}_\phi}{\mathrm{d}\bar{t}}=\sqrt{2}\frac{\hat{a}}{\hat{H}}\frac{\mathrm{d}\mathcal{I}_\phi}{\mathrm{d}\hat{t}}. \tag{9.59}$$

Therefore, the evolution equation (9.57) is parametrization-independent and also has the same functional form for tensor and scalar perturbations. The two asymptotic solutions for the scalar field ν corresponding to the subhorizon and the superhorizon limit can be written respectively as

$$\nu\to\begin{cases}\frac{1}{\sqrt{2k}}e^{-ik\tau} & \text{as} \quad -k\tau\to\infty,\\ A_k z & \text{as} \quad -k\tau\to 0.\end{cases} \tag{9.60}$$

The power spectrum for cosmological perturbations is usually defined by the two-point correlation function for $\mathcal{R}_k$ in the following way:

$$\langle\mathcal{R}_k,\mathcal{R}_{k'}\rangle=(2\pi)^2\delta^3(\mathbf{k}-\mathbf{k}')P_{\mathcal{R}}(k), \tag{9.61}$$

where all quantities are calculated at the time when the mode k crosses the horizon [when k^{-1} equals the Hubble radius $(aH)^{-1}$]. Note that the horizon-crossing condition is not the same in the two frames. In the EF one has the condition $k=\hat{a}\hat{H}$ while in the JF using (9.6),(9.7) and (9.30) one should use $k=\bar{a}\bar{H}(1-\bar{\lambda}_0)$ to evaluate quantities at the time of horizon crossing. Now, using the relation between $\mathcal{R}_k$ and the Mukhanov field and the asymptotic superhorizon limit (9.60) we can rewrite the power spectrum as

$$P(k)=\left(\frac{k^3}{2\pi^2}\right)\lim_{-k\tau\to 0}\left|\frac{\nu}{z}\right|^2=\frac{k^3}{2\pi^2}|A_k|^2. \tag{9.62}$$

This way the calculation of the spectrum reduces to simply finding the form of the amplitude of the field ν in the superhorizon limit. The MSE is usually solved in terms of Hankel functions by treating the slow-roll parameters as constant during inflation [53]. Since we want to obtain higher-order results for the power spectra and the spectral indices we cannot adhere to this assumption. Instead, we employ the Green's function method introduced by Stewart and Gong [55] which is valid to any order.

Now, in order to compute A_k one has to solve the MSE (9.57) which is a second-order differential equation. Thus in order to uniquely specify the solution for the field ν the use of two boundary conditions is necessary. To this end, one can use the asymptotic solutions (9.60) as boundary conditions. By introducing the dimensionless variable $x\equiv -k\tau$ and redefining the field as $y\equiv\sqrt{2k}\nu$, the

asymptotic solutions become

$$y \to \begin{cases} e^{-ix} & \text{as } x \to \infty, \\ \sqrt{2k}A_k z & \text{as } x \to 0. \end{cases} . \tag{9.63}$$

Also, by assuming the following ansatz for z:

$$z = \frac{1}{x} f(\ln x), \tag{9.64}$$

we can recast the MSE in the form

$$\frac{\mathrm{d}^2 y}{\mathrm{d}x^2} + \left(1 - \frac{2}{x^2}\right) y = \frac{1}{x^2} g(\ln x) y, \tag{9.65}$$

where the function g is defined through

$$g(\ln x) = \frac{1}{f(\ln x)} \left[-3 \frac{\mathrm{d}f(\ln x)}{\mathrm{d}\ln x} + \frac{\mathrm{d}^2 f(\ln x)}{\mathrm{d}(\ln x)^2} \right]. \tag{9.66}$$

The homogeneous solution with the appropriate asymptotic behavior at $x \to \infty$ is

$$y_0(x) = \left(1 + \frac{i}{x}\right) e^{ix}. \tag{9.67}$$

By “appropriate behavior" we mean that (9.67) reduces to the usual Minkowski modes in the deep subhorizon regime. Combining (9.65) and (9.63) we can rewrite the MSE as an integral equation

$$y(x) = y_0(x) + \frac{i}{2} \int_x^\infty \mathrm{d}u \frac{1}{u^2} g(\ln u) y(u) \left[y_0^*(u) y_0(x) - y_0^*(x) y_0(u) \right] \tag{9.68}$$

and seek a perturbative solution to (9.68). We start by Taylor-expanding xz around $x = 1$ in the following way:

$$xz = f(\ln x) = \sum_{n=0}^{\infty} \frac{f_n}{n!} (\ln x)^n, \tag{9.69}$$

where the n–th order coefficient of the expansion is of the same order in slow-roll and is given by

$$f_n = \frac{\mathrm{d}^n (xz)}{\mathrm{d}(\ln x)^n}. \tag{9.70}$$

In terms of the slow-roll parameters

$$\bar{\epsilon}_n = \frac{(-1)^{n+1}}{\bar{H}} \frac{\bar{H}^{(n+1)}}{\bar{H}^{(n)}} \tag{9.71}$$

we can expand the conformal time up to second order corrections and thus have the following approximation [49]:

$$x = -k\tau = -k \int \frac{\mathrm{d}\bar{t}}{\bar{a}} = \frac{k}{\bar{a}\bar{H}} (1 + \bar{\epsilon}_0 + 3\bar{\epsilon}_0^2 + \bar{\epsilon}_0 \bar{\epsilon}_1). \tag{9.72}$$

Then, using the relations

$$\bar{\epsilon}_0 = \bar{\lambda}_0 + \frac{\bar{\kappa}_0}{(1 - \bar{\lambda}_0)} - \frac{\bar{\lambda}_0 \bar{\lambda}_1}{(1 - \bar{\lambda}_0)}, \tag{9.73}$$

$$\bar{\epsilon}_0^2 \approx \bar{\lambda}_0^2 + \frac{\bar{\kappa}_0^2}{(1-\bar{\lambda}_0)^2} + 2\frac{\bar{\lambda}_0\bar{\kappa}_0}{(1-\bar{\lambda}_0)}, \tag{9.74}$$

$$2\bar{\epsilon}_0^2 + \bar{\epsilon}_0\bar{\epsilon}_1 \approx \bar{\lambda}_0\bar{\lambda}_1 + \frac{\bar{\kappa}_0\bar{\kappa}_1}{(1-\bar{\lambda}_0)}, \tag{9.75}$$

we can express x in terms of the $\bar{\kappa}$ and $\bar{\lambda}$ slow-roll parameters,

$$x = \frac{k}{\bar{a}\bar{H}}\left(1 + \bar{\lambda}_0 + \bar{\kappa}_0 + 3\bar{\lambda}_0\bar{\kappa}_0 + \bar{\kappa}_0\bar{\kappa}_1 + \bar{\kappa}_0^2 + \bar{\lambda}_0^2\right). \tag{9.76}$$

The second-order power spectrum is then given in terms of the coefficients f_0, f_1 and f_2 as [55]

$$P(k) = \frac{k^2}{(2\pi)^2}\frac{1}{f_0^2}\left[1 - 2\alpha\,\frac{f_1}{f_0} + \left(3\alpha^2 - 4 + \frac{5\pi^2}{12}\right)\left(\frac{f_1}{f_0}\right)^2 + \left(-\alpha^2 + \frac{\pi^2}{12}\right)\frac{f_2}{f_0}\right], \tag{9.77}$$

where $\alpha \equiv (2 - \ln 2 - \gamma) \simeq 0.729637$ and $\gamma \simeq 0.577216$ is the Euler–Mascheroni constant [54]. For tensor perturbations in the JF we have that up to second order terms

$$f_0^T = \frac{k}{\bar{H}\sqrt{\mathcal{I}_m}}\left(1 + \bar{\lambda}_0 + \bar{\kappa}_0 + 3\bar{\lambda}_0\bar{\kappa}_0 + \bar{\kappa}_0\bar{\kappa}_1 + 2\bar{\kappa}_0^2 + \bar{\lambda}_0^2\right)\Big|_{k=\bar{a}\bar{H}(1-\bar{\lambda}_0)}, \tag{9.78}$$

$$f_1^T = \frac{k}{\bar{H}\sqrt{\mathcal{I}_m}}\left(-\bar{\kappa}_0 - 3\bar{\kappa}_0\bar{\lambda}_0 - 2\bar{\kappa}_0^2 - \bar{\kappa}_0\bar{\kappa}_1\right)\Big|_{k=\bar{a}\bar{H}(1-\bar{\lambda}_0)}, \tag{9.79}$$

$$f_2^T = \frac{k}{\bar{H}\sqrt{\mathcal{I}_m}}\left(\bar{\kappa}_0^2 + \bar{\kappa}_0\bar{\kappa}_1\right)\Big|_{k=\bar{a}\bar{H}(1-\bar{\lambda}_0)}, \tag{9.80}$$

where the slow-roll parameters are evaluated at the time of the horizon crossing. We have also introduced the superscript "T" to discriminate from the corresponding coefficients of the scalar perturbations which will be denoted by an "S".

Substitution of these coefficients into (9.77) results in the following expression for the second order corrected tensor power spectrum in the slow-roll approximation:

$$\begin{aligned}\bar{P}_T = \left[\frac{\bar{H}^2\mathcal{I}_m}{(2\pi)^2}\right]\Bigg[1 - 2\bar{\lambda}_0 + (2\alpha-2)\bar{\kappa}_0 + \bar{\lambda}_0^2 + \left(2\alpha^2 - 2\alpha - 5 + \frac{\pi^2}{2}\right)\bar{\kappa}_0^2 \\ + \left(-\alpha^2 + 2\alpha - 2 + \frac{\pi^2}{12}\right)\bar{\kappa}_0\bar{\kappa}_1\Bigg].\end{aligned} \tag{9.81}$$

The tensor spectral index is defined as the logarithmic derivative of the power spectrum

$$\bar{n}_T \equiv \frac{\mathrm{d}\ln\bar{P}_T(k)}{\mathrm{d}\ln k} \tag{9.82}$$

and thus the third order JF tensor scalar spectral index is obtained to be

$$\begin{aligned}\bar{n}_T = &-2\bar{\kappa}_0 - 2\bar{\kappa}_0^2 - 4\bar{\lambda}_0\bar{\kappa}_0 + (2\alpha-2)\bar{\kappa}_0\bar{\kappa}_1 - 6\bar{\lambda}_0^2\bar{\kappa}_0 + (4\alpha-2)\bar{\lambda}_0\bar{\lambda}_1\bar{\kappa}_0 - 8\bar{\lambda}_0\bar{\kappa}_0^2 \\ &+ (6\alpha-6)\bar{\lambda}_0\bar{\kappa}_0\bar{\kappa}_1 - 2\bar{\kappa}_0^3 + (6\alpha - 16 + \pi^2)\bar{\kappa}_0^2\bar{\kappa}_1 + \left(-\alpha^2 + 2\alpha - 2 + \frac{\pi^2}{12}\right)(\bar{\kappa}_0\bar{\kappa}_1^2 + \bar{\kappa}_0\bar{\kappa}_1\bar{\kappa}_2).\end{aligned} \tag{9.83}$$

For scalar perturbations in the JF the coefficients f^S are slightly more complicated than their f^T counterparts and have the following second order forms:

$$f_0^S = \frac{k}{\bar{H}^2}\sqrt{\frac{2}{\mathcal{I}_m}}\frac{\mathrm{d}\mathcal{I}_\phi}{\mathrm{d}\bar{t}}\left[1+2\bar{\lambda}_0+\bar{\kappa}_0+4\bar{\lambda}_0\bar{\kappa}_0+\frac{3}{2}\bar{\kappa}_0\bar{\kappa}_1+2\bar{\kappa}_0^2+3\bar{\lambda}_0^2\right]\Big|_{k=\bar{a}\bar{H}(1-\bar{\lambda}_0)}, \tag{9.84}$$

$$f_1^S = -\frac{k}{\bar{H}^2}\sqrt{\frac{2}{\mathcal{I}_m}}\frac{\mathrm{d}\mathcal{I}_\phi}{\mathrm{d}\bar{t}}\left[\bar{\kappa}_0+\frac{\bar{\kappa}_1}{2}+2\bar{\kappa}_0\bar{\kappa}_1+4\bar{\kappa}_0\bar{\lambda}_0+\frac{3}{2}\bar{\lambda}_0\bar{\kappa}_1+\bar{\lambda}_0\bar{\lambda}_1+2\bar{\kappa}_0^2\right]\Big|_{k=\bar{a}\bar{H}(1-\bar{\lambda}_0)}, \tag{9.85}$$

$$f_2^S = \frac{k}{\bar{H}^2}\sqrt{\frac{2}{\mathcal{I}_m}}\frac{\mathrm{d}\mathcal{I}_\phi}{\mathrm{d}\bar{t}}\left[\frac{\bar{\kappa}_1^2}{4}+2\bar{\kappa}_0\bar{\kappa}_1+\bar{\kappa}_0^2+\frac{\bar{\kappa}_1\bar{\kappa}_2}{2}\right]\Big|_{k=\bar{a}\bar{H}(1-\bar{\lambda}_0)}. \tag{9.86}$$

Then the scalar power spectrum in the JF is

$$\begin{aligned}\bar{P}_S = \left[\frac{\bar{H}^4}{(2\pi)^2}\frac{\mathcal{I}_m}{2}\left(\frac{\mathrm{d}\mathcal{I}_\phi}{\mathrm{d}\bar{t}}\right)^{-2}\right]\Bigg[&1-4\bar{\lambda}_0+(2\alpha-2)\bar{\kappa}_0+\alpha\bar{\kappa}_1+\left(2\alpha^2-2\alpha-5+\frac{\pi^2}{2}\right)\bar{\kappa}_0^2\\&+(4-4\alpha)\bar{\lambda}_0\bar{\kappa}_0+(-3\alpha)\bar{\lambda}_0\bar{\kappa}_1+\left(\frac{\alpha^2}{2}-1+\frac{\pi^2}{8}\right)\bar{\kappa}_1^2+6\bar{\lambda}_0^2\\&+2\bar{\alpha}\bar{\lambda}_0\bar{\lambda}_1+\left(\alpha^2+\alpha-7+\frac{7\pi^2}{12}\right)\bar{\kappa}_0\bar{\kappa}_1+\left(-\frac{\alpha^2}{2}+\frac{\pi^2}{24}\right)\bar{\kappa}_1\bar{\kappa}_2\Bigg].\end{aligned} \tag{9.87}$$

Substitution of the latter in the definition of the scalar spectral index

$$\bar{n}_S \equiv 1+\frac{\mathrm{d}\ln\bar{P}_S}{\mathrm{d}\ln k} \tag{9.88}$$

results in the following third order expression for the scalar index in the JF:

$$\begin{aligned}\bar{n}_S =&1-2\bar{\kappa}_0-\bar{\kappa}_1-2\bar{\kappa}_0^2-2\bar{\lambda}_0\bar{\lambda}_1+\alpha\bar{\kappa}_1\bar{\kappa}_2-\bar{\kappa}_1\bar{\lambda}_0-4\bar{\kappa}_0\bar{\lambda}_0+(2\alpha-3)\bar{\kappa}_1\bar{\kappa}_0-2\bar{\kappa}_0^3-8\bar{\lambda}_0\bar{\kappa}_0^2\\&-6\bar{\lambda}_0^2\bar{\kappa}_0+(6\alpha-17+\pi^2)\bar{\kappa}_0^2\bar{\kappa}_1-\bar{\kappa}_1\bar{\lambda}_0^2+\left(-2+\frac{\pi^2}{4}\right)\bar{\kappa}_1^2\bar{\kappa}_2-4\bar{\lambda}_0^2\bar{\lambda}_1+2\alpha\bar{\lambda}_0\bar{\lambda}_1^2\\&+\left(-\frac{\alpha^2}{2}+\frac{\pi^2}{24}\right)\bar{\kappa}_1\bar{\kappa}_2^2+\left(-\alpha^2+3\alpha-7+\frac{7\pi^2}{12}\right)\bar{\kappa}_0\bar{\kappa}_1^2+2\alpha\bar{\lambda}_0\bar{\lambda}_1\bar{\lambda}_2+(6\alpha-9)\bar{\lambda}_0\bar{\kappa}_0\bar{\kappa}_1\\&+(4\alpha-4)\bar{\lambda}_0\bar{\lambda}_1\bar{\kappa}_0+(\alpha+1)\bar{\kappa}_1\bar{\lambda}_0\bar{\lambda}_1+2\alpha\bar{\lambda}_0\bar{\kappa}_1\bar{\kappa}_2+\left(-\frac{\alpha^2}{2}+\frac{\pi^2}{24}\right)\bar{\kappa}_1\bar{\kappa}_2\bar{\kappa}_3\\&+\left(-\alpha^2+4\alpha-7+\frac{7\pi^2}{12}\right)\bar{\kappa}_0\bar{\kappa}_1\bar{\kappa}_2.\end{aligned} \tag{9.89}$$

Finally, with the higher order corrected expressions for the power spectra for scalar and tensor perturbations in the JF at our disposal, it is trivial to compute the tensor-to-scalar ratio,

$$\begin{aligned}\bar{r} =&16\bar{\kappa}_0\Bigg[1+2\bar{\lambda}_0-\alpha\bar{\kappa}_1+3\bar{\lambda}_0^2-2\alpha\bar{\lambda}_0\bar{\lambda}_1-3\alpha\bar{\lambda}_0\bar{\kappa}_1+\left(-\alpha+5-\frac{\pi^2}{2}\right)\bar{\kappa}_0\bar{\kappa}_1\\&+\left(\frac{\alpha^2}{2}+1-\frac{\pi^2}{8}\right)\bar{\kappa}_1^2+\left(\frac{\alpha^2}{2}-\frac{\pi^2}{24}\right)\bar{\kappa}_1\bar{\kappa}_2\Bigg].\end{aligned} \tag{9.90}$$

9.3.2 Einstein frame results

Repeating the same analysis in the EF, we obtain the tensor power spectrum

$$\hat{P}_T = \frac{\hat{H}^2}{(2\pi)^2}\left[1+(2\alpha-2)\hat{\kappa}_0+\left(2\alpha^2-2\alpha-5+\frac{\pi^2}{2}\right)\hat{\kappa}_0^2+\left(-\alpha^2+2\alpha-2+\frac{\pi^2}{12}\right)\hat{\kappa}_0\hat{\kappa}_1\right], \tag{9.91}$$

the tensor spectral index

$$\begin{aligned}\hat{n}_T =& -2\hat{\kappa}_0-2\hat{\kappa}_0^2+(2\alpha-2)\hat{\kappa}_0\hat{\kappa}_1-2\hat{\kappa}_0^3+(6\alpha-16+\pi^2)\hat{\kappa}_0^2\hat{\kappa}_1\\ &+\left(-\alpha^2+2\alpha-2+\frac{\pi^2}{12}\right)(\hat{\kappa}_0\hat{\kappa}_1^2+\hat{\kappa}_0\hat{\kappa}_1\hat{\kappa}_2),\end{aligned} \tag{9.92}$$

the scalar power spectrum

$$\begin{aligned}\hat{P}_S =& \left[\frac{\hat{H}^4}{2(2\pi)^2}\left(\frac{\mathrm{d}\mathcal{I}_\phi}{\mathrm{d}\hat{t}}\right)^{-2}\right]\left[1+(2\alpha-2)\hat{\kappa}_0+\alpha\hat{\kappa}_1+\left(2\alpha^2-2\alpha-5+\frac{\pi^2}{2}\right)\hat{\kappa}_0^2\right.\\ &+\left(\frac{\alpha^2}{2}-1+\frac{\pi^2}{8}\right)\hat{\kappa}_1^2+\left(\alpha^2+\alpha-7+\frac{7\pi^2}{12}\right)\hat{\kappa}_0\hat{\kappa}_1\\ &\left.+\left(-\frac{\alpha^2}{2}+\frac{\pi^2}{24}\right)\hat{\kappa}_1\hat{\kappa}_2\right],\end{aligned} \tag{9.93}$$

the scalar spectral index

$$\begin{aligned}\hat{n}_S =& 1-2\hat{\kappa}_0-\hat{\kappa}_1-2\hat{\kappa}_0^2+\alpha\hat{\kappa}_1\hat{\kappa}_2+(2\alpha-3)\hat{\kappa}_0\hat{\kappa}_1-2\hat{\kappa}_0^3+(6\alpha-17+\pi^2)\hat{\kappa}_0^2\hat{\kappa}_1\\ &+\left(-2+\frac{\pi^2}{4}\right)\hat{\kappa}_1^2\hat{\kappa}_2+\left(-\frac{\alpha^2}{2}+\frac{\pi^2}{24}\right)\hat{\kappa}_1\hat{\kappa}_2^2+\left(-\alpha^2+3\alpha-7+\frac{7\pi^2}{12}\right)\hat{\kappa}_0\hat{\kappa}_1^2\\ &+\left(-\frac{\alpha^2}{2}+\frac{\pi^2}{24}\right)\hat{\kappa}_1\hat{\kappa}_2\hat{\kappa}_3+\left(-\alpha^2+4\alpha-7+\frac{7\pi^2}{12}\right)\hat{\kappa}_0\hat{\kappa}_1\hat{\kappa}_2,\end{aligned} \tag{9.94}$$

and finally the tensor-to-scalar ratio

$$\hat{r} = 16\hat{\kappa}_0\left[1-\alpha\hat{\kappa}_1+\left(-\alpha+5-\frac{\pi^2}{2}\right)\hat{\kappa}_0\hat{\kappa}_1+\left(\frac{\alpha^2}{2}+1-\frac{\pi^2}{8}\right)\hat{\kappa}_1^2+\left(\frac{\alpha^2}{2}-\frac{\pi^2}{24}\right)\hat{\kappa}_1\hat{\kappa}_2\right]. \tag{9.95}$$

Note that the above results have been obtained using the condition $k = \hat{a}\hat{H}$ at the time of horizon crossing.

9.3.3 Equivalence of the frames up to third order

It has been reported by the authors of [205] that the EF and JF spectral indices are equivalent up to second order in the slow-roll expansion. In this work we have obtained the third-order corrected expressions for the indices in the two frames. It is thus intriguing to see whether this equivalence extends to the third-order expressions also. Expanding the EF slow-roll parameters (9.50) up to third order in the JF slow-roll parameters we have

$$\hat{\kappa}_0 \approx \bar{\kappa}_0+2\bar{\kappa}_0\bar{\lambda}_0+3\bar{\kappa}_0\bar{\lambda}_0^2, \tag{9.96}$$

$$\hat{\kappa}_1 \approx \bar{\kappa}_1+\bar{\kappa}_1\bar{\lambda}_0+\bar{\kappa}_1\bar{\lambda}_0^2+2\bar{\lambda}_0\bar{\lambda}_1+4\bar{\lambda}_0^2\bar{\lambda}_1, \tag{9.97}$$

$$\hat{\kappa}_1\hat{\kappa}_2 \approx \bar{\kappa}_1\bar{\kappa}_2 + 2\bar{\kappa}_1\bar{\kappa}_2\bar{\lambda}_0 + \bar{\kappa}_1\bar{\lambda}_0\bar{\lambda}_1 + 2\bar{\lambda}_0\bar{\lambda}_1^2 + 2\bar{\lambda}_0\bar{\lambda}_1\bar{\lambda}_2, \tag{9.98}$$

$$\hat{\kappa}_0\hat{\kappa}_1\hat{\kappa}_2 \approx \bar{\kappa}_0\bar{\kappa}_1\bar{\kappa}_2\,, \quad \hat{\kappa}_1\hat{\kappa}_2\hat{\kappa}_3 \approx \bar{\kappa}_1\bar{\kappa}_2\bar{\kappa}_3. \tag{9.99}$$

Then, plugging (9.96) - (9.99) in the EF expressions for the indices (9.92) - (9.95) we find

$$\hat{n}_T = \bar{n}_T, \tag{9.100}$$

$$\hat{n}_S = \bar{n}_S, \tag{9.101}$$

$$\hat{r} = \bar{r}. \tag{9.102}$$

Therefore, the spectral indices calculated in the EF and JF coincide. Finally, since the Green's function method is valid up to arbitrary order in the slow-roll expansion, we expect the equivalence between the spectral indices in the JF and EF to also hold to all orders.

9.3.4 Invariant expressions for the inflationary observables

So far we have obtained the spectral indices and the tensor-to-scalar ratio in both the EF and JF. We have also shown that up to third order in the slow-roll expansion the results in the two frames are equivalent. We can take advantage of this equivalence and write down expressions for the inflationary observables only in terms of the invariant potential and its derivatives. The equivalence between the two frames allows then one to rewrite the EF results in terms of the invariant PSRPs and expect these results to hold in the JF too. In order to express the spectral indices in terms of the PSRPs defined in (9.52) - (9.56) we first use the following relations between the EF HSRPs (9.42) - (9.44) and the ones defined in [32]:

$$\begin{aligned}
\hat{\kappa}_0 &= \epsilon_H, && (9.103)\\
\hat{\kappa}_1 &= -2\eta_H + 2\epsilon_H, && (9.104)\\
\hat{\kappa}_1\hat{\kappa}_2 &= 4\epsilon_H^2 - 6\epsilon_H\eta_H + 2\zeta_H^2, && (9.105)\\
\hat{\kappa}_1\hat{\kappa}_2^2 + \hat{\kappa}_1\hat{\kappa}_2\hat{\kappa}_3 &= 16\epsilon_H^3 - 22\epsilon_H^2\eta_H + 12\epsilon_H\eta_H^2 + 10\epsilon_H\zeta_H^2 - 2\eta_H\zeta_H^2 - 2\rho_H^3. && (9.106)
\end{aligned}$$

Then, using the third-order Taylor expansions of the HSRPs in terms of the PSRPs [32], presented in Appendix C, we obtain the inflationary indices up to third order in the PSRPs

$$\begin{aligned}
n_T = &-2\epsilon_V + \left(8\alpha - \frac{22}{3}\right)\epsilon_V^2 - \left(4\alpha - \frac{8}{3}\right)\epsilon_V\eta_V + \left(-32\alpha^2 + \frac{189}{3}\alpha - \frac{996}{9} + \frac{20\pi^2}{3}\right)\epsilon_V^3\\
&+ \left(-4\alpha^2 + 4\alpha - \frac{46}{9} + \frac{\pi^2}{3}\right)\epsilon_V\eta_V^2 + \left(28\alpha^2 - 44\alpha + 68 - \frac{13\pi^2}{3}\right)\epsilon_V^2\eta_V\\
&+ \left(-2\alpha^2 + \frac{8}{3}\alpha - \frac{28}{9} + \frac{\pi^2}{6}\right)\epsilon_V\zeta_V^2,
\end{aligned} \tag{9.107}$$

$$
\begin{aligned}
n_S =& 1 - 6\epsilon_V + 2\eta_V + \left(24\alpha - \frac{10}{3}\right)\epsilon_V^2 - (16\alpha + 2)\,\epsilon_V\eta_V + \frac{2}{3}\eta_V^2 + \left(2\alpha + \frac{2}{3}\right)\zeta_V^2 \\
&- \left(90\alpha^2 - \frac{104}{3}\alpha + \frac{3734}{9} - \frac{87\pi^2}{2}\right)\epsilon_V^3 + \left(90\alpha^2 + \frac{4}{3}\alpha + \frac{1190}{3} - \frac{87\pi^2}{2}\right)\epsilon_V^2\eta_V \\
&- \left(16\alpha^2 + 12\alpha + \frac{742}{9} - \frac{28\pi^2}{3}\right)\epsilon_V\eta_V^2 - \left(12\alpha^2 + 4\alpha + \frac{98}{3} - 4\pi^2\right)\epsilon_V\zeta_V^2 \\
&+ \left(\alpha^2 + \frac{8}{3}\alpha + \frac{28}{3} - \frac{13\pi^2}{2}\right)\eta_V\zeta_V^2 + \frac{4}{9}\eta_V^3 + \left(\alpha^2 + \frac{2}{3}\alpha + \frac{2}{9} - \frac{\pi^2}{12}\right)\rho_V^3,
\end{aligned}
\tag{9.108}
$$

$$
\begin{aligned}
r =& 16\epsilon_V\left[1 - \left(4\alpha + \frac{4}{3}\right)\epsilon_V + \left(2\alpha + \frac{2}{3}\right)\eta_V + \left(16\alpha^2 + \frac{28}{3}\alpha + \frac{356}{9} - \frac{14\pi^2}{3}\right)\epsilon_V^2\right. \\
&- \left(14\alpha^2 + 10\alpha + \frac{88}{3} - \frac{7\pi^2}{2}\right)\epsilon_V\eta_V + \left(2\alpha^2 + 2\alpha + \frac{41}{9} - \frac{\pi^2}{2}\right)\eta_V^2 \\
&\left.+ \left(\alpha^2 + \frac{2}{3}\alpha + \frac{2}{9} - \frac{\pi^2}{12}\right)\zeta_V^2\right]
\end{aligned}
\tag{9.109}
$$

In a given model, once we derive the invariant potential $\mathcal{I}_\mathcal{V}$ in terms of the invariant $\mathcal{I}_\phi$, we can readily obtain the PSRPs and express the inflationary observables in an invariant way in terms of $\mathcal{I}_\mathcal{V}$ and its derivatives.

9.4 Number of e-folds

In this section, we consider the difference between the definitions for the number of e-folds in the EF and JF and study how it affects the values of the observables. Furthermore, we discuss various approaches for a more accurate determination of the value of the inflaton field at the end of inflation.

9.4.1 Einstein vs Jordan

The number of e-folds is usually defined in the EF as

$$
\mathrm{d}\hat{N} \equiv \hat{H}\mathrm{d}\hat{t} = \mathrm{d}\ln\hat{a} = -\frac{1}{\sqrt{\hat{\kappa}_0}}\,\mathrm{d}\mathcal{I}_\phi = -\frac{1}{\sqrt{\hat{\epsilon}_0}}\,\mathrm{d}\mathcal{I}_\phi = -\frac{1}{\sqrt{\epsilon_H}}\,\mathrm{d}\mathcal{I}_\phi. \tag{9.110}
$$

Using (9.6) the number of e-folds in the JF becomes

$$
\mathrm{d}\bar{N} = \mathrm{d}\hat{N} + \frac{1}{2}\,\mathrm{d}\ln\mathcal{I}_m = \left(-\frac{1}{\sqrt{\epsilon_H}} + \frac{1}{2}\frac{\mathrm{d}\ln\mathcal{I}_m}{\mathrm{d}\mathcal{I}_\phi}\right)\mathrm{d}\mathcal{I}_\phi. \tag{9.111}
$$

We see that the definitions for the number of e-folds in the two frames differ by the invariant factor $\frac{1}{2}\,\mathrm{d}\ln\mathcal{I}_m$ which includes the nonminimal coupling in a given theory. Of course, when the scalar field is minimally coupled to gravity the two definitions coincide. Therefore, in general, the same number of e-folds in the two frames will translate to different values for the invariant $\mathcal{I}_\phi$. This means that we will get different predictions for the observables depending on whether we use (9.110) or (9.111). Typically the difference is small, but still comparable to (if not larger than) the difference for the observables if one chooses to use the first, second or third order results for n_S and r in terms of

the slow-roll parameters. Furthermore, these types of differences can play a significant role in the future, with the advent of more precise measurements [52, 666], in regards to the characterization of an inflationary model as viable or not.

In order to quantify the aforementioned effects, we will next consider the nonminimal Coleman-Weinberg model introduced in [148]. The model functions are

$$\mathcal{A}(\Phi) = \xi\Phi^2, \tag{9.112}$$
$$\mathcal{B}(\Phi) = 1, \tag{9.113}$$
$$\sigma(\Phi) = 0, \tag{9.114}$$
$$\mathcal{V}(\Phi) = \Lambda^4 + \frac{1}{8}\beta_{\lambda_\Phi}\left(\ln\frac{\Phi^2}{v_\Phi^2} - \frac{1}{2}\right)\Phi^4, \tag{9.115}$$

where the cosmological constant Λ^4 was included in order to realize $\mathcal{V}(v_\Phi) = 0$ and β_{λ_Φ} is the beta function of the quartic scalar coupling λ_Φ. Furthermore, in this model the Planck scale is dynamically generated through the VEV of the scalar field v_Φ and we have

$$1 = \xi v_\Phi^2. \tag{9.116}$$

Minimization of the potential (9.115) yields

$$\beta_{\lambda_\Phi} = 16\,\frac{\Lambda^4}{v_\Phi^4}. \tag{9.117}$$

This means we can eliminate β_{λ_Φ} in (9.115) and rewrite the potential as

$$\mathcal{V}(\Phi) = \Lambda^4\left\{1 + \left[2\ln\left(\frac{\Phi^2}{v_\Phi^2}\right) - 1\right]\frac{\Phi^4}{v_\Phi^4}\right\} \tag{9.118}$$

From the expressions of the model functions (9.112) - (9.115) we can readily obtain the invariants $\mathcal{I}_m$, $\mathcal{I}_\mathcal{V}$ and $\mathcal{I}_\phi$. The invariant field takes the form

$$\mathcal{I}_\phi = \sqrt{\frac{1+6\xi}{2\xi}}\ln\left(\frac{\Phi}{v_\Phi}\right). \tag{9.119}$$

By inverting the above equation we can express the invariant $\mathcal{I}_m$ in terms of $\mathcal{I}_\phi$ as

$$\mathcal{I}_m = e^{-2\sqrt{\frac{2\xi}{1+6\xi}}\mathcal{I}_\phi}, \tag{9.120}$$

and also the invariant potential $\mathcal{I}_\mathcal{V}$ in terms of $\mathcal{I}_\phi$ as

$$\mathcal{I}_\mathcal{V} = \Lambda^4\left(4\sqrt{\frac{2\xi}{1+6\xi}}\,\mathcal{I}_\phi + e^{-4\sqrt{\frac{2\xi}{1+6\xi}}\mathcal{I}_\phi} - 1\right), \tag{9.121}$$

where we used (9.116). From the invariant potential (9.121) we can calculate the PSRPs (9.52), (9.54) - (9.56) and then the scalar index n_S [c.f. (9.108)] and the tensor-to-scalar ratio r [c.f. (9.109)] and compare them with the experimental bounds. Another important observable is the amplitude of scalar perturbations $A_S = (2.14 \pm 0.05) \times 10^{-9}$ [51], which can be used to constrain the value of Λ (see Fig. 3 in [148]).

Now, depending on whether the field Φ rolls down from values larger or smaller than its VEV, the invariant $\mathcal{I}_\phi$ can have positive or negative values. Since negative field inflation produces $r \gtrsim$

	$n_S^{(\mathrm{I})}$	$n_S^{(\mathrm{III})}$	$r^{(\mathrm{I})}$	$r^{(\mathrm{III})}$	ξ
$\hat{N}=60$	0.96702	0.96712	0.12782	0.12552	10^{-5}
$\bar{N}=60$	0.96699	0.96709	0.12792	0.12562	10^{-5}
$\hat{N}=60$	0.96935	0.96956	0.09655	0.09466	10^{-3}
$\bar{N}=60$	0.96911	0.96933	0.09736	0.09544	10^{-3}
$\hat{N}=60$	0.97451	0.97477	0.06796	0.06675	0.1
$\bar{N}=60$	0.97320	0.97348	0.07148	0.07013	0.1
$\hat{N}=60$	0.97482	0.97507	0.06716	0.06597	10
$\bar{N}=60$	0.97276	0.97305	0.07264	0.07125	10

Table 9.1: First and third order results for the observables of the nonminimal Coleman-Weinberg model considered in [148] for various values of the nonminimal coupling ξ and for $\hat{N}=\bar{N}=60$. We see that as ξ grows so does the difference between the observables, depending on which definition for the e-folds we use.

0.15 [148], which is excluded by observations [1, 51], we will not consider it further. Instead, we will only focus on positive field inflation which interpolates between quadratic [31] and linear [667] inflation depending on the value of the nonminimal coupling ξ. In the limit $\xi \to 0$, the invariant potential is approximated as

$$\mathcal{I}_{\mathcal{V}}|_{\xi\to 0} \sim 16\,\xi\,\Lambda^4\,\mathcal{I}_\phi^2, \tag{9.122}$$

while in the limit $\xi \to \infty$,

$$\mathcal{I}_{\mathcal{V}}|_{\xi\to \infty} \sim \frac{4}{\sqrt{3}}\,\Lambda^4\,\mathcal{I}_\phi. \tag{9.123}$$

Quadratic inflation is excluded by the Planck and BICEP2/Keck results [1,51] but linear inflation still lies within the 2σ allowed region. In Table 9.1 we present our results for the first and third order scalar index n_S and tensor-to-scalar ratio r for various values of the nonminimal coupling ξ. For simplicity, we have assumed that inflation ends at $\Phi = v_\Phi$, or equivalently $\mathcal{I}_\phi^{\mathrm{end}} = 0$, where the two frames coincide. Furthermore, we have approximated $\epsilon_H \approx \epsilon_V$ in the expressions (9.110) and (9.111). In each case, for every value of ξ considered, we have varied $\mathcal{I}_\phi^{\mathrm{HC}}$ at horizon crossing in order to get $\hat{N}=60$ and $\bar{N}=60$. This means that we obtain a different value for $\mathcal{I}_\phi$ depending on which definition for the e-folds we use. Consequently, the predictions for n_S and r differ. For small ξ the difference between the frames is negligible. However, for larger ξ the difference grows and becomes around 0.002 (or 0.2%) for n_S and 0.005 (or 8%) for r around $\xi = 10$. For large ξ, such a difference is actually larger than the difference between the first and third order results for the observables (0.03% for n_S and 1.9% for r). Both of these types of differences however should be within the reach of future experiments such as CORE and LiteBIRD [52, 666] which are expected to measure r with an accuracy of 10^{-3}.

Another way to illustrate the disparity between the two definitions for the e-folds is to examine how the same field excursion affects the number of e-folds itself. In Fig. 9.2, for a wide range of values of ξ, we calculate the invariant $\mathcal{I}_\phi^{\mathrm{HC}}$ for which $\hat{N}=50$ and $\hat{N}=60$. Then, for the same value of $\mathcal{I}_\phi$ we calculate the corresponding JF e-folds $\bar{N}$ and plot the difference with the EF e-folds $\hat{N}$. One can see that, as expected, the difference asymptotes to zero for $\xi \to 0$ due to the vanishing second term in (9.111). On the other hand, as ξ grows so does the difference $\bar{N}-\hat{N}$ until it reaches a value of about 4.3 e-folds for $\hat{N}=50$ and 4.7 e-folds for $\hat{N}=60$. Note that for $\xi \gtrsim 10$ the difference stops growing since the model has reached the linear inflation attractor. We perceive the JF definition for

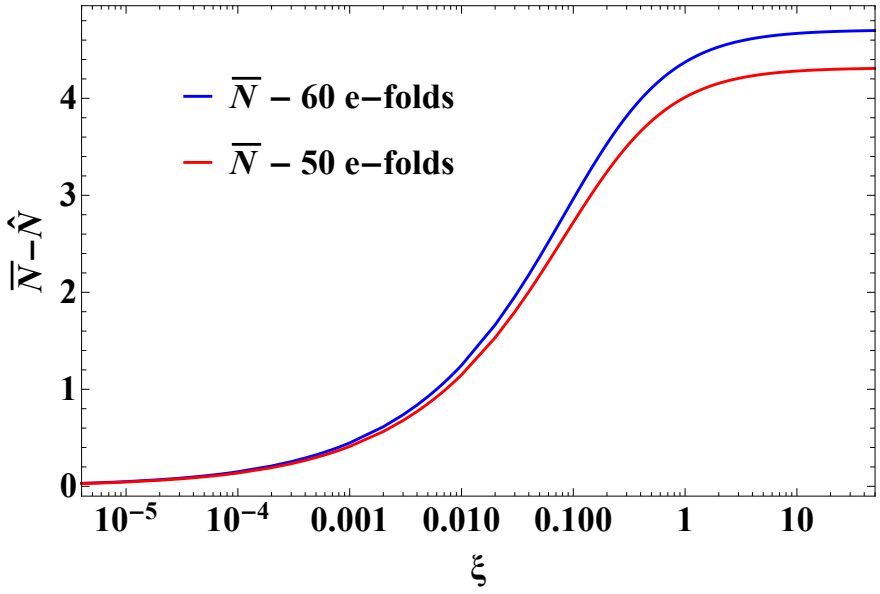

Figure 9.2: The difference between the JF ($\bar{N}$) and the EF ($\hat{N}$) number of e-folds as a function of the nonminimal coupling ξ for $\hat{N} = 60$ (top curve) and $\hat{N} = 50$ (bottom curve). We see that as ξ grows we need more e-folds in the Jordan frame for the same inflaton field excursion.

the number of e-folds as the fundamental one since it is composed of all three invariants (9.1)–(9.3) and also accommodates the EF definition.

9.4.2 Taylor vs Padé

Let us also examine how the end-of-inflation condition affects the observables. Inflation ends *exactly* at $\epsilon_H = 1$. Most authors usually adopt the slow-roll approximation and consider the relation between ϵ_H and the PSRPs at first order in the Taylor expansion and solve

$$\epsilon_H^{(\mathrm{I})} = \epsilon_V = 1 \tag{9.124}$$

in order to obtain the inflaton field value at the end of inflation. In our case, since we have obtained n_S and r at third order in the PSRPs, it would seem prudent to also approximate ϵ_H in the definition of e-folds with the third order Taylor expansion and solve

$$\epsilon_H^{(\mathrm{III})} = \epsilon_V - \frac{4}{3}\epsilon_V^2 + \frac{2}{3}\epsilon_V\eta_V + \frac{32}{9}\epsilon_V^3 + \frac{5}{9}\epsilon_V\eta_V^2 - \frac{10}{3}\epsilon_V^2\eta_V + \frac{2}{9}\epsilon_V\zeta_V^2 = 1 \tag{9.125}$$

in order to obtain $\mathcal{I}_\phi^{\mathrm{end}}$. Nevertheless, even though the third order Taylor expansion is a very good approximation around the time of horizon crossing when the slow-roll parameters are small, the same does not hold near the end of inflation when ϵ_V and η_V become of order one since the third order expansion actually blows up and thus fails to accurately describe the entirety of the inflationary epoch. A more accurate option, as pointed out in [32], is to consider a Padé approximation for ϵ_H. The $[1/1]$ Padé approximant is given by

$$\epsilon_H^{[1/1]} = \frac{\epsilon_V}{1 + \frac{4}{3}\epsilon_V - \frac{2}{3}\eta_V}, \tag{9.126}$$

$\hat{\mathbf{N}} = \mathbf{50}$	$n_S^{(\mathrm{I})}$	$n_S^{(\mathrm{III})}$	$r^{(\mathrm{I})}$	$r^{(\mathrm{III})}$	ξ
end: $\epsilon_H^{(\mathrm{I})} = 1$	0.96078	0.96092	0.15238	0.14914	10^{-5}
end: $\epsilon_H^{[1/1]} = 1$	0.95979	0.95994	0.15626	0.15285	10^{-5}
end: $\epsilon_H^{(\mathrm{III})} = 1$	0.96032	0.96047	0.15417	0.15085	10^{-5}
end: $\epsilon_H^{[2/2]} = 1$	0.96019	0.96034	0.15468	0.15134	10^{-5}
end: $\epsilon_H^{(\mathrm{I})} = 1$	0.96955	0.96991	0.08121	0.07948	0.1
end: $\epsilon_H^{[1/1]} = 1$	0.96870	0.96908	0.08348	0.08165	0.1
end: $\epsilon_H^{(\mathrm{III})} = 1$	0.96922	0.96959	0.08208	0.08031	0.1
end: $\epsilon_H^{[2/2]} = 1$	0.96909	0.96946	0.08244	0.08066	0.1

Table 9.2: First and third order results for the observables of the model [148] for two values of the nonminimal coupling ξ and for $\hat{N} = 50$ using the four end-of-inflation conditions described in the text. We see that the differences are small albeit comparable to the differences between the first and third order results.

while the $[2/2]$ approximant has the form

$$\epsilon_H^{[2/2]} = \frac{\epsilon_V + \frac{17}{4}\epsilon_V^2 - \frac{5}{3}\epsilon_V\eta_V}{1 + \frac{67}{12}\epsilon_V - \frac{7}{3}\eta_V - \frac{7}{2}\epsilon_V\eta_V + \frac{35}{9}\epsilon_V^2 + \eta_V^2 - \frac{2}{9}\zeta_V^2} + \frac{2}{27}\epsilon_V\rho_V^3 - \frac{1}{54}\epsilon_V^3\eta_V + \frac{35}{108}\epsilon_V^2\eta_V^2 - \frac{13}{54}\epsilon_V^2\zeta_V^2 - \frac{1}{9}\epsilon_V\eta_V^3. \tag{9.127}$$

In Table 9.2 we present the results for n_S and r for $\xi = 10^{-5}$, $\xi = 0.1$ and $\hat{N} = 50$ having employed the four end-of-inflation conditions for $\mathcal{I}_\phi^{\mathrm{end}}$ described above and the corresponding expressions (9.124) - (9.127) for ϵ_H in the e-folds integral. We find that the difference between the four methods is small for n_S but larger for r which has a greater dependence on ϵ_H. The largest difference for r between the methods occurs for small ξ since its value is sizeable ($r \simeq 0.15$) and a small change in the value of $\mathcal{I}_\phi^{\mathrm{end}}$ affects it noticeably. In any case, the differences between the end-of-inflation methods on n_S and r are comparable to the differences between the first and third order results.

Chapter 10

Conclusions and Outlook

In this thesis, we have considered classical scale invariance to be a fundamental property of Nature and have constructed models where the electroweak, neutrino, dark matter and Planck scales can by dynamically generated through the Coleman-Weinberg mechanism. In Chapters 2 through 5 we set up the stage by reviewing the ΛCDM model, the theory of cosmic inflation, the Standard Model of Particle Physics and the dark matter problem. Then, Chapter 6 was devoted to classical scale invariance.

In Chapter 7 we considered a classically scale invariant version of the Standard Model, enlarged by a dark $SU(2)_X$ gauge group which incorporates three vector bosons and a scalar field in the fundamental representation. We also included a real singlet scalar field and Majorana neutrinos coupled to it. The dark sector was radiatively broken through the Coleman-Weinberg mechanism and a mass scale was communicated to the electroweak and neutrino sectors through the portal interactions of the dark doublet with the Higgs and singlet scalars. We started by determining the necessary conditions for the stability of the potential and then proceeded in studying the full one-loop scalar potential, employing the Gildener-Weinberg formalism. We obtained the scalar masses through a particular parametrization of the scalar VEVs, and saw that one of these masses, although zero at tree level, received large quantum corrections. Neutrinos obtained masses through the realization of a type-I low-energy seesaw mechanism. After setting up the model, we proceeded to consider constraints to its set of free parameters through stability and perturbativity considerations, as well as bounds set by the LHC.

We identified the extra gauge bosons as WIMP dark matter candidates. We considered the Boltzmann equation and solved it semi-analytically in the non-relativistic approximation after calculating the total thermally averaged annihilation and semi-annihilation cross sections. In this way, we obtained the dark matter relic density, and by matching it to the observed value we constrained the dark matter mass to be in the range $M_X \sim 710 - 740$ GeV (Fig. 7.7). Then, considering the dark matter elastic scattering off a nucleon we computed the spin-independent scattering cross section and compared it with existing and projected limits from direct detection experiments. We found that dark matter masses above ~ 700 GeV evade limits set by LUX (2013) but can nevertheless be tested by XENON 1T.

In conclusion, the classically scale invariant model that we considered in Chapter 7 is a perfectly viable extension of the Standard Model, able to dynamically generate the dark matter, neutrino and electroweak scales through the multi-Higgs portal while stabilizing the vacuum. It predicts new scalar states that future collider searches may be able to discover and predicts vector dark matter with a definite mass range that can be probed by direct detection experiments in the years to come.

This model was reconsidered in Ref. [412], were the authors examined how oscillations between the right-handed neutrinos can lead to lepton number asymmetry which can then be converted

to the baryon asymmetry by electro-weak sphalerons. In this way, the problem of the matter-antimatter asymmetry is also solved.

In Chapter 8 we examined a classically scale-invariant extension of the SM, enlarged by a weakly coupled dark $SU(3)_X$ gauge group. The extra sector consists of the eight dark gauge bosons and two complex scalar triplets. Under mild assumptions on the parameters of the scalar potential of the model the scalar triplets can develop nonvanishing VEVs and break the extra $SU(3)_X$ completely via the Coleman-Weinberg mechanism. Eight of the 12 scalar degrees of freedom are absorbed by the dark gauge bosons, rendering them all massive. We focused on and analyzed the case in which the symmetry breaking pattern involves two VEVs. As a result of the portal couplings of the dark scalars to the Higgs field, the dark gauge symmetry breakdown triggers electroweak symmetry breaking. In the framework of the Gildener-Weinberg formalism, we considered the full one-loop effective potential. At one-loop level the pseudo–Nambu-Goldstone boson of broken classical scale symmetry receives a large radiative mass. Out of the massive dark gauge bosons the lightest three of them are almost degenerate in mass and also stable due to an intrinsic $Z_2 \times Z_2'$ discrete symmetry of $SU(3)_X$. These are identified as DM candidates.

The parameters of the model and the mass patterns resulting from symmetry breaking were subsequently subjected to the various existing theoretical and experimental constraints. The requirements on the tree-level and one-loop effective scalar potential to be bounded from below were analyzed. Constraints arising from LHC searches and measurements of the electroweak parameters S and T were also examined. Thus, we obtained five benchmark points for the parameters of the model that stabilize the vacuum, satisfy the experimental constraints, and reproduce the measured mass for the observed Higgs boson.

Having analyzed the phenomenological viability of the model, a comprehensive DM analysis was undertaken. After identifying the relevant DM processes (annihilations, semiannihilations, coannihilations, and DM conversions), the set of coupled Boltzmann equations was constructed, describing the number density evolution of the DM candidates in order to obtain their total relic density and compare it to the measured value. The Boltzmann equations were solved numerically in two cases defined by the VEVs of the $SU(3)_X$ scalar fields.

In the first case, the VEV separation was large ($v_1^2 \gg v_2^2$) and the three dark gauge boson candidates X^1, X^2, and $X^{3'}$ were nearly degenerate in mass. This case may seem similar to the dark $SU(2)_X$ model where the extra gauge symmetry gets broken by a complex scalar doublet. There, the three dark gauge bosons are completely degenerate in mass and contribute equally to the DM relic density. In the $SU(3)_X$ model, however, even though $X^{1,2,3'}$ are nearly degenerate in mass, the lightest of the three ($X^{3'}$) is the predominant DM component. This occurs mainly due to the mixing between $X^{3'}$ and $X^{8'}$ which means that more Feynman diagrams contribute to the semi-annihilation processes $X^{1,2}X^{1,2} \to X^{3'}h_i$ and the annihilation processes $X^{3'}X^{3'} \to h_i h_j$. Also, even though the mass splitting is small, some of the $X^{1,2}$ particles are converted to $X^{3'}$ and increase its final relic density. Finally, as it is transparent in the framework of the GW formalism employed, the pNGB mass depends on all the other masses of the model. Consequently, there can be only one resonant dip for the DM relic density in the $SU(2)_X$ model (corresponding to $M_{\text{Higgs}}/2$) and two in the $SU(3)_X$ model (corresponding to $M_{h_1}/2$ and $M_{h_3}/2$). Therefore, in general, enlarging the gauge group means that more scalars are needed in order to break it, which leads to a larger parameter space that may be compatible with cosmological observations.

In the second case, the VEVs were very close ($v_1 \simeq v_2$). This resulted in $X^{3'}$ being around 20% lighter than X^1, X^2 (which were exactly degenerate) and X^4, X^5 (which were exactly degenerate too) now being close in mass with X^1 and X^2. Therefore, possible coannihilation effects had to be examined. Nevertheless, it turned out that the dominant process was DM conversion and $X^{3'}$ was

again the predominant DM component. Finally, we determined that the DM candidates have viable prospects of being directly detected by future underground experiments.

This model was reconsidered in [422], albeit without classical scale invariance. There, the authors examined all possible combinations for the particles that could constitute dark matter.

In Chapter 9, we began by briefly reviewing the frame and reparametrization invariant formalism of scalar-tensor theories developed in [203–206, 655]. This formalism proves to be useful for inflation since it allows us to classify various models based on their invariant potentials. Therefore, it becomes transparent why theories with very different physical motivations yield similar predictions for the inflationary observables.

Motivated by the imminent advancement in the sensitivity of the experiments, we then calculated the tensor and scalar spectral indices as well as the tensor-to-scalar ratio up to third order in the HSRPs in both the Einstein and Jordan frames employing the Green's function method introduced in [55]. After this, utilizing the relation between the HSRPs in the two frames, we showed the equivalence of the frames. By construction, the Green's function method is valid to arbitrary order in the slow-roll expansion. Therefore, we expect the equivalence to hold up to any order. In addition, since the HSRPs are related to the PSRPs, we expressed the spectral indices and the ratio in terms of the PSRPs which are manifestly invariant.

Nevertheless, since the definition of the number of e-folds is different in the two frames, this can result to different predictions for the observables. We demonstrated this difference by considering the nonminimally coupled Coleman-Weinberg model examined in [148] and saw that as the nonminimal coupling grows so does the difference in the predictions. Such a difference can in fact be larger than the differences between the first and third order results and will be detectable by the planned future experiments. We regard the Jordan frame definition for the number of e-folds (9.111) as *the* fundamental one since it can be expressed in terms of all the principal invariants and also includes the Einstein definition. Furthermore, we examined how various end-of-inflation conditions affect the inflationary observables. We found that the differences between the methods are comparable to the differences between the first and third order results.

The above discussion proves that with the advent of precision experiments, care must be taken when analyzing a given inflationary model since the underlying methods and assumptions used may play an instrumental role in determining the viability of said model.

A possible future direction would be to construct classically scale-invariant models where the strong CP problem and the rest of the SM problems are also solved. Furthermore, it would be worth investigating how a viable inflationary model where the Planck mass is dynamically generated could be connected through the reheating process to the rest of the scales examined here and explore what possible phenomenological implications such a model could have.

Appendix A

Oblique parameters

The S and T parameters are given in the model discussed in Chapter 8 by the expressions (see also [379, 405, 518])

$$\begin{aligned} S &= \frac{1}{24\pi}\Bigg\{\mathcal{R}_{11}^2\left[\log R_{h_1 h} + G(M_{h_1}^2, M_Z^2) - G(M_h^2, M_Z^2)\right] \\ &\quad + \mathcal{R}_{12}^2\left[\log R_{h_2 h} + G(M_{h_2}^2, M_Z^2) - G(M_h^2, M_Z^2)\right] \\ &\quad + \mathcal{R}_{13}^2\left[\log R_{h_3 h} + G(M_{h_3}^2, M_Z^2) - G(M_h^2, M_Z^2)\right]\Bigg\}, \end{aligned} \tag{A.1}$$

$$\begin{aligned} T &= \frac{3}{16\pi \sin^2\theta_W}\Bigg\{\mathcal{R}_{11}^2\left[\frac{1}{\cos^2\theta_W}\left(\frac{\log R_{Zh_1}}{1-R_{Zh_1}} - \frac{\log R_{Zh}}{1-R_{Zh}}\right) - \left(\frac{\log R_{Wh_1}}{1-R_{Wh_1}} - \frac{\log R_{Wh}}{1-R_{Wh}}\right)\right] \\ &\quad + \mathcal{R}_{12}^2\left[\frac{1}{\cos^2\theta_W}\left(\frac{\log R_{Zh_2}}{1-R_{Zh_2}} - \frac{\log R_{Zh}}{1-R_{Zh}}\right) - \left(\frac{\log R_{Wh_2}}{1-R_{Wh_2}} - \frac{\log R_{Wh}}{1-R_{Wh}}\right)\right] \\ &\quad + \mathcal{R}_{13}^2\left[\frac{1}{\cos^2\theta_W}\left(\frac{\log R_{Zh_3}}{1-R_{Zh_3}} - \frac{\log R_{Zh}}{1-R_{Zh}}\right) - \left(\frac{\log R_{Wh_3}}{1-R_{Wh_3}} - \frac{\log R_{Wh}}{1-R_{Wh}}\right)\right]\Bigg\}, \end{aligned} \tag{A.2}$$

where the functions R_{AB}, $G(m_A^2, m_B^2)$, and $f(R_{AB})$ are given by

$$R_{AB} = \frac{M_A^2}{M_B^2}, \tag{A.3}$$

$$\begin{aligned} G(M_A^2, M_B^2) &= -\frac{79}{3} + 9R_{AB} - 2R_{AB}^2 + (12 - 4R_{AB} + R_{AB}^2) f(R_{AB}) \\ &\quad + (-10 + 18R_{AB} - 6R_{AB}^2 + R_{AB}^3 - 9\frac{R_{AB}+1}{R_{AB}-1})\log R_{AB}, \end{aligned} \tag{A.4}$$

$$f(R_{AB}) = \begin{cases} \sqrt{R_{AB}(R_{AB}-4)}\log\left|\frac{R_{AB}-2-\sqrt{R_{AB}(R_{AB}-4)}}{2}\right| & R_{AB} > 4, \\ 0 & R_{AB} = 4, \\ 2\sqrt{R_{AB}(4-R_{AB})}\arctan\sqrt{\frac{4-R_{AB}}{R_{AB}}} & R_{AB} < 4. \end{cases} \tag{A.5}$$

Appendix B

Renormalization group equations

In this appendix, we present the two-loop gauge RGEs, as well as the one-loop RGEs for the Yukawa and scalar couplings for the model discussed in Chapter 8. However, in our numerical analysis we used the full set of two-loop RGEs obtained using SARAH [612,613]. Defining $\beta_\kappa \equiv (4\pi)^2 \frac{d\kappa}{d\ln\mu}$, the RGEs have the form

$$\beta_{g_1} = \frac{41}{10}g_1^3 + \frac{1}{(4\pi)^2}\frac{1}{50}g_1^3\Big(199g_1^2 + 135g_2^2 + 440g_3^2 - 85y_t^2\Big), \tag{B.1}$$

$$\beta_{g_2} = -\frac{19}{6}g_2^3 + \frac{1}{(4\pi)^2}\frac{1}{30}g_2^3\Big(27g_1^2 + 175g_2^2 + 360g_3^2 - 45y_t^2\Big), \tag{B.2}$$

$$\beta_{g_3} = -7g_3^3 + \frac{1}{(4\pi)^2}\frac{1}{10}g_3^3\Big(11g_1^2 + 45g_2^2 - 260g_3^2 - 20y_t^2\Big), \tag{B.3}$$

$$\beta_{g_X} = -\frac{32}{3}g_X^3 - \frac{1}{(4\pi)^2}\frac{284}{3}g_X^5, \tag{B.4}$$

$$\beta_{y_t} = y_t\left(\frac{9}{2}y_t^2 - \frac{17}{20}g_1^2 - \frac{9}{4}g_2^2 - 8g_3^2\right), \tag{B.5}$$

$$\beta_{\lambda_h} = -6y_t^4 + 24\lambda_h^2 + \lambda_h\left(12y_t^2 - \frac{9}{5}g_1^2 - 9g_2^2\right) + \frac{27}{200}g_1^4 + \frac{9}{20}g_1^2g_2^2 + \frac{9}{8}g_2^4 + 3\lambda_{h1}^2 + 3\lambda_{h2}^2, \tag{B.6}$$

$$\beta_{\lambda_1} = -16g_X^2\lambda_1 + 28\lambda_1^2 - 2\lambda_3\lambda_4 + 2\lambda_{h1}^2 + 3\lambda_3^2 + \frac{13}{6}g_X^4 + \lambda_4^2 + \lambda_5^2, \tag{B.7}$$

$$\beta_{\lambda_2} = -16g_X^2\lambda_2 + 28\lambda_2^2 - 2\lambda_3\lambda_4 + 2\lambda_{h2}^2 + 3\lambda_3^2 + \frac{13}{6}g_X^4 + \lambda_4^2 + \lambda_5^2, \tag{B.8}$$

$$\beta_{\lambda_{h1}} = \lambda_{h1}\left(-\frac{9}{10}g_1^2 - \frac{9}{2}g_2^2 - 8g_X^2 + 12\lambda_h - 4\lambda_{h1} + 16\lambda_1 + 6y_t^2\right) + 6\lambda_{h2}\lambda_3 - 2\lambda_{h2}\lambda_4, \tag{B.9}$$

$$\beta_{\lambda_{h2}} = \lambda_{h2}\left(-\frac{9}{10}g_1^2 - \frac{9}{2}g_2^2 - 8g_X^2 + 12\lambda_h - 4\lambda_{h2} + 16\lambda_1 + 6y_t^2\right) + 6\lambda_{h1}\lambda_3 - 2\lambda_{h1}\lambda_4, \tag{B.10}$$

$$\beta_{\lambda_3} = \lambda_3\left(-16g_X^2 + 16\lambda_2 + 16\lambda_1 - 4\lambda_3\right) - 2\lambda_4^2 - 2\lambda_5^2 - 4\lambda_1\lambda_4 - 4\lambda_2\lambda_4 + 4\lambda_{h1}\lambda_{h2} - \frac{11}{6}g_X^4, \tag{B.11}$$

$$\beta_{\lambda_4} = 10\lambda_5^2 - 16g_X^2\lambda_4 + 4\lambda_1\lambda_4 + 4\lambda_2\lambda_4 + 6\lambda_4^2 - 8\lambda_3\lambda_4 + \frac{5}{2}g_X^4, \tag{B.12}$$

$$\beta_{\lambda_5} = 4\lambda_5\left(-2\lambda_3 - 4g_X^2 + 4\lambda_4 + \lambda_1 + \lambda_2\right). \tag{B.13}$$

For the SM gauge couplings and the top quark Yukawa coupling we specify the boundary conditions at the top quark pole mass M_t [4,571],

$$g_1(\mu = M_t) = \sqrt{\frac{5}{3}}\left(0.35830 + 0.00011\left(\frac{M_t}{\text{GeV}} - 173.34\right) - 0.00020\left(\frac{M_W - 80.384\,\text{GeV}}{0.014\,\text{GeV}}\right)\right), \tag{B.14}$$

$$g_2(\mu = M_t) = 0.64779 + 0.00004\left(\frac{M_t}{\text{GeV}} - 173.34\right) + 0.00011\left(\frac{M_W - 80.384\,\text{GeV}}{0.014\,\text{GeV}}\right), \tag{B.15}$$

$$g_3(\mu = M_t) = 1.1666 + 0.00314\left(\frac{\alpha_s(M_Z) - 0.1184}{0.0007}\right) - 0.00046\left(\frac{M_t}{\text{GeV}} - 173.34\right), \tag{B.16}$$

$$y_t(\mu = M_t) = 0.93690 + 0.00556\left(\frac{M_t}{\text{GeV}} - 173.34\right) - 0.00042\left(\frac{\alpha_s(M_Z) - 0.1184}{0.0007}\right), \tag{B.17}$$

whereas the dark gauge coupling is defined at the scale of the lightest dark gauge boson $g_X(M_{X^{3'}})$. The boundary conditions for the scalar couplings are specified at the renormalization scale Λ where the tree-level potential is minimized.

Appendix C

From Hubble to potential slow-roll parameters

The HSRPs are related to the PSRPs up to third order in the Taylor expansion via the following expressions [32]:

$$\epsilon_H = \epsilon_V - \frac{4}{3}\epsilon_V^2 + \frac{2}{3}\epsilon_V\eta_V + \frac{32}{9}\epsilon_V^3 + \frac{5}{9}\epsilon_V\eta_V^2 - \frac{10}{3}\epsilon_V^2\eta_V + \frac{2}{9}\epsilon_V\zeta_V^2, \tag{C.1}$$

$$\eta_H = \eta_V - \epsilon_V + \frac{8}{3}\epsilon_V^2 + \frac{1}{3}\eta_V^2 - \frac{8}{3}\epsilon_V\eta_V + \frac{1}{3}\zeta_V^2 - 12\epsilon_V^3 + \frac{2}{9}\eta_V^3 + 16\epsilon_V^2\eta_V - \frac{46}{9}\epsilon_V\eta_V^2 - \frac{17}{9}\epsilon_V\zeta_V^2 + \frac{2}{3}\eta_V\zeta_V^2 + \frac{1}{9}\rho_V^3, \tag{C.2}$$

$$\zeta_H^2 = \zeta_V^2 - 3\epsilon_V\eta_V + 3\epsilon_V^2 - 20\epsilon_V^3 + 26\epsilon_V^2\eta_V - 7\epsilon_V\eta_V^2 - \frac{13}{3}\epsilon_V\zeta_V^2 + \frac{4}{3}\eta_V\zeta_V^2 + \frac{1}{3}\rho_V^3, \tag{C.3}$$

$$\rho_H^3 = \rho_V^3 - 3\epsilon_V\eta_V^2 + 18\epsilon_V^2\eta_V - 15\epsilon_V^3 - 4\epsilon_V\zeta_V^2. \tag{C.4}$$

Appendix D

Runnings of the spectral indices

The runnings of the tensor and scalar spectral indices up to third order in the HSRPs are given in the JF by

$$\frac{\mathrm{d}\bar{n}_T}{\mathrm{d}\ln k} = -2\bar{\kappa}_0\bar{\kappa}_1 - 6\bar{\kappa}_0\bar{\kappa}_1\bar{\lambda}_0 - 4\bar{\kappa}_0\bar{\lambda}_0\bar{\lambda}_1 - 6\bar{\kappa}_0^2\bar{\kappa}_1 + (2\alpha-2)\left(\bar{\kappa}_0\bar{\kappa}_1^2 + \bar{\kappa}_0\bar{\kappa}_1\bar{\kappa}_1\right), \tag{D.1}$$

$$\begin{aligned}\frac{\mathrm{d}\bar{n}_S}{\mathrm{d}\ln k} = {} & -2\bar{\kappa}_0\bar{\kappa}_1 - \bar{\kappa}_1\bar{\kappa}_2 - 6\bar{\kappa}_0\bar{\kappa}_1\bar{\lambda}_0 - 4\bar{\kappa}_0\bar{\lambda}_0\bar{\lambda}_1 - \bar{\kappa}_1\bar{\lambda}_0\bar{\lambda}_1 - 2\bar{\kappa}_1\bar{\kappa}_2\bar{\lambda}_0 - 2\bar{\lambda}_0\bar{\lambda}_1\bar{\lambda}_2 \\ & -2\bar{\lambda}_0\bar{\lambda}_1^2 - 6\bar{\kappa}_0^2\bar{\kappa}_1 + (2\alpha-3)\,\bar{\kappa}_0\bar{\kappa}_1^2 + (2\alpha-4)\,\bar{\kappa}_0\bar{\kappa}_1\bar{\kappa}_2 + \alpha\left(\bar{\kappa}_1\bar{\kappa}_2^2 + \bar{\kappa}_1\bar{\kappa}_2\bar{\kappa}_3\right),\end{aligned} \tag{D.2}$$

while in the EF the runnings have the form

$$\frac{\mathrm{d}\hat{n}_T}{\mathrm{d}\ln k} = -2\hat{\kappa}_0\hat{\kappa}_1 - 6\hat{\kappa}_0^2\hat{\kappa}_1 + (2\alpha-2)\left(\hat{\kappa}_0\hat{\kappa}_1^2 + \hat{\kappa}_0\hat{\kappa}_1\hat{\kappa}_1\right), \tag{D.3}$$

$$\begin{aligned}\frac{\mathrm{d}\hat{n}_S}{\mathrm{d}\ln k} = {} & -2\hat{\kappa}_0\hat{\kappa}_1 - \hat{\kappa}_1\hat{\kappa}_2 - 6\hat{\kappa}_0^2\hat{\kappa}_1 + (2\alpha-3)\,\hat{\kappa}_0\hat{\kappa}_1^2 + (2\alpha-4)\,\hat{\kappa}_0\hat{\kappa}_1\hat{\kappa}_2 \\ & +\alpha\left(\hat{\kappa}_1\hat{\kappa}_2^2 + \hat{\kappa}_1\hat{\kappa}_2\hat{\kappa}_3\right).\end{aligned} \tag{D.4}$$

Again, plugging (9.96) - (9.99) into the EF expressions, one can see that the expressions for the runnings of the spectral indices in the two frames coincide. Finally, the runnings of the spectral indices can be written in terms of the PSRPs as

$$\begin{aligned}\frac{\mathrm{d}n_T}{\mathrm{d}\ln k} = {} & -8\epsilon_V^2 + 4\epsilon_V\eta_V + \left(52\alpha - \frac{148}{3}\right)\epsilon_V^3 - (50\alpha-38)\,\epsilon_V^2\eta_V \\ & + (16\alpha-12)\,\epsilon_V\eta_V^2 + \left(4\alpha - \frac{8}{3}\right)\epsilon_V\zeta_V^2,\end{aligned} \tag{D.5}$$

$$\begin{aligned}\frac{\mathrm{d}n_S}{\mathrm{d}\ln k} = {} & -24\epsilon_V^2 + 16\epsilon_V\eta_V - 2\zeta_V^2 + \left(180\alpha - \frac{104}{3}\right)\epsilon_V^3 - \left(180\alpha + \frac{4}{3}\right)\epsilon_V^2\eta_V \\ & + (32\alpha+12)\,\epsilon_V\eta_V^2 + (24\alpha+4)\,\epsilon_V\zeta_V^2 - \left(2\alpha - \frac{8}{3}\right)\eta_V\zeta_V^2 - \left(2\alpha + \frac{2}{3}\right)\rho_V^3.\end{aligned} \tag{D.6}$$

Appendix E

Equation of motion in terms of e-folds

We can rewrite the equation of motion for the invariant $\mathcal{I}_\phi$ as a nonlinear second order differential equation with respect to the number of e-folds. In the Einstein frame we have

$$\frac{\mathrm{d}^2\mathcal{I}_\phi}{\mathrm{d}\hat{N}^2}+3\frac{\mathrm{d}\mathcal{I}_\phi}{\mathrm{d}\hat{N}}-\left(\frac{\mathrm{d}\mathcal{I}_\phi}{\mathrm{d}\hat{N}}\right)^3+\left[1-\frac{1}{3}\left(\frac{\mathrm{d}\mathcal{I}_\phi}{\mathrm{d}\hat{N}}\right)^2\right]3\sqrt{\epsilon_V}=0, \tag{E.1}$$

while in the Jordan frame the equation of motion can be brought to the following form:

$$\begin{aligned}\frac{\mathrm{d}^2\mathcal{I}_\phi}{\mathrm{d}\bar{N}^2}+3\frac{\mathrm{d}\mathcal{I}_\phi}{\mathrm{d}\bar{N}}+\frac{\mathrm{d}\mathcal{I}_\phi}{\mathrm{d}\bar{N}}\left[1-\frac{1}{2}\frac{\mathrm{d}\ln\mathcal{I}_m}{\mathrm{d}\bar{N}}\right]^{-1}\left[-\frac{1}{2}\frac{\mathrm{d}\ln\mathcal{I}_m}{\mathrm{d}\bar{N}}+\frac{1}{4}\left(\frac{\mathrm{d}\ln\mathcal{I}_m}{\mathrm{d}\bar{N}}\right)^2-\left(\frac{\mathrm{d}\mathcal{I}_\phi}{\mathrm{d}\bar{N}}\right)^2+\frac{1}{2}\frac{\mathrm{d}^2\ln\mathcal{I}_m}{\mathrm{d}\bar{N}^2}\right]\\ -\frac{\mathrm{d}\ln\mathcal{I}_m}{\mathrm{d}\bar{N}}\frac{\mathrm{d}\mathcal{I}_\phi}{\mathrm{d}\bar{N}}+\left[1+\frac{1}{4}\left(\frac{\mathrm{d}\ln\mathcal{I}_m}{\mathrm{d}\bar{N}}\right)^2-\frac{\mathrm{d}\ln\mathcal{I}_m}{\mathrm{d}\bar{N}}-\frac{1}{3}\left(\frac{\mathrm{d}\mathcal{I}_\phi}{\mathrm{d}\bar{N}}\right)^2\right]3\sqrt{\epsilon_V}=0.\end{aligned} \tag{E.2}$$

By numerically solving these equations we can obtain the invariant field as a function of the number of e-folds in the two frames. Of course, in the case with minimal coupling we have $\frac{\mathrm{d}\ln\mathcal{I}_m}{\mathrm{d}\bar{N}}=\frac{\mathrm{d}^2\ln\mathcal{I}_m}{\mathrm{d}\bar{N}^2}=0$ and $\bar{N}=\hat{N}$, which means that (E.2) reduces to (E.1).

Bibliography

[1] **Planck** Collaboration, P. A. R. Ade *et al.*, "Planck 2015 results. XIII. Cosmological parameters," *Astron. Astrophys.* **594** (2015) A13, arXiv:1502.01589 [astro-ph.CO].

[2] V. Faraoni, *Cosmology in scalar tensor gravity*. 2004.

[3] G. Degrassi, S. Di Vita, J. Elias-Miro, J. R. Espinosa, G. F. Giudice, *et al.*, "Higgs mass and vacuum stability in the Standard Model at NNLO," *JHEP* **1208** (2012) 098, arXiv:1205.6497 [hep-ph].

[4] D. Buttazzo, G. Degrassi, P. P. Giardino, G. F. Giudice, F. Sala, *et al.*, "Investigating the near-criticality of the Higgs boson," *JHEP* **1312** (2013) 089, arXiv:1307.3536 [hep-ph].

[5] G. 't Hooft, "Naturalness, chiral symmetry, and spontaneous chiral symmetry breaking," *NATO Sci. Ser. B* **59** (1980) 135–157.

[6] W. A. Bardeen, "On naturalness in the standard model," in *Ontake Summer Institute on Particle Physics Ontake Mountain, Japan, August 27-September 2, 1995*. 1995. http://lss.fnal.gov/cgi-bin/find_paper.pl?conf-95-391.

[7] S. R. Coleman and E. J. Weinberg, "Radiative Corrections as the Origin of Spontaneous Symmetry Breaking," *Phys.Rev.* **D7** (1973) 1888–1910.

[8] A. Einstein, "The Foundation of the General Theory of Relativity," *Annalen Phys.* **49** no. 7, (1916) 769–822. [Annalen Phys.14,517(2005)].

[9] A. A. Penzias and R. W. Wilson, "A Measurement of excess antenna temperature at 4080-Mc/s," *Astrophys. J.* **142** (1965) 419–421.

[10] G. Efstathiou, J. R. Bond, and S. D. M. White, "COBE Background radiation anisotropies and large scale structure in the universe," *Mon. Not. Roy. Astron. Soc.* **258** (1992) 1–6.

[11] L. A. Kofman, N. Y. Gnedin, and N. A. Bahcall, "Cosmological constant, COBE cosmic microwave background anisotropy, and large scale clustering," *Astrophys. J.* **413** (1993) 1–9.

[12] V. Mukhanov, *Physical Foundations of Cosmology*. Cambridge University Press, Oxford, 2005. http://www-spires.fnal.gov/spires/find/books/www?cl=QB981.M89::2005.

[13] S. Weinberg, *The First Three Minutes. A Modern View of the Origin of the Universe*. 1977. http://www.amazon.com/The-First-Three-Minutes-Universe/dp/0465024378.

[14] **Supernova Search Team** Collaboration, A. G. Riess *et al.*, "Observational evidence from supernovae for an accelerating universe and a cosmological constant," *Astron. J.* **116** (1998) 1009–1038, arXiv:astro-ph/9805201 [astro-ph].

[15] **Supernova Cosmology Project** Collaboration, S. Perlmutter *et al.*, "Measurements of Omega and Lambda from 42 high redshift supernovae," *Astrophys. J.* **517** (1999) 565–586, arXiv:astro-ph/9812133 [astro-ph].

[16] A. Friedman, "On the Curvature of space," *Z. Phys.* **10** (1922) 377–386. [Gen. Rel. Grav.31,1991(1999)].

[17] A. Friedmann, "On the Possibility of a world with constant negative curvature of space," *Z. Phys.* **21** (1924) 326–332. [Gen. Rel. Grav.31,2001(1999)].

[18] H. P. Robertson, "Relativistic Cosmology," *Rev. Mod. Phys.* **5** (1933) 62–90.

[19] H. P. Robertson, "Kinematics and World-Structure," *Astrophys. J.* **82** (1935) 284–301.

[20] H. P. Robertson, "Kinematics and World-Structure. 2," *Astrophys. J.* **83** (1935) 187–201.

[21] H. P. Robertson, "Kinematics and World-Structure. 3," *Astrophys. J.* **83** (1936) 257–271.

[22] G. Lemaitre, "The expanding universe," *Gen. Rel. Grav.* **29** (1997) 641–680. [Annales Soc. Sci. Bruxelles A53,51(1933)].

[23] W. O. Kermack and W. H. McCrea, "On Milne's theory of world structure," *MNRAS* **93** (May, 1933) 519–529.

[24] A. Raychaudhuri, "Relativistic cosmology. 1.," *Phys. Rev.* **98** (1955) 1123–1126.

[25] N. Suzuki *et al.*, "The Hubble Space Telescope Cluster Supernova Survey: V. Improving the Dark Energy Constraints Above z>1 and Building an Early-Type-Hosted Supernova Sample," *Astrophys. J.* **746** (2012) 85, arXiv:1105.3470 [astro-ph.CO].

[26] A. H. Guth, "The Inflationary Universe: A Possible Solution to the Horizon and Flatness Problems," *Phys. Rev.* **D23** (1981) 347–356.

[27] A. D. Linde, "A New Inflationary Universe Scenario: A Possible Solution of the Horizon, Flatness, Homogeneity, Isotropy and Primordial Monopole Problems," *Phys. Lett.* **108B** (1982) 389–393.

[28] S. W. Hawking, "The Development of Irregularities in a Single Bubble Inflationary Universe," *Phys. Lett.* **115B** (1982) 295.

[29] A. A. Starobinsky, "Dynamics of Phase Transition in the New Inflationary Universe Scenario and Generation of Perturbations," *Phys. Lett.* **117B** (1982) 175–178.

[30] A. H. Guth and S. Y. Pi, "Fluctuations in the New Inflationary Universe," *Phys. Rev. Lett.* **49** (1982) 1110–1113.

[31] A. D. Linde, "Chaotic Inflation," *Phys. Lett.* **129B** (1983) 177–181.

[32] A. R. Liddle, P. Parsons, and J. D. Barrow, "Formalizing the slow roll approximation in inflation," *Phys. Rev.* **D50** (1994) 7222–7232, arXiv:astro-ph/9408015 [astro-ph].

[33] D. H. Lyth and A. Riotto, "Particle physics models of inflation and the cosmological density perturbation," *Physics Reports* **314** no. 1, (1999) 1–146, arXiv:hep-ph/9807278 [hep-ph].

[34] A. D. Linde, "Inflationary Cosmology," *Lect. Notes Phys.* **738** (2008) 1–54, arXiv:0705.0164 [hep-th].

[35] D. Baumann, "Inflation," in *Physics of the large and the small, TASI 09, proceedings of the Theoretical Advanced Study Institute in Elementary Particle Physics, Boulder, Colorado, USA, 1-26 June 2009*, pp. 523–686. 2011. arXiv:0907.5424 [hep-th]. http://inspirehep.net/record/827549/files/arXiv:0907.5424.pdf.

[36] J. Martin, C. Ringeval, and V. Vennin, "Encyclopaedia inflationaris," 1303.3787v3.

[37] L. Kofman, A. D. Linde, and A. A. Starobinsky, "Reheating after inflation," *Phys. Rev. Lett.* **73** (1994) 3195–3198, arXiv:hep-th/9405187 [hep-th].

[38] L. Kofman, A. D. Linde, and A. A. Starobinsky, "Towards the theory of reheating after inflation," *Phys. Rev.* **D56** (1997) 3258–3295, arXiv:hep-ph/9704452 [hep-ph].

[39] B. A. Bassett, S. Tsujikawa, and D. Wands, "Inflation dynamics and reheating," *Rev. Mod. Phys.* **78** (2006) 537–589, arXiv:astro-ph/0507632 [astro-ph].

[40] A. R. Liddle and S. M. Leach, "How long before the end of inflation were observable perturbations produced?," *Phys. Rev.* **D68** (2003) 103503, arXiv:astro-ph/0305263 [astro-ph].

[41] S. Dodelson and L. Hui, "A Horizon ratio bound for inflationary fluctuations," *Phys. Rev. Lett.* **91** (2003) 131301, arXiv:astro-ph/0305113 [astro-ph].

[42] C. F. Steinwachs, *Non-minimal Higgs inflation and frame dependence in cosmology*. PhD thesis, Cologne U., New York, 2012. http://www.springer.com/astronomy/cosmology/book/978-3-319-01841-6.

[43] E. Bertschinger, "Cosmological perturbation theory and structure formation," in *Cosmology 2000: Proceedings, Conference, Lisbon, Portugal, 12-15 Jul 2000*, pp. 1–25. 2001. arXiv:astro-ph/0101009 [astro-ph].

[44] J. M. Stewart, "Perturbations of Friedmann-Robertson-Walker cosmological models," *Class. Quant. Grav.* **7** (1990) 1169–1180.

[45] J. M. Bardeen, "Gauge Invariant Cosmological Perturbations," *Phys. Rev.* **D22** (1980) 1882–1905.

[46] V. F. Mukhanov, "Quantum Theory of Gauge Invariant Cosmological Perturbations," *Sov. Phys. JETP* **67** (1988) 1297–1302. [Zh. Eksp. Teor. Fiz.94N7,1(1988)].

[47] M. Sasaki, "Large Scale Quantum Fluctuations in the Inflationary Universe," *Prog. Theor. Phys.* **76** (1986) 1036.

[48] V. F. Mukhanov, H. A. Feldman, and R. H. Brandenberger, "Theory of cosmological perturbations. Part 1. Classical perturbations. Part 2. Quantum theory of perturbations. Part 3. Extensions," *Phys. Rept.* **215** (1992) 203–333.

[49] A. L. Alinea, T. Kubota, and W. Naylor, "Logarithmic divergences in the k-inflationary power spectra computed through the uniform approximation," *JCAP* **1602** no. 02, (2016) 028, arXiv:1506.08344 [gr-qc].

[50] T. S. Bunch and P. C. W. Davies, "Quantum Field Theory in de Sitter Space: Renormalization by Point Splitting," *Proc. Roy. Soc. Lond.* **A360** (1978) 117–134.

[51] **Planck** Collaboration, P. A. R. Ade *et al.*, "Planck 2015 results. XX. Constraints on inflation," *Astron. Astrophys.* **594** (2016) A20, arXiv:1502.02114 [astro-ph.CO].

[52] **CORE** Collaboration, F. Finelli *et al.*, "Exploring Cosmic Origins with CORE: Inflation," arXiv:1612.08270 [astro-ph.CO].

[53] E. D. Stewart and D. H. Lyth, "A More accurate analytic calculation of the spectrum of cosmological perturbations produced during inflation," *Phys. Lett.* **B302** (1993) 171–175, arXiv:gr-qc/9302019 [gr-qc].

[54] E. D. Stewart, "The Spectrum of density perturbations produced during inflation to leading order in a general slow roll approximation," *Phys. Rev.* **D65** (2002) 103508, arXiv:astro-ph/0110322 [astro-ph].

[55] J.-O. Gong and E. D. Stewart, "The Density perturbation power spectrum to second order corrections in the slow roll expansion," *Phys. Lett.* **B510** (2001) 1–9, arXiv:astro-ph/0101225 [astro-ph].

[56] J.-O. Gong, "General slow-roll spectrum for gravitational waves," *Class. Quant. Grav.* **21** (2004) 5555–5562, arXiv:gr-qc/0408039 [gr-qc].

[57] H.-s. Kim, G. S. Lee, H. W. Lee, and Y. S. Myung, "Second order corrections to noncommutative space-time inflation," *Phys. Rev.* **D70** (2004) 043521, arXiv:hep-th/0402198 [hep-th].

[58] H. Wei, R.-G. Cai, and A. Wang, "Second-order corrections to the power spectrum in the slow-roll expansion with a time-dependent sound speed," *Phys. Lett.* **B603** (2004) 95–106, arXiv:hep-th/0409130 [hep-th].

[59] H.-s. Kim, G. S. Lee, and Y. S. Myung, "Noncommutative space-time effect on the slow roll period of inflation," *Mod. Phys. Lett.* **A20** (2005) 271–284, arXiv:hep-th/0402018 [hep-th].

[60] K. Kadota, S. Dodelson, W. Hu, and E. D. Stewart, "Precision of inflaton potential reconstruction from CMB using the general slow-roll approximation," *Phys. Rev.* **D72** (2005) 023510, arXiv:astro-ph/0505158 [astro-ph].

[61] M. Joy, E. D. Stewart, J.-O. Gong, and H.-C. Lee, "From the spectrum to inflation: An Inverse formula for the general slow-roll spectrum," *JCAP* **0504** (2005) 012, arXiv:astro-ph/0501659 [astro-ph].

[62] C. Dvorkin and W. Hu, "Complete WMAP Constraints on Bandlimited Inflationary Features," *Phys. Rev.* **D84** (2011) 063515, arXiv:1106.4016 [astro-ph.CO].

[63] P. Adshead, W. Hu, C. Dvorkin, and H. V. Peiris, "Fast Computation of Bispectrum Features with Generalized Slow Roll," *Phys. Rev.* **D84** (2011) 043519, arXiv:1102.3435 [astro-ph.CO].

[64] K. Kumazaki, S. Yokoyama, and N. Sugiyama, "Fine Features in the Primordial Power Spectrum," *JCAP* **1112** (2011) 008, arXiv:1105.2398 [astro-ph.CO].

[65] V. Miranda, W. Hu, and P. Adshead, "Warp Features in DBI Inflation," *Phys. Rev.* **D86** (2012) 063529, arXiv:1207.2186 [astro-ph.CO].

[66] P. Adshead, W. Hu, and V. Miranda, "Bispectrum in Single-Field Inflation Beyond Slow-Roll," *Phys. Rev.* **D88** no. 2, (2013) 023507, arXiv:1303.7004 [astro-ph.CO].

[67] J. Beltran Jimenez, M. Musso, and C. Ringeval, "Exact Mapping between Tensor and Most General Scalar Power Spectra," *Phys. Rev.* **D88** (2013) 043524, arXiv:1303.2788 [astro-ph.CO].

[68] P. Adshead and W. Hu, "Bounds on nonadiabatic evolution in single-field inflation," *Phys. Rev.* **D89** no. 8, (2014) 083531, arXiv:1402.1677 [astro-ph.CO].

[69] J.-O. Gong, K. Schalm, and G. Shiu, "Correlating correlation functions of primordial perturbations," *Phys. Rev.* **D89** no. 6, (2014) 063540, arXiv:1401.4402 [astro-ph.CO].

[70] A. Achucarro, V. Atal, B. Hu, P. Ortiz, and J. Torrado, "Inflation with moderately sharp features in the speed of sound: Generalized slow roll and in-in formalism for power

spectrum and bispectrum," *Phys. Rev.* **D90** no. 2, (2014) 023511, arXiv:1404.7522 [astro-ph.CO].

[71] H. Motohashi and W. Hu, "Running from Features: Optimized Evaluation of Inflationary Power Spectra," *Phys. Rev.* **D92** no. 4, (2015) 043501, arXiv:1503.04810 [astro-ph.CO].

[72] H. Motohashi and W. Hu, "Generalized Slow Roll in the Unified EFT of Inflation," arXiv:1704.01128 [hep-th].

[73] D. J. Schwarz, C. A. Terrero-Escalante, and A. A. Garcia, "Higher order corrections to primordial spectra from cosmological inflation," *Phys. Lett.* **B517** (2001) 243–249, arXiv:astro-ph/0106020 [astro-ph].

[74] J. Martin and D. J. Schwarz, "WKB approximation for inflationary cosmological perturbations," *Phys. Rev.* **D67** (2003) 083512, arXiv:astro-ph/0210090 [astro-ph].

[75] R. Casadio, F. Finelli, M. Luzzi, and G. Venturi, "Improved WKB analysis of slow-roll inflation," *Phys. Rev.* **D72** (2005) 103516, arXiv:gr-qc/0510103 [gr-qc].

[76] R. Casadio, F. Finelli, M. Luzzi, and G. Venturi, "Improved WKB analysis of cosmological perturbations," *Phys. Rev.* **D71** (2005) 043517, arXiv:gr-qc/0410092 [gr-qc].

[77] R. Casadio, F. Finelli, M. Luzzi, and G. Venturi, "Higher order slow-roll predictions for inflation," *Phys. Lett.* **B625** (2005) 1–6, arXiv:gr-qc/0506043 [gr-qc].

[78] S. Habib, A. Heinen, K. Heitmann, G. Jungman, and C. Molina-Paris, "Characterizing inflationary perturbations: The Uniform approximation," *Phys. Rev.* **D70** (2004) 083507, arXiv:astro-ph/0406134 [astro-ph].

[79] S. Habib, A. Heinen, K. Heitmann, and G. Jungman, "Inflationary perturbations and precision cosmology," *Phys. Rev.* **D71** (2005) 043518, arXiv:astro-ph/0501130 [astro-ph].

[80] L. Lorenz, J. Martin, and C. Ringeval, "K-inflationary Power Spectra in the Uniform Approximation," *Phys. Rev.* **D78** (2008) 083513, arXiv:0807.3037 [astro-ph].

[81] T. Zhu, A. Wang, G. Cleaver, K. Kirsten, and Q. Sheng, "Power spectra and spectral indices of k-inflation: high-order corrections," *Phys. Rev.* **D90** no. 10, (2014) 103517, arXiv:1407.8011 [astro-ph.CO].

[82] T. Zhu, A. Wang, G. Cleaver, K. Kirsten, and Q. Sheng, "Gravitational quantum effects on power spectra and spectral indices with higher-order corrections," *Phys. Rev.* **D90** no. 6, (2014) 063503, arXiv:1405.5301 [astro-ph.CO].

[83] C. Rojas and V. M. Villalba, "Computation of inflationary cosmological perturbations in chaotic inflationary scenarios using the phase-integral method," *Phys. Rev.* **D79** (2009) 103502, arXiv:0904.4295 [gr-qc].

[84] C. Rojas and V. M. Villalba, "Computation of the Power Spectrum in Chaotic $1/4\lambda\phi^4$ Inflation," *JCAP* **1201** (2012) 003, arXiv:1112.1342 [astro-ph.CO].

[85] Q. Wu, T. Zhu, and A. Wang, "Primordial Spectra of slow-roll inflation at second-order with the Gauss-Bonnet correction," arXiv:1707.08020 [gr-qc].

[86] G. Ballesteros and C. Tamarit, "Radiative plateau inflation," *JHEP* **02** (2016) 153, arXiv:1510.05669 [hep-ph].

[87] A. A. Starobinsky, "A New Type of Isotropic Cosmological Models Without Singularity," *Phys. Lett.* **91B** (1980) 99–102.

[88] C. Pallis and N. Toumbas, "Starobinsky Inflation: From Non-SUSY To SUGRA Realizations," *Adv. High Energy Phys.* **2017** (2017) 6759267, arXiv:1612.09202 [hep-ph].

[89] C. van de Bruck and L. E. Paduraru, "Simplest extension of Starobinsky inflation," *Phys. Rev.* **D92** (2015) 083513, arXiv:1505.01727 [hep-th].

[90] E. J. Copeland, C. Rahmede, and I. D. Saltas, "Asymptotically Safe Starobinsky Inflation," *Phys. Rev.* **D91** no. 10, (2015) 103530, arXiv:1311.0881 [gr-qc].

[91] A. Kehagias, A. M. Dizgah, and A. Riotto, "Remarks on the Starobinsky model of inflation and its descendants," *Phys. Rev.* **D89** no. 4, (2014) 043527, arXiv:1312.1155 [hep-th].

[92] T. Asaka, S. Iso, H. Kawai, K. Kohri, T. Noumi, and T. Terada, "Reinterpretation of the Starobinsky model," *PTEP* **2016** no. 12, (2016) 123E01, arXiv:1507.04344 [hep-th].

[93] F. L. Bezrukov and M. Shaposhnikov, "The Standard Model Higgs boson as the inflaton," *Phys. Lett.* **B659** (2008) 703–706, arXiv:0710.3755 [hep-th].

[94] F. Bezrukov and M. Shaposhnikov, "Standard Model Higgs boson mass from inflation: Two loop analysis," *JHEP* **07** (2009) 089, arXiv:0904.1537 [hep-ph].

[95] A. De Simone, M. P. Hertzberg, and F. Wilczek, "Running Inflation in the Standard Model," *Phys. Lett.* **B678** (2009) 1–8, arXiv:0812.4946 [hep-ph].

[96] J. L. F. Barbon and J. R. Espinosa, "On the Naturalness of Higgs Inflation," *Phys. Rev.* **D79** (2009) 081302, arXiv:0903.0355 [hep-ph].

[97] F. L. Bezrukov, A. Magnin, and M. Shaposhnikov, "Standard Model Higgs boson mass from inflation," *Phys. Lett.* **B675** (2009) 88–92, arXiv:0812.4950 [hep-ph].

[98] A. O. Barvinsky, A. Yu. Kamenshchik, C. Kiefer, A. A. Starobinsky, and C. Steinwachs, "Asymptotic freedom in inflationary cosmology with a non-minimally coupled Higgs field," *JCAP* **0912** (2009) 003, arXiv:0904.1698 [hep-ph].

[99] R. N. Lerner and J. McDonald, "Higgs Inflation and Naturalness," *JCAP* **1004** (2010) 015, arXiv:0912.5463 [hep-ph].

[100] R. N. Lerner and J. McDonald, "A Unitarity-Conserving Higgs Inflation Model," *Phys. Rev.* **D82** (2010) 103525, arXiv:1005.2978 [hep-ph].

[101] L. A. Popa, "Observational consequences of the Standard Model Higgs inflation variants," *JCAP* **1110** (2011) 025, arXiv:1107.3436 [astro-ph.CO].

[102] F. Bezrukov, A. Magnin, M. Shaposhnikov, and S. Sibiryakov, "Higgs inflation: consistency and generalisations," *JHEP* **01** (2011) 016, arXiv:1008.5157 [hep-ph].

[103] K. Kamada, T. Kobayashi, T. Takahashi, M. Yamaguchi, and J. Yokoyama, "Generalized Higgs inflation," *Phys. Rev.* **D86** (2012) 023504, arXiv:1203.4059 [hep-ph].

[104] F. Bezrukov, "The Higgs field as an inflaton," *Class. Quant. Grav.* **30** (2013) 214001, arXiv:1307.0708 [hep-ph].

[105] D. P. George, S. Mooij, and M. Postma, "Quantum corrections in Higgs inflation: the real scalar case," *JCAP* **1402** (2014) 024, arXiv:1310.2157 [hep-th].

[106] Y. Hamada, H. Kawai, and K.-y. Oda, "Minimal Higgs inflation," *PTEP* **2014** (2014) 023B02, arXiv:1308.6651 [hep-ph].

[107] Y. Hamada, H. Kawai, K.-y. Oda, and S. C. Park, "Higgs Inflation is Still Alive after the Results from BICEP2," *Phys. Rev. Lett.* **112** no. 24, (2014) 241301, arXiv:1403.5043 [hep-ph].

[108] Y. Hamada, H. Kawai, K.-y. Oda, and S. C. Park, "Higgs inflation from Standard Model criticality," *Phys. Rev.* **D91** (2015) 053008, arXiv:1408.4864 [hep-ph].

[109] F. Bezrukov and M. Shaposhnikov, "Higgs inflation at the critical point," *Phys. Lett.* **B734** (2014) 249–254, arXiv:1403.6078 [hep-ph].

[110] K. Allison, C. T. Hill, and G. G. Ross, "Ultra-weak sector, Higgs boson mass, and the dilaton," *Phys.Lett.* **B738** (2014) 191–195, arXiv:1404.6268 [hep-ph].

[111] A. Salvio and A. Mazumdar, "Classical and Quantum Initial Conditions for Higgs Inflation," *Phys. Lett.* **B750** (2015) 194–200, arXiv:1506.07520 [hep-ph].

[112] C. van de Bruck and C. Longden, "Higgs Inflation with a Gauss-Bonnet term in the Jordan Frame," *Phys. Rev.* **D93** no. 6, (2016) 063519, arXiv:1512.04768 [hep-ph].

[113] X. Calmet and I. Kuntz, "Higgs Starobinsky Inflation," *Eur. Phys. J.* **C76** no. 5, (2016) 289, arXiv:1605.02236 [hep-th].

[114] R. Kallosh and A. Linde, "Multi-field conformal cosmological attractors," *Journal of Cosmology and Astroparticle Physics* **2013** no. 12, (2013) 006.

[115] R. Kallosh, A. Linde, and D. Roest, "Superconformal Inflationary α-Attractors," *JHEP* **11** (2013) 198, arXiv:1311.0472 [hep-th].

[116] R. Kallosh and A. Linde, "Non-minimal Inflationary Attractors," *JCAP* **1310** (2013) 033, arXiv:1307.7938 [hep-th].

[117] R. Kallosh, A. Linde, and D. Roest, "The double attractor behavior of induced inflation," *JHEP* **09** (2014) 062, arXiv:1407.4471 [hep-th].

[118] A. Linde, "Single-field α-attractors," *JCAP* **1505** (2015) 003, arXiv:1504.00663 [hep-th].

[119] M. Galante, R. Kallosh, A. Linde, and D. Roest, "Unity of Cosmological Inflation Attractors," *Phys. Rev. Lett.* **114** no. 14, (2015) 141302, arXiv:1412.3797 [hep-th].

[120] B. J. Broy, D. Roest, and A. Westphal, "Power Spectrum of Inflationary Attractors," *Phys. Rev.* **D91** no. 2, (2015) 023514, arXiv:1408.5904 [hep-th].

[121] R. Kallosh and A. Linde, "Planck, LHC, and α-attractors," *Phys. Rev.* **D91** (2015) 083528, arXiv:1502.07733 [astro-ph.CO].

[122] J. J. M. Carrasco, R. Kallosh, and A. Linde, "Cosmological Attractors and Initial Conditions for Inflation," *Phys. Rev.* **D92** no. 6, (2015) 063519, arXiv:1506.00936 [hep-th].

[123] Z. Yi and Y. Gong, "Nonminimal coupling and inflationary attractors," *Phys. Rev.* **D94** no. 10, (2016) 103527, arXiv:1608.05922 [gr-qc].

[124] S. D. Odintsov and V. K. Oikonomou, "Inflationary α-attractors from $F(R)$ gravity," *Phys. Rev.* **D94** no. 12, (2016) 124026, arXiv:1612.01126 [gr-qc].

[125] S. Bhattacharya, K. Das, and K. Dutta, "Attractor Models in Scalar-Tensor Theories of Inflation," arXiv:1706.07934 [gr-qc].

[126] K. Dimopoulos and C. Owen, "Quintessential Inflation with α-attractors," *JCAP* **1706** no. 06, (2017) 027, arXiv:1703.00305 [gr-qc].

[127] V. Faraoni, "Nonminimal coupling of the scalar field and inflation," *Phys. Rev.* **D53** (1996) 6813–6821, arXiv:astro-ph/9602111 [astro-ph].

[128] T. P. Sotiriou and V. Faraoni, "f(R) Theories Of Gravity," *Rev. Mod. Phys.* **82** (2010) 451–497, arXiv:0805.1726 [gr-qc].

[129] S. Capozziello and M. De Laurentis, "Extended Theories of Gravity," *Phys. Rept.* **509** (2011) 167–321, arXiv:1108.6266 [gr-qc].

[130] S. Nojiri and S. D. Odintsov, "Unified cosmic history in modified gravity: from F(R) theory to Lorentz non-invariant models," *Phys. Rept.* **505** (2011) 59–144, arXiv:1011.0544 [gr-qc].

[131] A. De Felice and S. Tsujikawa, "f(R) theories," *Living Rev. Rel.* **13** (2010) 3, arXiv:1002.4928 [gr-qc].

[132] T. Clifton, P. G. Ferreira, A. Padilla, and C. Skordis, "Modified Gravity and Cosmology," *Phys. Rept.* **513** (2012) 1–189, arXiv:1106.2476 [astro-ph.CO].

[133] M. Rinaldi, G. Cognola, L. Vanzo, and S. Zerbini, "Reconstructing the inflationary $f(R)$ from observations," *JCAP* **1408** (2014) 015, arXiv:1406.1096 [gr-qc].

[134] K. Bamba, S. Nojiri, S. D. Odintsov, and D. Sáez-Gómez, "Inflationary universe from perfect fluid and $F(R)$ gravity and its comparison with observational data," *Phys. Rev.* **D90** (2014) 124061, arXiv:1410.3993 [hep-th].

[135] S. Nojiri, S. D. Odintsov, and V. K. Oikonomou, "Modified Gravity Theories on a Nutshell: Inflation, Bounce and Late-time Evolution," *Phys. Rept.* **692** (2017) 1–104, arXiv:1705.11098 [gr-qc].

[136] M. Shaposhnikov and D. Zenhausern, "Scale invariance, unimodular gravity and dark energy," *Phys. Lett.* **B671** (2009) 187–192, arXiv:0809.3395 [hep-th].

[137] V. V. Khoze, "Inflation and Dark Matter in the Higgs Portal of Classically Scale Invariant Standard Model," *JHEP* **1311** (2013) 215, arXiv:1308.6338 [hep-ph].

[138] K. Kannike, A. Racioppi, and M. Raidal, "Embedding inflation into the Standard Model - more evidence for classical scale invariance," *JHEP* **1406** (2014) 154, arXiv:1405.3987 [hep-ph].

[139] E. Gabrielli, M. Heikinheimo, K. Kannike, A. Racioppi, M. Raidal, *et al.*, "Towards Completing the Standard Model: Vacuum Stability, EWSB and Dark Matter," *Phys.Rev.* **D89** no. 1, (2014) 015017, arXiv:1309.6632 [hep-ph].

[140] A. Salvio and A. Strumia, "Agravity," *Journal of High Energy Physics* **2014** no. 6, (2014) 1–26.

[141] C. Csaki, N. Kaloper, J. Serra, and J. Terning, "Inflation from Broken Scale Invariance," *Phys. Rev. Lett.* **113** (2014) 161302, arXiv:1406.5192 [hep-th].

[142] K. Kannike, G. Hütsi, L. Pizza, A. Racioppi, M. Raidal, A. Salvio, and A. Strumia, "Dynamically induced planck scale and inflation," *Journal of High Energy Physics* **2015** no. 5, (2015) 1–31.

[143] N. D. Barrie, A. Kobakhidze, and S. Liang, "Natural Inflation with Hidden Scale Invariance," *Phys. Lett.* **B756** (2016) 390–393, arXiv:1602.04901 [gr-qc].

[144] L. Marzola and A. Racioppi, "Minimal but non-minimal inflation and electroweak symmetry breaking," *JCAP* **1610** no. 10, (2016) 010, arXiv:1606.06887 [hep-ph].

[145] L. Marzola, A. Racioppi, M. Raidal, F. R. Urban, and H. Veermäe, "Non-minimal CW inflation, electroweak symmetry breaking and the 750 GeV anomaly," *JHEP* **03** (2016) 190, arXiv:1512.09136 [hep-ph].

[146] M. Rinaldi and L. Vanzo, "Inflation and reheating in theories with spontaneous scale invariance symmetry breaking," *Phys. Rev.* **D94** no. 2, (2016) 024009, arXiv:1512.07186 [gr-qc].

[147] A. Farzinnia and S. Kouwn, "Classically scale invariant inflation, supermassive WIMPs, and adimensional gravity," *Phys. Rev.* **D93** no. 6, (2016) 063528, arXiv:1512.05890 [hep-ph].

[148] K. Kannike, "Vacuum stability of a general scalar potential of a few fields," *Eur.Phys.J. C* **76** (Mar., 2016) 324, 1603.02680.

[149] M. Rinaldi, L. Vanzo, S. Zerbini, and G. Venturi, "Inflationary quasiscale-invariant attractors," *Phys. Rev.* **D93** (2016) 024040, arXiv:1505.03386 [hep-th].

[150] G. K. Karananas and J. Rubio, "On the geometrical interpretation of scale-invariant models of inflation," *Phys. Lett.* **B761** (2016) 223–228, arXiv:1606.08848 [hep-ph].

[151] G. Tambalo and M. Rinaldi, "Inflation and reheating in scale-invariant scalar-tensor gravity," *Gen. Rel. Grav.* **49** no. 4, (2017) 52, arXiv:1610.06478 [gr-qc].

[152] K. Kannike, M. Raidal, C. Spethmann, and H. Veermäe, "The evolving Planck mass in classically scale-invariant theories," *JHEP* **04** (2017) 026, arXiv:1610.06571 [hep-ph].

[153] P. G. Ferreira, C. T. Hill, and G. G. Ross, "Weyl Current, Scale-Invariant Inflation and Planck Scale Generation," *Phys. Rev.* **D95** no. 4, (2017) 043507, arXiv:1610.09243 [hep-th].

[154] A. Salvio, "Inflationary Perturbations in No-Scale Theories," *Eur. Phys. J.* **C77** no. 4, (2017) 267, arXiv:1703.08012 [astro-ph.CO].

[155] K. Kannike, A. Racioppi, and M. Raidal, "Super-heavy dark matter âĂŞ Towards predictive scenarios from inflation," *Nucl. Phys.* **B918** (2017) 162–177, arXiv:1605.09378 [hep-ph].

[156] R. Fakir and W. G. Unruh, "Improvement on cosmological chaotic inflation through nonminimal coupling," *Phys. Rev.* **D41** (1990) 1783–1791.

[157] N. Makino and M. Sasaki, "The Density perturbation in the chaotic inflation with nonminimal coupling," *Prog. Theor. Phys.* **86** (1991) 103–118.

[158] D. F. Torres, "Slow roll inflation in nonminimally coupled theories: Hyperextended gravity approach," *Phys. Lett.* **A225** (1997) 13–17, arXiv:gr-qc/9610021 [gr-qc].

[159] V. Faraoni, "Inflation and quintessence with nonminimal coupling," *Phys. Rev.* **D62** (2000) 023504, arXiv:gr-qc/0002091 [gr-qc].

[160] S. Koh, S. P. Kim, and D. J. Song, "Inflationary solutions in nonminimally coupled scalar field theory," *Phys. Rev.* **D72** (2005) 043523, arXiv:astro-ph/0505188 [astro-ph].

[161] S. C. Park and S. Yamaguchi, "Inflation by non-minimal coupling," *JCAP* **0808** (2008) 009, arXiv:0801.1722 [hep-ph].

[162] K. Nozari and S. D. Sadatian, "Non-Minimal Inflation after WMAP3," *Mod. Phys. Lett.* **A23** (2008) 2933–2945, arXiv:0710.0058 [astro-ph].

[163] F. Bauer and D. A. Demir, "Inflation with Non-Minimal Coupling: Metric versus Palatini Formulations," *Phys. Lett.* **B665** (2008) 222–226, arXiv:0803.2664 [hep-ph].

[164] K. Nozari and S. Shafizadeh, "Non-minimal inflation revisited," *Physica Scripta* **82** no. 1, (2010) 015901, arXiv:1006.1027 [gr-qc].

[165] N. Okada, M. U. Rehman, and Q. Shafi, "Tensor to Scalar Ratio in Non-Minimal ϕ^4 Inflation," *Phys. Rev.* **D82** (2010) 043502, arXiv:1005.5161 [hep-ph].

[166] C. Pallis, "Non-Minimally Gravity-Coupled Inflationary Models," *Phys. Lett.* **B692** (2010) 287–296, arXiv:1002.4765 [astro-ph.CO].

[167] D. C. Edwards and A. R. Liddle, "The observational position of simple non-minimally coupled inflationary scenarios," *JCAP* **1409** no. 09, (2014) 052, arXiv:1406.5768 [astro-ph.CO].

[168] T. Inagaki, R. Nakanishi, and S. D. Odintsov, "Non-Minimal Two-Loop Inflation," *Phys. Lett.* **B745** (2015) 105–111, arXiv:1502.06301 [hep-ph].

[169] M. Artymowski and A. Racioppi, "Scalar-tensor linear inflation," *JCAP* **1704** no. 04, (2017) 007, arXiv:1610.09120 [astro-ph.CO].

[170] A. Yu. Kamenshchik and C. F. Steinwachs, "Question of quantum equivalence between Jordan frame and Einstein frame," *Phys. Rev.* **D91** no. 8, (2015) 084033, arXiv:1408.5769 [gr-qc].

[171] M. Herrero-Valea, "Anomalies, equivalence and renormalization of cosmological frames," *Phys. Rev.* **D93** no. 10, (2016) 105038, arXiv:1602.06962 [hep-th].

[172] S. Pandey, S. Pal, and N. Banerjee, "Equivalence of Einstein and Jordan frames in quantized cosmological models," arXiv:1611.07043 [gr-qc].

[173] S. Pandey and N. Banerjee, "Equivalence of Jordan and Einstein frames at the quantum level," *Eur. Phys. J. Plus* **132** no. 3, (2017) 107, arXiv:1610.00584 [gr-qc].

[174] S. Capozziello, R. de Ritis, and A. A. Marino, "Some aspects of the cosmological conformal equivalence between 'Jordan frame' and 'Einstein frame'," *Class. Quant. Grav.* **14** (1997) 3243–3258, arXiv:gr-qc/9612053 [gr-qc].

[175] R. Dick, "Inequivalence of Jordan and Einstein frame: What is the low-energy gravity in string theory?," *Gen. Rel. Grav.* **30** (1998) 435–444.

[176] V. Faraoni, E. Gunzig, and P. Nardone, "Conformal transformations in classical gravitational theories and in cosmology," *Fund. Cosmic Phys.* **20** (1999) 121, arXiv:gr-qc/9811047 [gr-qc].

[177] V. Faraoni and E. Gunzig, "Einstein frame or Jordan frame?," *Int. J. Theor. Phys.* **38** (1999) 217–225, arXiv:astro-ph/9910176 [astro-ph].

[178] E. E. Flanagan, "The Conformal frame freedom in theories of gravitation," *Class. Quant. Grav.* **21** (2004) 3817, arXiv:gr-qc/0403063 [gr-qc].

[179] A. Bhadra, K. Sarkar, D. P. Datta, and K. K. Nandi, "Brans-Dicke theory: Jordan versus Einstein frame," *Mod. Phys. Lett.* **A22** (2007) 367–376, arXiv:gr-qc/0605109 [gr-qc].

[180] K. Nozari and S. Davood Sadatian, "Comparison of Frames: Jordan vs Einstein Frame for a Non-minimal Dark Energy Model," *Mod. Phys. Lett.* **A24** (2009) 3143–3155, arXiv:0905.0241 [gr-qc].

[181] S. Capozziello, P. Martin-Moruno, and C. Rubano, "Physical non-equivalence of the Jordan and Einstein frames," *Phys. Lett.* **B689** (2010) 117–121, arXiv:1003.5394 [gr-qc].

[182] C. Corda, "Gravitational wave astronomy: the definitive test for the 'Einstein frame versus Jordan frame' controversy," *Astropart. Phys.* **34** (2011) 412–419, arXiv:1010.2086 [gr-qc].

[183] T. Qiu, "Reconstruction of a Nonminimal Coupling Theory with Scale-invariant Power Spectrum," *JCAP* **1206** (2012) 041, arXiv:1204.0189 [hep-ph].

[184] T. Qiu, "Reconstruction of f(R) models with Scale-invariant Power Spectrum," *Phys. Lett.* **B718** (2012) 475–481, arXiv:1208.4759 [astro-ph.CO].

[185] I. Quiros, R. Garcia-Salcedo, J. E. Madriz Aguilar, and T. Matos, "The conformal transformation's controversy: what are we missing?," *Gen. Rel. Grav.* **45** (2013) 489–518, arXiv:1108.5857 [gr-qc].

[186] T. Chiba and M. Yamaguchi, "Conformal-Frame (In)dependence of Cosmological Observations in Scalar-Tensor Theory," *JCAP* **1310** (2013) 040, arXiv:1308.1142 [gr-qc].

[187] M. Postma and M. Volponi, "Equivalence of the Einstein and Jordan frames," *Phys. Rev.* **D90** no. 10, (2014) 103516, arXiv:1407.6874 [astro-ph.CO].

[188] T. Qiu and J.-Q. Xia, "Perturbations of Single-field Inflation in Modified Gravity Theory," *Phys. Lett.* **B744** (2015) 273–279, arXiv:1406.5902 [astro-ph.CO].

[189] G. DomÃĺnech and M. Sasaki, "Conformal Frame Dependence of Inflation," *JCAP* **1504** no. 04, (2015) 022, arXiv:1501.07699 [gr-qc].

[190] S. Bahamonde, S. D. Odintsov, V. K. Oikonomou, and M. Wright, "Correspondence of $F(R)$ Gravity Singularities in Jordan and Einstein Frames," *Annals Phys.* **373** (2016) 96–114, arXiv:1603.05113 [gr-qc].

[191] D. J. Brooker, S. D. Odintsov, and R. P. Woodard, "Precision predictions for the primordial power spectra from $f(R)$ models of inflation," *Nucl. Phys.* **B911** (2016) 318–337, arXiv:1606.05879 [gr-qc].

[192] K. Bhattacharya and B. R. Majhi, "Fresh look at the scalar-tensor theory of gravity in Jordan and Einstein frames from undiscussed standpoints," *Phys. Rev.* **D95** no. 6, (2017) 064026, arXiv:1702.07166 [gr-qc].

[193] S. Bahamonde, S. D. Odintsov, V. K. Oikonomou, and P. V. Tretyakov, "Deceleration versus acceleration universe in different frames of $F(R)$ gravity," *Phys. Lett.* **B766** (2017) 225–230, arXiv:1701.02381 [gr-qc].

[194] B. Boisseau, G. Esposito-Farese, D. Polarski, and A. A. Starobinsky, "Reconstruction of a scalar tensor theory of gravity in an accelerating universe," *Phys. Rev. Lett.* **85** (2000) 2236, arXiv:gr-qc/0001066 [gr-qc].

[195] G. Esposito-Farese and D. Polarski, "Scalar tensor gravity in an accelerating universe," *Phys. Rev.* **D63** (2001) 063504, arXiv:gr-qc/0009034 [gr-qc].

[196] C. Brans and R. H. Dicke, "Mach's principle and a relativistic theory of gravitation," *Phys. Rev.* **124** (1961) 925–935.

[197] P. G. Bergmann, "Comments on the scalar tensor theory," *Int. J. Theor. Phys.* **1** (1968) 25–36.

[198] R. V. Wagoner, "Scalar tensor theory and gravitational waves," *Phys. Rev.* **D1** (1970) 3209–3216.

[199] R. H. Dicke, "Mach's principle and invariance under transformation of units," *Phys. Rev.* **125** (1962) 2163–2167.

[200] Y. M. Cho, "Violation of equivalence principle in Brans-Dicke theory," *Class. Quant. Grav.* **14** (1997) 2963–2970.

[201] R. Catena, M. Pietroni, and L. Scarabello, "Einstein and Jordan reconciled: a frame-invariant approach to scalar-tensor cosmology," *Phys. Rev.* **D76** (2007) 084039, arXiv:astro-ph/0604492 [astro-ph].

[202] L. Jarv, P. Kuusk, M. Saal, and O. Vilson, "The formalism of invariants in scalar-tensor and multiscalar-tensor theories of gravitation," in *14th Marcel Grossmann Meeting on Recent Developments in Theoretical and Experimental General Relativity, Astrophysics, and Relativistic Field Theories (MG14) Rome, Italy, July 12-18, 2015*. 2015. arXiv:1512.09166 [gr-qc]. http://inspirehep.net/record/1411793/files/arXiv:1512.09166.pdf.

[203] L. Järv, P. Kuusk, M. Saal, and O. Vilson, "Invariant quantities in the scalar-tensor theories of gravitation," *Physical Review D* **91** no. 2, (2015) 024041, arXiv:1411.1947 [gr-qc].

[204] L. Järv, P. Kuusk, M. Saal, and O. Vilson, "Transformation properties and general relativity regime in scalar–tensor theories," *Classical and Quantum Gravity* **32** no. 23, (2015) 235013, arXiv:1504.02686 [gr-qc].

[205] P. Kuusk, M. Rünkla, M. Saal, and O. Vilson, "Invariant slow-roll parameters in scalarâĂŞtensor theories," *Class. Quant. Grav.* **33** no. 19, (2016) 195008, arXiv:1605.07033 [gr-qc].

[206] P. Kuusk, L. Järv, and O. Vilson, "Invariant quantities in the multiscalar-tensor theories of gravitation," *Int. J. Mod. Phys.* **A31** no. 02n03, (2016) 1641003, arXiv:1509.02903 [gr-qc].

[207] O. Vilson, "Some remarks concerning invariant quantities in scalar-tensor gravity," *Adv. Appl. Clifford Algebras* **27** no. 1, (2017) 321–332, arXiv:1509.02481 [gr-qc].

[208] J. C. Hwang, "Cosmological perturbations in generalized gravity theories: Formulation," *Class. Quant. Grav.* **7** (1990) 1613–1631.

[209] J. C. Hwang, "Cosmological perturbations in generalized gravity theories: Solutions," *Phys. Rev.* **D42** (1990) 2601–2606.

[210] J.-c. Hwang, "Unified analysis of cosmological perturbations in generalized gravity," *Phys. Rev.* **D53** (1996) 762–765, arXiv:gr-qc/9509044 [gr-qc].

[211] J.-c. Hwang and H. Noh, "Cosmological perturbations in generalized gravity theories," *Phys. Rev.* **D54** (1996) 1460–1473.

[212] J.-c. Hwang, "Quantum fluctuations of cosmological perturbations in generalized gravity," *Class. Quant. Grav.* **14** (1997) 3327–3336, arXiv:gr-qc/9607059 [gr-qc].

[213] J. chan Hwang and H. Noh, "Density spectra from pole-like inflations based on generalized gravity theories," *Classical and Quantum Gravity* **15** no. 5, (1998) 1387. http://stacks.iop.org/0264-9381/15/i=5/a=020.

[214] J.-c. Hwang, "Gravitational wave spectrums from pole - like inflations based on generalized gravity theories," *Class. Quant. Grav.* **15** (1998) 1401–1413, arXiv:gr-qc/9710061 [gr-qc].

[215] H. Noh and J.-c. Hwang, "Inflationary spectra in generalized gravity: Unified forms," *Phys. Lett.* **B515** (2001) 231–237, arXiv:astro-ph/0107069 [astro-ph].

[216] D. Burns, S. Karamitsos, and A. Pilaftsis, "Frame-Covariant Formulation of Inflation in Scalar-Curvature Theories," *Nucl. Phys.* **B907** (2016) 785–819, arXiv:1603.03730 [hep-ph].

[217] S. Glashow, "Partial Symmetries of Weak Interactions," *Nucl.Phys.* **22** (1961) 579–588.

[218] S. Weinberg, "A Model of Leptons," *Phys.Rev.Lett.* **19** (1967) 1264–1266.

[219] A. Salam, "Weak and Electromagnetic Interactions," *Conf.Proc.* **C680519** (1968) 367–377.

[220] **ATLAS** Collaboration, G. Aad *et al.*, "Observation of a new particle in the search for the Standard Model Higgs boson with the ATLAS detector at the LHC," *Phys.Lett.* **B716** (2012) 1–29, arXiv:1207.7214 [hep-ex].

[221] **CMS** Collaboration, S. Chatrchyan *et al.*, "Observation of a new boson at a mass of 125 GeV with the CMS experiment at the LHC," *Phys.Lett.* **B716** (2012) 30–61, arXiv:1207.7235 [hep-ex].

[222] F. Englert and R. Brout, "Broken Symmetry and the Mass of Gauge Vector Mesons," *Phys.Rev.Lett.* **13** (1964) 321–323.

[223] P. W. Higgs, "Broken symmetries, massless particles and gauge fields," *Phys.Lett.* **12** (1964) 132–133.

[224] P. W. Higgs, "Broken Symmetries and the Masses of Gauge Bosons," *Phys.Rev.Lett.* **13** (1964) 508–509.

[225] G. Guralnik, C. Hagen, and T. Kibble, "Global Conservation Laws and Massless Particles," *Phys.Rev.Lett.* **13** (1964) 585–587.

[226] **KamLAND** Collaboration, S. Abe *et al.*, "Precision Measurement of Neutrino Oscillation Parameters with KamLAND," *Phys. Rev. Lett.* **100** (2008) 221803, arXiv:0801.4589 [hep-ex].

[227] **LSND** Collaboration, A. Aguilar-Arevalo *et al.*, "Evidence for neutrino oscillations from the observation of anti-neutrino(electron) appearance in a anti-neutrino(muon) beam," *Phys. Rev.* **D64** (2001) 112007, arXiv:hep-ex/0104049 [hep-ex].

[228] **K2K** Collaboration, M. H. Ahn *et al.*, "Indications of neutrino oscillation in a 250 km long baseline experiment," *Phys. Rev. Lett.* **90** (2003) 041801, arXiv:hep-ex/0212007 [hep-ex].

[229] **K2K** Collaboration, E. Aliu *et al.*, "Evidence for muon neutrino oscillation in an accelerator-based experiment," *Phys. Rev. Lett.* **94** (2005) 081802, arXiv:hep-ex/0411038 [hep-ex].

[230] **KamLAND** Collaboration, T. Araki *et al.*, "Measurement of neutrino oscillation with KamLAND: Evidence of spectral distortion," *Phys. Rev. Lett.* **94** (2005) 081801, arXiv:hep-ex/0406035 [hep-ex].

[231] **Super-Kamiokande** Collaboration, Y. Ashie *et al.*, "Evidence for an oscillatory signature in atmospheric neutrino oscillation," *Phys. Rev. Lett.* **93** (2004) 101801, arXiv:hep-ex/0404034 [hep-ex].

[232] F. Boehm *et al.*, "Final results from the Palo Verde neutrino oscillation experiment," *Phys. Rev.* **D64** (2001) 112001, arXiv:hep-ex/0107009 [hep-ex].

[233] **Super-Kamiokande** Collaboration, Y. Fukuda *et al.*, "Evidence for oscillation of atmospheric neutrinos," *Phys. Rev. Lett.* **81** (1998) 1562–1567, arXiv:hep-ex/9807003 [hep-ex].

[234] **Particle Data Group** Collaboration, C. Patrignani *et al.*, "Review of Particle Physics," *Chin. Phys.* **C40** no. 10, (2016) 100001.

[235] **CMS** Collaboration, W. de Boer, "The Discovery of the Higgs Boson with the CMS Detector and its Implications for Supersymmetry and Cosmology," in *Time and Matter 2013 (TAM2013) Venice, Italy*. 2013. arXiv:1309.0721 [hep-ph]. http://inspirehep.net/record/1252561/files/arXiv:1309.0721.pdf.

[236] **SLD Electroweak Group, DELPHI, ALEPH, SLD, SLD Heavy Flavour Group, OPAL, LEP Electroweak Working Group, L3** Collaboration, S. Schael *et al.*, "Precision electroweak measurements on the Z resonance," *Phys. Rept.* **427** (2006) 257–454, arXiv:hep-ex/0509008 [hep-ex].

[237] R. Bouchendira, P. Clade, S. Guellati-Khelifa, F. Nez, and F. Biraben, "New determination of the fine structure constant and test of the quantum electrodynamics," *Phys. Rev. Lett.* **106** (2011) 080801, arXiv:1012.3627 [physics.atom-ph].

[238] **MuLan** Collaboration, D. B. Chitwood *et al.*, "Improved measurement of the positive muon lifetime and determination of the Fermi constant," *Phys. Rev. Lett.* **99** (2007) 032001, arXiv:0704.1981 [hep-ex].

[239] M. E. Peskin and T. Takeuchi, "A New constraint on a strongly interacting Higgs sector," *Phys. Rev. Lett.* **65** (1990) 964–967.

[240] G. Altarelli and R. Barbieri, "Vacuum polarization effects of new physics on electroweak processes," *Phys. Lett.* **B253** (1991) 161–167.

[241] M. E. Peskin and T. Takeuchi, "Estimation of oblique electroweak corrections," *Phys. Rev.* **D46** (1992) 381–409.

[242] G. Altarelli, R. Barbieri, and S. Jadach, "Toward a model independent analysis of electroweak data," *Nucl. Phys.* **B369** (1992) 3–32. [Erratum: Nucl. Phys.B376,444(1992)].

[243] **Particle Data Group** Collaboration, K. A. Olive *et al.*, "Review of Particle Physics," *Chin. Phys.* **C38** (2014) 090001.

[244] M. F. Zoller, "Vacuum stability in the SM and the three-loop β-function for the Higgs self-interaction," *Subnucl. Ser.* **50** (2014) 557–566, arXiv:1209.5609 [hep-ph].

[245] V. Branchina and E. Messina, "Stability, Higgs Boson Mass and New Physics," *Phys. Rev. Lett.* **111** (2013) 241801, arXiv:1307.5193 [hep-ph].

[246] V. Branchina, E. Messina, and A. Platania, "Top mass determination, Higgs inflation, and vacuum stability," *JHEP* **09** (2014) 182, arXiv:1407.4112 [hep-ph].

[247] A. Andreassen, W. Frost, and M. D. Schwartz, "Consistent Use of the Standard Model Effective Potential," *Phys.Rev.Lett.* **113** no. 24, (2014) 241801, arXiv:1408.0292 [hep-ph].

[248] V. Branchina and E. Messina, "Stability and UV completion of the Standard Model," arXiv:1507.08812 [hep-ph].

[249] F. Bezrukov, J. Rubio, and M. Shaposhnikov, "Living beyond the edge: Higgs inflation and vacuum metastability," *Phys. Rev.* **D92** no. 8, (2015) 083512, arXiv:1412.3811 [hep-ph].

[250] J. R. Espinosa, G. F. Giudice, E. Morgante, A. Riotto, L. Senatore, *et al.*, "The cosmological Higgstory of the vacuum instability," arXiv:1505.04825 [hep-ph].

[251] A. V. Bednyakov, B. A. Kniehl, A. F. Pikelner, and O. L. Veretin, "Fate of the Universe: Gauge Independence and Advanced Precision," arXiv:1507.08833 [hep-ph].

[252] L. Susskind, "Dynamics of Spontaneous Symmetry Breaking in the Weinberg-Salam Theory," *Phys. Rev.* **D20** (1979) 2619–2625.

[253] M. Heikinheimo, A. Racioppi, M. Raidal, C. Spethmann, and K. Tuominen, "Physical Naturalness and Dynamical Breaking of Classical Scale Invariance," *Mod.Phys.Lett.* **A29** (2014) 1450077, arXiv:1304.7006 [hep-ph].

[254] C. P. Burgess, "Goldstone and pseudoGoldstone bosons in nuclear, particle and condensed matter physics," *Phys. Rept.* **330** (2000) 193–261, arXiv:hep-th/9808176 [hep-th].

[255] M. Schmaltz and D. Tucker-Smith, "Little Higgs review," *Ann. Rev. Nucl. Part. Sci.* **55** (2005) 229–270, arXiv:hep-ph/0502182 [hep-ph].

[256] M. Perelstein, "Little Higgs models and their phenomenology," *Prog. Part. Nucl. Phys.* **58** (2007) 247–291, arXiv:hep-ph/0512128 [hep-ph].

[257] H.-C. Cheng and I. Low, "Little hierarchy, little Higgses, and a little symmetry," *JHEP* **08** (2004) 061, arXiv:hep-ph/0405243 [hep-ph].

[258] N. Arkani-Hamed, A. G. Cohen, E. Katz, and A. E. Nelson, "The Littlest Higgs," *JHEP* **07** (2002) 034, arXiv:hep-ph/0206021 [hep-ph].

[259] J. L. Hewett, F. J. Petriello, and T. G. Rizzo, "Constraining the littlest Higgs," *JHEP* **10** (2003) 062, arXiv:hep-ph/0211218 [hep-ph].

[260] G. Panico and A. Wulzer, "The Composite Nambu-Goldstone Higgs," *Lect. Notes Phys.* **913** (2016) pp.1–316, arXiv:1506.01961 [hep-ph].

[261] Z. Chacko, H.-S. Goh, and R. Harnik, "The Twin Higgs: Natural electroweak breaking from mirror symmetry," *Phys. Rev. Lett.* **96** (2006) 231802, arXiv:hep-ph/0506256 [hep-ph].

[262] Z. Chacko, H.-S. Goh, and R. Harnik, "A Twin Higgs model from left-right symmetry," *JHEP* **01** (2006) 108, arXiv:hep-ph/0512088 [hep-ph].

[263] G. Altarelli and F. Feruglio, "Models of neutrino masses and mixings," *New J. Phys.* **6** (2004) 106, arXiv:hep-ph/0405048 [hep-ph].

[264] R. N. Mohapatra *et al.*, "Theory of neutrinos: A White paper," *Rept. Prog. Phys.* **70** (2007) 1757–1867, arXiv:hep-ph/0510213 [hep-ph].

[265] R. N. Mohapatra and A. Y. Smirnov, "Neutrino Mass and New Physics," *Ann. Rev. Nucl. Part. Sci.* **56** (2006) 569–628, arXiv:hep-ph/0603118 [hep-ph].

[266] F. Zwicky, "Die Rotverschiebung von extragalaktischen Nebeln," *Helv. Phys. Acta* **6** (1933) 110–127. [Gen. Rel. Grav.41,207(2009)].

[267] E. Corbelli and P. Salucci, "The Extended Rotation Curve and the Dark Matter Halo of M33," *Mon. Not. Roy. Astron. Soc.* **311** (2000) 441–447, arXiv:astro-ph/9909252 [astro-ph].

[268] R. Massey, T. Kitching, and J. Richard, "The dark matter of gravitational lensing," *Rept. Prog. Phys.* **73** (2010) 086901, arXiv:1001.1739 [astro-ph.CO].

[269] D. Clowe, A. Gonzalez, and M. Markevitch, "Weak lensing mass reconstruction of the interacting cluster 1E0657-558: Direct evidence for the existence of dark matter," *Astrophys. J.* **604** (2004) 596–603, arXiv:astro-ph/0312273 [astro-ph].

[270] D. Clowe, M. Bradac, A. H. Gonzalez, M. Markevitch, S. W. Randall, C. Jones, and D. Zaritsky, "A direct empirical proof of the existence of dark matter," *Astrophys. J.* **648** (2006) L109–L113, arXiv:astro-ph/0608407 [astro-ph].

[271] A. J. Benson, A. Farahi, S. Cole, L. A. Moustakas, A. Jenkins, M. Lovell, R. Kennedy, J. Helly, and C. Frenk, "Dark Matter Halo Merger Histories Beyond Cold Dark Matter: I - Methods and Application to Warm Dark Matter," *Mon. Not. Roy. Astron. Soc.* **428** (2013) 1774, arXiv:1209.3018 [astro-ph.CO].

[272] M. R. Lovell, C. S. Frenk, V. R. Eke, A. Jenkins, L. Gao, and T. Theuns, "The properties of warm dark matter haloes," *Mon. Not. Roy. Astron. Soc.* **439** (2014) 300–317, arXiv:1308.1399 [astro-ph.CO].

[273] R. Kennedy, C. Frenk, S. Cole, and A. Benson, "Constraining the warm dark matter particle mass with Milky Way satellites," *Mon. Not. Roy. Astron. Soc.* **442** no. 3, (2014) 2487–2495, arXiv:1310.7739 [astro-ph.CO].

[274] K. Griest, "Galactic Microlensing as a Method of Detecting Massive Compact Halo Objects," *Astrophys. J.* **366** (1991) 412–421.

[275] **MACHO** Collaboration, C. Alcock *et al.*, "The MACHO project: Microlensing results from 5.7 years of LMC observations," *Astrophys. J.* **542** (2000) 281–307, arXiv:astro-ph/0001272 [astro-ph].

[276] **EROS-2** Collaboration, P. Tisserand *et al.*, "Limits on the Macho Content of the Galactic Halo from the EROS-2 Survey of the Magellanic Clouds," *Astron. Astrophys.* **469** (2007) 387–404, arXiv:astro-ph/0607207 [astro-ph].

[277] S. Calchi Novati, L. Mancini, G. Scarpetta, and L. Wyrzykowski, "LMC self lensing for OGLE-II microlensing observations," *Mon. Not. Roy. Astron. Soc.* **400** (2009) 1625, arXiv:0908.3836 [astro-ph.GA].

[278] L. Wyrzykowski *et al.*, "The OGLE View of Microlensing towards the Magellanic Clouds. I. A Trickle of Events in the OGLE-II LMC data," *Mon. Not. Roy. Astron. Soc.* **397** (2009) 1228–1242, arXiv:0905.2044 [astro-ph.GA].

[279] **POINT-AGAPE** Collaboration, S. Calchi Novati *et al.*, "POINT-AGAPE pixel lensing survey of M31: Evidence for a MACHO contribution to galactic halos," *Astron. Astrophys.* **443** (2005) 911, arXiv:astro-ph/0504188 [astro-ph].

[280] B. J. Carr and S. W. Hawking, "Black holes in the early Universe," *Mon. Not. Roy. Astron. Soc.* **168** (1974) 399–415.

[281] P. Meszaros, "The behaviour of point masses in an expanding cosmological substratum," *Astron. Astrophys.* **37** (1974) 225–228.

[282] B. J. Carr, "The Primordial black hole mass spectrum," *Astrophys. J.* **201** (1975) 1–19.

[283] D. N. Page and S. W. Hawking, "Gamma rays from primordial black holes," *Astrophys. J.* **206** (1976) 1–7.

[284] **EGRET** Collaboration, P. Sreekumar *et al.*, "EGRET observations of the extragalactic gamma-ray emission," *Astrophys. J.* **494** (1998) 523–534, arXiv:astro-ph/9709257 [astro-ph].

[285] B. J. Carr, K. Kohri, Y. Sendouda, and J. Yokoyama, "New cosmological constraints on primordial black holes," *Phys. Rev.* **D81** (2010) 104019, arXiv:0912.5297 [astro-ph.CO].

[286] F. Capela, M. Pshirkov, and P. Tinyakov, "Constraints on Primordial Black Holes as Dark Matter Candidates from Star Formation," *Phys. Rev.* **D87** no. 2, (2013) 023507, arXiv:1209.6021 [astro-ph.CO].

[287] A. Barnacka, J. F. Glicenstein, and R. Moderski, "New constraints on primordial black holes abundance from femtolensing of gamma-ray bursts," *Phys. Rev.* **D86** (2012) 043001, arXiv:1204.2056 [astro-ph.CO].

[288] K. Griest, A. M. Cieplak, and M. J. Lehner, "Experimental Limits on Primordial Black Hole Dark Matter from the First 2 yr of Kepler Data," *Astrophys. J.* **786** no. 2, (2014) 158, arXiv:1307.5798 [astro-ph.CO].

[289] M. Ricotti, J. P. Ostriker, and K. J. Mack, "Effect of Primordial Black Holes on the Cosmic Microwave Background and Cosmological Parameter Estimates," *Astrophys. J.* **680** (2008) 829, arXiv:0709.0524 [astro-ph].

[290] M. A. Monroy-RodrÃ■guez and C. Allen, "The end of the MACHO era- revisited: new limits on MACHO masses from halo wide binaries," *Astrophys. J.* **790** no. 2, (2014) 159, arXiv:1406.5169 [astro-ph.GA].

[291] S. W. Hawking, "Black hole explosions," *Nature* **248** (1974) 30–31.

[292] C. G. Lacey and J. P. Ostriker, "Massive black holes in galactic halos?," *The Astrophysical Journal* **299** (Dec., 1985) 633–652.

[293] **Virgo, LIGO Scientific** Collaboration, B. P. Abbott *et al.*, "Observation of Gravitational Waves from a Binary Black Hole Merger," *Phys. Rev. Lett.* **116** no. 6, (2016) 061102, arXiv:1602.03837 [gr-qc].

[294] A. M. Green, "Microlensing and dynamical constraints on primordial black hole dark matter with an extended mass function," *Phys. Rev.* **D94** no. 6, (2016) 063530, arXiv:1609.01143 [astro-ph.CO].

[295] F. KÃijhnel and K. Freese, "Constraints on Primordial Black Holes with Extended Mass Functions," *Phys. Rev.* **D95** no. 8, (2017) 083508, arXiv:1701.07223 [astro-ph.CO].

[296] B. Carr, M. Raidal, T. Tenkanen, V. Vaskonen, and H. VeermÃd'e, "Primordial black hole constraints for extended mass functions," *Phys. Rev.* **D96** no. 2, (2017) 023514, arXiv:1705.05567 [astro-ph.CO].

[297] N. Bellomo, J. L. Bernal, A. Raccanelli, and L. Verde, "Primordial Black Holes as Dark Matter: Converting Constraints from Monochromatic to Extended Mass Distributions," *JCAP* **1801** no. 01, (2018) 004, arXiv:1709.07467 [astro-ph.CO].

[298] G. Ballesteros and M. Taoso, "Primordial black hole dark matter from single field inflation," *Phys. Rev.* **D97** no. 2, (2018) 023501, arXiv:1709.05565 [hep-ph].

[299] S. Clesse and J. GarcÃ■a-Bellido, "Seven Hints for Primordial Black Hole Dark Matter," arXiv:1711.10458 [astro-ph.CO].

[300] G. F. Giudice, M. McCullough, and A. Urbano, "Hunting for Dark Particles with Gravitational Waves," *JCAP* **1610** no. 10, (2016) 001, arXiv:1605.01209 [hep-ph].

[301] G. Bertone, D. Hooper, and J. Silk, "Particle dark matter: Evidence, candidates and constraints," *Phys. Rept.* **405** (2005) 279–390, arXiv:hep-ph/0404175 [hep-ph].

[302] R. D. Peccei and H. R. Quinn, "CP Conservation in the Presence of Instantons," *Phys. Rev. Lett.* **38** (1977) 1440–1443.

[303] R. D. Peccei and H. R. Quinn, "Constraints Imposed by CP Conservation in the Presence of Instantons," *Phys. Rev.* **D16** (1977) 1791–1797.

[304] D. J. E. Marsh, "Axion Cosmology," *Phys. Rept.* **643** (2016) 1–79, arXiv:1510.07633 [astro-ph.CO].

[305] J. Preskill, M. B. Wise, and F. Wilczek, "Cosmology of the Invisible Axion," *Phys. Lett.* **120B** (1983) 127–132.

[306] L. F. Abbott and P. Sikivie, "A Cosmological Bound on the Invisible Axion," *Phys. Lett.* **120B** (1983) 133–136.

[307] M. Dine and W. Fischler, "The Not So Harmless Axion," *Phys. Lett.* **120B** (1983) 137–141.

[308] C. Abel *et al.*, "Search for Axionlike Dark Matter through Nuclear Spin Precession in Electric and Magnetic Fields," *Phys. Rev.* **X7** no. 4, (2017) 041034, arXiv:1708.06367 [hep-ph].

[309] S. Dodelson and L. M. Widrow, "Sterile-neutrinos as dark matter," *Phys. Rev. Lett.* **72** (1994) 17–20, arXiv:hep-ph/9303287 [hep-ph].

[310] H. J. de Vega and N. G. Sanchez, "Model independent analysis of dark matter points to a particle mass at the keV scale," *Mon. Not. Roy. Astron. Soc.* **404** (2010) 885, arXiv:0901.0922 [astro-ph.CO].

[311] H. J. de Vega, P. Salucci, and N. G. Sanchez, "The mass of the dark matter particle from theory and observations," *New Astron.* **17** (2012) 653–666, arXiv:1004.1908 [astro-ph.CO].

[312] A. Merle, "keV Neutrino Model Building," *Int. J. Mod. Phys.* **D22** (2013) 1330020, arXiv:1302.2625 [hep-ph].

[313] M. Drewes *et al.*, "A White Paper on keV Sterile Neutrino Dark Matter," *JCAP* **1701** no. 01, (2017) 025, arXiv:1602.04816 [hep-ph].

[314] M. Milgrom, "A Modification of the Newtonian dynamics as a possible alternative to the hidden mass hypothesis," *Astrophys. J.* **270** (1983) 365–370.

[315] J. Bekenstein and M. Milgrom, "Does the missing mass problem signal the breakdown of Newtonian gravity?," *Astrophys. J.* **286** (1984) 7–14.

[316] J. D. Bekenstein, "Relativistic gravitation theory for the MOND paradigm," *Phys. Rev.* **D70** (2004) 083509, arXiv:astro-ph/0403694 [astro-ph]. [Erratum: Phys. Rev.D71,069901(2005)].

[317] J. D. Bekenstein, "Alternatives to Dark Matter: Modified Gravity as an Alternative to dark Matter," arXiv:1001.3876 [astro-ph.CO].

[318] B. Famaey and S. McGaugh, "Modified Newtonian Dynamics (MOND): Observational Phenomenology and Relativistic Extensions," *Living Rev. Rel.* **15** (2012) 10, arXiv:1112.3960 [astro-ph.CO].

[319] S. Dodelson, "The Real Problem with MOND," *Int. J. Mod. Phys.* **D20** (2011) 2749–2753, arXiv:1112.1320 [astro-ph.CO].

[320] P. Bull *et al.*, "Beyond ΛCDM: Problems, solutions, and the road ahead," *Phys. Dark Univ.* **12** (2016) 56–99, arXiv:1512.05356 [astro-ph.CO].

[321] S. Boran, S. Desai, E. O. Kahya, and R. P. Woodard, "GW170817 Falsifies Dark Matter Emulators," arXiv:1710.06168 [astro-ph.HE].

[322] E. W. Kolb and M. S. Turner, "The Early Universe," *Front. Phys.* **69** (1990) 1–547.

[323] K. Griest and M. Kamionkowski, "Unitarity Limits on the Mass and Radius of Dark Matter Particles," *Phys. Rev. Lett.* **64** (1990) 615.

[324] J. Edsjo and P. Gondolo, "Neutralino relic density including coannihilations," *Phys.Rev.* **D56** (1997) 1879–1894, arXiv:hep-ph/9704361 [hep-ph].

[325] P. Gondolo and G. Gelmini, "Cosmic abundances of stable particles: Improved analysis," *Nuclear Physics B* **360** no. 1, (1991) 145–179.

[326] J. R. Ellis, T. Falk, K. A. Olive, and M. Srednicki, "Calculations of neutralino-stau coannihilation channels and the cosmologically relevant region of MSSM parameter space," *Astropart. Phys.* **13** (2000) 181–213, arXiv:hep-ph/9905481 [hep-ph]. [Erratum: Astropart. Phys.15,413(2001)].

[327] G. Belanger, F. Boudjema, A. Pukhov, and A. Semenov, "MicrOMEGAs 2.0: A Program to calculate the relic density of dark matter in a generic model," *Comput. Phys. Commun.* **176** (2007) 367–382, arXiv:hep-ph/0607059 [hep-ph].

[328] G. Belanger, F. Boudjema, A. Pukhov, and A. Semenov, "Dark matter direct detection rate in a generic model with micrOMEGAs 2.2," *Comput. Phys. Commun.* **180** (2009) 747–767, arXiv:0803.2360 [hep-ph].

[329] M. Cirelli, E. Del Nobile, and P. Panci, "Tools for model-independent bounds in direct dark matter searches," *JCAP* **1310** (2013) 019, arXiv:1307.5955 [hep-ph].

[330] G. Belanger, F. Boudjema, A. Pukhov, and A. Semenov, "micrOMEGAs 3: A program for calculating dark matter observables," *Comput. Phys. Commun.* **185** (2014) 960–985, arXiv:1305.0237 [hep-ph].

[331] G. BÃl'langer, F. Boudjema, A. Pukhov, and A. Semenov, "micrOMEGAs4.1: two dark matter candidates," *Comput. Phys. Commun.* **192** (2015) 322–329, arXiv:1407.6129 [hep-ph].

[332] **The GAMBIT Dark Matter Workgroup** Collaboration, T. Bringmann *et al.*, "DarkBit: A GAMBIT module for computing dark matter observables and likelihoods," *Eur. Phys. J.* **C77** no. 12, (2017) 831, arXiv:1705.07920 [hep-ph].

[333] T. Bringmann, J. Edsjo, P. Gondolo, P. Ullio, and L. Bergstrom, "DarkSUSY 6 : An Advanced Tool to Compute Dark Matter Properties Numerically," arXiv:1802.03399 [hep-ph].

[334] G. Arcadi, M. Dutra, P. Ghosh, M. Lindner, Y. Mambrini, M. Pierre, S. Profumo, and F. S. Queiroz, "The waning of the WIMP? A review of models, searches, and constraints," *Eur. Phys. J.* **C78** no. 3, (2018) 203, arXiv:1703.07364 [hep-ph].

[335] F. Takayama and M. Yamaguchi, "Gravitino dark matter without R-parity," *Phys. Lett.* **B485** (2000) 388–392, arXiv:hep-ph/0005214 [hep-ph].

[336] F. D. Steffen, "Gravitino dark matter and cosmological constraints," *JCAP* **0609** (2006) 001, arXiv:hep-ph/0605306 [hep-ph].

[337] W. Buchmuller, L. Covi, K. Hamaguchi, A. Ibarra, and T. Yanagida, "Gravitino Dark Matter in R-Parity Breaking Vacua," *JHEP* **03** (2007) 037, arXiv:hep-ph/0702184 [HEP-PH].

[338] J. Pradler and F. D. Steffen, "Thermal gravitino production and collider tests of leptogenesis," *Phys. Rev.* **D75** (2007) 023509, arXiv:hep-ph/0608344 [hep-ph].

[339] L. Covi, J. Hasenkamp, S. Pokorski, and J. Roberts, "Gravitino Dark Matter and general neutralino NLSP," *JHEP* **11** (2009) 003, arXiv:0908.3399 [hep-ph].

[340] C. Arina and N. Fornengo, "Sneutrino cold dark matter, a new analysis: Relic abundance and detection rates," *JHEP* **11** (2007) 029, arXiv:0709.4477 [hep-ph].

[341] D. G. Cerdeno, C. Munoz, and O. Seto, "Right-handed sneutrino as thermal dark matter," *Phys. Rev.* **D79** (2009) 023510, arXiv:0807.3029 [hep-ph].

[342] D. G. Cerdeno and O. Seto, "Right-handed sneutrino dark matter in the NMSSM," *JCAP* **0908** (2009) 032, arXiv:0903.4677 [hep-ph].

[343] H. Goldberg, "Constraint on the Photino Mass from Cosmology," *Phys. Rev. Lett.* **50** (1983) 1419. [Erratum: Phys. Rev. Lett.103,099905(2009)].

[344] J. R. Ellis, J. S. Hagelin, D. V. Nanopoulos, K. A. Olive, and M. Srednicki, "Supersymmetric Relics from the Big Bang," *Nucl. Phys.* **B238** (1984) 453–476.

[345] K. Griest, "Cross-Sections, Relic Abundance and Detection Rates for Neutralino Dark Matter," *Phys. Rev.* **D38** (1988) 2357. [Erratum: Phys. Rev.D39,3802(1989)].

[346] G. Jungman, M. Kamionkowski, and K. Griest, "Supersymmetric dark matter," *Phys. Rept.* **267** (1996) 195–373, arXiv:hep-ph/9506380 [hep-ph].

[347] J. L. Feng, K. T. Matchev, and F. Wilczek, "Neutralino dark matter in focus point supersymmetry," *Phys. Lett.* **B482** (2000) 388–399, arXiv:hep-ph/0004043 [hep-ph].

[348] H. Baer, V. Barger, and A. Mustafayev, "Implications of a 125 GeV Higgs scalar for LHC SUSY and neutralino dark matter searches," *Phys. Rev.* **D85** (2012) 075010, arXiv:1112.3017 [hep-ph].

[349] N. G. Deshpande and E. Ma, "Pattern of Symmetry Breaking with Two Higgs Doublets," *Phys. Rev.* **D18** (1978) 2574.

[350] G. C. Branco, P. M. Ferreira, L. Lavoura, M. N. Rebelo, M. Sher, and J. P. Silva, "Theory and phenomenology of two-Higgs-doublet models," *Phys. Rept.* **516** (2012) 1–102, arXiv:1106.0034 [hep-ph].

[351] R. Barbieri, L. J. Hall, and V. S. Rychkov, "Improved naturalness with a heavy Higgs: An Alternative road to LHC physics," *Phys. Rev.* **D74** (2006) 015007, arXiv:hep-ph/0603188 [hep-ph].

[352] E. Ma, "Verifiable radiative seesaw mechanism of neutrino mass and dark matter," *Phys. Rev.* **D73** (2006) 077301, arXiv:hep-ph/0601225 [hep-ph].

[353] L. Lopez Honorez, E. Nezri, J. F. Oliver, and M. H. G. Tytgat, "The Inert Doublet Model: An Archetype for Dark Matter," *JCAP* **0702** (2007) 028, arXiv:hep-ph/0612275 [hep-ph].

[354] A. Goudelis, B. Herrmann, and O. StÃěl, "Dark matter in the Inert Doublet Model after the discovery of a Higgs-like boson at the LHC," *JHEP* **09** (2013) 106, arXiv:1303.3010 [hep-ph].

[355] I. Low, "T parity and the littlest Higgs," *JHEP* **10** (2004) 067, arXiv:hep-ph/0409025 [hep-ph].

[356] J. Hubisz and P. Meade, "Phenomenology of the littlest Higgs with T-parity," *Phys. Rev.* **D71** (2005) 035016, arXiv:hep-ph/0411264 [hep-ph].

[357] J. Hubisz, P. Meade, A. Noble, and M. Perelstein, "Electroweak precision constraints on the littlest Higgs model with T parity," *JHEP* **01** (2006) 135, arXiv:hep-ph/0506042 [hep-ph].

[358] I. Garcia Garcia, R. Lasenby, and J. March-Russell, "Twin Higgs WIMP Dark Matter," *Phys. Rev.* **D92** no. 5, (2015) 055034, arXiv:1505.07109 [hep-ph].

[359] M. Farina, "Asymmetric Twin Dark Matter," *JCAP* **1511** no. 11, (2015) 017, arXiv:1506.03520 [hep-ph].

[360] N. Craig and A. Katz, "The Fraternal WIMP Miracle," *JCAP* **1510** no. 10, (2015) 054, arXiv:1505.07113 [hep-ph].

[361] I. Garcia Garcia, R. Lasenby, and J. March-Russell, "Twin Higgs Asymmetric Dark Matter," *Phys. Rev. Lett.* **115** no. 12, (2015) 121801, arXiv:1505.07410 [hep-ph].

[362] V. Silveira and A. Zee, "SCALAR PHANTOMS," *Phys. Lett.* **161B** (1985) 136–140.

[363] J. McDonald, "Gauge singlet scalars as cold dark matter," *Phys. Rev.* **D50** (1994) 3637–3649, arXiv:hep-ph/0702143 [HEP-PH].

[364] C. P. Burgess, M. Pospelov, and T. ter Veldhuis, "The Minimal model of nonbaryonic dark matter: A Singlet scalar," *Nucl. Phys.* **B619** (2001) 709–728, arXiv:hep-ph/0011335 [hep-ph].

[365] J. M. Cline, K. Kainulainen, P. Scott, and C. Weniger, "Update on scalar singlet dark matter," *Phys. Rev.* **D88** (2013) 055025, arXiv:1306.4710 [hep-ph]. [Erratum: Phys. Rev.D92,no.3,039906(2015)].

[366] L. Feng, S. Profumo, and L. Ubaldi, "Closing in on singlet scalar dark matter: LUX, invisible Higgs decays and gamma-ray lines," *JHEP* **03** (2015) 045, arXiv:1412.1105 [hep-ph].

[367] Y. G. Kim and K. Y. Lee, "The Minimal model of fermionic dark matter," *Phys. Rev.* **D75** (2007) 115012, arXiv:hep-ph/0611069 [hep-ph].

[368] R. Harnik and G. D. Kribs, "An Effective Theory of Dirac Dark Matter," *Phys. Rev.* **D79** (2009) 095007, arXiv:0810.5557 [hep-ph].

[369] P. Ciafaloni, M. Cirelli, D. Comelli, A. De Simone, A. Riotto, and A. Urbano, "On the Importance of Electroweak Corrections for Majorana Dark Matter Indirect Detection," *JCAP* **1106** (2011) 018, arXiv:1104.2996 [hep-ph].

[370] L. Lopez-Honorez, T. Schwetz, and J. Zupan, "Higgs portal, fermionic dark matter, and a Standard Model like Higgs at 125 GeV," *Phys. Lett.* **B716** (2012) 179–185, arXiv:1203.2064 [hep-ph].

[371] Y. Bai and J. Berger, "Fermion Portal Dark Matter," *JHEP* **11** (2013) 171, arXiv:1308.0612 [hep-ph].

[372] S. Baek, P. Ko, and W.-I. Park, "Search for the Higgs portal to a singlet fermionic dark matter at the LHC," *JHEP* **02** (2012) 047, arXiv:1112.1847 [hep-ph].

[373] S. Baek, P. Ko, W.-I. Park, and E. Senaha, "Vacuum structure and stability of a singlet fermion dark matter model with a singlet scalar messenger," *JHEP* **11** (2012) 116, arXiv:1209.4163 [hep-ph].

[374] M. Fairbairn and R. Hogan, "Singlet Fermionic Dark Matter and the Electroweak Phase Transition," *JHEP* **09** (2013) 022, arXiv:1305.3452 [hep-ph].

[375] A. Freitas, S. Westhoff, and J. Zupan, "Integrating in the Higgs Portal to Fermion Dark Matter," *JHEP* **09** (2015) 015, arXiv:1506.04149 [hep-ph].

[376] M. Cirelli, F. Sala, and M. Taoso, "Wino-like Minimal Dark Matter and future colliders," *JHEP* **10** (2014) 033, arXiv:1407.7058 [hep-ph]. [Erratum: JHEP01,041(2015)].

[377] A. Dedes and D. Karamitros, "Doublet-Triplet Fermionic Dark Matter," *Phys. Rev.* **D89** no. 11, (2014) 115002, arXiv:1403.7744 [hep-ph].

[378] A. Dedes, D. Karamitros, and V. C. Spanos, "Effective Theory for Electroweak Doublet Dark Matter," *Phys. Rev.* **D94** no. 9, (2016) 095008, arXiv:1607.05040 [hep-ph].

[379] T. Hambye, "Hidden vector dark matter," *JHEP* **0901** (2009) 028, arXiv:0811.0172 [hep-ph].

[380] T. Hambye and M. H. Tytgat, "Confined hidden vector dark matter," *Phys.Lett.* **B683** (2010) 39–41, arXiv:0907.1007 [hep-ph].

[381] H. Zhang, C. S. Li, Q.-H. Cao, and Z. Li, "A Dark Matter Model with Non-Abelian Gauge Symmetry," *Phys.Rev.* **D82** (2010) 075003, arXiv:0910.2831 [hep-ph].

[382] C. Arina, T. Hambye, A. Ibarra, and C. Weniger, "Intense Gamma-Ray Lines from Hidden Vector Dark Matter Decay," *JCAP* **1003** (2010) 024, arXiv:0912.4496 [hep-ph].

[383] S. Bhattacharya, J. L. Diaz-Cruz, E. Ma, and D. Wegman, "Dark Vector-Gauge-Boson Model," *Phys.Rev.* **D85** (2012) 055008, arXiv:1107.2093 [hep-ph].

[384] C.-W. Chiang, T. Nomura, and J. Tandean, "Nonabelian Dark Matter with Resonant Annihilation," *JHEP* **1401** (2014) 183, arXiv:1306.0882 [hep-ph].

[385] C. Boehm, M. J. Dolan, and C. McCabe, "A weighty interpretation of the Galactic Centre excess," *Phys.Rev.* **D90** no. 2, (2014) 023531, arXiv:1404.4977 [hep-ph].

[386] S. Baek, P. Ko, W.-I. Park, and E. Senaha, "Higgs Portal Vector Dark Matter : Revisited," *JHEP* **1305** (2013) 036, arXiv:1212.2131 [hep-ph].

[387] F. D'Eramo, M. McCullough, and J. Thaler, "Multiple Gamma Lines from Semi-Annihilation," *JCAP* **1304** (2013) 030, arXiv:1210.7817 [hep-ph].

[388] Y. Farzan and A. R. Akbarieh, "VDM: A model for Vector Dark Matter," *JCAP* **1210** (2012) 026, arXiv:1207.4272 [hep-ph].

[389] A. Djouadi, O. Lebedev, Y. Mambrini, and J. Quevillon, "Implications of lhc searches for higgs-portal dark matter," *Physics Letters B* **709** no. 1, (2012) 65–69.

[390] K.-Y. Choi, H. M. Lee, and O. Seto, "Vector Higgs-portal dark matter and Fermi-LAT gamma ray line," *Phys. Rev.* **D87** no. 12, (2013) 123541, arXiv:1304.0966 [hep-ph].

[391] S. Baek, P. Ko, and W.-I. Park, "Hidden sector monopole, vector dark matter and dark radiation with Higgs portal," *JCAP* **1410** no. 10, (2014) 067, arXiv:1311.1035 [hep-ph].

[392] S. Baek, P. Ko, W.-I. Park, and Y. Tang, "Indirect and direct signatures of Higgs portal decaying vector dark matter for positron excess in cosmic rays," *JCAP* **1406** (2014) 046, arXiv:1402.2115 [hep-ph].

[393] P. Ko, W.-I. Park, and Y. Tang, "Higgs portal vector dark matter for GeV scale γ-ray excess from galactic center," *JCAP* **1409** (2014) 013, arXiv:1404.5257 [hep-ph].

[394] C. BalÃązs and T. Li, "Simplified Dark Matter Models Confront the Gamma Ray Excess," *Phys. Rev.* **D90** no. 5, (2014) 055026, arXiv:1407.0174 [hep-ph].

[395] Y. Farzan and A. R. Akbarieh, "Decaying Vector Dark Matter as an Explanation for the 3.5 keV Line from Galaxy Clusters," *JCAP* **1411** no. 11, (2014) 015, arXiv:1408.2950 [hep-ph].

[396] S. Fraser, E. Ma, and M. Zakeri, "$SU(2)_N$ model of vector dark matter with a leptonic connection," *Int. J. Mod. Phys.* **A30** no. 03, (2015) 1550018, arXiv:1409.1162 [hep-ph].

[397] C.-R. Chen, Y.-K. Chu, and H.-C. Tsai, "An Elusive Vector Dark Matter," *Phys. Lett.* **B741** (2015) 205–209, arXiv:1410.0918 [hep-ph].

[398] W. Chao, "First order electroweak phase transition triggered by the Higgs portal vector dark matter," *Phys. Rev.* **D92** no. 1, (2014) 015025, arXiv:1412.3823 [hep-ph].

[399] M. Duch, B. Grzadkowski, and M. McGarrie, "A stable Higgs portal with vector dark matter," *JHEP* **09** (2015) 162, arXiv:1506.08805 [hep-ph].

[400] S. Di Chiara and K. Tuominen, "A minimal model for SU(N) vector dark matter," *JHEP* **11** (2015) 188, arXiv:1506.03285 [hep-ph].

[401] C. Gross, O. Lebedev, and Y. Mambrini, "Non-Abelian gauge fields as dark matter," *JHEP* **08** (2015) 158, arXiv:1505.07480 [hep-ph].

[402] N. Bernal, X. Chu, C. Garcia-Cely, T. Hambye, and B. Zaldivar, "Production Regimes for Self-Interacting Dark Matter," *JCAP* **1603** no. 03, (2016) 018, arXiv:1510.08063 [hep-ph].

[403] F. S. Sage and R. Dick, "Gamma ray signals of the annihilation of Higgs-portal singlet dark matter," arXiv:1604.04589 [astro-ph.HE].

[404] V. V. Khoze and G. Ro, "Dark matter monopoles, vectors and photons," *JHEP* **10** (2014) 61, arXiv:1406.2291 [hep-ph].

[405] L. Bian, T. Li, J. Shu, and X.-C. Wang, "Two component dark matter with multi-Higgs portals," *JHEP* **1503** (2015) 126, arXiv:1412.5443 [hep-ph].

[406] C.-H. Chen, C.-W. Chiang, and T. Nomura, "Dark matter for excess of AMS-02 positrons and antiprotons," *Phys. Lett.* **B747** (2015) 495–499, arXiv:1504.07848 [hep-ph].

[407] C.-H. Chen and T. Nomura, "$SU(2)_X$ vector DM and Galactic Center gamma-ray excess," *Phys.Lett.* **B746** (2015) 351–358, arXiv:1501.07413 [hep-ph].

[408] C.-H. Chen and T. Nomura, "Searching for Vector Dark Matter by Higgs Portal at the LHC," *Phys. Rev.* **D93** no. 7, (2015) 074019, arXiv:1507.00886 [hep-ph].

[409] T. Hambye and A. Strumia, "Dynamical generation of the weak and Dark Matter scale," *Phys.Rev.* **D88** (2013) 055022, arXiv:1306.2329 [hep-ph].

[410] C. D. Carone and R. Ramos, "Classical scale-invariance, the electroweak scale and vector dark matter," *Phys.Rev.* **D88** (2013) 055020, arXiv:1307.8428 [hep-ph].

[411] V. V. Khoze, C. McCabe, and G. Ro, "Higgs vacuum stability from the dark matter portal," *JHEP* **1408** (2014) 026, arXiv:1403.4953 [hep-ph].

[412] V. V. Khoze and A. D. Plascencia, "Dark Matter and Leptogenesis Linked by Classical Scale Invariance," *JHEP* **11** (2016) 025, arXiv:1605.06834 [hep-ph].

[413] G. M. Pelaggi, "Predictions of a model of weak scale from dynamical breaking of scale invariance," *Nucl.Phys.* **B893** (2015) 443–458, arXiv:1406.4104 [hep-ph].

[414] A. Karam and K. Tamvakis, "Dark matter and neutrino masses from a scale-invariant multi-Higgs portal," *Phys. Rev.* **D92** no. 7, (2015) 075010, arXiv:1508.03031 [hep-ph].

[415] A. DiFranzo, P. J. Fox, and T. M. P. Tait, "Vector Dark Matter through a Radiative Higgs Portal," *JHEP* **04** (2016) 135, arXiv:1512.06853 [hep-ph].

[416] P. Ko and H. Yokoya, "Search for Higgs portal DM at the ILC," arXiv:1603.04737 [hep-ph].

[417] A. Karam and K. Tamvakis, "Dark matter and neutrino masses from a classically scale-invariant multi-Higgs portal," *PoS* **CORFU2015** (2016) 073, arXiv:1603.08470 [hep-ph].

[418] A. Karam and K. Tamvakis, "Dark Matter from a Classically Scale-Invariant $SU(3)_X$," *Phys. Rev.* **D94** no. 5, (2016) 055004, arXiv:1607.01001 [hep-ph].

[419] J. Kopp, J. Liu, T. R. Slatyer, X.-P. Wang, and W. Xue, "Impeded Dark Matter," *JHEP* **12** (2016) 033, arXiv:1609.02147 [hep-ph].

[420] P. Ko and Y. Tang, "Residual Non-Abelian Dark Matter and Dark Radiation," *Phys. Lett.* **B768** (2017) 12–17, arXiv:1609.02307 [hep-ph].

[421] A. DiFranzo and G. Mohlabeng, "Multi-component Dark Matter through a Radiative Higgs Portal," *JHEP* **01** (2017) 080, arXiv:1610.07606 [hep-ph].

[422] G. Arcadi, C. Gross, O. Lebedev, Y. Mambrini, S. Pokorski, and T. Toma, "Multicomponent Dark Matter from Gauge Symmetry," *JHEP* **12** (2016) 081, arXiv:1611.00365 [hep-ph].

[423] G. Arcadi, C. Gross, O. Lebedev, S. Pokorski, and T. Toma, "Evading Direct Dark Matter Detection in Higgs Portal Models," *Phys. Lett.* **B769** (2017) 129–133, arXiv:1611.09675 [hep-ph].

[424] M. Heikinheimo, T. Tenkanen, and K. Tuominen, "WIMP miracle of the second kind," *Phys. Rev.* **D96** no. 2, (2017) 023001, arXiv:1704.05359 [hep-ph].

[425] S.-M. Choi, Y. Hochberg, E. Kuflik, H. M. Lee, Y. Mambrini, H. Murayama, and M. Pierre, "Vector SIMP dark matter," *JHEP* **10** (2017) 162, arXiv:1707.01434 [hep-ph].

[426] G. Arcadi, F. S. Queiroz, and C. Siqueira, "The Semi-Hooperon: Gamma-ray and anti-proton excesses in the Galactic Center," *Phys. Lett.* **B775** (2017) 196–205, arXiv:1706.02336 [hep-ph].

[427] M. Duch, B. Grzadkowski, and D. Huang, "Strongly self-interacting vector dark matter via freeze-in," *JHEP* **01** (2018) 020, arXiv:1710.00320 [hep-ph].

[428] **PICO** Collaboration, C. Amole *et al.*, "Dark Matter Search Results from the PICO-60 C_3F_8 Bubble Chamber," *Phys. Rev. Lett.* **118** no. 25, (2017) 251301, arXiv:1702.07666 [astro-ph.CO].

[429] **CoGeNT** Collaboration, C. E. Aalseth *et al.*, "CoGeNT: A Search for Low-Mass Dark Matter using p-type Point Contact Germanium Detectors," *Phys. Rev.* **D88** (2013) 012002, arXiv:1208.5737 [astro-ph.CO].

[430] **CoGeNT** Collaboration, C. E. Aalseth *et al.*, "Search for An Annual Modulation in Three Years of CoGeNT Dark Matter Detector Data," arXiv:1401.3295 [astro-ph.CO].

[431] C. E. Aalseth *et al.*, "The DarkSide Multiton Detector for the Direct Dark Matter Search," *Adv. High Energy Phys.* **2015** (2015) 541362.

[432] **ANTARES** Collaboration, S. Adrian-Martinez *et al.*, "First results on dark matter annihilation in the Sun using the ANTARES neutrino telescope," *JCAP* **1311** (2013) 032, arXiv:1302.6516 [astro-ph.HE].

[433] **ANTARES** Collaboration, S. Adrian-Martinez *et al.*, "Limits on Dark Matter Annihilation in the Sun using the ANTARES Neutrino Telescope," *Phys. Lett.* **B759** (2016) 69–74, arXiv:1603.02228 [astro-ph.HE].

[434] **DarkSide** Collaboration, P. Agnes *et al.*, "First Results from the DarkSide-50 Dark Matter Experiment at Laboratori Nazionali del Gran Sasso," *Phys. Lett.* **B743** (2015) 456–466, arXiv:1410.0653 [astro-ph.CO].

[435] **DarkSide** Collaboration, P. Agnes *et al.*, "Results from the first use of low radioactivity argon in a dark matter search," *Phys. Rev.* **D93** no. 8, (2016) 081101, arXiv:1510.00702 [astro-ph.CO]. [Addendum: Phys. Rev.D95,no.6,069901(2017)].

[436] **CDMS** Collaboration, R. Agnese *et al.*, "Silicon Detector Dark Matter Results from the Final Exposure of CDMS II," *Phys. Rev. Lett.* **111** no. 25, (2013) 251301, arXiv:1304.4279 [hep-ex].

[437] **CDMS** Collaboration, R. Agnese *et al.*, "Silicon detector results from the first five-tower run of CDMS II," *Phys. Rev.* **D88** (2013) 031104, arXiv:1304.3706 [astro-ph.CO]. [Erratum: Phys. Rev.D88,no.5,059901(2013)].

[438] **CDMS-II** Collaboration, Z. Ahmed *et al.*, "Search for annual modulation in low-energy CDMS-II data," arXiv:1203.1309 [astro-ph.CO].

[439] **LUX** Collaboration, D. S. Akerib *et al.*, "Improved Limits on Scattering of Weakly Interacting Massive Particles from Reanalysis of 2013 LUX Data," *Phys. Rev. Lett.* **116** no. 16, (2016) 161301, arXiv:1512.03506 [astro-ph.CO].

[440] **LUX** Collaboration, D. S. Akerib *et al.*, "Results on the Spin-Dependent Scattering of Weakly Interacting Massive Particles on Nucleons from the Run 3 Data of the LUX Experiment," *Phys. Rev. Lett.* **116** no. 16, (2016) 161302, arXiv:1602.03489 [hep-ex].

[441] **LUX** Collaboration, D. S. Akerib *et al.*, "Results from a search for dark matter in the complete LUX exposure," *Phys. Rev. Lett.* **118** no. 2, (2017) 021303, arXiv:1608.07648 [astro-ph.CO].

[442] **PICO** Collaboration, C. Amole *et al.*, "Dark matter search results from the PICO-60 CF_3I bubble chamber," *Phys. Rev.* **D93** no. 5, (2016) 052014, arXiv:1510.07754 [hep-ex].

[443] **PICO** Collaboration, C. Amole *et al.*, "Dark Matter Search Results from the PICO-2L C_3F_8 Bubble Chamber," *Phys. Rev. Lett.* **114** no. 23, (2015) 231302, arXiv:1503.00008 [astro-ph.CO].

[444] **PICO** Collaboration, C. Amole *et al.*, "Improved dark matter search results from PICO-2L Run 2," *Phys. Rev.* **D93** no. 6, (2016) 061101, arXiv:1601.03729 [astro-ph.CO].

[445] **CRESST-II** Collaboration, G. Angloher *et al.*, "Results on low mass WIMPs using an upgraded CRESST-II detector," *Eur. Phys. J.* **C74** no. 12, (2014) 3184, arXiv:1407.3146 [astro-ph.CO].

[446] **CRESST** Collaboration, G. Angloher *et al.*, "Results on light dark matter particles with a low-threshold CRESST-II detector," *Eur. Phys. J.* **C76** no. 1, (2016) 25, arXiv:1509.01515 [astro-ph.CO].

[447] **XENON100** Collaboration, E. Aprile *et al.*, "First Dark Matter Results from the XENON100 Experiment," *Phys. Rev. Lett.* **105** (2010) 131302, arXiv:1005.0380 [astro-ph.CO].

[448] **XENON100** Collaboration, E. Aprile *et al.*, "Dark Matter Results from 100 Live Days of XENON100 Data," *Phys. Rev. Lett.* **107** (2011) 131302, arXiv:1104.2549 [astro-ph.CO].

[449] **XENON100** Collaboration, E. Aprile *et al.*, "Dark Matter Results from 225 Live Days of XENON100 Data," *Phys. Rev. Lett.* **109** (2012) 181301, arXiv:1207.5988 [astro-ph.CO].

[450] **XENON100** Collaboration, E. Aprile *et al.*, "Limits on spin-dependent WIMP-nucleon cross sections from 225 live days of XENON100 data," *Phys.Rev.Lett.* **111** no. 2, (2013) 021301, arXiv:1301.6620 [astro-ph.CO].

[451] **XENON100** Collaboration, E. Aprile *et al.*, "First Axion Results from the XENON100 Experiment," *Phys. Rev.* **D90** no. 6, (2014) 062009, arXiv:1404.1455 [astro-ph.CO]. [Erratum: Phys. Rev.D95,no.2,029904(2017)].

[452] **XENON100** Collaboration, E. Aprile *et al.*, "Search for Event Rate Modulation in XENON100 Electronic Recoil Data," *Phys. Rev. Lett.* **115** no. 9, (2015) 091302, arXiv:1507.07748 [astro-ph.CO].

[453] **XENON100** Collaboration, E. Aprile *et al.*, "XENON100 Dark Matter Results from a Combination of 477 Live Days," *Phys. Rev.* **D94** no. 12, (2016) 122001, arXiv:1609.06154 [astro-ph.CO].

[454] **EDELWEISS** Collaboration, E. Armengaud *et al.*, "Constraints on low-mass WIMPs from the EDELWEISS-III dark matter search," *JCAP* **1605** no. 05, (2016) 019, arXiv:1603.05120 [astro-ph.CO].

[455] **Super-Kamiokande** Collaboration, K. Choi *et al.*, "Search for neutrinos from annihilation of captured low-mass dark matter particles in the Sun by Super-Kamiokande," *Phys. Rev. Lett.* **114** no. 14, (2015) 141301, arXiv:1503.04858 [hep-ex].

[456] **EDELWEISS** Collaboration, L. Hehn *et al.*, "Improved EDELWEISS-III sensitivity for low-mass WIMPs using a profile likelihood approach," *Eur. Phys. J.* **C76** no. 10, (2016) 548, arXiv:1607.03367 [astro-ph.CO].

[457] **Super-Kamiokande** Collaboration, T. Tanaka *et al.*, "An Indirect Search for WIMPs in the Sun using 3109.6 days of upward-going muons in Super-Kamiokande," *Astrophys. J.* **742** (2011) 78, arXiv:1108.3384 [astro-ph.HE].

[458] R. Catena and P. Ullio, "A novel determination of the local dark matter density," *JCAP* **1008** (2010) 004, arXiv:0907.0018 [astro-ph.CO].

[459] M. Weber and W. de Boer, "Determination of the Local Dark Matter Density in our Galaxy," *Astron. Astrophys.* **509** (2010) A25, arXiv:0910.4272 [astro-ph.CO].

[460] J. I. Read, "The Local Dark Matter Density," *J. Phys.* **G41** (2014) 063101, arXiv:1404.1938 [astro-ph.GA].

[461] Q. Xia, C. Liu, S. Mao, Y. Song, L. Zhang, R. J. Long, Y. Zhang, Y. Hou, Y. Wang, and Y. Wu, "Determining the local dark matter density with LAMOST data," *Mon. Not. Roy. Astron. Soc.* **458** no. 4, (2016) 3839–3850, arXiv:1510.06810 [astro-ph.GA].

[462] F. Iocco, M. Pato, and G. Bertone, "Reply to Comment on "Evidence for dark matter in the inner Milky Way"," arXiv:1503.08784 [astro-ph.GA].

[463] F. Iocco, M. Pato, and G. Bertone, "Evidence for dark matter in the inner Milky Way," *Nature Phys.* **11** (2015) 245–248, arXiv:1502.03821 [astro-ph.GA].

[464] S. McGaugh *et al.*, "Comment on "Evidence for dark matter in the inner Milky Way"," arXiv:1503.07813 [astro-ph.GA].

[465] G. Duda, A. Kemper, and P. Gondolo, "Model Independent Form Factors for Spin Independent Neutralino-Nucleon Scattering from Elastic Electron Scattering Data," *JCAP* **0704** (2007) 012, arXiv:hep-ph/0608035 [hep-ph].

[466] V. A. Bednyakov and F. Simkovic, "Nuclear spin structure in dark matter search: The Finite momentum transfer limit," *Phys. Part. Nucl.* **37** (2006) S106–S128, arXiv:hep-ph/0608097 [hep-ph].

[467] R. W. Schnee, "Introduction to dark matter experiments," in *Physics of the large and the small, TASI 09, proceedings of the Theoretical Advanced Study Institute in Elementary Particle Physics, Boulder, Colorado, USA, 1-26 June 2009*, pp. 775–829. 2011. arXiv:1101.5205 [astro-ph.CO]. http://inspirehep.net/record/885795/files/arXiv:1101.5205.pdf.

[468] **DAMA, LIBRA** Collaboration, R. Bernabei *et al.*, "New results from DAMA/LIBRA," *Eur. Phys. J.* **C67** (2010) 39–49, arXiv:1002.1028 [astro-ph.GA].

[469] R. Bernabei *et al.*, "Final model independent result of DAMA/LIBRA-phase1," *Eur. Phys. J.* **C73** (2013) 2648, arXiv:1308.5109 [astro-ph.GA].

[470] C. E. Aalseth *et al.*, "Search for an Annual Modulation in a P-type Point Contact Germanium Dark Matter Detector," *Phys. Rev. Lett.* **107** (2011) 141301, arXiv:1106.0650 [astro-ph.CO].

[471] **CoGeNT** Collaboration, C. E. Aalseth *et al.*, "Results from a Search for Light-Mass Dark Matter with a P-type Point Contact Germanium Detector," *Phys. Rev. Lett.* **106** (2011) 131301, arXiv:1002.4703 [astro-ph.CO].

[472] M. Felizardo *et al.*, "Final Analysis and Results of the Phase II SIMPLE Dark Matter Search," *Phys. Rev. Lett.* **108** (2012) 201302, arXiv:1106.3014 [astro-ph.CO].

[473] **PICASSO** Collaboration, S. Archambault *et al.*, "Constraints on Low-Mass WIMP Interactions on ^{19}F from PICASSO," *Phys. Lett.* **B711** (2012) 153–161, arXiv:1202.1240 [hep-ex].

[474] **COUPP** Collaboration, E. Behnke *et al.*, "First Dark Matter Search Results from a 4-kg CF_3I Bubble Chamber Operated in a Deep Underground Site," *Phys. Rev.* **D86** no. 5, (2012) 052001, arXiv:1204.3094 [astro-ph.CO]. [Erratum: Phys. Rev.D90,no.7,079902(2014)].

[475] **SuperCDMS** Collaboration, R. Agnese *et al.*, "Search for Low-Mass Weakly Interacting Massive Particles with SuperCDMS," *Phys. Rev. Lett.* **112** no. 24, (2014) 241302, arXiv:1402.7137 [hep-ex].

[476] **SuperCDMS** Collaboration, R. Agnese *et al.*, "Improved WIMP-search reach of the CDMS II germanium data," *Phys. Rev.* **D92** no. 7, (2015) 072003, arXiv:1504.05871 [hep-ex].

[477] **SuperCDMS** Collaboration, R. Agnese *et al.*, "New Results from the Search for Low-Mass Weakly Interacting Massive Particles with the CDMS Low Ionization Threshold Experiment," *Phys. Rev. Lett.* **116** no. 7, (2016) 071301, arXiv:1509.02448 [astro-ph.CO].

[478] **PandaX-II** Collaboration, A. Tan *et al.*, "Dark Matter Results from First 98.7 Days of Data from the PandaX-II Experiment," *Phys. Rev. Lett.* **117** no. 12, (2016) 121303, arXiv:1607.07400 [hep-ex].

[479] **XENON** Collaboration, E. Aprile *et al.*, "First Dark Matter Search Results from the XENON1T Experiment," *Phys. Rev. Lett.* **119** no. 18, (2017) 181301, arXiv:1705.06655 [astro-ph.CO].

[480] **LUX, LZ** Collaboration, M. Szydagis, "The Present and Future of Searching for Dark Matter with LUX and LZ," *PoS* **ICHEP2016** (2016) 220, arXiv:1611.05525 [astro-ph.CO].

[481] M. Schumann, L. Baudis, L. BÃijtikofer, A. Kish, and M. Selvi, "Dark matter sensitivity of multi-ton liquid xenon detectors," *JCAP* **1510** no. 10, (2015) 016, arXiv:1506.08309 [physics.ins-det].

[482] **SuperCDMS** Collaboration, R. Agnese *et al.*, "Projected Sensitivity of the SuperCDMS SNOLAB experiment," *Phys. Rev.* **D95** no. 8, (2017) 082002, arXiv:1610.00006 [physics.ins-det].

[483] J. Billard, L. Strigari, and E. Figueroa-Feliciano, "Implication of neutrino backgrounds on the reach of next generation dark matter direct detection experiments," *Phys. Rev.* **D89** no. 2, (2014) 023524, arXiv:1307.5458 [hep-ph].

[484] L. Roszkowski, E. M. Sessolo, and S. Trojanowski, "WIMP dark matter candidates and searches - current issues and future prospects," arXiv:1707.06277 [hep-ph].

[485] **Fermi-LAT** Collaboration, A. A. Abdo *et al.*, "Observations of Milky Way Dwarf Spheroidal galaxies with the Fermi-LAT detector and constraints on Dark Matter models," *Astrophys. J.* **712** (2010) 147–158, arXiv:1001.4531 [astro-ph.CO].

[486] **Fermi-LAT** Collaboration, M. Ackermann *et al.*, "Constraining Dark Matter Models from a Combined Analysis of Milky Way Satellites with the Fermi Large Area Telescope," *Phys. Rev. Lett.* **107** (2011) 241302, arXiv:1108.3546 [astro-ph.HE].

[487] **H.E.S.S.** Collaboration, A. Abramowski *et al.*, "Search for a Dark Matter annihilation signal from the Galactic Center halo with H.E.S.S," *Phys. Rev. Lett.* **106** (2011) 161301, arXiv:1103.3266 [astro-ph.HE].

[488] **H.E.S.S.** Collaboration, A. Abramowski *et al.*, "Search for Dark Matter Annihilation Signals from the Fornax Galaxy Cluster with H.E.S.S," *Astrophys. J.* **750** (2012) 123, arXiv:1202.5494 [astro-ph.HE]. [Erratum: Astrophys. J.783,63(2014)].

[489] **Fermi-LAT** Collaboration, M. Ackermann *et al.*, "Search for Dark Matter Satellites using the FERMI-LAT," *Astrophys. J.* **747** (2012) 121, arXiv:1201.2691 [astro-ph.HE].

[490] **Fermi-LAT** Collaboration, M. Ackermann *et al.*, "Search for Gamma-ray Spectral Lines with the Fermi Large Area Telescope and Dark Matter Implications," *Phys. Rev.* **D88** (2013) 082002, arXiv:1305.5597 [astro-ph.HE].

[491] **Fermi-LAT** Collaboration, M. Ackermann *et al.*, "Dark matter constraints from observations of 25 MilkyÂăWay satellite galaxies with the Fermi Large Area Telescope," *Phys. Rev.* **D89** (2014) 042001, arXiv:1310.0828 [astro-ph.HE].

[492] **H.E.S.S.** Collaboration, A. Abramowski *et al.*, "Search for dark matter annihilation signatures in H.E.S.S. observations of Dwarf Spheroidal Galaxies," *Phys. Rev.* **D90** (2014) 112012, arXiv:1410.2589 [astro-ph.HE].

[493] **H.E.S.S.** Collaboration, A. Abramowski *et al.*, "Constraints on an Annihilation Signal from a Core of Constant Dark Matter Density around the MilkyÂăWay Center with H.E.S.S.," *Phys. Rev. Lett.* **114** no. 8, (2015) 081301, arXiv:1502.03244 [astro-ph.HE].

[494] **Fermi-LAT** Collaboration, M. Ackermann *et al.*, "Limits on Dark Matter Annihilation Signals from the Fermi LAT 4-year Measurement of the Isotropic Gamma-Ray Background," *JCAP* **1509** no. 09, (2015) 008, arXiv:1501.05464 [astro-ph.CO].

[495] **Fermi-LAT** Collaboration, M. Ackermann *et al.*, "Updated search for spectral lines from Galactic dark matter interactions with pass 8 data from the Fermi Large Area Telescope," *Phys. Rev.* **D91** no. 12, (2015) 122002, arXiv:1506.00013 [astro-ph.HE].

[496] **Fermi-LAT** Collaboration, M. Ackermann *et al.*, "Searching for Dark Matter Annihilation from MilkyÂăWay Dwarf Spheroidal Galaxies with Six Years of Fermi Large Area Telescope Data," *Phys. Rev. Lett.* **115** no. 23, (2015) 231301, arXiv:1503.02641 [astro-ph.HE].

[497] **H.E.S.S.** Collaboration, H. Abdalla *et al.*, "H.E.S.S. Limits on Linelike Dark Matter Signatures in the 100ÂăGeV to 2ÂăTeV Energy Range Close to the Galactic Center," *Phys. Rev. Lett.* **117** no. 15, (2016) 151302, arXiv:1609.08091 [astro-ph.HE].

[498] **H.E.S.S.** Collaboration, H. Abdallah *et al.*, "Search for dark matter annihilations towards the inner Galactic halo from 10 years of observations with H.E.S.S," *Phys. Rev. Lett.* **117** no. 11, (2016) 111301, arXiv:1607.08142 [astro-ph.HE].

[499] **DES, Fermi-LAT** Collaboration, A. Albert *et al.*, "Searching for Dark Matter Annihilation in Recently Discovered Milky Way Satellites with Fermi-LAT," *Astrophys. J.* **834** no. 2, (2017) 110, arXiv:1611.03184 [astro-ph.HE].

[500] C. Rott, "Status of Dark Matter Searches (Rapporteur Talk)," arXiv:1712.00666 [astro-ph.HE]. [PoSICRC2017,1119(2017)].

[501] H. Baer, T. Barklow, K. Fujii, Y. Gao, A. Hoang, S. Kanemura, J. List, H. E. Logan, A. Nomerotski, M. Perelstein, *et al.*, "The International Linear Collider Technical Design Report - Volume 2: Physics," arXiv:1306.6352 [hep-ph].

[502] G. F. Giudice, B. Gripaios, and R. Mahbubani, "Counting dark matter particles in LHC events," *Phys. Rev.* **D85** (2012) 075019, arXiv:1108.1800 [hep-ph].

[503] E. A. Baltz, M. Battaglia, M. E. Peskin, and T. Wizansky, "Determination of dark matter properties at high-energy colliders," *Phys. Rev.* **D74** (2006) 103521, arXiv:hep-ph/0602187 [hep-ph].

[504] G. Kane and S. Watson, "Dark Matter and LHC: What is the Connection?," *Mod. Phys. Lett.* **A23** (2008) 2103–2123, arXiv:0807.2244 [hep-ph].

[505] K. G. Wilson and J. B. Kogut, "The Renormalization group and the epsilon expansion," *Phys. Rept.* **12** (1974) 75–200.

[506] K. G. Wilson, "The Renormalization Group: Critical Phenomena and the Kondo Problem," *Rev. Mod. Phys.* **47** (1975) 773.

[507] C. T. Hill, "Conjecture on the physical implications of the scale anomaly," arXiv:hep-th/0510177 [hep-th].

[508] A. Dymarsky, Z. Komargodski, A. Schwimmer, and S. Theisen, "On Scale and Conformal Invariance in Four Dimensions," *JHEP* **10** (2015) 171, arXiv:1309.2921 [hep-th].

[509] M. Shaposhnikov and D. Zenhausern, "Quantum scale invariance, cosmological constant and hierarchy problem," *Phys. Lett.* **B671** (2009) 162–166, arXiv:0809.3406 [hep-th].

[510] G. Marques Tavares, M. Schmaltz, and W. Skiba, "Higgs mass naturalness and scale invariance in the UV," *Phys.Rev.* **D89** no. 1, (2014) 015009, arXiv:1308.0025 [hep-ph].

[511] S. Abel and A. Mariotti, "Novel Higgs Potentials from Gauge Mediation of Exact Scale Breaking," *Phys.Rev.* **D89** no. 12, (2014) 125018, arXiv:1312.5335 [hep-ph].

[512] A. Gorsky, A. Mironov, A. Morozov, and T. Tomaras, "Is the Standard Model saved asymptotically by conformal symmetry?," *J.Exp.Theor.Phys.* **120** no. 3, (2015) 344–353, arXiv:1409.0492 [hep-ph].

[513] C. Englert, J. Jaeckel, V. Khoze, and M. Spannowsky, "Emergence of the Electroweak Scale through the Higgs Portal," *JHEP* **1304** (2013) 060, arXiv:1301.4224 [hep-ph].

[514] E. Gildener and S. Weinberg, "Symmetry Breaking and Scalar Bosons," *Phys.Rev.* **D13** (1976) 3333.

[515] L. Alexander-Nunneley and A. Pilaftsis, "The Minimal Scale Invariant Extension of the Standard Model," *JHEP* **1009** (2010) 021, arXiv:1006.5916 [hep-ph].

[516] S. Benic and B. Radovcic, "Electroweak breaking and Dark Matter from the common scale," *Phys. Lett.* **B732** (2014) 91–94, arXiv:1401.8183 [hep-ph].

[517] W.-F. Chang, J. N. Ng, and J. M. Wu, "Shadow Higgs from a scale-invariant hidden U(1)(s) model," *Phys.Rev.* **D75** (2007) 115016, arXiv:hep-ph/0701254 [HEP-PH].

[518] A. Farzinnia, H.-J. He, and J. Ren, "Natural electroweak symmetry breaking from scale invariant higgs mechanism," *Physics Letters B* **727** no. 1, (2013) 141–150.

[519] A. G. Dias, "Neutrino Mass Through Concomitant Breakdown of the U(1) Chiral and Scale Symmetries," *Phys. Rev.* **D73** (2006) 096002, arXiv:hep-ph/0604219 [hep-ph].

[520] K. A. Meissner and H. Nicolai, "Conformal Symmetry and the Standard Model," *Phys.Lett.* **B648** (2007) 312–317, arXiv:hep-th/0612165 [hep-th].

[521] R. Foot, A. Kobakhidze, K. McDonald, and R. Volkas, "Neutrino mass in radiatively-broken scale-invariant models," *Phys.Rev.* **D76** (2007) 075014, arXiv:0706.1829 [hep-ph].

[522] R. Foot, A. Kobakhidze, and R. R. Volkas, "Electroweak Higgs as a pseudo-Goldstone boson of broken scale invariance," *Phys.Lett.* **B655** (2007) 156–161, arXiv:0704.1165 [hep-ph].

[523] R. Foot, A. Kobakhidze, K. L. McDonald, and R. R. Volkas, "A Solution to the hierarchy problem from an almost decoupled hidden sector within a classically scale invariant theory," *Phys.Rev.* **D77** (2008) 035006, arXiv:0709.2750 [hep-ph].

[524] R. Foot, A. Kobakhidze, and R. R. Volkas, "Stable mass hierarchies and dark matter from hidden sectors in the scale-invariant standard model," *Phys.Rev.* **D82** (2010) 035005, arXiv:1006.0131 [hep-ph].

[525] R. Foot and A. Kobakhidze, "Electroweak Scale Invariant Models with Small Cosmological Constant," arXiv:1112.0607 [hep-ph].

[526] R. Foot, A. Kobakhidze, and R. R. Volkas, "Cosmological constant in scale-invariant theories," *Phys. Rev.* **D84** (2011) 075010, arXiv:1012.4848 [hep-ph].

[527] K. Ishiwata, "Dark Matter in Classically Scale-Invariant Two Singlets Standard Model," *Phys.Lett.* **B710** (2012) 134–138, arXiv:1112.2696 [hep-ph].

[528] J. S. Lee and A. Pilaftsis, "Radiative Corrections to Scalar Masses and Mixing in a Scale Invariant Two Higgs Doublet Model," *Phys.Rev.* **D86** (2012) 035004, arXiv:1201.4891 [hep-ph].

[529] D. Chway, T. H. Jung, H. D. Kim, and R. Dermisek, "Radiative Electroweak Symmetry Breaking Model Perturbative All the Way to the Planck Scale," *Phys.Rev.Lett.* **113** no. 5, (2014) 051801, arXiv:1308.0891 [hep-ph].

[530] M. Lindner, S. Schmidt, and J. Smirnov, "Neutrino Masses and Conformal Electro-Weak Symmetry Breaking," *JHEP* **1410** (2014) 177, arXiv:1405.6204 [hep-ph].

[531] H. Davoudiasl and I. M. Lewis, "Right-Handed Neutrinos as the Origin of the Electroweak Scale," *Phys.Rev.* **D90** no. 3, (2014) 033003, arXiv:1404.6260 [hep-ph].

[532] O. Antipin, M. Mojaza, and F. Sannino, "Conformal Extensions of the Standard Model with Veltman Conditions," *Phys.Rev.* **D89** no. 8, (2014) 085015, arXiv:1310.0957 [hep-ph].

[533] W.-L. Guo and Y.-L. Wu, "The Real singlet scalar dark matter model," *JHEP* **1010** (2010) 083, arXiv:1006.2518 [hep-ph].

[534] A. Farzinnia and J. Ren, "Higgs Partner Searches and Dark Matter Phenomenology in a Classically Scale Invariant Higgs Boson Sector," *Phys.Rev.* **D90** no. 1, (2014) 015019, arXiv:1405.0498 [hep-ph].

[535] Z. Kang, "Upgrading sterile neutrino dark matter to FI*m*P using scale invariance," *Eur. Phys. J.* **C75** no. 10, (2015) 471, arXiv:1411.2773 [hep-ph].

[536] P. Humbert, M. Lindner, and J. Smirnov, "The Inverse Seesaw in Conformal Electro-Weak Symmetry Breaking and Phenomenological Consequences," arXiv:1503.03066 [hep-ph].

[537] K. Endo and K. Ishiwata, "Direct detection of singlet dark matter in classically scale-invariant standard model," *Phys. Lett.* **B749** (2015) 583–588, arXiv:1507.01739 [hep-ph].

[538] F. Sannino and J. VirkajÎŞÂd'rvi, "First Order Electroweak Phase Transition from (Non)Conformal Extensions of the Standard Model," *Phys. Rev.* **D92** no. 4, (2015) 045015, arXiv:1505.05872 [hep-ph].

[539] Z. Kang, "View FImP miracle (by scale invariance) Ãă la self-interaction," *Phys. Lett.* **B751** (2015) 201–204, arXiv:1505.06554 [hep-ph].

[540] K. Endo and Y. Sumino, "A Scale-invariant Higgs Sector and Structure of the Vacuum," *JHEP* **1505** (2015) 030, arXiv:1503.02819 [hep-ph].

[541] A. Farzinnia, "Prospects for Discovering the Higgs-like Pseudo-Nambu-Goldstone Boson of the Classical Scale Symmetry," *Phys. Rev.* **D92** no. 9, (2015) 095012, arXiv:1507.06926 [hep-ph].

[542] K. Endo, K. Ishiwata, and Y. Sumino, "*WW* scattering in a radiative electroweak symmetry breaking scenario," *Phys. Rev.* **D94** no. 7, (2016) 075007, arXiv:1601.00696 [hep-ph].

[543] A. Ahriche, A. Manning, K. L. McDonald, and S. Nasri, "Scale-Invariant Models with One-Loop Neutrino Mass and Dark Matter Candidates," arXiv:1604.05995 [hep-ph].

[544] Z.-W. Wang, F. S. Sage, T. G. Steele, and R. B. Mann, "Can an Asymptotically-Safe Conformal $U(1)'$ Model Address the LHC Diboson Excess?," arXiv:1511.02531 [hep-ph].

[545] K. Ghorbani and H. Ghorbani, "Scalar Dark Matter in Scale Invariant Standard Model," *JHEP* **04** (2016) 024, arXiv:1511.08432 [hep-ph].

[546] A. J. Helmboldt, P. Humbert, M. Lindner, and J. Smirnov, "Minimal Conformal Extensions of the Higgs Sector," arXiv:1603.03603 [hep-ph].

[547] K. Hashino, M. Kakizaki, S. Kanemura, and T. Matsui, "Synergy between measurements of gravitational waves and the triple-Higgs coupling in probing the first-order electroweak phase transition," *Phys. Rev.* **D94** no. 1, (2016) 015005, arXiv:1604.02069 [hep-ph].

[548] P. G. Ferreira, C. T. Hill, and G. G. Ross, "Scale-Independent Inflation and Hierarchy Generation," *Submitted to: Phys. Rev. Lett.* (2016) , arXiv:1603.05983 [hep-th].

[549] A. Ahriche, K. L. McDonald, and S. Nasri, "A Radiative Model for the Weak Scale and Neutrino Mass via Dark Matter," *JHEP* **02** (2016) 038, arXiv:1508.02607 [hep-ph].

[550] A. Ahriche, K. L. McDonald, and S. Nasri, "The Scale-Invariant Scotogenic Model," arXiv:1604.05569 [hep-ph].

[551] K. Kawana, "Classical conformality in the Standard Model from Coleman's theory," arXiv:1605.00436 [hep-ph].

[552] F. Wu, "Aspects of a Non-minimal Conformal Extension of the Standard Model," *Phys. Rev.* **D94** no. 5, (2016) 055011, arXiv:1606.08112 [hep-ph].

[553] K. Hashino, M. Kakizaki, S. Kanemura, P. Ko, and T. Matsui, "Gravitational waves and Higgs boson couplings for exploring first order phase transition in the model with a singlet scalar field," *Phys. Lett.* **B766** (2017) 49–54, arXiv:1609.00297 [hep-ph].

[554] L. Marzola, A. Racioppi, and V. Vaskonen, "Phase transition and gravitational wave phenomenology of scalar conformal extensions of the Standard Model," *Eur. Phys. J.* **C77** no. 7, (2017) 484, arXiv:1704.01034 [hep-ph].

[555] A. Lewandowski, K. A. Meissner, and H. Nicolai, "Conformal Standard Model, Leptogenesis and Dark Matter," *Phys. Rev.* **D97** no. 3, (2018) 035024, arXiv:1710.06149 [hep-ph].

[556] R. Hempfling, "The Next-to-minimal Coleman-Weinberg model," *Phys.Lett.* **B379** (1996) 153–158, arXiv:hep-ph/9604278 [hep-ph].

[557] S. Iso, N. Okada, and Y. Orikasa, "Classically conformal B^- L extended Standard Model," *Phys.Lett.* **B676** (2009) 81–87, arXiv:0902.4050 [hep-ph].

[558] S. Iso, N. Okada, and Y. Orikasa, "The minimal B-L model naturally realized at TeV scale," *Phys.Rev.* **D80** (2009) 115007, arXiv:0909.0128 [hep-ph].

[559] M. Holthausen, M. Lindner, and M. A. Schmidt, "Radiative Symmetry Breaking of the Minimal Left-Right Symmetric Model," *Phys.Rev.* **D82** (2010) 055002, arXiv:0911.0710 [hep-ph].

[560] S. Iso and Y. Orikasa, "TeV Scale B-L model with a flat Higgs potential at the Planck scale - in view of the hierarchy problem -," *PTEP* **2013** (2013) 023B08, arXiv:1210.2848 [hep-ph].

[561] E. J. Chun, S. Jung, and H. M. Lee, "Radiative generation of the Higgs potential," *Phys. Lett.* **B725** (2013) 158–163, arXiv:1304.5815 [hep-ph]. [Erratum: Phys. Lett.B730,357(2014)].

[562] R. S. Chivukula, A. Farzinnia, J. Ren, and E. H. Simmons, "Constraints on the Scalar Sector of the Renormalizable Coloron Model," *Phys.Rev.* **D88** no. 7, (2013) 075020, arXiv:1307.1064 [hep-ph].

[563] V. V. Khoze and G. Ro, "Leptogenesis and Neutrino Oscillations in the Classically Conformal Standard Model with the Higgs Portal," *JHEP* **1310** (2013) 075, arXiv:1307.3764.

[564] M. Holthausen, J. Kubo, K. S. Lim, and M. Lindner, "Electroweak and Conformal Symmetry Breaking by a Strongly Coupled Hidden Sector," *JHEP* **1312** (2013) 076, arXiv:1310.4423 [hep-ph].

[565] M. Hashimoto, S. Iso, and Y. Orikasa, "Radiative symmetry breaking at the Fermi scale and flat potential at the Planck scale," *Phys.Rev.* **D89** no. 1, (2014) 016019, arXiv:1310.4304 [hep-ph].

[566] S. Benic and B. Radovcic, "Majorana dark matter in a classically scale invariant model," *JHEP* **1501** (2015) 143, arXiv:1409.5776 [hep-ph].

[567] J. Kubo, K. S. Lim, and M. Lindner, "Gamma-ray Line from Nambu-Goldstone Dark Matter in a Scale Invariant Extension of the Standard Model," *JHEP* **1409** (2014) 016, arXiv:1405.1052 [hep-ph].

[568] J. Guo, Z. Kang, P. Ko, and Y. Orikasa, "Accidental Dark Matter: Case in the Scale Invariant Local $B-L$ Models," arXiv:1502.00508 [hep-ph].

[569] N. Haba, H. Ishida, N. Okada, and Y. Yamaguchi, "Bosonic seesaw mechanism in a classically conformal extension of the Standard Model," *Phys. Lett.* **B754** (2016) 349–352, arXiv:1508.06828 [hep-ph].

[570] Y. Orikasa, "The Classically Conformal B−L Extended Ma Model," arXiv:1504.07953 [hep-ph].

[571] S. Oda, N. Okada, and D.-s. Takahashi, "Classically conformal U(1)′ extended Standard Model and Higgs vacuum stability," *Phys. Rev.* **D92** no. 1, (2015) 015026, arXiv:1504.06291 [hep-ph].

[572] N. Haba and Y. Yamaguchi, "Vacuum stability in the $U(1)_\chi$ extended model with vanishing scalar potential at the Planck scale," *PTEP* **2015** no. 9, (2015) 093B05, arXiv:1504.05669 [hep-ph].

[573] Y. Ametani, M. Aoki, H. Goto, and J. Kubo, "Nambu-Goldstone Dark Matter in a Scale Invariant Bright Hidden Sector," *Phys. Rev.* **D91** no. 11, (2015) 115007, arXiv:1505.00128 [hep-ph].

[574] C. D. Carone and R. Ramos, "Dark chiral symmetry breaking and the origin of the electroweak scale," *Phys.Lett.* **B746** (2015) 424–429, arXiv:1505.04448 [hep-ph].

[575] W. Altmannshofer, W. A. Bardeen, M. Bauer, M. Carena, and J. D. Lykken, "Light Dark Matter, Naturalness, and the Radiative Origin of the Electroweak Scale," *JHEP* **1501** (2015) 032, arXiv:1408.3429 [hep-ph].

[576] A. D. Plascencia, "Classical scale invariance in the inert doublet model," *JHEP* **09** (2015) 026, arXiv:1507.04996 [hep-ph].

[577] A. Das, N. Okada, and N. Papapietro, "Electroweak vacuum stability in classically conformal B-L extension of the Standard Model," arXiv:1509.01466 [hep-ph].

[578] N. Haba, H. Ishida, R. Takahashi, and Y. Yamaguchi, "Gauge coupling unification in a classically scale invariant model," *JHEP* **02** (2016) 058, arXiv:1511.02107 [hep-ph].

[579] H. Okada, Y. Orikasa, and K. Yagyu, "Higgs Triplet Model with Classically Conformal Invariance," arXiv:1510.00799 [hep-ph].

[580] R. Jinno and M. Takimoto, "Probing classically conformal $B-L$ model with gravitational waves," arXiv:1604.05035 [hep-ph].

[581] A. Das, S. Oda, N. Okada, and D.-s. Takahashi, "Classically conformal U(1)′ extended standard model, electroweak vacuum stability, and LHC Run-2 bounds," *Phys. Rev.* **D93** no. 11, (2016) 115038, arXiv:1605.01157 [hep-ph].

[582] K. Kannike, G. M. Pelaggi, A. Salvio, and A. Strumia, "The diphoton as the Higgs of the Higgs," *JHEP* **07** (2016) 101, arXiv:1605.08681 [hep-ph].

[583] H. Hatanaka, D.-W. Jung, and P. Ko, "AdS/QCD approach to the scale invariant extension of the standard model with a strongly interacting hidden sector," *JHEP* **08** (2016) 094, arXiv:1606.02969 [hep-ph].

[584] J. Kubo and M. Yamada, "Scale genesis and gravitational wave in a classically scale invariant extension of the standard model," *JCAP* **1612** no. 12, (2016) 001, arXiv:1610.02241 [hep-ph].

[585] S. Oda, N. Okada, and D.-s. Takahashi, "Right-handed neutrino dark matter in the classically conformal U(1)âĂŠ extended standard model," *Phys. Rev.* **D96** no. 9, (2017) 095032, arXiv:1704.05023 [hep-ph].

[586] A. Salvio and A. Strumia, "Agravity," *JHEP* **06** (2014) 080, arXiv:1403.4226 [hep-ph].

[587] M. B. Einhorn and D. R. T. Jones, "Naturalness and Dimensional Transmutation in Classically Scale-Invariant Gravity," *JHEP* **1503** (2015) 047, arXiv:1410.8513 [hep-th].

[588] K. Kannike, G. HÎŞÎŇtsi, L. Pizza, A. Racioppi, M. Raidal, *et al.*, "Dynamically Induced Planck Scale and Inflation," *JHEP* **1505** (2015) 065, arXiv:1502.01334 [astro-ph.CO].

[589] K. Kannike, A. Racioppi, and M. Raidal, "Linear inflation from quartic potential," *JHEP* **01** (2016) 035, arXiv:1509.05423 [hep-ph].

[590] M. B. Einhorn and D. R. T. Jones, "Gauss-Bonnet coupling constant in classically scale-invariant gravity," *Phys. Rev.* **D91** no. 8, (2015) 084039, arXiv:1412.5572 [hep-th].

[591] M. Rinaldi, G. Cognola, L. Vanzo, and S. Zerbini, "Inflation in scale-invariant theories of gravity," *Phys. Rev.* **D91** no. 12, (2015) 123527, arXiv:1410.0631 [gr-qc].

[592] G. Narain, "Exorcising Ghosts in Induced Gravity," *Eur. Phys. J.* **C77** no. 10, (2017) 683, arXiv:1612.04930 [hep-th].

[593] A. Salvio and A. Strumia, "Agravity up to infinite energy," *Eur. Phys. J.* **C78** no. 2, (2018) 124, arXiv:1705.03896 [hep-th].

[594] K. Kaneta, O. Seto, and R. Takahashi, "Very low scale Coleman-Weinberg inflation with non-minimal coupling," *Phys. Rev.* **D97** no. 6, (2017) 063004, arXiv:1708.06455 [hep-ph].

[595] P. G. Ferreira, C. T. Hill, and G. G. Ross, "Inertial Spontaneous Symmetry Breaking and Quantum Scale Invariance," arXiv:1801.07676 [hep-th].

[596] P. G. Ferreira, C. T. Hill, J. Noller, and G. G. Ross, "Inflation in a scale invariant universe," arXiv:1802.06069 [astro-ph.CO].

[597] A. Karam, L. Marzola, T. Pappas, A. Racioppi, and K. Tamvakis, "Constant-Roll (Quasi-)Linear Inflation," arXiv:1711.09861 [astro-ph.CO].

[598] A. Racioppi, "Coleman-Weinberg linear inflation: metric vs. Palatini formulation," *JCAP* **1712** no. 12, (2017) 041, arXiv:1710.04853 [astro-ph.CO].

[599] A. Racioppi, "A new universal attractor: linear inflation," arXiv:1801.08810 [astro-ph.CO].

[600] E. Gildener, "Radiatively Induced Spontaneous Symmetry Breaking for Asymptotically Free Gauge Theories," *Phys.Rev.* **D13** (1976) 1025.

[601] K. Hadeler, "On copositive matrices," *Linear Algebra and its Applications* **49** (1983) 79–89.

[602] L. Ping and F. Y. Yu, "Criteria for copositive matrices of order four," *Linear algebra and its applications* **194** (1993) 109–124.

[603] G. Chang and T. W. Sederberg, "Nonnegative quadratic bézier triangular patches," *Computer aided geometric design* **11** no. 1, (1994) 113–116.

[604] K. Kannike, "Vacuum Stability Conditions From Copositivity Criteria," *Eur.Phys.J.* **C72** (2012) 2093, arXiv:1205.3781 [hep-ph].

[605] J. Chakrabortty, P. Konar, and T. Mondal, "Copositive criteria and boundedness of the scalar potential," *Physical Review D* **89** no. 9, (2014) 095008.

[606] **ATLAS, CDF, CMS, D0** Collaboration, "First combination of Tevatron and LHC measurements of the top-quark mass," arXiv:1403.4427 [hep-ex].

[607] M. E. Machacek and M. T. Vaughn, "Two Loop Renormalization Group Equations in a General Quantum Field Theory. 1. Wave Function Renormalization," *Nucl. Phys.* **B222** (1983) 83.

[608] M. E. Machacek and M. T. Vaughn, "Two Loop Renormalization Group Equations in a General Quantum Field Theory. 2. Yukawa Couplings," *Nucl. Phys.* **B236** (1984) 221.

[609] M. E. Machacek and M. T. Vaughn, "Two Loop Renormalization Group Equations in a General Quantum Field Theory. 3. Scalar Quartic Couplings," *Nucl. Phys.* **B249** (1985) 70.

[610] M.-x. Luo, H.-w. Wang, and Y. Xiao, "Two loop renormalization group equations in general gauge field theories," *Phys.Rev.* **D67** (2003) 065019, arXiv:hep-ph/0211440 [hep-ph].

[611] M.-x. Luo and Y. Xiao, "Two loop renormalization group equations in the standard model," *Phys. Rev. Lett.* **90** (2003) 011601, arXiv:hep-ph/0207271 [hep-ph].

[612] F. Staub, "SARAH 4 : A tool for (not only SUSY) model builders," *Comput. Phys. Commun.* **185** (2014) 1773–1790, arXiv:1309.7223 [hep-ph].

[613] F. Staub, "Exploring new models in all detail with SARAH," *Adv. High Energy Phys.* **2015** (2015) 840780, arXiv:1503.04200 [hep-ph].

[614] **LHC Higgs Cross Section Working Group** Collaboration, S. Heinemeyer *et al.*, "Handbook of LHC Higgs Cross Sections: 3. Higgs Properties," arXiv:1307.1347 [hep-ph].

[615] K. Cheung, J. S. Lee, and P.-Y. Tseng, "Higgs precision analysis updates 2014," *Phys. Rev.* **D90** (2014) 095009, arXiv:1407.8236 [hep-ph].

[616] **ATLAS** Collaboration, G. Aad *et al.*, "Measurement of the Higgs boson mass from the $H \to \gamma\gamma$ and $H \to ZZ^* \to 4\ell$ channels with the ATLAS detector using 25 fb^{-1} of pp collision data," *Phys.Rev.* **D90** no. 5, (2014) 052004, arXiv:1406.3827 [hep-ex].

[617] **CMS** Collaboration, V. Khachatryan *et al.*, "Precise determination of the mass of the Higgs boson and tests of compatibility of its couplings with the standard model predictions using proton collisions at 7 and 8 TeV," *Eur. Phys. J.* **C75** no. 5, (2015) 212, arXiv:1412.8662 [hep-ex].

[618] A. Falkowski, C. Gross, and O. Lebedev, "A second Higgs from the Higgs portal," *JHEP* **05** (2015) 057, arXiv:1502.01361 [hep-ph].

[619] M. Srednicki, R. Watkins, and K. A. Olive, "Calculations of Relic Densities in the Early Universe," *Nucl. Phys.* **B310** (1988) 693.

[620] F. D'Eramo and J. Thaler, "Semi-annihilation of Dark Matter," *JHEP* **1006** (2010) 109, arXiv:1003.5912 [hep-ph].

[621] G. Belanger, K. Kannike, A. Pukhov, and M. Raidal, "Impact of semi-annihilations on dark matter phenomenology - an example of Z_N symmetric scalar dark matter," *JCAP* **1204** (2012) 010, arXiv:1202.2962 [hep-ph].

[622] Y. Cai and A. Spray, "A Systematic Effective Operator Analysis of Semi-Annihilating Dark Matter," *JHEP* **02** (2017) 120, arXiv:1611.09360 [hep-ph].

[623] M. Srednicki, R. Watkins, and K. A. Olive, "Calculations of relic densities in the early universe," *Nuclear Physics B* **310** no. 3, (1988) 693–713.

[624] K. Griest and D. Seckel, "Three exceptions in the calculation of relic abundances," *Phys. Rev.* **D43** (1991) 3191–3203.

[625] P. Junnarkar and A. Walker-Loud, "Scalar strange content of the nucleon from lattice QCD," *Phys. Rev.* **D87** (2013) 114510, arXiv:1301.1114 [hep-lat].

[626] A. Crivellin, M. Hoferichter, and M. Procura, "Accurate evaluation of hadronic uncertainties in spin-independent WIMP-nucleon scattering: Disentangling two- and three-flavor effects," *Phys. Rev.* **D89** (2014) 054021, arXiv:1312.4951 [hep-ph].

[627] M. Hoferichter, J. Ruiz de Elvira, B. Kubis, and U.-G. MeiÃ§ner, "High-precision determination of the pion-nucleon σ-term from Roy-Steiner equations," arXiv:1506.04142 [hep-ph].

[628] **LUX** Collaboration, D. Akerib *et al.*, "First results from the LUX dark matter experiment at the Sanford Underground Research Facility," *Phys.Rev.Lett.* **112** (2014) 091303, arXiv:1310.8214 [astro-ph.CO].

[629] K. Agashe, D. Kim, D. G. E. Walker, and L. Zhu, "Using MT2 to Distinguish Dark Matter Stabilization Symmetries," *Phys. Rev.* **D84** (2011) 055020, arXiv:1012.4460 [hep-ph].

[630] G. Belanger, K. Kannike, A. Pukhov, and M. Raidal, "Z_3 Scalar Singlet Dark Matter," *JCAP* **1301** (2013) 022, arXiv:1211.1014 [hep-ph].

[631] M. Aoki and T. Toma, "Impact of semi-annihilation of $\mathbb{Z}_3$ symmetric dark matter with radiative neutrino masses," *JCAP* **1409** (2014) 016, arXiv:1405.5870 [hep-ph].

[632] P. Ko and Y. Tang, "Galactic center γ-ray excess in hidden sector DM models with dark gauge symmetries: local Z_3 symmetry as an example," *JCAP* **1501** (2015) 023, arXiv:1407.5492 [hep-ph].

[633] N. Bernal, C. Garcia-Cely, and R. Rosenfeld, "WIMP and SIMP Dark Matter from the Spontaneous Breaking of a Global Group," *JCAP* **1504** no. 04, (2015) 012, arXiv:1501.01973 [hep-ph].

[634] S. Bhattacharya, S. Jana, and S. Nandi, "Neutrino Masses and Scalar Singlet Dark Matter," *Phys. Rev.* **D95** no. 5, (2017) 055003, arXiv:1609.03274 [hep-ph].

[635] I. P. Ivanov and V. Keus, "Zp scalar dark matter from multi-Higgs-doublet models," *Phys. Rev.* **D86** (2012) 016004, arXiv:1203.3426 [hep-ph].

[636] G. BÃl'langer, K. Kannike, A. Pukhov, and M. Raidal, "Minimal semi-annihilating $\mathbb{Z}_N$ scalar dark matter," *JCAP* **1406** (2014) 021, arXiv:1403.4960 [hep-ph].

[637] Y. Cai and A. P. Spray, "Fermionic Semi-Annihilating Dark Matter," *JHEP* **01** (2016) 087, arXiv:1509.08481 [hep-ph].

[638] G. Belanger and J.-C. Park, "Assisted freeze-out," *JCAP* **1203** (2012) 038, arXiv:1112.4491 [hep-ph].

[639] M. Aoki, M. Duerr, J. Kubo, and H. Takano, "Multi-Component Dark Matter Systems and Their Observation Prospects," *Phys. Rev.* **D86** (2012) 076015, arXiv:1207.3318 [hep-ph].

[640] M. Aoki, J. Kubo, and H. Takano, "Two-loop radiative seesaw mechanism with multicomponent dark matter explaining the possible Îş excess in the Higgs boson decay and at the Fermi LAT," *Phys. Rev.* **D87** no. 11, (2013) 116001, arXiv:1302.3936 [hep-ph].

[641] S. Bhattacharya, P. Poulose, and P. Ghosh, "Multipartite Interacting Scalar Dark Matter in the light of updated LUX data," *JCAP* **1704** no. 04, (2017) 043, arXiv:1607.08461 [hep-ph].

[642] S. Bhattacharya, P. Ghosh, T. N. Maity, and T. S. Ray, "Mitigating Direct Detection Bounds in Non-minimal Higgs Portal Scalar Dark Matter Models," *JHEP* **10** (2017) 088, arXiv:1706.04699 [hep-ph].

[643] M. Pandey, D. Majumdar, and K. P. Modak, "Two Component Feebly Interacting Massive Particle (FIMP) Dark Matter," arXiv:1709.05955 [hep-ph].

[644] J. Ellis, J. L. Evans, F. Luo, and K. A. Olive, "Scenarios for Gluino Coannihilation," *JHEP* **02** (2016) 071, arXiv:1510.03498 [hep-ph].

[645] T. Hahn, "Generating Feynman diagrams and amplitudes with FeynArts 3," *Comput. Phys. Commun.* **140** (2001) 418–431, arXiv:hep-ph/0012260 [hep-ph].

[646] T. Hahn and M. Perez-Victoria, "Automatized one loop calculations in four-dimensions and D-dimensions," *Comput. Phys. Commun.* **118** (1999) 153–165, arXiv:hep-ph/9807565 [hep-ph].

[647] S. Di Chiara, V. Keus, and O. Lebedev, "Stabilizing the Higgs potential with a Z′," *Phys.Lett.* **B744** (2015) 59–66, arXiv:1412.7036 [hep-ph].

[648] J. M. Alarcon, J. Martin Camalich, and J. A. Oller, "The chiral representation of the πN scattering amplitude and the pion-nucleon sigma term," *Phys. Rev.* **D85** (2012) 051503, arXiv:1110.3797 [hep-ph].

[649] J. M. Alarcon, L. S. Geng, J. Martin Camalich, and J. A. Oller, "The strangeness content of the nucleon from effective field theory and phenomenology," *Phys. Lett.* **B730** (2014) 342–346, arXiv:1209.2870 [hep-ph].

[650] M. Aoki, J. Kubo, and H. Takano, "Multicomponent Dark Matter in Radiative Seesaw Model and Monochromatic Neutrino Flux," *Phys.Rev.* **D90** no. 7, (2014) 076011, arXiv:1408.1853 [hep-ph].

[651] S. Esch, M. Klasen, and C. E. Yaguna, "A minimal model for two-component dark matter," *JHEP* **09** (2014) 108, arXiv:1406.0617 [hep-ph].

[652] D. C. Malling *et al.*, "After LUX: The LZ Program," arXiv:1110.0103 [astro-ph.IM].

[653] **XENON** Collaboration, E. Aprile *et al.*, "Physics reach of the XENON1T dark matter experiment," *JCAP* **1604** no. 04, (2016) 027, arXiv:1512.07501 [physics.ins-det].

[654] A. Karam, T. Pappas, and K. Tamvakis, "Frame-dependence of higher-order inflationary observables in scalar-tensor theories," *Phys. Rev.* **D96** no. 6, (2017) 064036, arXiv:1707.00984 [gr-qc].

[655] L. Järv, K. Kannike, L. Marzola, A. Racioppi, M. Raidal, M. Rünkla, M. Saal, and H. Veermäe, "Frame-Independent Classification of Single-Field Inflationary Models," *Phys. Rev. Lett.* **118** no. 15, (2017) 151302, arXiv:1612.06863 [hep-ph].

[656] H. PadÃľ, "Sur la reprÃľsentation approchÃľe d'une fonction par des fractions rationnelles," *Annales scientifiques de l'ÃĽcole Normale SupÃľrieure* **9** (1892) 3–93. http://eudml.org/doc/81047.

[657] F. S. Accetta, D. J. Zoller, and M. S. Turner, "Induced Gravity Inflation," *Phys. Rev.* **D31** (1985) 3046.

[658] E. Carugno, S. Capozziello, and F. Occhionero, "Tunneling from nothing toward induced gravity inflation," *Phys. Rev.* **D47** (1993) 4261–4266.

[659] D. I. Kaiser, "Constraints in the context of induced gravity inflation," *Phys. Rev.* **D49** (1994) 6347–6353, arXiv:astro-ph/9308043 [astro-ph].

[660] D. I. Kaiser, "Induced gravity inflation and the density perturbation spectrum," *Phys. Lett.* **B340** (1994) 23–28, arXiv:astro-ph/9405029 [astro-ph].

[661] J. L. Cervantes-Cota and H. Dehnen, "Induced gravity inflation in the standard model of particle physics," *Nucl. Phys.* **B442** (1995) 391–412, arXiv:astro-ph/9505069 [astro-ph].

[662] A. Cerioni, F. Finelli, A. Tronconi, and G. Venturi, "Inflation and Reheating in Induced Gravity," *Phys. Lett.* **B681** (2009) 383–386, arXiv:0906.1902 [astro-ph.CO].

[663] G. F. Giudice and H. M. Lee, "Starobinsky-like inflation from induced gravity," *Phys. Lett.* **B733** (2014) 58–62, arXiv:1402.2129 [hep-ph].

[664] C. van de Bruck, P. Dunsby, and L. E. Paduraru, "Reheating and preheating in the simplest extension of Starobinsky inflation," arXiv:1606.04346 [gr-qc].

[665] R. Kallosh, A. Linde, and D. Roest, "Large field inflation and double α-attractors," *JHEP* **08** (2014) 052, arXiv:1405.3646 [hep-th].

[666] T. Matsumura *et al.*, "Mission design of LiteBIRD," arXiv:1311.2847 [astro-ph.IM]. [J. Low. Temp. Phys.176,733(2014)].

[667] L. McAllister, E. Silverstein, and A. Westphal, "Gravity Waves and Linear Inflation from Axion Monodromy," *Phys. Rev.* **D82** (2010) 046003, arXiv:0808.0706 [hep-th].